Localized Corrosion of Stainless Steels in High Temperature Potash Brine

A Thesis

Submitted to the College of Graduate Studies and Research

University of Saskatchewan

in Partial Fulfillment of the Requirements

for the Degree of

Master of Science in Chemical Engineering

by

Mehdi Shirazi

Summer, 1996

In presenting this thesis in partial fulfillment of the requirements for a Postgraduate degree from the University of Saskatchewan, I agree that the libraries of this University may make it freely available for inspection. I further agree that permission for copying of this thesis in any manner, in whole or in part, for scholarly purposes may be granted by the professor or professors who supervised my thesis work or, in their absence, by the Head of the Department or the Dean of the College in which my thesis work was done. It is Understood that any copying or publication or use of this thesis or parts thereof for financial gain shall not be allowed without my written permission. It is also understood that due recognition shall be given to me and to the University of Saskatchewan in any scholarly use that may be made of any material in my thesis.

Requests for permission to copy or to make other use of material in this thesis in whole or part should be addressed to:

The Head of the Department of Chemical Engineering
University of Saskatchewan
Saskatoon, Saskatchewan
Canada
S7N 5C9

ACKNOWLEDGMENTS

I would like to thank my supervisors, Dr. J. Postlethwaite and Dr. S. Yannacopoulos, for their guidance and support throughout my work. I would also like to thank the remaining members of my advisory committee, Drs. Macdonald, Watson, Dalai and Hedayat.

My special thanks goes to my dearest friend, my wife, Hedi for her support in all aspects of my life and especially throughout the last two years.

Many individuals helped me with this project. I truly appreciate my friends C. Blackmore, R. Evitts, T. Davis, F. Wang and Y. Wang for helping me in the laboratory. I would also thank Anita Johnson for helping proof-reading the manuscript and many more things. My thanks also goes to Ted Wallentiny and Philip Siminoff for their technical assistance.

The project was made possible by financial support provided by the Potash Corporation of Saskatchewan. I express my sincere appreciation to Dr. Strathdee and Mr. Popiel for support throughout the project. Laboratory facilities provided by the Departments of Chemical Engineering and Mechanical Engineering, University of Saskatchewan and PCS pilot plant are also appreciated.

To my Father

Localized Corrosion of Stainless Steels in High Temperature Potash Brine

ABSTRACT

Potash brines are highly corrosive at the elevated temperatures found in potash processing. Cyclic potentiodynamic polarization and exposure tests have been carried out with a wide range of stainless steels used in the potash industry.

Hastelloy C276 (a nickel alloy) showed excellent resistance to localized corrosion in high chloride concentration solutions over wide range of temperatures. A wide range of lower cost alloys with less resistance to localized corrosion have been investigated to determine their corrosion behavior at 22 and 90°C in saturated potash brine. The alloys studied included: austenitic, duplex and cast stainless steel alloys.

The results of the electrochemical polarization and exposure tests are compared to the predictions of Localized Corrosion Resistance Index [$LCRI_{wt.\%}$ = %Cr + 3.3 (%Mo) + 16 (%N)]. The electrochemical polarization results show that LCRI can roughly predict the resistance of stainless steel alloys (in the same group i.e. austenitic, duplex) to initiation of localized corrosion. The average pit depth and the five deepest pits have been measured and compared to LCRI for the tested alloys. The deepest pits (the cause of metal failure) found in the exposure tests show that the LCRI cannot predict the propagation of the pits.

Austenitic stainless steels are very sensitive to initiation of pits at the edges. The pits on the edges are deep and wide. Residual stresses adjacent to the edges produce stress corrosion cracking at the bottom of each pit which accelerates corrosion.

Comparing austenitic and duplex stainless steels to identical LCRIs shows a better resistance of duplex stainless steels to localized corrosion. Duplex stainless steels consist of ferrite-austenite phases with more chromium and molybdenum in the ferrite than in the austenite phase. It was found that the austenite-ferrite interface is prone to the initiation of localized attack, but the attack propagates preferentially in the ferrite phase. The immunity of the austenite phase is related to the higher nitrogen concentration in that phase.

Table of Contents

List of Tables

List of Figures

List of Abbreviations

AES	Auger Electron Spectroscopy
ASTM	American Society for Testing and Materials
CPT	Critical Pitting Temperature, °C
CCT	Critical Crevice Temperature, °C
CE	Counter Electrode
CRE	Crevice Resistance Equivalent
$\mathbf{E_{corr}}$	Corrosion Poential, mV
$\mathbf{E_p}$	Repassivation Potential, mV
$\mathbf{E_{pp}}$	Pitting or Breakdown Potential, mV
LCRI	Localized Corrosion Resistance Index
MCA	Multiple Crevice Assembly
PRE	Pitting Resistance Equivalent
PCS	Potash Corporation of Saskatchewan Inc.
RE	Reference Electrode
SCE	Standard Calomel Electrode
SHE	Standard Hydrogen Electrode
STM	Scanning Tunneling Microscopy
SEM	Scanning Electron Microscopy
WE	Working Electrode
XPS	X-ray Photoelectron Spectroscopy

Nomenclature

A	Constant
A'	Constant
B	Constant
B'	Constant
E	Potential, mV
K	Equilibrium Constant
R	Resistance, Ω
i	Current Density, A/cm^2

1. Introduction

Potash was first discovered in Saskatchewan in 1943 during oil exploration. Potash is primarily used as a source of potassium in fertilizers. It is estimated that potash resources in Saskatchewan are large enough to supply the world fertilizer demand for thousands of years. Saskatchewan potash mines are capable of producing more than 16 million tons annually[1].

One of the major problems in potash production processes is localized corrosion of the equipment and pipelines. In this type of attack, metals are perforated without any significant uniform corrosion. This is caused primarily by the presence of chloride in potash, which initiates and propagates the localized corrosion. The presence of solid crystals, high temperature and oxygen makes the corrosion mechanism more complex. Typically, chemical composition and mechanical properties are the main characteristics which are used in material selection.

The most popular stainless steels (i.e. 304L, 316L) are susceptible to localized corrosion at elevated temperatures and high chloride ion concentrations. The new duplex stainless steels containing high chromium and molybdenum show better resistance to localized corrosion. The resistance of stainless steels is increased by passivation in moderate to highly corrosive media. However, the passive film will be destroyed at high temperatures, high oxygen contents and high concentrations of chloride and solid

particles in the process. Therefore, when selecting construction materials, there needs to be a balance between resistance to localized corrosion along with favorable mechanical properties and affordable cost.

1.1. Potash and Potash Chemistry

Potash is composed of potassium chloride, any soluble potassium salt or the potassium oxide (K_2O) equivalent of any potassium compound[2]. Potassium, in combination with nitrogen and phosphorus, has no substitute in agricultural applications. Table 1.1 lists the water soluble potassium minerals which are abundant in the earth's crust and are convertible to fertilizers[2]. Sylvinite, which is a mechanical mixture of sylvite and halite, is the source of over 90% of the world's potash and potassium compounds[3]. Analysis of typical ores from Saskatchewan are shown in Table 1.2[4]. The physical properties of some chloride salts which are present in potash ore are shown in Table 1.3[2].

Table 1.1 Water soluble potash brine on earth[2]

Mineral	Chemical Formula	Potash (K_2O) wt%	Potassium wt%
Sylvite	KCl	63.2	52.5
Sylvinite	nKCl-mNaCl	Varies	Varies
Carnallite	$KCl.MgCl_2.6H_2O$	17.0	14.1
Kainite	$KCl.MgSO_4.3H_2O$	18.9	15.7
Langbeinite	$K_2SO_4.2MgSO_4$	22.6	18.8
Polyhalite	$K_2SO_4.MgSO_4.2CaSO_4.2H_2O$	15.5	13.0
Niter	KNO_3	46.5	38.6

Table 1.2 Analysis of typical potash ore in Saskatchewan[4]

Chemical analysis	wt%	Mineralogical analysis	wt%
KCl	37.724	Sylvinite	96-99
NaCl	59.18	Langbeinite	nil
MgO	0.58	Kainite	0-trace
SO_4^{2-}	0.10	Carnallite	1.0-1.5
Combined H_2O	1.61	Polyhalite	0-trace
Free H_2O	0.30	Others	trace-0.1
Water insoluble	0.50	Water insoluble	0.7-1.0

Table 1.3 Physical properties of chloride salts[2]

Property	NaCl	KCl	$MgCl_2$	$CaCl_2$
Specific gravity at 20°C	2.163	1.988	$2.325_{25°}$	2.152
Melting point, °C	804	790	712	772
Boiling point, °C	1413	1500	1412	>1600
Solubility, parts/100 H_2O at 0°C	35.7	27.6	52.8	59.3
Specific heat, Cal/grmole °C	10.79	10.93	17.3	16.9
Heat of formation, Kcal/ grmole	-98.32	-104.35	153.22	-190.6
Heat of solution, Kcal/grmole	1.16	4.40	-35.95	-18.52

1.2. Objective

The objective of this study is to determine the localized corrosion behavior of commercial stainless steels in potash brine at both the room temperature and 90°C. The highest temperature for the potash brine to achieve in the process is about 90°C in which localized corrosion is a major problem for the equipment and pipelines in this condition. Electrochemical polarization techniques, exposure tests and metallography were used to examine the selected alloys and compare their resistance to localized corrosion.

2. Literature Review

2.1. Passivity

Passivity is defined as a state of a metal surface characterized by low corrosion rates in a potential region that is strongly oxidizing for the metal[5]. The resistance of a passive metal to localized corrosion is closely related to the quality of the passive film on the metal surface. Therefore, the chemical composition of the passive film, its chemical and physical properties, structure, coherence and thickness are significant in the localized corrosion resistance of the metal.

The concept of passivity can be seen in the schematic polarization curve for a passive metal in chloride solution, shown in Fig. 2.1. The passive potential range is defined by the low current density regime between the active-passive transition (passivation potential) and the breakdown potential. The polarization curve is produced by potentiodynamic techniques[5] (see also 2.3).

Films are classified into two categories; *(i)* non-continuous films, which partially insulate the metal from the electrolytic solution; and *(ii)* continuous films, which totally cover the metal surface. Non-continuous films slow down the corrosion of the metal by producing a non-protective oxide film which provides a barrier to oxygen diffusion to the metal surface. These types of films are porous and can be as thick as 1 mm. The red

rusty film often found on iron is an example of non-continuous film. Continuous films completely cover the metal surface. The films are invisible and the thickness of these films varies from 1 to 10 nanometer. Examples of these films are the passive films formed on aluminum, zirconium and stainless steels[6,7].

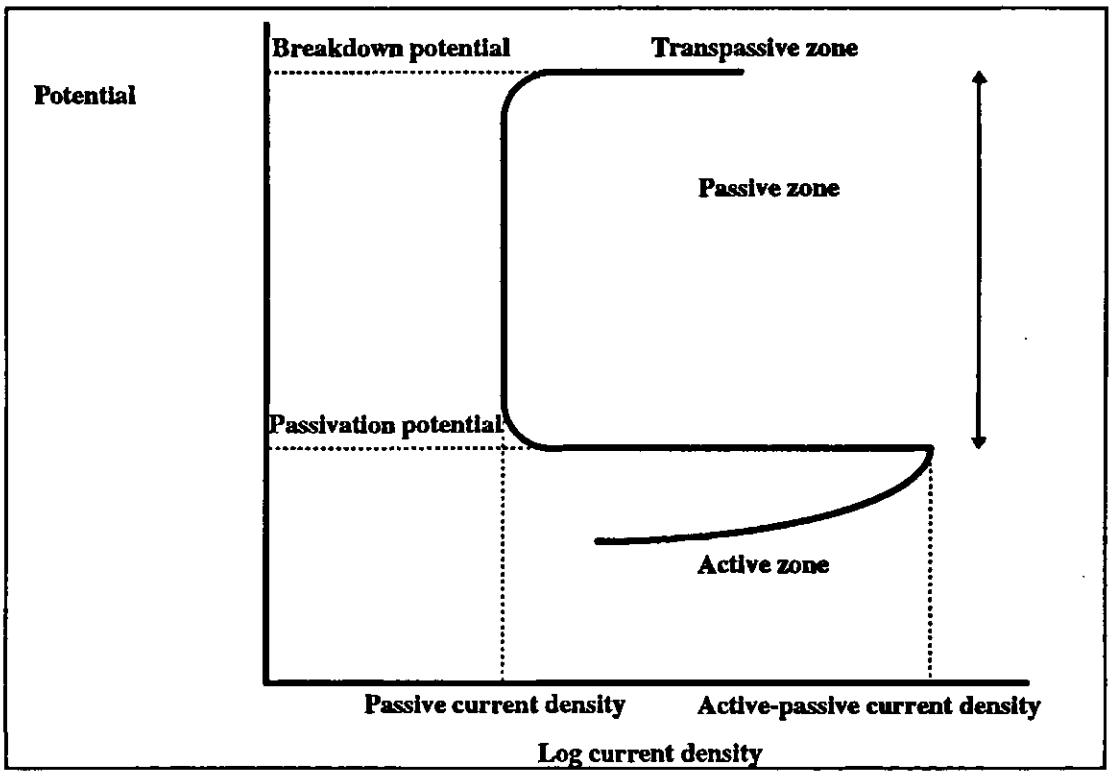

Fig. 2.1 Anodic polarization curve of a passive metal

The continuous oxide films can be semiconducting or insulating. Stainless steels are examples of the first group. The growth of the passive film in this group depends on the applied anodic potential to the metal surface, but the thickness of the film is limited by the oxygen evolution or any other anodic reaction (see also Fig. 2.4). In the second

group, passive film on aluminum has a low electronic conductivity, therefore, the oxygen evolution is hindered at high potentials and the passive film thickens.

Increasing the potential in the passive region thickens the passive film. This phenomenon is known as anodizing and is widely used to make a thick oxide film on aluminum by applying an external voltage[7]. The required driving force (potential) under corrosion conditions is provided by cathodic reactions. In aqueous systems, the cathodic reaction is oxygen reduction or hydrogen evolution, as in equations (2.1) and (2.2):

$$O_2 + 2H_2O + 4e^- \rightarrow 4OH^- \qquad ...2.1$$

$$2H^+ + 2e^- \rightarrow H_2 \qquad ...2.2$$

While the anodic reaction is metal dissolution, as in equation (2.3):

$$M \rightarrow M^{n+} + ne^- \qquad ...2.3$$

Other reduction reactions can be involved in the passivation process. For example, chromate in aqueous solutions not only accelerates cathodic reactions but also reinforces the passive film by depositing chromium oxide [Cr_2O_3] into it.

The effect of chromate oxidizing agents on the passivity of metals is shown in Fig. 2.2. Corrosion is an electrochemical phenomenon and the rates of anodic and cathodic reactions must be equal rates at the corrosion potential. Therefore, in the polarization curve, the intersection point of these two kinetic lines indicates the corrosion potential. This potential should be compared to the passive region.

Different cathodic reactions are shown in Fig. 2.2. The solid line is the anodic reaction. Open circuit potential is determined by the intersection between the anodic and

cathodic reaction rates. The oxidizing power of cathodic reactions increases from *(a)* to *(c)*. The cathodic reaction *(b)*, intersects the anodic reaction at three points, indicating that the metal may actively corrode or passivate, but the passivity may be unstable. The cathodic reaction *(c)*, provides a stable passivity, which can also be achieved by higher oxidizing agent concentrations.

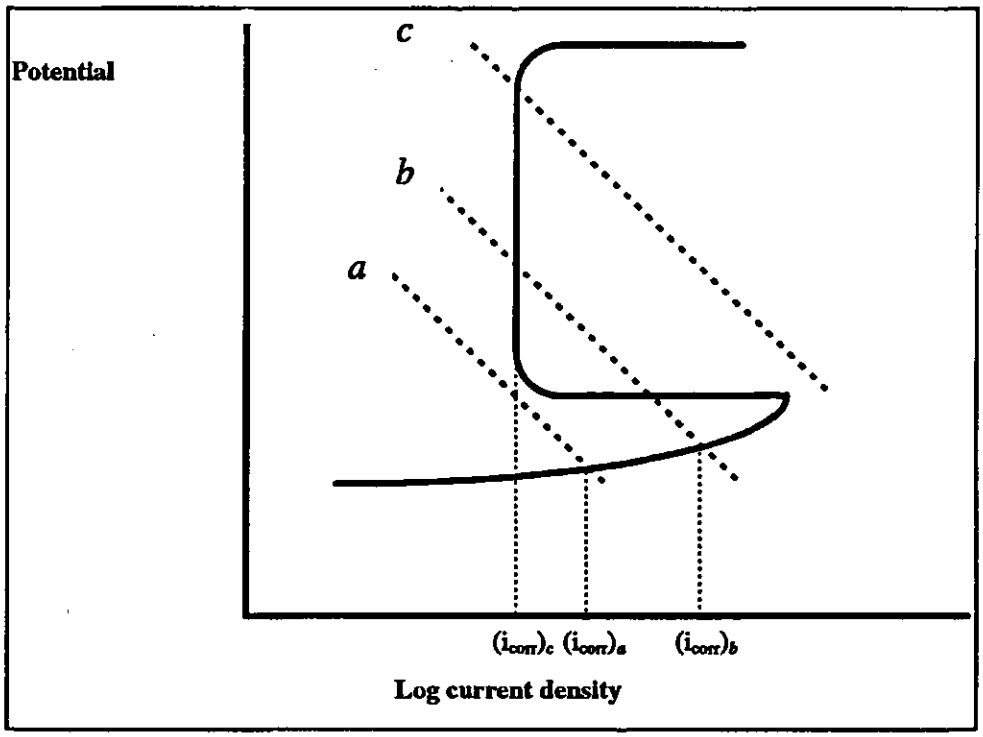

Fig. 2.2 Effect of oxidizing agent on the cathodic reaction
(a): active corrosion *(b)*: unstable passivation *(c)*: stable passivation

Other passivating agents do not passivate metals with increasing cathodic reaction and do not have an oxidizing action. Instead, they produce insoluble salts which act the same as a passive film. Phosphate inhibitors are among the agents in this group. The effect of these inhibitors on polarization curves is shown in Fig. 2.3. A decrease in the passive current density combined with a decrease in passivation potential is observed in

this case. The agent form a compound with the corroded ions present in the solution forming an insoluble salt deposit on the active site[7].

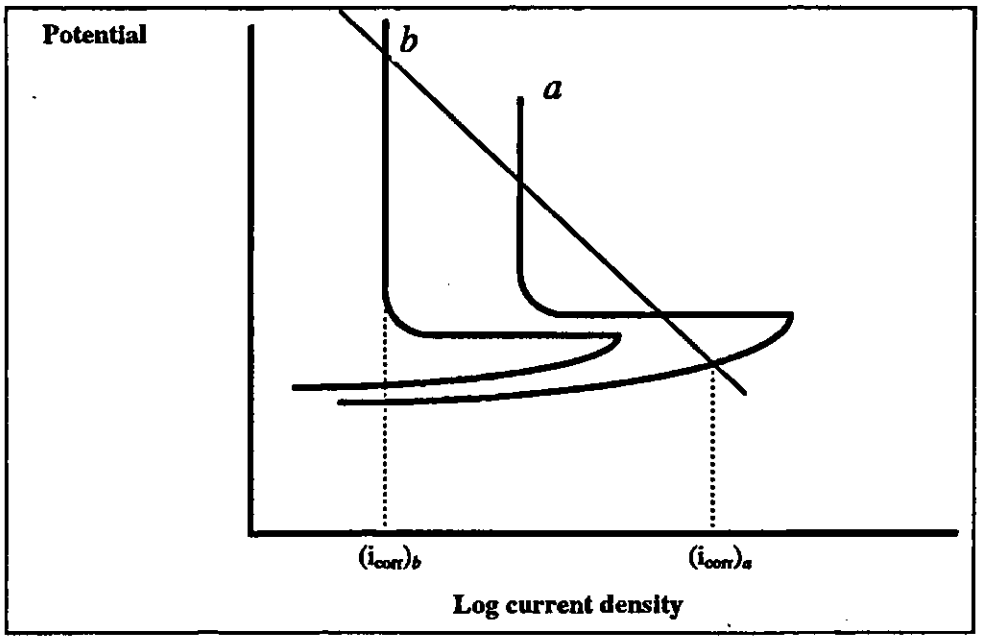

Fig. 2.3 Effect of insoluble salt on the passivity of a metal
(a): without the passivating agent
(b): with passivating agent and insoluble film formation

Formation of the passive film has been explained by various theories. According to the first theory, formation of the passive film (which separates the metal from its surrounding) is due to the thin oxide layer on the metal surface. The passive film has a low ionic conductivity and separates the metal ions movement from the metal and the solution, thus reducing the rate of the oxidation reaction. This theory is called oxide-film theory. The second theory proposes that the passive metal is covered by a chemisorbed film of oxygen or passivating ions. The film adsorbs the water molecules and slows the rate of anodic dissolution involving hydration of the metal ions. In other words, the exchange current density of the metal dissolution is decreased by the adsorbed species.

The film consists of a mono-layer on the metal surface and it cannot be considered as a diffusion barrier layer. The theory is called adsorption theory of passivity. Formation of a passive film on the transition metals is confirmed by this theory. Transition metals with uncoupled electrons in the *d* orbital of the atoms can make a strong bond with oxygen which also contains uncoupled electrons[8].

2.1.1. Polarization Curves

At potentials higher than those in the passivity range, the metal may exhibit a transpassive state and is corroded. The potential range for active, passive and transpassive regions is the characteristic of the metal/environment system, and the available cathodic reaction.

The presence of highly aggressive ions, such as chlorides, impacts the passivity of metals. Chlorides or other halides produce anodic reactions at potentials lower than the transpassive potentials for passive metals, by nucleation of pits on the metal surface (line *de* in Fig. 2.4). In the absence of halides, this passive film may be oxidized itself at point *f* and produce a soluble anion. This can alter the passive state of the metal. For example, chromium oxide [Cr_2O_3] can be oxidized to chromate [CrO_4^{2-}][7]. At higher potentials, the aqueous solution itself begins to be oxidized. The reaction is the oxidation of water to oxygen, as in equation (2.4):

$$2H_2O \rightarrow O_2 + 4H^+ + 4e^- \qquad ...2.4$$

The rise in current density with the increase in potential is shown by line *hi* which indicates the oxygen evolution rate. This reaction occurs only if the passive film is an

electron conductor, since the oxidation of water requires the passing of electrons from the water to the metal surface. When the passive film is a poor electron conductor, the electrons cannot pass through the oxide film. In this situation, the oxide film is thickened by the increase in potential and the metal remains passive. This process is widely used in industries for anodizing aluminum[7].

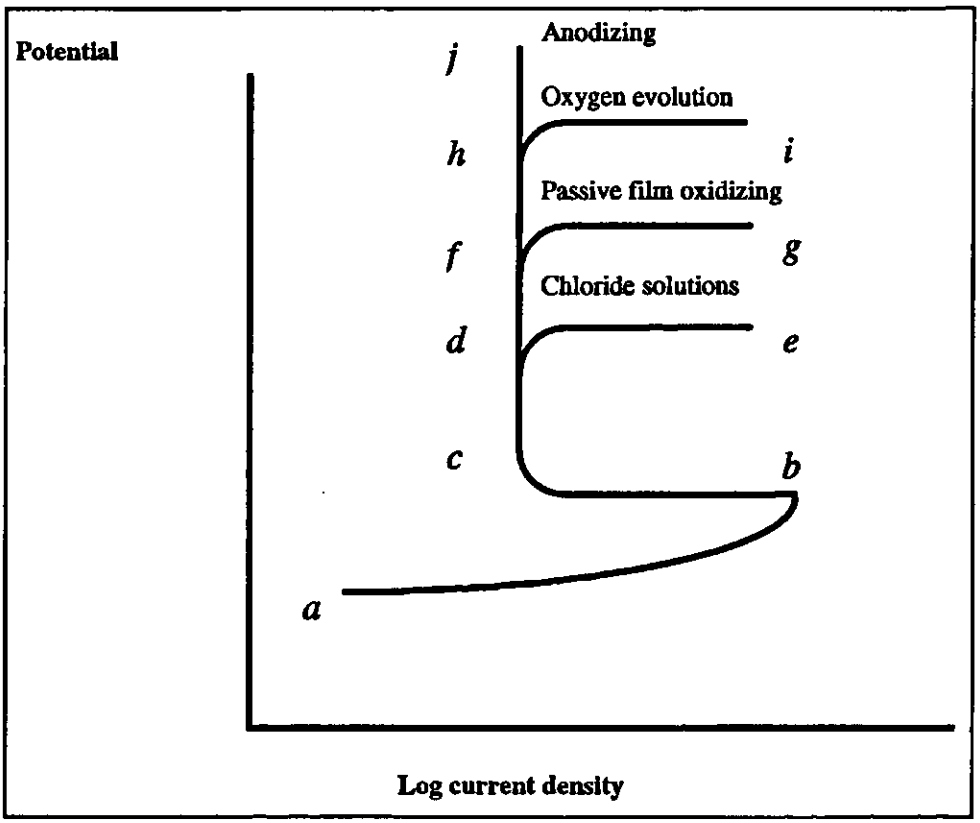

Fig. 2.4 Typical anodic polarization curve with different passivation behaviors

2.1.2. Passivity of Alloys

Passive alloys, such as stainless steels, owe their passivity to their chemistry. It has been shown that chromium-iron alloys with more than 12% chromium have a stable potential range (passive potential) in 4% sodium chloride solution[8]. The effect of

chromium on anodic polarization of iron is shown in Fig. 2.5. Chromium shifts the corrosion potential to more noble potentials. It also reduces the active-passive and passivation current density. Advanced surface analytical techniques, such as AES (Auger Electron Spectroscopy) and XPS (X-ray Photoelectron Spectroscopy) have shown enrichment of chromium in the passive film on stainless steels. The main reason for this enrichment is the dissolution of iron during passivation[9,10]. At higher passive potentials, the Cr^{3+} in the oxide film is oxidized to other Cr^{6+} and the passive state of the alloy gives way to the transpassive zone (line *fg* in Fig. 2.4). If the chromium concentration in the passive film is depleted locally and the chromium concentration drops below 12%, this region is no longer passive and is prone to localized attack. Such a depletion is very common in heat affected zones after welding of stainless steels. In this case, chromium carbide precipitates at the grain boundaries during welding and the enrichment of chromium at the grain boundaries causes depletion of chromium around the carbides. This phenomenon is known as sensitization[11].

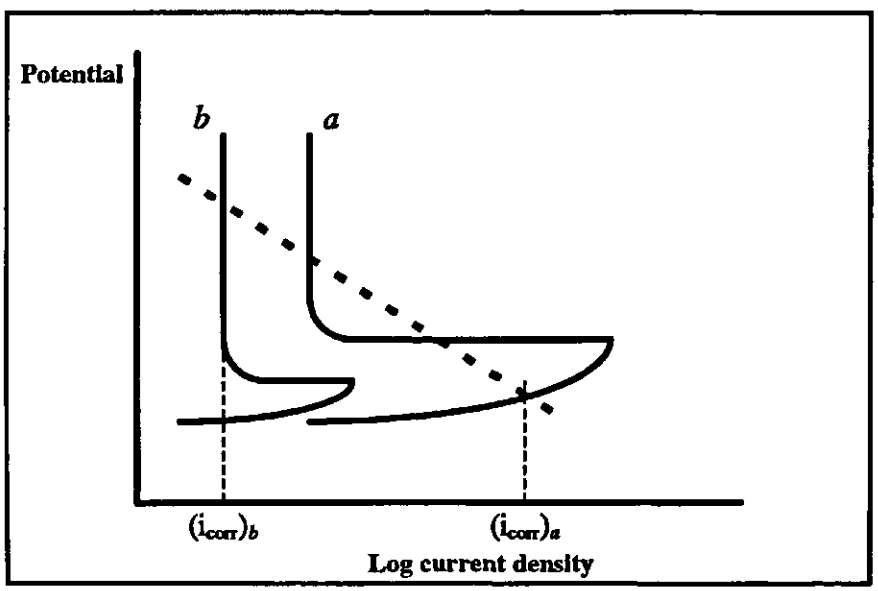

Fig 2.5 Effect of chromium on anodic polarization of iron
(a) Fe, *(b)* Fe + 12% Cr

2.1.3. Chemistry of Passive Film

Passive films are very thin and it is very difficult to determine their exact composition and structure. New advanced surface analysis techniques are both *ex-situ* (e.g. AES and XPS) and *in-situ* (e.g. ellipsometry and STM) tests, and developments of these methods are in progress[12,13].

While the composition of passive film depends on metal composition and environment, the film thickness is determined by the potential attained. It has been shown that the passive film consists of two layers, an outer hydroxide and an inner oxide layer[14,15]. The contact of passive film with aqueous solution may explain hydroxide formation on the outer layer[7]. In Fe-Cr-Ni-Mo stainless steels, the presence of iron, chromium and molybdenum in the oxide film has been proven. However, there is no agreement on the presence of nickel oxide in the passive film[7,10].

2.1.4. Passivity Breakdown

The passive film is a very thin layer and its stability depends on the composition of the solution and the electric field it carries[7]. This thin film may be removed due to impact of particles on the metal surface in slurry pipelines, or due to gas bubbling (cavitation) in pump casings. Lowering the extent of the cathodic reaction such as oxygen reduction (which supports the passivity) may also destroy the passive film at oxygen depleted areas resulting in crevice corrosion. Depletion of the passive element at a point in the alloy matrix can also cause localized corrosion. Segregation of other

elements can induce localized corrosion. Precipitation of sulfides at grain boundaries of stainless steels can retard oxide formation and provide sites for pit nucleation[6,16,17].

The most common reason for the breakdown of the passive film is the presence of an aggressive anion such as chloride in solution. Localized corrosion in the form of pitting usually takes place in passive regions at high potentials. The potential at which pits initiate in the chloride solutions is called the pitting or breakdown potential. It has been shown that small, unstable pits can initiate at lower potentials than the pitting potential in chloride solutions[18]. The small pits repassivate spontaneously and do not cause problems. Only those pits which initiate at potentials higher than the pitting potential are stable and propagate[7].

The presence of non-aggressive cations such as sulfate [$SO4^{2-}$] can reduce the ability of pits to propagate on the metal. This is attribute to the fact that its migration to the pits can postpone the achievement of the critical chloride concentration (60-70% saturation of metal chloride) inside the pits[15].

The breakdown of a passive film in a chloride solutions can be explained by the adsorption theory. This theory describes the formation of pits as a result of the competitive adsorption between chloride ions in the solution and the oxygen mono-layer on the surface. According to this theory, passive alloys have a greater affinity for oxygen than chloride ions. At high potentials, the adsorbed oxygen on the surface is displaced by chloride ions. Therefore, it can be expected that the initiation of pits requires an induction period. The decrease of induction period in the solutions with high chloride concentration can be described by this theory[7,8].

The failure of the passive film has also been described by considering the breakdown of the passive film as an equilibrium state between the metal salt of aggressive ion (i.e. aluminum chloride [$AlCl_3$]), and the passive film (i.e. aluminum oxide [Al_2O_3]). According to this theory, at potentials higher than the pitting potential, metal dissolution is accelerated due to the strong electric field across the passive film and a tendency to form metal salts instead of metal oxides[6].

2.2. Localized Corrosion

The mechanisms of pitting and crevice corrosion are described in the following sections. It is shown that these mechanisms are similar to one another. In this study, our premise is that localized corrosion refers to crevice and pitting corrosion.

2.2.1. Crevice Corrosion

Crevice corrosion is characterized by a geometrical configuration in which the anodic reaction takes place within the crevice, while the cathodic reaction occurs on the bold surfaces (the area surrounding a crevice). The formation of the crevice may be due to the contact of metal/metal, metal/nonmetal or the area under deposits on the surface. The cathodic reaction on the bold surface is usually oxygen reduction. The oxygen is supplied to the metal surface by convection and diffusion. The oxygen inside the crevice is supplied only by diffusion and the stagnant condition of the solution inside the crevice is a barrier to the supply of more oxygen to this area. Therefore, after a while all the oxygen within the crevice is depleted. This differential aeration on the bold surface and

within the crevice makes a differential aeration cell. The high ratio of cathode to anode areas intensifies the attack inside the crevice.

To describe the mechanism of crevice corrosion, first consider the crevice corrosion of a mild steel without a passive film in an aerated solution of sodium chloride (Fig. 2.6). Initially, the whole surface is in contact with the aerated solution. The similarity in solution inside and outside the crevice causes identical electrochemical reactions to occur on the bold surfaces and inside the crevice. This means that metal dissolution (anodic reaction) and oxygen reduction (cathodic reaction) have the same rate on the both surfaces. After a while the oxygen inside the crevice is consumed. The oxygen transfer rate to the bold surface is much greater than that inside the crevice and oxygen reduction ceases within the crevice. This creates two different areas; *(i)* the area around the crevice where oxygen reduction occurs, and *(ii)* the area inside the crevice where metal dissolution takes place.

$$Fe \rightarrow Fe^{2+} + 2e^{-} \qquad ...2.5$$

$$O_2 + 2H_2O + 4e^{-} \rightarrow 4OH^{-} \qquad ...2.1$$

$$Fe^{2+} + 2OH^{-} \rightarrow Fe(OH)_2(s) \qquad ...2.6$$

$$Fe^{2+} + 2Cl^{-} \rightarrow FeCl_2 \qquad ...2.7$$

$$FeCl_2 + 2H_2O \rightarrow Fe(OH)_2(s) + 2HCl \qquad ...2.8$$

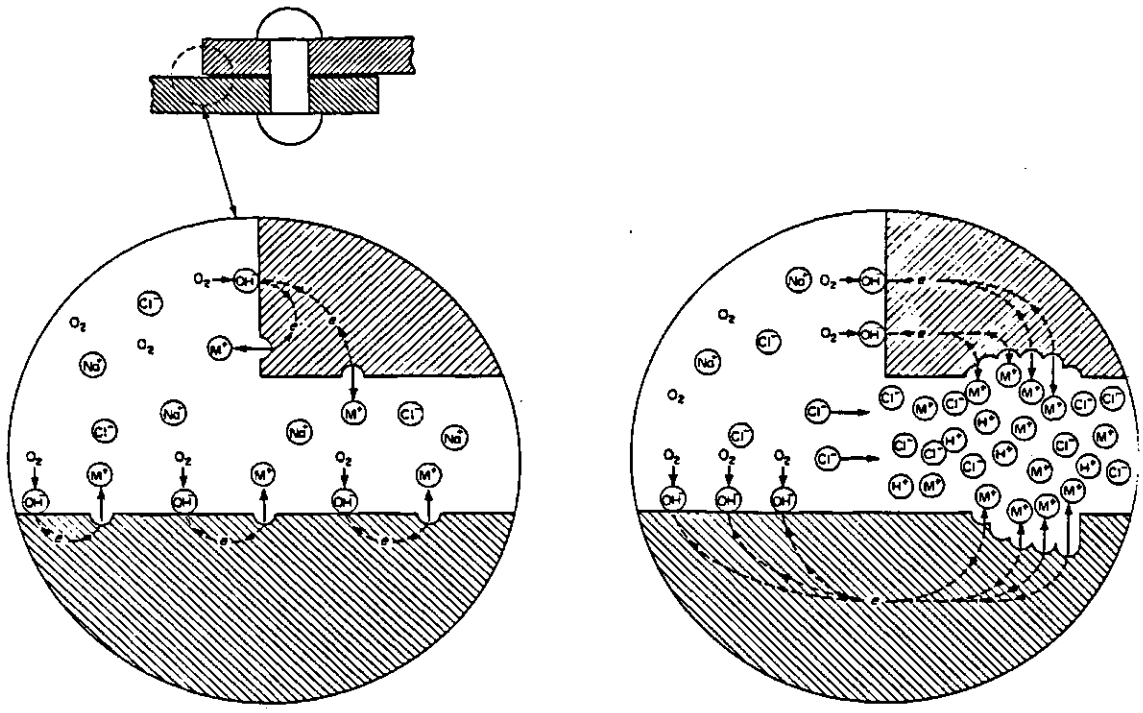

(a) *(b)*

Fig. 2.6 Crevice corrosion mechanism[11]
(a) Initiation *(b)* Propagation

To balance the positive charges resulting from metal dissolution inside the crevice, chloride and hydroxide anions migrate into the crevice. Despite the migration of the hydroxide ions towards the crevice, the pH value of the solution will not change significantly because of the low concentration of hydroxide ion in the solution. On the other hand, chloride ions and metal ions combine to produce metal chlorides. Hydrolysis of these metal chlorides yields ferrous hydroxide [$Fe(OH)_2$] which is not a protective film. Instead, an acid solution is formed within the crevice. High concentrations of chloride and hydrogen ions prevent the formation of a passive film and facilitate anodic

dissolution. The potential within the crevice becomes more negative and the rate of the anodic reaction become faster. This sequence of reactions gives rise to an autocatalytic process which intensifies localized attack.

In the case of passive metals like stainless steels, the rapid oxygen reduction reaction on bold surfaces increases the current density until its value exceeds the critical current density, and subsequently the metal surface becomes passive. Low current density due to passivation on the large bold surfaces balances with the high current density of the small anodic area of metal in the active zone inside the pit. Increasing hydrogen ions inside the pit shift to the passivation potential to a more noble potential and the active zone extends. In such a situation the dominant cations inside the pit are both ferrous [Fe^{2+}] and chromium [Cr^{3+}] ions[7].

2.2.2. Pitting Corrosion

Pitting corrosion can be defined as an intensive localized attack on the metal surface yielding small pits that penetrate into the metal and lead to perforation. Pitting corrosion may be divided into two steps, pit initiation and pit propagation. Pit initiation is the rupturing of the passive film without the film reforming. The propagation step is a rapid metal dissolution process in the absence of the passive film. While pit initiation depends on the characteristics of the passive film, pit propagation depends on the metal composition and structure[7].

Any discontinuity in the passive film which is caused by mechanical, geometrical or compositional non-homogenities can be the initiation site for pits on the metal surface.

Therefore, pitting is less likely on smooth, polished surfaces than on rough or ground surfaces. In other words, the more homogeneous the metal surface is, the better is the resistance of passive film to localized corrosion.

The potential of the metal during pitting is in the passive region so that the major part of the surface remains passive. On the other hand, the redox potential of the solution has to be higher than a critical value for the pits to initiate. This redox potential can be affected by oxygen reduction on the metal surface around the pits. This redox potential is higher for some oxidizing metal cations like ferric chloride [$FeCl_3$] and cupric chloride [$CuCl_2$], and that is why ferric chloride is widely used in testing alloys for their resistance to pitting.

Almost all the factors which are considered for crevice corrosion act the same as in pitting corrosion. Some of these factors are anode/cathode area ratio, autocatalytic reaction during the propagation step, and differential aeration between pits and the metal surface.

The most important parameter in the pitting of passive alloys is the breakdown potential. This is the most negative potential to cause initiation of pits on the metal surface along with distortion of the passive film. The breakdown potential for a given alloy depends on the nature of the solution. It also depends on many other parameters such as the surface condition, and the duration of the test. The breakdown potential is not a precise value, but provides a good comparison for the resistance of different metals to pitting corrosion in identical conditions.

2.3. pH Changes During Localized Corrosion

It has been shown that in an aerated solution of sodium chloride, localized corrosion may begin. The cathodic reactions are oxygen reduction and hydrogen evolution.

$$O_2 + 2H_2O + 4e^- \rightarrow 4OH^- \quad ...2.1$$

$$2H^+ + 2e^- \rightarrow H_2 \quad ...2.2$$

Both reactions result in an increase in the pH value in the cathodic area around the pit or crevice. On the other hand, the hydrolysis of metal ions within the pit or crevice increases the H^+ concentration which decreases the pH value.

$$M^{2+} + 2H_2O \rightarrow M(OH)_2 + 2H^+ \quad ...2.9$$

Consider iron hydrolysis inside the pits during the pitting corrosion of iron.

$$Fe^{3+} + 3H_2O \rightarrow Fe(OH)_3\,(s) + 3H^+ \quad ...2.10$$

The equilibrium constant for the above reaction is:

$$K = [H^+]^3 / [Fe^{3+}] \quad ...2.11$$

$$\log K = 3 \log [H^+] - \log [Fe^{3+}] \quad ...2.12$$

$$pH = -\log [H^+] \quad ...2.13$$

$$pH = 1/3 (-\log K - \log [Fe^{3+}]) \quad ...2.14$$

The values in the brackets indicate the activity of the species. The K value can be found in thermodynamic tables. The pH values, based on the hydrolysis reaction of most common stainless steel elements, are given in Table 2.1[19].

Table 2.1 Hydrolysis reactions and equilibrium pHs for metal ions in localized corrosion of stainless steels[19]

Hydrolysis Reaction	Equilibrium pH
$Fe^{2+} + 2H_2O \rightarrow Fe(OH)_2 + 2H^+$	pH = 6.64 - 1/2 log [Fe^{2+}]
$Cr^{3+} + 3H_2O \rightarrow Cr(OH)_3 + 3H^+$	pH = 1.53 - 1/3 log [Cr^{3+}]
$Ni^{2+} + 2H_2O \rightarrow Ni(OH)_2 + 2H^+$	pH = 6.1 - 1/2 log [Ni^{2+}]
$Mo^{3+} + 2H_2O \rightarrow MoO_2 + 4H^+ + e^-$	pH = (0.311-0.059 log [Mo^{3+}] -E°)/0.236
$Mn^{2+} + 2H_2O \rightarrow Mn(OH)_2 + 2H^+$	pH = 7.66 - 1/2 log [Mn^{2+}]

E° = -0.2 V (vs. Standard Calomel Electrode).

It is shown that the pH value decrease in the anodic area for molybdenum is greater than that for chromium, and the pH value decrease is for chromium is greater than that for iron. This conclusion cannot be made in the case of Fe-Cr-Mo stainless steels because of the presence of cations and the effect of these cations on the thermodynamic equilibrium between species. Therefore, the pH value is lower than the expected value. The pH values and chloride concentrations for three types of austenitic stainless steels in 0.5N sodium chloride at 70°C by creating an artificial pit are shown in Table 2.2[20]. The pH values for Cr, Fe, Ni and Mo inside the artificial pits are shown in Table 2.3[20]. The results show that the real pHs for pure metals are lower than the pH values estimated by the equilibrium constants in Table 2.1. A disagreement is observed between the results of Table 2.1 and Table 2.3 if it is assumed that the concentration of the metal ion inside the pit is 10^{-6} M. This disagreement is related to the high concentration of a chloride and the formation of hydroxy-chloro complex. The results of pH value measurements for austenitic stainless steels reveal the effect of Cr and Mo in lowering the pH inside the pit. As mentioned before, low pH values move the

passivation potential to higher values. This shifts the potential in the pit to the active region.

The nature of pitting and crevice corrosion makes the situation for measuring the pH value and chloride concentration in pits or crevices rather difficult. No instrument can measure the pH inside a deep crevice within a 1 micron gap size. However, computer programs can simulate electrochemical reactions during localized corrosion and can be used to estimate the pH and the chloride concentration profiles inside the crevice. The crevice corrosion simulation for 304 and 316 austenitic stainless steels is consistent with the results shown in Table 2.2[21].

Table 2.2 pH, chloride concentration and potential for artificial pits in stainless steel[20]

	304L*	316L*	Fe-18Cr-16Ni-5Mo
pH	0.6 to 0.8	0.06 to 0.17	-0.13 to -0.08
Cl^- conc. (N)	3.87	6.47	6.20
Steady state potential, V (vs. S.C.E)	-0.25 to -0.021	-0.02 to -0.22	-0.18 to -0.20

* See section 3.1 for the chemical composition

Table 2.3 pH of selected metals in the artificial pits*[20]

Metal	Fe	Cr	Ni	Mo
pH	4.71	0.09	2.93	0.020

* The data for 0.5 NaCl solution at 70°C

2.4. Stainless Steel

Stainless steels are iron-based alloys containing more than 11% chromium. The chromium gives the steel its ability to form a protective or passive film that increases corrosion resistance. The passive film consists of chromium oxide and hydroxide[7]. Other

elements such as iron, nickel and molybdenum have also been detected in the passive film[7,10]. When stainless steel is exposed to an oxidizing environment such as air or aerated water, its corrosion resistance approaches that of a noble metal. However, when exposed to a harsher environment that destroys the passive film, its resistance becomes less than that of iron. The corrosion behavior of stainless steels depends on the type and percentage of alloying elements. Varying amounts of nickel, copper, molybdenum, nitrogen, vanadium, titanium, tungsten, silicon, manganese and niobium are used for different purposes in stainless steels. These elements affect both the mechanical and physical properties as well as the corrosion resistance of stainless steels. Improving the corrosion resistance of stainless steels by alloying may adversely influence other desirable mechanical properties.

Stainless steels have conventionally been classified into several categories (e.g. martensitic, ferritic, austenitic, precipitation-hardening and duplex)[1,16,22,23]. A simple, but approximate way to categorize stainless steels is relating metallurgical structure with composition elements. The most popular diagram which shows the effect of alloying on structure is the Schaeffler diagram[7,16,22,23] (Fig. 2.7). This particular diagram indicates the structure obtained for stainless steel after being cooled rapidly from a solution heat treatment temperature of 1050°C to room temperature[7,16].

The alloying elements in stainless steels are usually regarded either as ferrite or austenite stabilizers. Nickel is considered as an element for austenite stabilizing, and chromium for ferrite stabilizing. On this basis, nickel and chromium have been defined and used as the two axes in the Schaeffler diagram. Different coefficients have been

considered for each alloying element to determine nickel and chromium equivalents[10,17,24]. In the Schaeffler diagram (Fig. 2.7) the following equations have been used in calculating the nickel and chromium equivalents.

$$\%Ni\ equivalent = \%Ni + \%Co + 30\,(\%C) + 25\,(\%N) + 0.5\,(\%Mn) + 0.3\,(\%Cu) \quad ...2.15$$

$$\%Cr\ equivalent = \%Cr + 2\,(\%Si) + 1.5\,(\%Mo) + 5\,(\%V) + 5.5\,(\%Al) + 1.75\,(\%Cb) + 1.5\,(\%Ti) + 0.75\,(\%W) \quad ...2.16$$

Based on the Schaeffler diagram, it can be seen that there are four major areas according to the structures: martensite, ferrite, austenite and ferrite plus austenite. These four areas provide a convenient basis for classification of stainless steels.

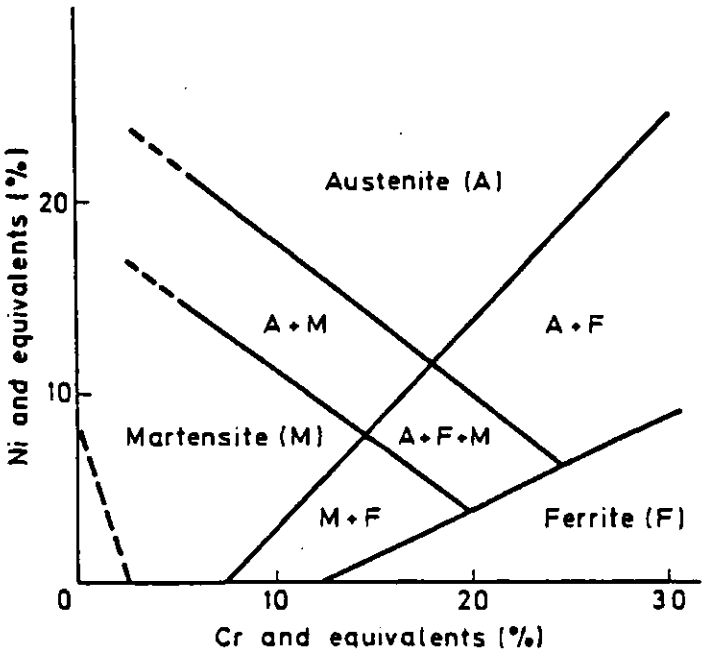

Fig. 2.7 Structure of steels as determined by composition; (A) Austenite, (M) Martensite and (F) Ferrite[7]

2.4.1. Martensitic Stainless Steels

A plain carbon steel at high temperature has a face centered cubic structure (austenite). At high carbon content, the steel can be transformed into martensite by rapid cooling to room temperature instead of ferrite. During this transformation the structure of the steel changes from face-centered cubic to a distorted body-centered cubic, called body-centered tetragonal. The resulting steel is hard and consequently more brittle. The hardness depends on the amount of distortion in the lattice which is related to the carbon content in the metal . The presence of chromium decreases the minimum cooling rate required for this transformation making it easier to obtain martensite in steels containing lower carbon contents. However, a very high chromium content in steels causes the final structure to be ferritic instead of martensitic. Addition of up to 3 wt% Ni can prevent ferrite from forming[22]. Fig. 2.7 shows the limitation of chromium in obtaining the martensitic phase. Most martensitic stainless steels contain 11.5% to 13.5% chromium[7]. Table 2.4 shows the chemical composition and mechanical properties of some commercial martensitic stainless steels. To obtain suitable mechanical properties for engineering applications, the martensitic steels must be tempered (a process in which martensite partially dissociates into ferrite-plus-carbide[25]). The final mechanical properties depend on the tempering time and temperature. Alloying the martensitic stainless steel with a carbide forming element like molybdenum, stabilizes the precipitation of carbides, and extends the tempering to have desirable properties at higher temperatures (e.g. toughness, weldability). It also prevents chromium carbide

precipitation which decreases corrosion resistance in the vicinity of precipitation areas due to the depletion of chromium.

Table 2.4 Typical chemical composition and mechanical properties of martensitic stainless steels*♦[26]

AISI type	%C	%Cr	%Ni	% Other	Yield strength kpi	Tensile strength kpi	Elongation %	Hardness HB
410	0.15	11.5-13	-	-	35	70	30	150
416	0.15	12-14	-	0.15S♣	40	75	30	155
420	0.15	12-14	-	-	50	95	20	195
431	0.2	15-17	1.25-2	-	95	125	20	260

* Single values are maximum values unless otherwise noted
♦ Typical room-temperature properties of annealed plates
♣ Minimum

The martensitic stainless steels are usually selected for special applications which, in addition to having moderate resistance in corrosive media, need special mechanical properties. For example, this material would be useful for a mine ore conveyor where high abrasion resistance associated with moderate corrosion resistance is needed.

2.4.2. Ferritic Stainless Steels

It can be seen in the Schaeffler diagram (Fig. 2.7) that at lower nickel equivalent areas, a ferritic structure is formed by increasing the chromium content. The ferritic alloys have a body-centered cubic structure. They are particularly noted for their stress corrosion cracking resistance. Increasing the chromium content in ferrite structure improves corrosion resistance but decreases some other properties like weldability, strength and hardness.

Super-ferritic steels with low amounts of interstitial elements (carbon and nitrogen) of less than 0.02% each contain molybdenum, which increases the corrosion resistance[22]. These steels are widely used in chemical industries, because of their workability, and good corrosion resistance. Table 2.5 shows the chemical composition and mechanical properties of some ferritic stainless steel alloys. A description of ferritic stainless steels would be incomplete without mentioning their disadvantages, which are: sigma-phase embrittlement, intergranular corrosion, and ductile to brittle transition. Detailed descriptions of these problems are available in the literature[16,23].

Table 2.5 Typical chemical composition and mechanical properties of ferritic stainless steels*♦[26]

AISI type	%C	%Cr	%Mn	Si%	%Other	Yield strength kpi	Tensile strength kpi	Elongation %	Hardness HB
405	0.08	11.5-14	1.0	1.0	P, S, Al	40	65	30	150
409	0.08	10.5-12	1.0	1.0	P, S, Ti	35	65	25	137
430	0.12	16-18	1.0	1.0	P, S	40	75	30	160
442	0.2	18-23	1.0	1.0	P, S	45	80	20	185

* Single values are maximum values unless otherwise noted

♦ Typical room-temperature properties of annealed plates

2.4.3. Austenitic Stainless Steels

The high temperature (910-1400°C) form of iron is known as austenite and it can be retained at room temperature by appropriate alloying. Such a structure has the advantages of high ductility and toughness. The most common austenitic phase stabilizer is nickel. The traditional and familiar austenitic stainless steel has a composition which contains sufficient chromium to offer corrosion resistance, together with nickel to ensure

an austenite form at room temperature and below. In fact, many elements to differing degrees, depress the temperature range for the transition of austenite to martensite. Alloying also has a significant effect on the corrosion resistance of this group. Addition of molybdenum and nitrogen increases the localized corrosion resistance[7,22]. The austenitic stainless steels are particularly susceptible to stress corrosion cracking in chloride environments at high temperatures. This form of corrosion can be minimized by increasing the percentage of nickel in the alloys. Decreasing the carbon content can prevent intergranular corrosion. Titanium or niobium can also stabilize heat affected zones and reduce the risk of intergranular cracking.

Sulfur is present in austenitic stainless steels as an impurity. The sulfur is usually available in amounts larger than the saturation amount in the solid solution. Therefore, the excess sulfur precipitates as metal sulfide, (predominantly manganese sulfide at the grain boundaries. This inclusion in addition to reducing toughness, is a site for initiation of pits on the metal surface[16].

Austenitic stainless steels have been widely used in all industries, due to their good mechanical properties and corrosion resistance. Table 2.6 shows some commercial alloys in this group.

Table 2.6 Typical chemical composition and mechanical properties austenitic stainless steels*♦[26]

AISI type	%C	%Cr	%Ni	%Mo	%Other	Yield strength kpi	Tensile strength kpi	Elongation %	Hardness HB
304	0.08	18-20	8-10	-	Mn, Si	35	82	60	149
316	0.08	16-18	10-14	2-3	Si, Mn	36	82	55	149
316L	0.03	16-18	10-14	2-3	Si, Mn	34	81	55	146
347	0.08	17-19	9-13	-	Si,Cb,Ta	35	90	50	160

* Single values are maximum values unless otherwise noted

♦ Typical room-temperature properties of annealed plates

2.4.4. Duplex Stainless Steels

Duplex stainless steels are two-phase structures composed of austenitic and ferrite phases of approximately equivalent volumes. They have good resistance to stress corrosion cracking, coupled with better resistance to localized corrosion than the equivalent chromium and molybdenum content austenitic stainless steels. They also have better mechanical properties[27].

Generally, the effects of alloying on localized corrosion of duplex stainless steels are the same as those for austenitic stainless steels. The presence of two phases creates some difficulties such as galvanic effect between the two-phases, preferential attack in one phase during localized attack, and weld decay[27]. Balancing the alloying elements in each phase can prevent the above problems. High nitrogen content in the austenite phase balances the corrosion resistance of the two phases, while low carbon content in both phases decreases intergranular corrosion after welding[27].

The chemical compositions and mechanical properties of some duplex stainless steels are shown in Table 2.7. Duplex stainless steels have been successfully used in the construction of pulp & paper, oil & gas, food and other chemical processing equipment[28].

Table 2.7 Typical chemical composition and mechanical properties of duplex stainless steels[23]

AISI type	%C	%Cr	%Ni	%Mo	%Other	Yield strength kpi	Tensile strength kpi	Elongation %	Ferrite %
U50*	0.03♣	20-22	5.5-9	2-3	Mn,Si,N, P, S, Cu	46-64	86-116	20-25	30-50
3RE60♦	0.03♣	18.5	4.7	2.7	Mn,Si,N, P, S	65	102-131	30	50
2205♦	0.03	22	5.5	3	Mn,Si,N, P, S	59-65	99-131	25	45

* Trade name of Creusot-Loire
♦ Trade name of Sandvik AB
♣ Maximum

2.4.5. Precipitation-Hardening Stainless Steels

Precipitation-hardening stainless steels are iron-chromium-nickel alloys characterized by their high strengths obtained by precipitation hardening a martensitic or austenitic matrix with one or more of the following elements: copper, aluminum, titanium, niobium, and molybdenum. The precipitation-hardening stainless steels offer an alternative means to obtain high strength, relatively good ductility, excellent corrosion resistance, and ease of fabrication. Most of the applications for precipitation-hardening stainless steels are in the aerospace and other high-technology industries. The precipitation-hardening stainless steels are subdivided into martensitic, semi-austenitic, and austenitic types [16,23,29,30].

The first step in the heat treatment of all three types is solution annealing at temperatures in the single phase austenite region. The following steps are determined by the stability of the austenite on cooling from this region[16]. The mechanical properties of precipitation-hardening stainless steels are highly affected by heat treatments. The chemical composition of some alloys in this group are shown in Table 2.8[29].

Table 2.8 Typical chemical composition of precipitation-hardening stainless steels[29]

Alloy	Type	%C	%Mn	%Si	%Cr	%Ni	%Other
15-5PH	Martensitic	0.07	1.00	1.00	14-15.5	3.5-5.5	2.5-4.5 Cu
17-4PH	Martensitic	0.07	1.00	1.00	15-17.5	3-5	3-5 Cu
17-7PH	Semi-austenitic	0.09	1.00	1.00	16-18	6.5-7.5	0.75-1.5 Al
A-286	Austenitic	0.08	2.00	1.00	13.5-16	24-27	1.9-2.35 Ti 1-1.5 Mo

2.5. Effects of Cations

Electrolytes in dilute solutions are believed to be present entirely as ions. The degree of solubility and ionization of salts is larger in liquids, such as water, with a high dielectric constant. These liquids, referred to as polar solutions, contain molecules in which the geometrical contents of positive and negative charges do not coincide. Thus, the solvent molecules, attracted by the electrostatic charges, surround the solute ion and insulate it from other ions.

The mechanism of localized corrosion shows that the chloride ion is the major parameter in the autocatalytic reaction of this type of corrosion. At higher temperatures the corrosion rate could be accelerated due to the higher conductivity of the chloride ion. However, even at identical temperatures, the conductivity of chloride ions for two

different cation chlorides are not the same[31] (Fig. 2.8). This phenomena may be related to the effects of cations. For example, consider sodium chloride and potassium chloride solutions. Both sodium and potassium are in the first group of the periodic table of the elements with atomic numbers of 11 and 19, respectively. It means that in aqueous solutions, Na^+ has one atomic layer less than K^+, while both of them have the same positive charge. These positive charges attract the negative side of water molecules. The density of the positive charges around Na^+ is more than K^+ because of its ionic radii. Therefore it is expected that the number of water molecules (hydration number) which surrounds the Na^+ ions is more than for K^+. It means that in an electrolyte solution with the same normality of NaCl and KCl, Na^+ moves slower than K^+ and thus the conductivity of Na^+ is less than K^+.

In electrochemical cells, the charged particles move in opposite directions and the chloride ions in KCl move faster than those in NaCl due to the smaller cation atmosphere and less interference with other charged particles.

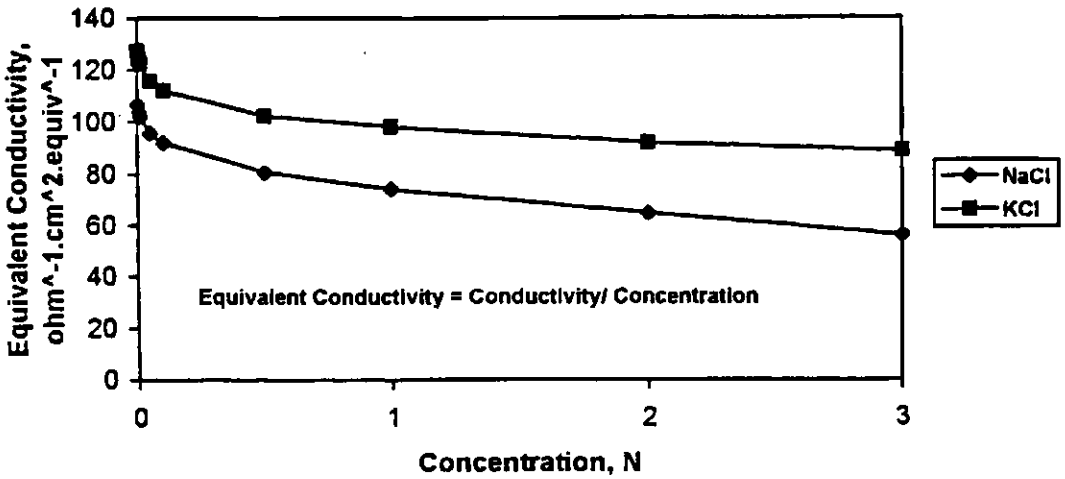

Fig. 2.8 Equivalent conductivity of NaCl & KCl at 18°C[31]

2.6. *Effects of Chemical Composition*

2.6.1. Chromium

Stainless steels derive their passivity from alloying with chromium. Alloying of iron with chromium moves the breakdown potential of stainless steels to more noble potentials in chloride solutions[17]. It has been reported that the passive film on iron-chromium alloys consists of two layers. The inner layer is mostly oxide and the outer layer comprised of iron and chromium hydroxide[10]. The iron is dissolved selectively during active corrosion; therefore, the chromium concentration is increased on the inner oxide film, and the metal becomes passive. The passive films are thickened by increasing the potential.

The enrichment of chromium in the passive film reduces the chromium concentration in the metallic phase under the passive film until this value becomes much lower than the chromium concentration in the bulk of the metal. The chromium depletion in this area makes the metal more susceptible to localized attack at potentials higher than the breakdown potential[10].

The effect of chromium content on breakdown potential for iron chromium alloys in a 0.1N deaerated solution of sodium chloride at 25°C is shown in Fig. 2.9[16].

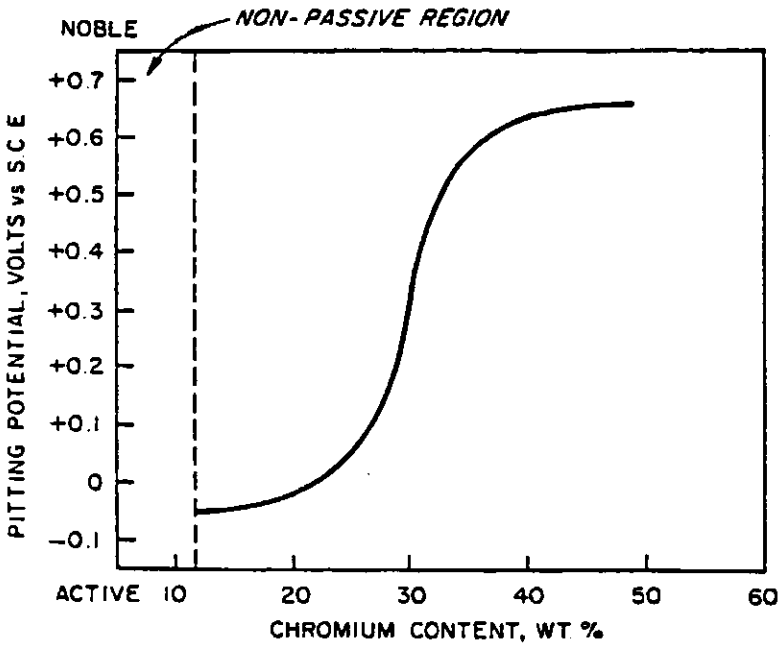

Fig. 2.9 Effect of chromium on pitting potential of Fe-Cr alloys in 0.1 N NaCl at 25°C[16]

2.6.2. Nickel

Investigating the effect of nickel on the corrosion behavior of stainless steels reveals two different ideas and mixed interpretations. Alloying with nickel is well known for increasing the strength and also increasing the resistance of austenitic stainless steels to stress corrosion cracking. It has been reported by Sedriks that increasing the nickel content in Fe-15% Cr stainless steels shifts the breakdown potential to more positive values[16]. It was reported that nickel affects the anodic polarization curve by extending the passivation potential and decreasing both passive potential and current density. Despite this idea, no positive effect on localized corrosion resistance indices due to the presence of nickel has been presented[17]. Nickel does not participate in passive films due to its higher required oxidation energy compared to the oxidation of chromium, iron and molybdenum[10]. Nickel is enriched on the metal/passive film interface where the

chromium and iron are depleted, due to the selective oxidation in this area. Fig. 2.10 shows the effect of nickel content on the pitting potential of Fe-15 %Cr alloys in a deaerated solution of 0.1 N sodium chloride at 25°C[16].

A few other investigations imply that there is a negative effect of nickel on localized corrosion resistance of stainless steels as well as on the Localized Corrosion Resistance Index (see section 2.7)[32,33].

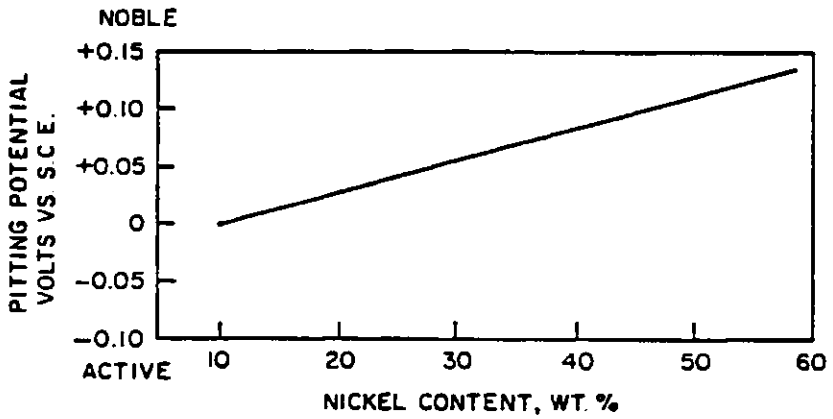

Fig. 2.10 Effect of nickel on pitting potential of Fe-15 %Cr alloys in 0.1 N NaCl at 25°C[16]

2.6.3. Molybdenum

Molybdenum is present in the passive film of stainless steels in the form of oxides and hydroxides. However, the molybdenum concentration in the passive film is much less than chromium because of the lower concentration of molybdenum in stainless steels. While molybdenum concentration in the passive film is less than the metal matrix, its concentration in the metal/passive film interface is much higher than that in the metal matrix[10]. In the presence of nitrogen, segregation of molybdenum nitride blocks the active site on the interfacial area. In austenitic stainless steels, the mixed nitride phase of

Ni_2Mo_3N forms a stable compound with a strong intermetallic bond at the metal/passive film interface[34]. The effect of molybdenum content on the pitting potential of Fe-15 %Cr-13 %Ni alloys in deaerated solution of 0.1 N sodium chloride is shown in Fig. 2.11[16].

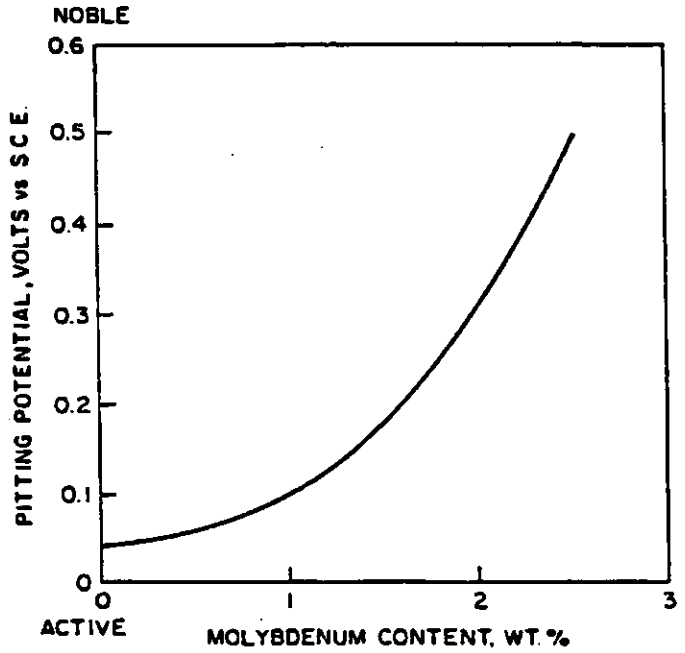

Fig. 2.11 Effect of molybdenum on pitting potential of Fe-15 %Cr-13 %Ni alloys in 0.1 N NaCl at 25°C[16]

In molybdenum-nickel stainless steels which contain nitrogen, the intermetallic phase of Ni_2Mo_3N segregates under the passive film and blocks the active site during active dissolution and passivation. Both molybdenum and nickel nitrides can form and precipitate. However, molybdenum nitride is more stable than nickel nitride. As mentioned before, selective oxidation of chromium, iron, and molybdenum over nickel enriches nickel on the metal/passive film interface. Nickel produces an intermetallic phase both with chromium and molybdenum in the presence of nitrogen. However, it has

been proposed that the intermetallic bond between molybdenum and nickel is much stronger than that between chromium and nickel[10,34].

Ives *et al* showed that the presence of molybdenum in stainless steels does not have a significant effect on the initiation of pits but segregation of molybdenum provides a barrier inside the pits and slows down the propagation of the pits. It was proposed that the composition of this segregation layer is mainly $NiMoO_4$ mixed oxide[35].

2.6.4. Nitrogen

Nitrogen in molybdenum-bearing stainless steels segregates as nitride and blocks the active dissolution of stainless steels in the absence of a passive film. Molybdenum-nitrogen synergism increases the austenitic stainless steels resistance dramatically due to the formation of an intermetallic phase of Ni_2Mo_3N during active dissolution and passivation. Even in the absence of nitrogen and molybdenum, the reaction between chromium nitride and water can reduce the acid concentration in the attacked location[34]:

$$2CrN + 3H_2O \rightarrow Cr_2O_3 + 2NH_3 \qquad ...2.17$$

It has been reported that the addition of less than 0.25 wt% nitrogen to Fe-Cr-Ni-Mo stainless steels results in lower passive and active-to-passive current densities. It also extends the passive potential region in chloride solutions[36]. Nitrogen can be present in the austenite phase more than in the ferrite phase because of the more interstitial opportunities in the face-centered cubic structure than in the body-centered cubic structure. It should be mentioned that the high level of nitrogen in stainless steels needs relatively high concentrations of manganese to keep the nitrogen in solid solution[17].

However, high levels of manganese increases MnS precipitation at grain boundaries which are the most susceptible places for initiation of pits. During localized corrosion, nitrogen (which is present in nitride phase) segregates inside the pits. This leads to the formation of ammonium ions which increases the pH and slows down the pit growth kinetics.

$$N + 4H^{+} + 3e^{-} \rightarrow NH_4^{+} \qquad ...2.18$$

2.7. Localized Corrosion Resistance Index (LCRI)

The useful corrosion resistance of a stainless steel is due almost entirely to the fact that it exhibits passivity in a wide range of environments. In solutions containing chlorides, however stainless steels are prone to localized corrosion. The resistance of an alloy to this type of corrosion depends mostly on its chemical composition. The beneficial effects of chromium, molybdenum and nitrogen, as well as the effects of nickel were discussed in previous sections. Equations for the localized corrosion resistance of stainless steels which have been proposed relate the resistance in chloride containing solutions to the chemical composition[7,37,38,39]. The most widely used equation in this regard is[7]:

$$LCRI_{wt.\%} = \%\ Cr + 3.3\ (\%\ Mo) + 16\ (\%N) \qquad ...2.19$$

Another expression for relating the localized corrosion resistance to stainless steel alloying is the Pitting Resistance Equivalent (PRE). Both LCRI and PRE have been developed by the multiple linear regression technique. The regressions have been performed based on the breakdown potential or the Critical Pitting Temperature (CPT).

Critical pitting temperature is the threshold temperature at which the breakdown potential of a given alloy drops sharply[37] (Fig. 2.12). The CPT has been related to PRE by the following linear equation:

$$CPT = A + B\,(PRE) \qquad ...2.20$$

Similar equations can be proposed for predicting the relation between Critical Crevice Temperature (CCT) and Crevice Resistance Equivalent (CRE)[12,6].

$$CCT = A' + B'\,(CRE) \qquad ...2.21$$

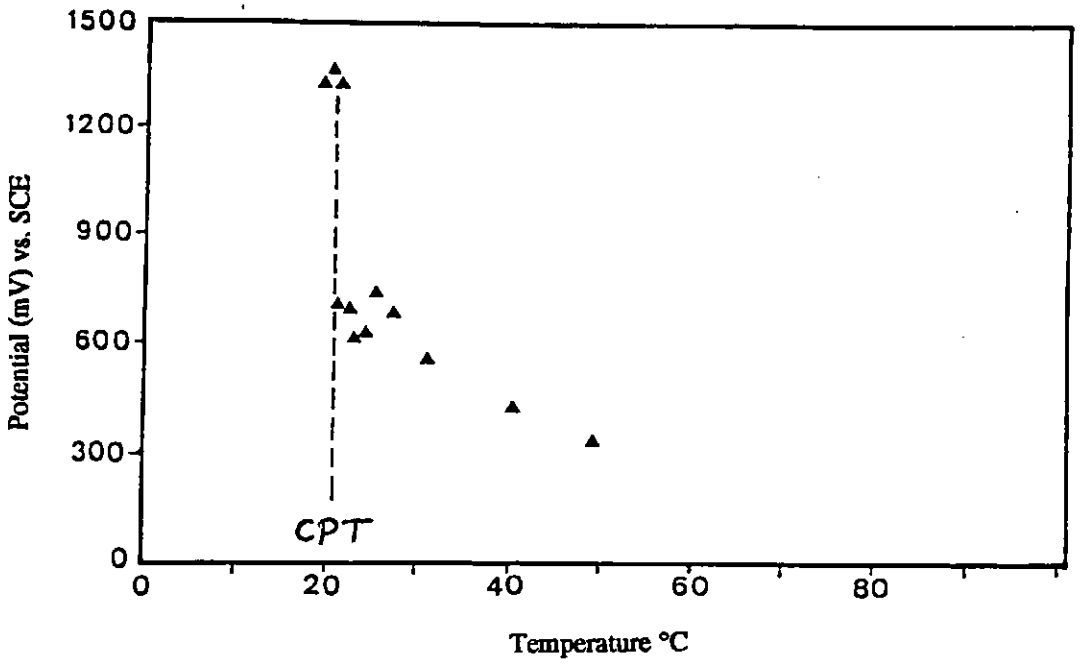

Fig. 2.12 Determining the critical pitting temperature (CPT) with electrochemical method[37]

Some of the proposed equations which indicate the relationship between alloying elements and resistance to localized corrosion are shown in Table 2.9.

Table 2.9 Selected equations for relating the localized corrosion resistance to the alloying elements

Ref	Formula*	Solution	Alloys
40	Cr + 3 Mo + 12.8 N	6% $FeCl_3$	Mo bearing stainless steels & Nickel alloys
41	Cr + 3.3 Mo + 13 N	%$FeCl_3$	Mo bearing stainless steels
42	Cr + 3.3 Mo + 16 N	0.6M NaCl + 0.1 M $NaHNO_3$	Wide range of alloys
43	Cr + 3 Mo + 27 N	6% $FeCl_3$	Mo bearing stainless steels & alloys with up to 42% Ni
33	Cr + 3.3 Mo + 16 N - 0.33 Ni	600ppm Cl^- + ClO_2	Austenitic and duplex stainless steels
32	Cr + 4.1 Mo + 6 N- 0.14 Ni	Potash brine	Austenitic and duplex stainless steels

* The given formulas are based on the weight percentages of the elements

In all the above equations for the evaluation of the metal resistance to localized corrosion, the effect of molybdenum is larger than that of chromium and nitrogen is more effective than each of them. There is a mixed interpretation for predicting the effect of nickel in localized corrosion. However, the majority of investigators have not considered any significant effect on localized corrosion for alloying with nickel in stainless steels[40,41,42,43].

Although LCRI or PRE are a good guide for evaluating and ranking different types of stainless steels, it should be considered that LCRI or PRE equations estimate only roughly the localized corrosion resistance of most stainless steels.

2.8. Effects of Surface Condition on Localized Corrosion

Breakdown potential for a given alloy/environment system is affected by the surface condition of the alloy. Grinding, polishing, brushing, sand blasting, degreasing

and acid washing are some of the mechanical and chemical treatments which are performed during metal fabrication and all of them affect the surface conditions and, therefore, the breakdown potential.

Both pitting and crevice corrosion can be affected by different treatments on the metal surface. One of the most effective methods of chemical surface finishing is "passivation". It consists of the immersion of an alloy in 20% HNO_3 solution. The main purpose of this process is cleaning the metal surface by dissolving inclusions and contaminants which are produced during fabrication. This treatment also removes manganese sulfide from the surface which makes the surface susceptible to initiation of pitting[16]. Passivation treatment is usually followed by an alkali treatment and then rinsing to neutralize and remove the chemical residual. It has been shown that chemical treatment improves the pitting potential for austenitic stainless steel 316[44]. The same result has been obtained by mechanical polishing of austenitic stainless steel 304, and it has been concluded that the pitting potential is raised by smoothing the metal surface[16].

Ogushi (after some AES experiments) found that the chromium level in 304 austenitic stainless steel is reduced as a consequence of the mechanical polishing which leads to an undesirable loss of corrosion resistance[45]. To prove the negative effect of mechanical polishing on passivity and breakdown potential, the chromium concentrations of passive films have been measured and are shown in Table 2.10. It is shown that chemical passivation is more effective than mechanical polishing, but no comparison was made to show the chromium concentration in the passive film at different mechanical polishing conditions(i.e. 400 grit and 600 grit). Higher concentrations of chromium in

wet polishing is related to lower temperature during polishing, and preventing the depletion of the chromium due to lower diffusion of chromium[45].

Table 2.10 Chromium concentration on the surface after different finishing for 304 stainless steel[45]

%Cr	Surface Condition
12.2	DP: Dry polish (60 sec. with #1000 emery paper).
13.9	$DP.N_{10}$: DP followed by passivation (30 min. in 10% HNO_3 at 50° C).
20.0	WP: Wet polish (60 sec. with #1000 emery paper with tap water).
18.0	$DP.N_{30}$: DP followed by passivation (30 min. in 30% HNO_3 at 50° C).
15.5	WPN_{10}: Mechanical polishing for 60 sec. using #1000 emery paper under a 10% HNO_3 dip
15.4	WPN_{30}: Mechanical polishing for 60 sec. using #1000 emery paper under a 30% HNO_3 dip.

Most of these works have confirmed that both chemical treatment and mechanical polishing increase the breakdown potential[16,44,46]. It has also been shown that the presence of additional chromium on the passive film after chemical treatment rather than after mechanical polishing, makes chemical treatment a better method to improve the localized corrosion resistance. The effects of chemical treatment, mechanical polishing and the combination of both of them on pitting and crevice corrosion are shown in Fig. 2.13[47] and Table 2.10[48], respectively.

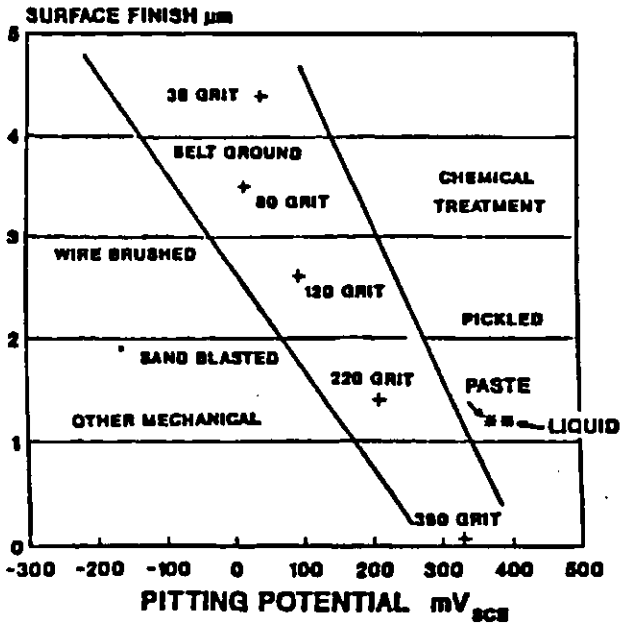

Fig. 2.13 Pitting potential of 316 stainless steel after various surface treatments[47]

Table 2.10 Surface chromium content and crevice corrosion initiation potentials after various surface treatments*[48]

Finish (Grit)	Chemical treatment	Surface chromium content %	Pitting potential mV (SCE)
36	None	42	125
36	Aqua Regia♦ 60°C, 5min	46.5	275
36	20% HNO_3, 25°C, 20 min	55	550
800	20% HNO_3, 25°C, 20 min	55.5	750

* Crevice corrosion potential was measured in aerated 0.5 M NaCl solution at room temperature

♦ 1 part HNO_3 + 3 parts HCl

Surface conditioning also affects crevice corrosion in another way. Smoother surfaces make smaller crevices. Therefore, the oxygen diffusion rate slows down and the crevice corrosion initiation gets faster. It was predicted that going from rough surfaces to fine surfaces decreases the crevice corrosion resistance[49], but the results in Table 2.10 show that the enrichment of the surface can overcome the effect of fast oxygen depletion due to the fine surface inside the crevice.

2.9. Effect of Cold Work

Most of the investigations on localized corrosion have been done on corrosion coupons which have been annealed. However, cold working of alloys during mechanical processing (i.e. forging, extrusion) may affect the metal resistance to localized corrosion. It was found that the breakdown potentials of Fe-Cr, Fe-Cr-Ni, and Fe-Cr-Ni-Mo alloys in chloride solutions are not greatly affected by cold work. For the cold worked specimens, the number of pits was higher and the pits were smaller. It was reported that plastic deformation, which does not cause fracture of the passive film, does not affect pitting[50]. However, an increase in the passive current density is observed with an increase in the cold work for iron and nickel[50,51]

2.10. Effects of Flow Rate

A previous study by Postlethwaite *et al.*, showed that the flow rate does not have a significant effect on the breakdown potential of nickel, but in their work, the pits were much less developed under the flowing conditions[52]. This suggests that the propagation step is slower at high flow rates. In this condition, the acidic solution inside the pits is swept away by the flowing condition. This phenomenon reduces the corrosion attack. In another work by the same author, it was found that pitting attack is retarded due to the current density decrease with increasing the flow rate over Zircaloy 2[53]. It was found that the current density in pits is controlled by mass transfer for 304 stainless steel and there is a threshold velocity which affects the current density. This means that the

smaller the pit, the higher the threshold velocity which affects the current density inside the pits[54].

The beneficial effect of solution flow to pitting corrosion cannot be extended for crevice corrosion and slurry flow[6]. In crevice corrosion, when the crevice is formed due to marine growth or deposits on the metal surface, increasing the flow rate removes the sedimentation from the surface and prevents crevices from forming. Otherwise the flowrate increases the crevice corrosion. This could be anticipated by assuming that the moving solution provides a greater supply of oxygen to the bold surface outside the crevice[16].

2.11. Rotating Cylinder Electrode

Simulating the effect of flow rate on metal corrosion is possible in a laboratory apparatus. The actual operating conditions including transport effects, were simulated in the laboratory so that polarization data could be applied to estimate the corrosion rate. A few equations have been presented which allow rotating cylinder rotation speeds to be chosen so that the mass transfer coefficients equal those in the pipes[55,56]. The limiting current density was used to correspond the mass transfer rate to the corrosion rate by correlation among Schmidt, Reynolds and Sherwood numbers[56].

These proposals can only be applied to single phase liquid flow and is not suitable for studying the effect of slurry or cavitation on corrosion of metals. More details about developing this equation and other equations for other geometries (i.e. annulus and impinging jet) are available in the literature[7,55,56,57].

3. Experimental

3.1. Alloys

In this study, mostly austenitic and duplex stainless steels were examined. However, two other samples from casting stainless steels were tested to compare the results with previous experiments performed by Blackmore[32]. The casting stainless steels may be categorized into two classes: heat-resistant and corrosion-resistant. Both CN7M and CD4MCu are corrosion-resistant stainless steels. The structure of most alloys in this group is austenitic but the dominant structure in CD4MCu is ferritic. The corrosion resistance of Hastelloy C-276, a nickel alloy which is one of the most resistant alloys to chloride solutions, was compared with the corrosion resistance of other alloys in the electrochemical polarization tests.

The alloys were selected based on their history of use in the potash industry. The most common alloys which are used in potash production process are 316L, 2304, 2205 and 254SMO[58]. The alloy samples were prepared by a materials sample producer*. Each sample was accompanied with its corresponding chemical composition and mechanical properties. The samples were wet ground to 600 grit by a SiC grinding belt. The actual chemical composition and mechanical properties of the samples are shown in

* Metal Samples Company, Munford, AL 36268, USA

Appendix A. The nominal and actual chemical compositions of tested alloys are shown in Table 3.1.

Table 3.1 Chemical composition of the alloys*♦

alloy	C	Cr	Mo	Ni	N	Alloy type
CD4MCu	0.022	25.50	1.80	5.40	0	Cast Corr. Resistant, Ferritic
	0.022	25.52	1.87	5.04	0	
	0.022	25.52	1.87	5.04	0	
CN7M	0.010	20.20	2.20	29.00	0	Cast Corr. Resistant, austenitic
	0.056	20.02	2.18	28.79	0	
	0.01	20.23	2.16	28.86	0	
304L	0.030	18.20	0.2	8.80	0.080	Austenitic
	0.030	18.13	0	8.79	0.050	
	0.026	18.23	0.24	8.83	0.086	
316L	0.020	16.30	2.10	11.00	0.03	Austenitic
	0.027	16.30	2.18	10.27	0.04	
	0.020	16.33	2.12	10.17	0.03	
904L	0.020	19.90	4.30	24.00	0.060	Austenitic
	0.016	20.27	4.32	24.04	0	
	0.014	19.90	4.30	24.20	0.064	
254SMO	0.010	20.10	6.20	18.0	0.200	Duplex
	0.009	20.10	6.15	18.0	0.200	
	0.010	20.10	6.20	18.0	0.200	
2304	0.03	22.5	0.30	4.5	0.12	Duplex
	0.03	22.5	0.37	4.5	0.12	
	-	-	-	-	-	
2205	0.020	22.30	2.80	5.80	0.120	Duplex
	0.016	22.20	3.00	5.60	0.150	
	0.020	22.33	2.77	5.82	0.117	
2507	0.020	25.00	4.00	7.00	0.300	Duplex
	0.019	24.80	3.90	6.80	0.300	
	0.016	24.87	3.81	6.93	0.263	
C-276	0.003	15.50	15.50	64	0	Nickel alloy
	0.002	15.48	15.60	Bal.	0	
	0.002	15.41	15.52	Bal.	0	

♦ The values in each row show the nominal chemical composition of samples, the chemical composition of samples in electrochemical polarization and exposure tests, respectively

* Chemical analysis of the samples were performed by Metal Samples Company

3.2. *Chemical Composition of Potash Brines*

Three samples of potash brine from different mills in Saskatchewan were received and analyzed under saturation conditions(Table 3.2). The samples were analyzed in chemical laboratory of PCS* pilot plant. Experimental results showed that the brines had almost similar compositions. The chemical composition of the brines depended on the type of process, the sample point, and the operating conditions. The brine samples were taken from the recycle line of the crystallizers.

In this study, only the potash brine from the Cory mill was used. Higher potassium and lower sodium concentrations in the Cory brine at the higher temperatures can be described with the NaCl-KCl-H_2O phase system diagram[59] (Fig. 3.1). Point A and point B show the Cory brine samples at 22°C and 90°C, respectively. Deviation of these points from saturation lines can be related to the presence of sulfate ions and other cations in the solution.

Table 3.2 Chemical composition of the saturated potash brines

	Concentration, %					
Mine source	Cl^-	SO_4^{2-}	Na^+	K^+	Ca^{2+}	Mg^{2+}
Cominco at 22°C	22.38	0.57	9.9	6.25	0.40	0.17
Central Canada at 22°C	22.43	0.56	9.62	6.59	0.38	0.16
Cory at 22°C	21.88	0.57	8.44	8.87	0.35	0.11
Cory at 90°C	23.45	0.20	7.65	12.00	0.41	0.10

* Potash Corporation of Saskatchewan Inc.

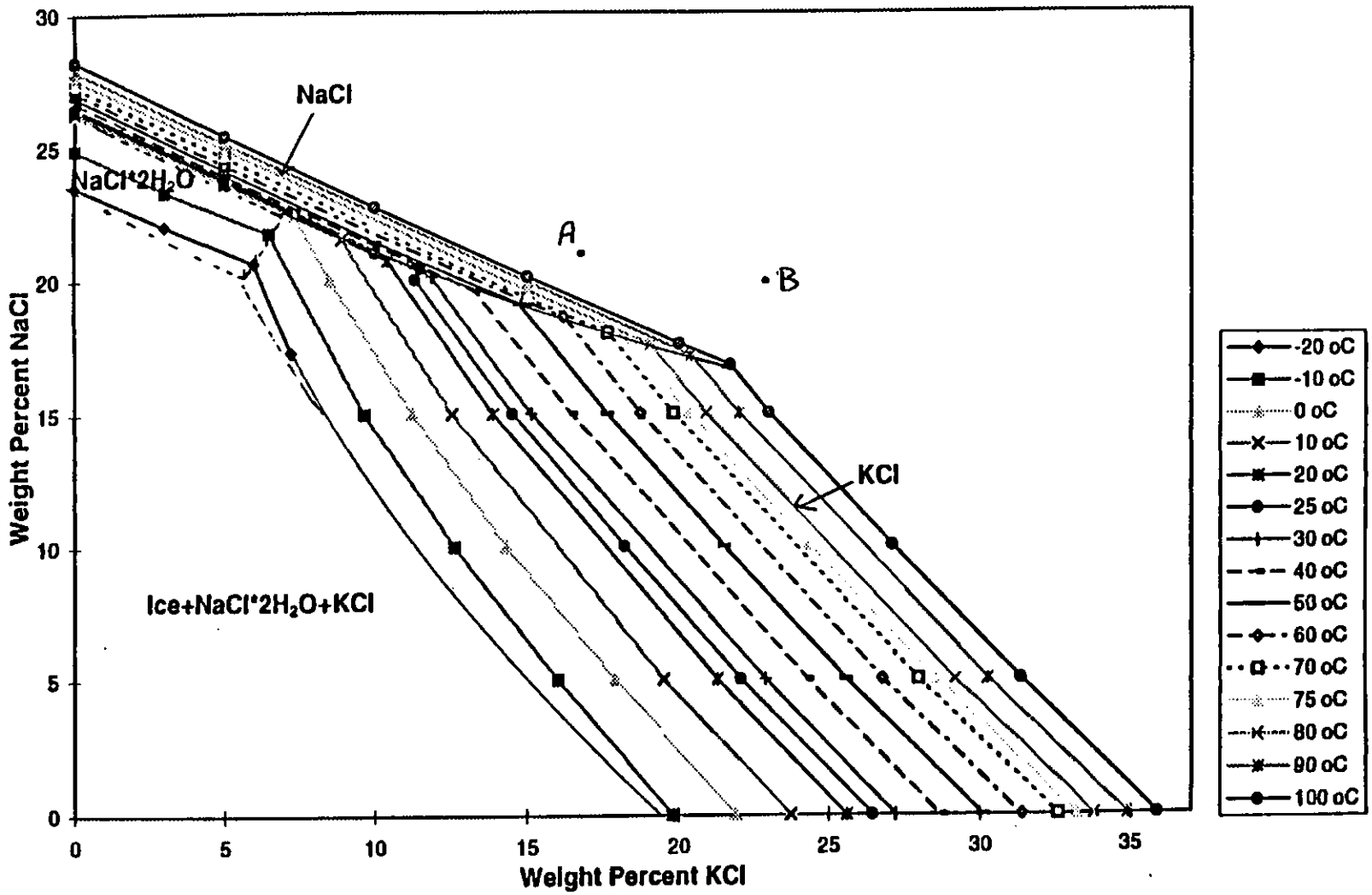

Fig. 3.1 Phase diagram for NaCl-KCl-H_2O system and the situation of the Cory potash brine at 22°C (point A)and 90°C (point B)[59]

3.3. *Electrochemical Polarization*

Electrochemical testing is the most rapid method of determining the possibility of localized corrosion. The main advantage of electrochemical testing is that a great deal of information can be gained about the dependence of corrosion on an external variable in a short time. For example, the determination of breakdown potentials and currents can be useful in devising accelerated tests to discriminate the alloy corrosion resistance. The validity of an accelerated corrosion test depends largely on how well the factors (which are accelerating the rate of corrosion in the test) simulate what is actually happening in the service environment.

The simple circuit diagram for an electrochemical polarization cell is shown in Fig. 3.2. The working electrode (WE) is the metal under study. The open circuit potential (corrosion potential) can be measured versus the reference electrode (RE) when the power supply is not in circuit. By switching the power supply on and changing the resistance (R), the potential of the working electrode with respect to the reference electrode sweeps stepwise to higher potentials than the open circuit potential. The current is measured by the ammeter in each step. The counter electrode (CE) is made of platinum or graphite and completes the electrical circuit (this is the cathode during anodic polarization of the working electrode). In practice, a potentiostat which is a proportional controller, controls the potential of the working electrode with respect to a reference electrode. The device produces the current between the working electrode and counter electrode to establish the required set potential.

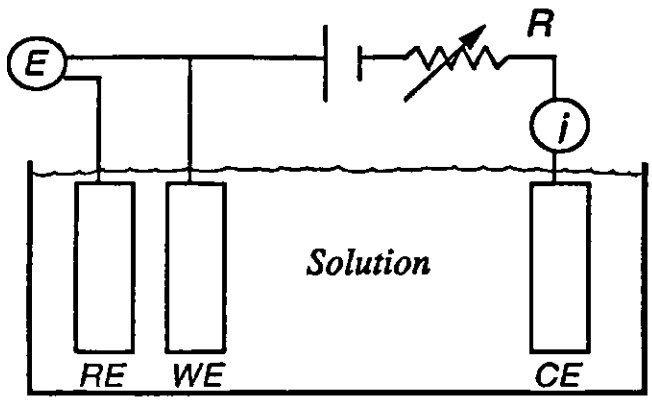

Fig. 3.2 Simple circuit diagram for an electrochemical polarization cell

A rotating electrode with variable rotation speed (an AFMSRX Rotator from the Pine Instrument Company*) was used to compare the effect of velocity on electrochemical polarization curves of alloys with those in stagnant solutions. More information about the rotating electrode is available in Appendix B. Under flowing conditions the speed of the rotating electrode was 1940 rpm.

By far, the most common electrochemical test for localized corrosion is cyclic polarization. In cyclic polarization, the potential is scanned from open circuit potential (E_{corr}) or slightly below it in the anodic direction until localized corrosion is initiated. This is indicated by a large increase in the applied current (Fig. 3.3). When the current density reaches 1 mA/cm^2, the direction of the scan is reversed, and the current decreases until the polarity is changed and a hysterisis loop on the *Log(i)-E* curve is presented. The breakdown or pitting potential (E_{rp}) is the potential above which pits initiate, while the repassivation potential (E_p) is the potential below which the pits repassivate.

---

* Pine Instrument Company, Grove City, PA 16127, USA

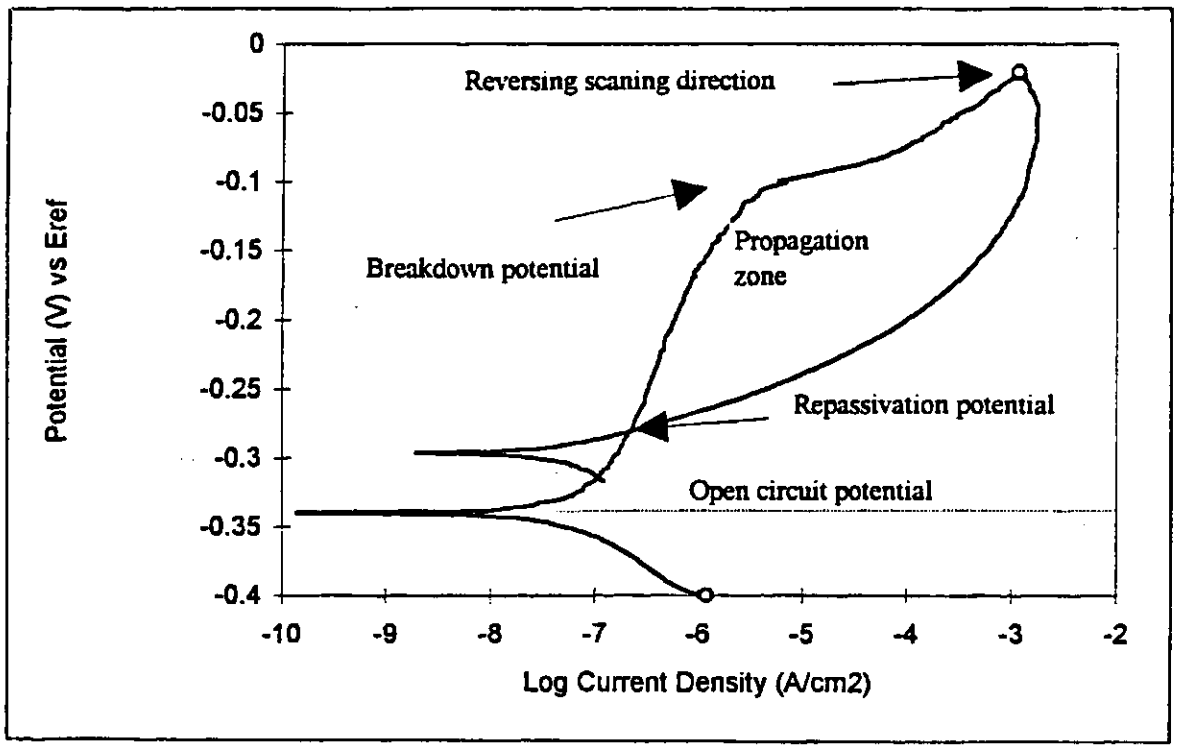

Fig. 3.3 Typical cyclic polarization curve

The breakdown potential is usually defined as the potential at which there is a large increase in the current density and repassivation potential is defined (on the reverse scan) as the potential at which the curve intersects the forward curve section. Together, these potentials make a hysterisis loop. Thus, the higher the value of the breakdown potential, the more the resistant the alloy is to the initiation of localized attack. The higher the repassivation potential and smaller the hysterisis loop, the more easily the alloy can repassivate. At potentials between breakdown and repassivation potentials, sites that have initiated can propagate. Based upon this argument, one would favor an alloy that has both a high breakdown potential and a small hysteresis loop. The test procedure was followed according to ASTM test methods G-5 ("Standard Reference Test Method for Making Potentiostatic and Potentiodynamic Anodic Polarization Peasurement") and G-

61 ("Conducting Cyclic Potentiodynamic Polarization Measurements for Localized Corrosion Susceptibility of Iron-, Nickel or Cobalt-Based Alloys")[5].

A one litre, round bottom flask with various necks is a suitable container in which to install the electrodes, the input and output gas connections, the salt-bridge, the thermometer and pH meter. A pH/ATC combination electrode from Fisher Scientific* was used to measure both pH and temperature. The salt-bridge maintained an electrical connection between the solution in the flask and the reference electrode. The reference electrode was inserted in a beaker with the same solution but at ambient temperature to protect it against high temperature solution in the flask. Most importantly, the reference electrode was maintained at room temperature to keep it at constant potential during the experiments. The salt-bridge tip was adjustable so that it could be easily adjusted to the specimen. The schematic of electrochemical polarization cell is shown in Fig. 3.4.

A scanning potentiostat/galvanostat built into a PC computer was used for the experiments. The Gamry CMS100 Corrosion Measurement System† was used for all electrochemical experiments. Software was installed on the computer which was used to control the test routine for different corrosion experiments. All the parameters during the experiments such as initial potential, final potential, highest current density, and scanning rate were controlled. More information about the Gamry CMS100 system is available in Appendix B. The cyclic polarization test was used in this study to determine the breakdown and repassivation potentials for the alloys.

---

* pH/ATC combination electrode for Accumet 1000 series meters, Fisher Scientific
† Gamry Instruments, Inc, Langhorne, PA 19047, USA

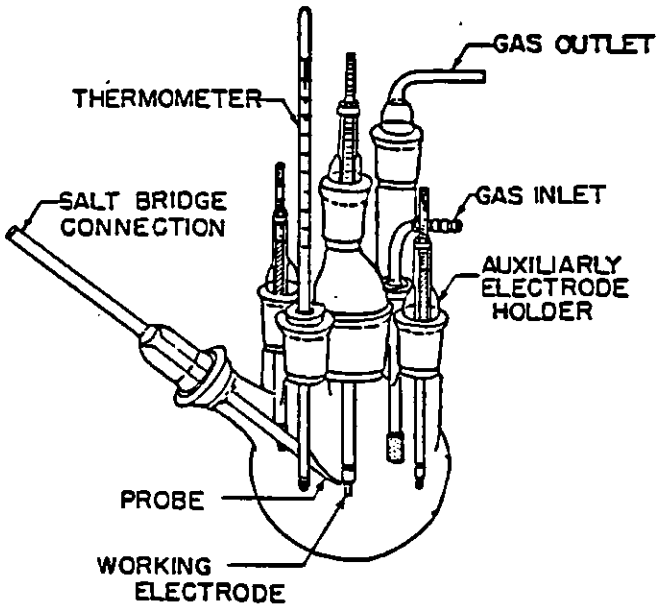

Fig. 3.4 Schematic of an electrochemical polarization cell

Alloy samples were cylindrical with a 11.95 mm in diameter and a height of 8 mm, with a 3 cm^2 exposed area to the solution. Fig. 3.5 shows the sample arrangement on the rotating electrode.

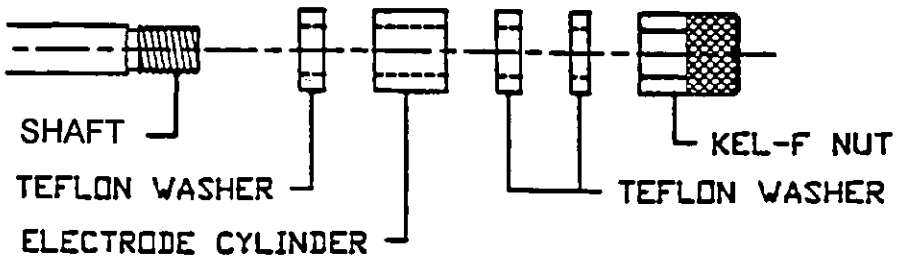

Fig. 3.5 Rotating electrode

The alloy sample surfaces were prepared and used less than one hour after preparation for testing. The samples were polished with wet SiC paper, starting from 240-grit and ending with 600-grit. Then, the samples were washed with alcohol and distilled water and dried. Meanwhile, the temperature of the brine solution was

controlled by a heater equipped with a thermostat. High purity nitrogen (99.999%) at a minimum rate of 200 cm^3/min was purged through the solution. The nitrogen source was a nitrogen cylinder which was under pressure and the gas temperature decreased when it passed through the throttling valve. The low nitrogen temperature caused plugging of the pores in the inlet gas port due to the saturation state and high temperature in the flask. To overcome this problem, the nitrogen line (a copper tube) was passed through a high temperature bath to increase its temperature before entering the flask. After half an hour of nitrogen injection, the specimen was put in the cell and left there for an hour for its potential to stabilize. The salt-bridge tip was adjusted about 2 mm from the specimen. If the experiment was running under flowing conditions, the rotating electrode was turned on after the sample was immersed. A rotating speed controller was used to set the rotation speed at the desirable value. The sample installed on the rotating electrode was connected to the working electrode probe of the potentiostat. A Fisher Scientific silver/silver chloride reference electrode with (4M) potassium chloride electrolyte was used. The potential of the reference electrode in this situation was 0.199 mV versus the standard hydrogen electrode (SHE). Once in a while, the potential of the reference electrode was checked with the other standard electrodes to verify that it remained at the standard potential. A graphite rod completed the electrical circuit as a counter electrode. First the program monitored the open circuit potential (corrosion potential) in 10 seconds and then started scanning at a constant rate. After a rapid increase of anodic current at potentials below the oxygen evolution potential, the current reached 1 mA/cm^2. At that point the scanning direction was reversed. The scanning rate was selected at 0.166

mV/sec (10 mV/min). The potential and current density were recorded over 9 second intervals (user defined) and monitored on an X-Y coordination curve on the computer screen. The data from the test was saved in a file which could be analyzed and plotted by Microsoft Excel. The most popular electrochemical curve is the *E-log i* curve which shows the potential versus the logarithm of the current density. Fig. 3.6 shows the schematic of a experimental set-up.

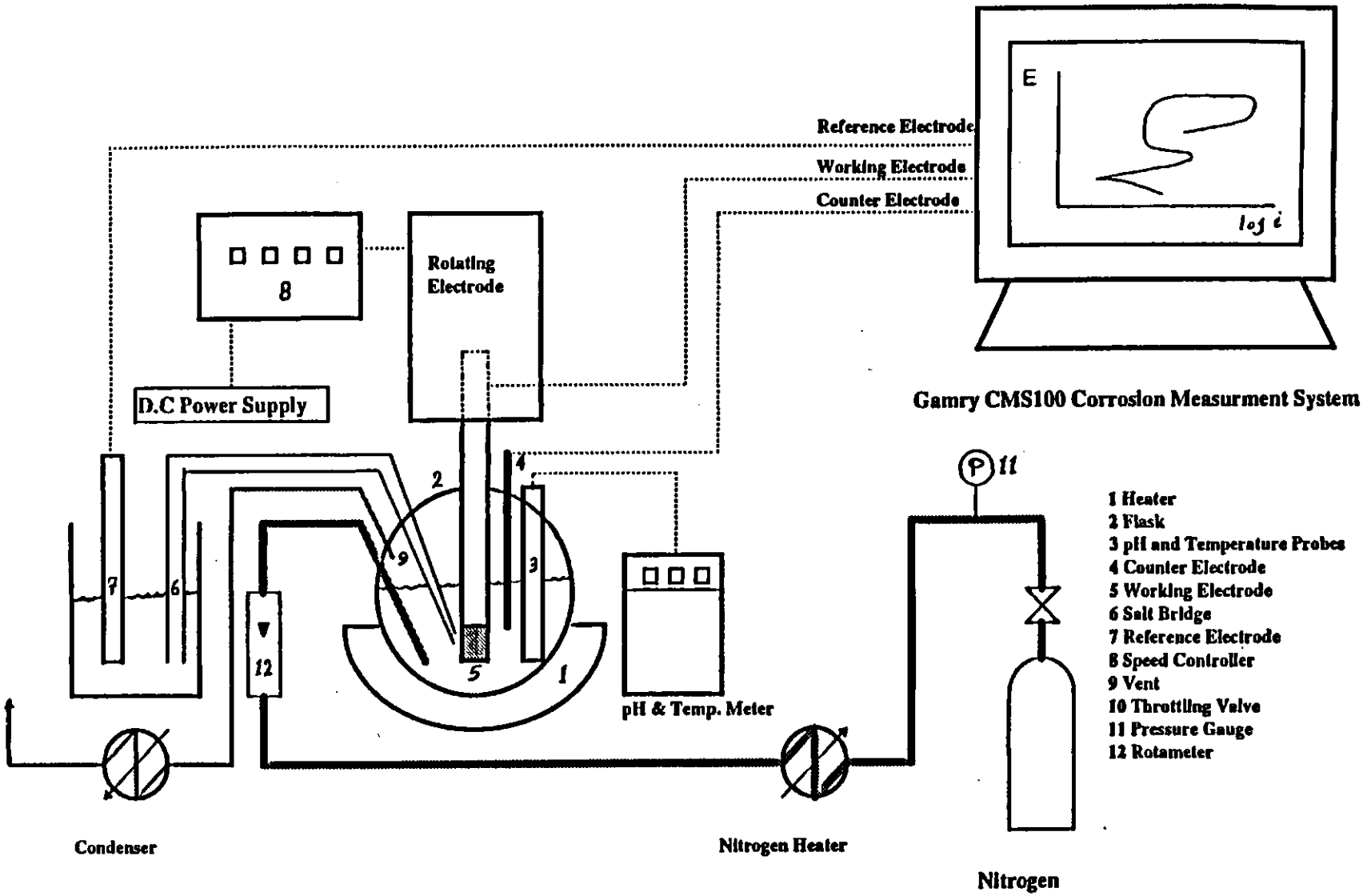

Fig. 3.6 The schematic of the experimental set-up

3.4. Exposure Tests

Generally, crevices can be categorized into two groups. First, natural crevices which are created by biofouling, sediments and deposits. Second group, crevices which are created during the manufacture, fabrication and maintenance of equipment. The second group of crevices utilized in laboratories could represent actual geometric formations in some service conditions.

An experimental procedure for exposure testing is described by ASTM G78 ("Standard Guide for Crevice Corrosion Testing of Iron-Based and Nickel-Based Stainless Alloys in Sea Water and Other Chloride Containing Aqueous Environments")[5]. The materials of interest are typically machined into coupon forms and then measured, cleaned, weighed, and exposed to the corrosive environment. After a period of time, the coupons are removed, their surfaces carefully cleaned, and then evaluated for attack. The minimum suggested exposure test period for recognizing the attacked area is 30 days. After the test, one should consider two surface areas: *(i)* the surface in contact with the solution without any crevice on the surface, and *(ii)* the area around the crevice assembly. The dominant mechanism for corrosion in area *(i)* is pitting and the mechanism for area *(ii)* is crevice corrosion.

The multiple crevice assembly (MCA) consisted of two bolted serrated washers and a hole drilled in the specimen as shown in Fig. 3.7. The advantage of MCA is that the crevice geometry can be made very tight by applying greater torque to the bolt and the multiple small contact points. The contact points on the washer were individually examined and then statistically analyzed as a group. The MCA consisted of 12 plateaus

and the bold/crevice (cathode/anode) area ratio in this work was 34. The specimen dimensions were 2" × 3/4" × 1/8" with a 0.375" diameter hole in the center. The exposure tests conditions are given in Table 3.3. The samples were held by a torque of 8.5 Nm (75 in.lb_f) on the MCA. The nuts, bolts, metallic washers and the flat bar rack were made of Hastelloy C-276 while the MCAs were made of Teflon. The solution container was warmed up in a high temperature oil bath by using a heater equipped with thermostat and circulating pump. All exposure tests were performed in stagnant and non-deaerated solutions.

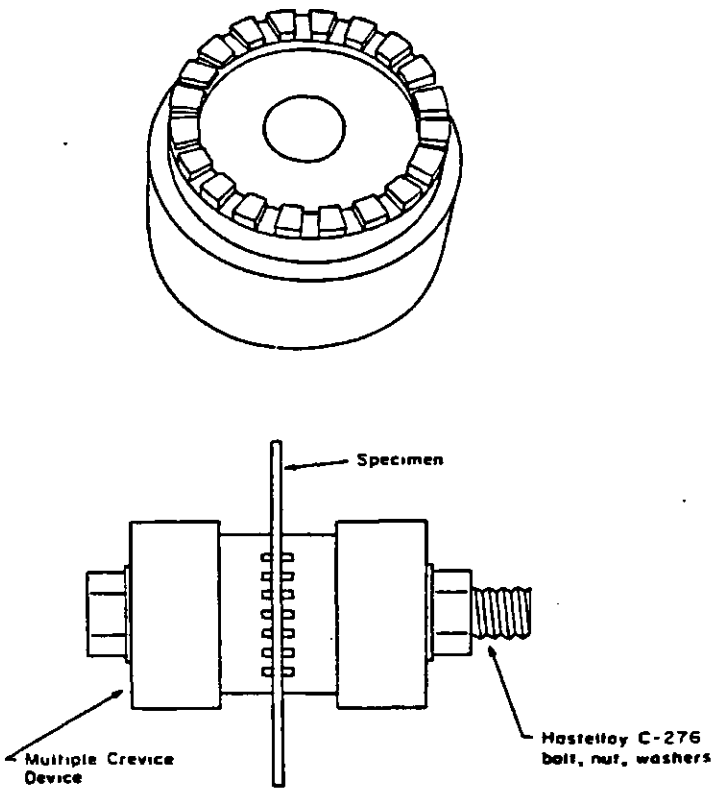

Fig. 3.7 Typical crevice corrosion test setup and MCA[60]

Table 3.3 Exposure test conditions

	Test 1	Test 2
Solution	Potash Brine from the Cory Mill	Potash Brine from the Cory Mill
Temperature, °C	90	90
Exposure Time	30 days	60 days
Solution Condition	Aerated, Stagnant	Aerated, Stagnant
pH	6.35-6.60	6.35-6.60
Surface Condition	600 grit	600 grit

After the exposure period, the exposed samples were rinsed, dried and weighed. The specimens were cleaned in a solution of 10% nitric acid at 60°C for 20 min. After each chemical cleaning, they were rinsed, dried and weighed again. Care was taken to remove the corrosion product only, and not the metal base, with the acid solution. ASTM G1 ("Standard Practice for Preparing, Cleaning, and Evaluating Corrosion Test Specimens") was a good guide in this regard[5]. When the difference between the sample weight before and after the cleaning cycle approached zero, the samples were assumed to be cleaned enough and they were ready for metallography.

3.5. Metallography

The approximate size and distribution of pits and attacked areas were determined by visual examination, followed by a more critical and detailed microscopic examination through a microscope to determine the exact size, shape and density of the pits.

It was a tedious and time-consuming job to determine the pit density. The pits depth is usually a more significant piece of data than the pit density or pit size. A finely calibrated, fine focusing knob built in the microscope was suitable for measuring the pit

depth. The microscope was equipped with four different objective lenses (2.5×, 5×, 10×,and 40×) and scaled eyepieces lenses (10×). Therefore the magnification of the microscope was ×25, ×50, ×100 and ×400. The specimens were cut by a low speed diamond saw to examine the cross section of the corroded area. The specimen parts were dried after removing grease with acetone and soap, washed with methanol, and rinsed with water. The sample parts were then mounted in a plastic mold to be ground and polished to a desirable surface condition and to be kept for further study. Compression molding techniques were used to produce hard mounts for specimens. Thermoplastic material (Lucite®) was used to produce clear molds. Lucite requires heat and pressure during the molding cycle. The temperature and pressure during the cycle were 280-300°F and 3000 psi, respectively. Lucite® remains fluid at maximum molding temperature and becomes transparent and dense with a decrease in temperature[61].

The mounted samples were polished by 660-grit SiC wet paper followed by 6 μm and 1μm diamond paste. Selected samples were electro-etched to investigate the microstructure of the attacked areas.

A solution of 10% oxalic acid was used in the electrolytic etching method. This solution is a conventional etchant for a wide range of stainless steels. Direct current electrolysis is usually used for electrolytic etching. The specimen was the anode and a stainless steel rod (316L) was the cathode in these cases. The voltage between electrodes was 6 V with 0.1 A/cm^2 and the total elapsed time was 20 seconds. The current was controlled by changing the distance between the electrodes.

Scanning Electron Microscopy (SEM) was used for a more detailed examination of a few selected specimens. The etched samples were brought out of the molds and cleaned ultrasonically. After this preparation, they were ready for examination using the SEM.

4. Results

4.1. *Electrochemical Polarization*

The cyclic potentiodynamic polarization method was used to determine the susceptibility of alloys to localized corrosion. The breakdown and repassivation potentials and the passive current density were determined for each alloy based on its polarization curve. The breakdown potential is usually defined as the potential at which the current density increases sharply with a small increase in the potential[62]. Some other researchers define the breakdown potential as the potential at which the current density is equal to 10 $\mu A/cm^2$ [7]. In this study, the former definition was used and in cases where the increase was not sharp, the breakdown potential was determined at the intersection of two extrapolated sections of the curve. Also, there are two different definitions for the repassivation potential; *(i)* the potential at which the reversed curve intersects the ordinate, as it is believed that the formed pit ceases to propagate at potentials below this value[62]; and *(ii)* the potential at which the polarity of the curve is changed[12]. In this study the first definition was used. In some cases it was difficult to determine a precise value for the above parameters because of the irregular behavior of the polarization curve. Fig. 4.1 shows the polarization curves for 904L, which shows an uncertainty in determining the breakdown and repassivation potentials and passive current density. The presence of two transpassive areas in the anodic curve was the main problem in determining the breakdown potential. This was related to the oxidation of molybdenum at lower potentials and chromium at higher potentials[63].

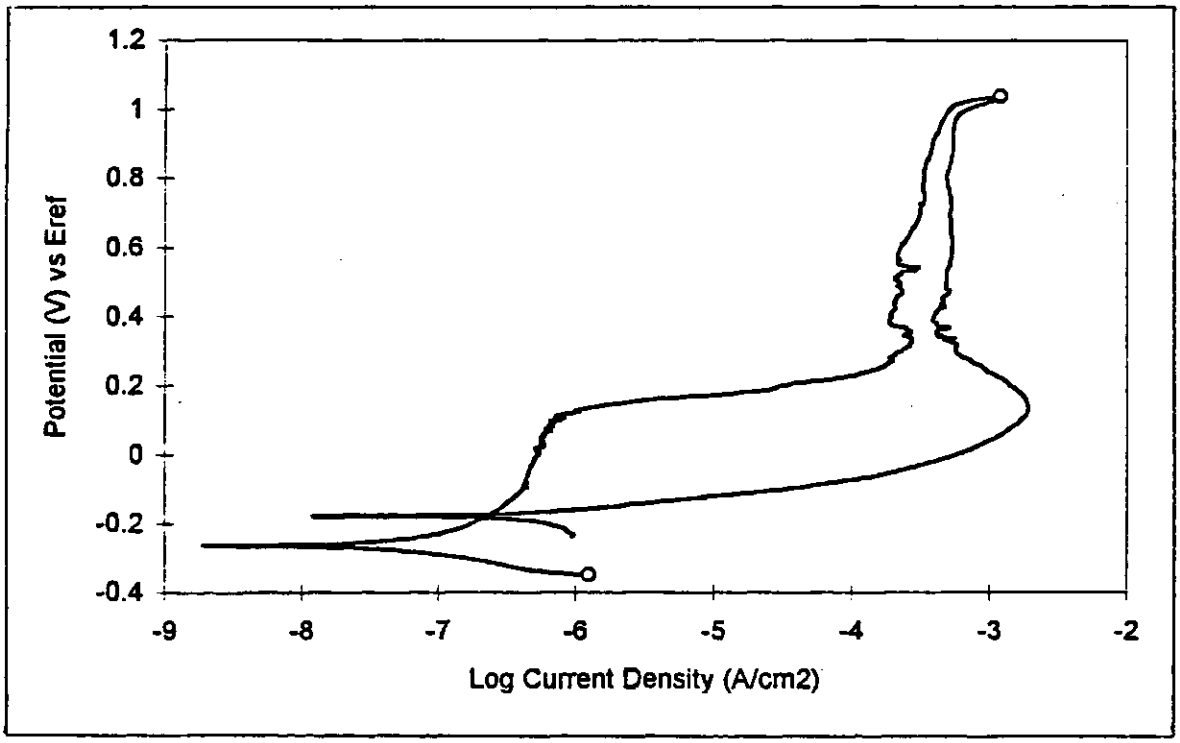

Fig. 4.1 Uncertainty in determining the breakdown and repassivation potentials and the passive current density due to presence of two transpassive zones (904L in the potash brine)

The uncertainty in determining the repassivation potential is due to the unusual behavior of alloys during reverse scanning. In this condition, the repassivation potential determination was based on the selected breakdown potential. The passive current density was determined in the area preceding the breakdown potential or where the current density was kept constant when the potential swept to more noble potentials.

Reproducibility of the curves was examined. Although in some cases shifting of the corrosion potential (open circuit potential) was observed, no significant changes in the breakdown and repassivation potential were distinguished. Fig. 4.2 shows reproducibility of the anodic polarization for cast corrosion-resistant CN7M.

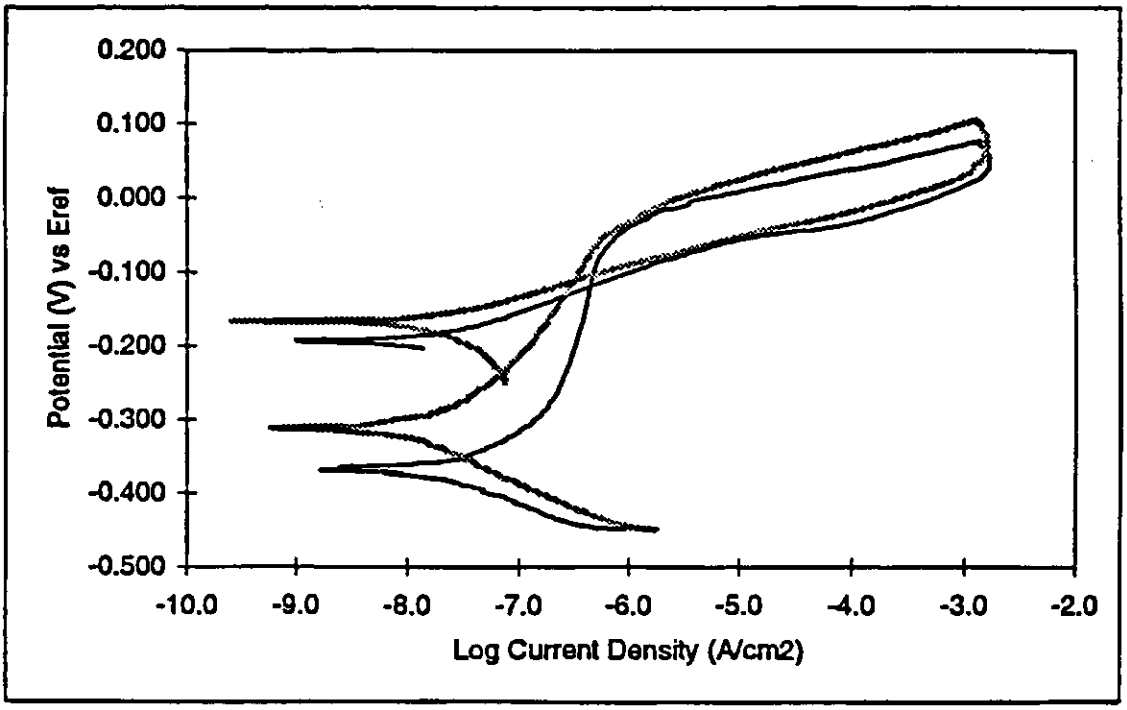

Fig. 4.2 The reproducibility of the electrochemical polarization curves (Cast corrosion resistant CN7M in potash brine)

The breakdown and repassivation potentials for the tested alloys both in stagnant and flowing conditions are shown in Tables 4.1 and 4.2. The passivation current densities for the alloys are shown in Table 4.3. The original curves from the experiments are attached in Appendix C.

In part of this study, two types of austenitic stainless steels (304L and 316L) were examined to compare the corrosivity of sodium chloride and potassium chloride. Electrochemical polarization was performed for this purpose. The breakdown potentials are given in Table 4.4.

Table 4.1 The breakdown and repassivation potentials of alloys in stagnant conditions

	22°C		90°C	
Alloy	E_{rp} (mV)	E_p (mV)	E_{rp} (mV)	E_p (mV)
304L	-128	-255	-288	-380
316L	15	-190	-212	-313
2304	-4	-230	-200	-425
CN7M	-43	-120	-161	-300
CD4MCu	-40	-290	-245	-288
2205	865	865	-176	-314
904L	85	-140	-120	-280
2507	886	886	-119	-275
254SMO	943	871	69	-261
C-276	927	844	883	728

Table 4.2 The breakdown and repassivation potentials of alloys in flowing conditions (1940 rpm)

	22°C		90°C	
Alloy	E_{rp} (mV)	E_p (mV)	E_{rp} (mV)	E_p (mV)
304L	-106	-280	-242	-430
316L	0	-250	-193	-303
2304	19	-181	-226	-426
CN7M	-53	-120	-160	-236
CD4MCu	-37	-322	-220	-270
2205	875	580	-129	-236
904L	100	-160	-56	-240
2507	932	932	-90	-245
254SMO	850	765	-38	-155
C-276	976	816	870	648

Table 4.3 Logarithm of passive current density at the electrochemical polarization tests

	22°C		90°C	
Alloy	**Stagnant**	**1940 rpm**	**Stagnant**	**1940 rpm**
304L	-5.89	-5.81	-5.70	-5.50
316L	-6.07	-6.51	-5.75	-5.71
2304	-6.13	-6.51	-5.83	-5.60
CN7M	-6.48	-6.35	-5.93	-5.83
CD4MCu	-5.40	-5.41	-4.93	-4.97
2205	-6.13	-6.32	-5.80	-5.79
904L	-6.27	-6.25	-5.95	-6.04
2507	-6.23	-6.21	-5.94	-5.72
254SMO	-6.24	-6.21	-5.97	-5.92
C-276	-6.04	-6.14	-5.84	-5.90

Table 4.4 Breakdown potentials of the austenitic stainless steels in 0.3N KCl and 0.3N NaCl solution at room temperature

Solution	E_{pp} (mV), Deaerated		E_{pp} (mV), Aerated	
	304L	316L	304L	316L
KCl	238	253	135	186
NaCl	244	258	200	286

4.1.1. pH Changes in the Bulk Solution

The pH changes during anodic polarization were measured in the bulk solution for 304L stainless steels in 0.3N NaCl solution (in both aerated and deaerated conditions). The pH values in the bulk of the solution increased during localized corrosion in both deaerated and aerated conditions (Fig. 4.3 and 4.4).

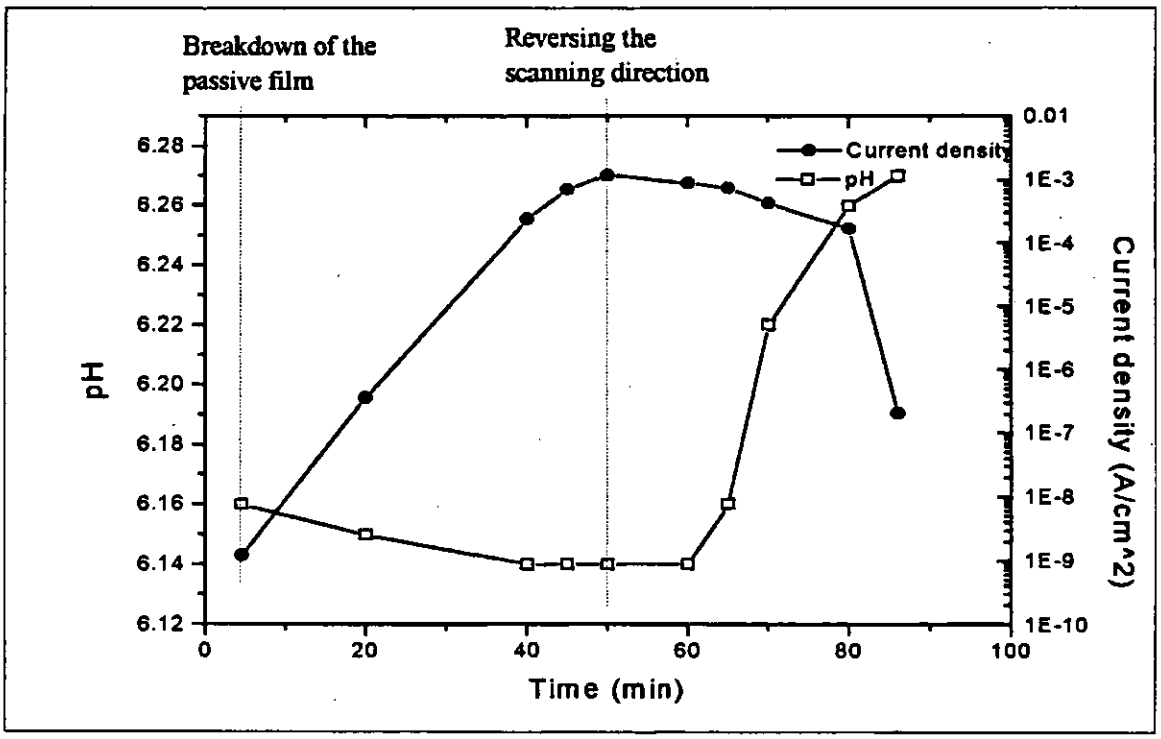

Fig. 4.3 pH changes in the bulk of 0.3N potassium chloride solution during polarization of 304L (aerated)

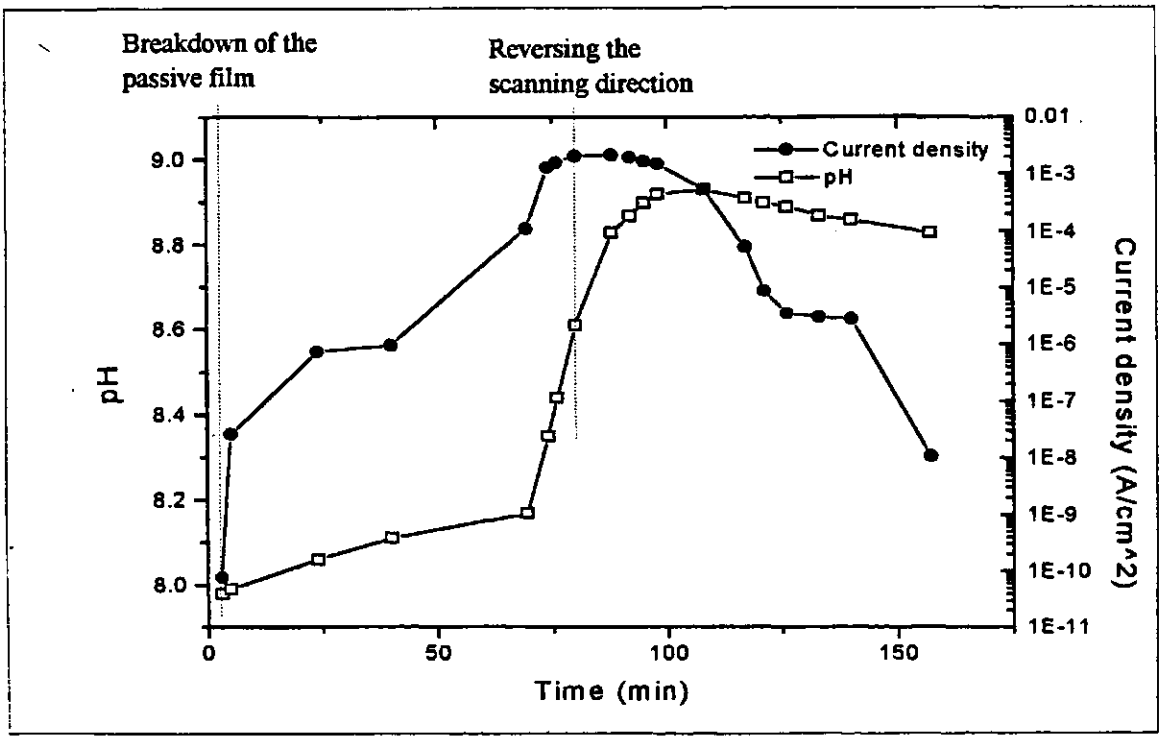

Fig. 4.4 pH changes in the bulk of 0.3N potassium chloride solution during polarization of 304L (deaerated)

4.2. Exposure Tests

The typical features of a specimen after the exposure test are shown in Fig. 4.5 and 4.6. The corrosion products surround the crevices as well as the bare metal surface.

The density, size and depth of pits are given in a typical pitting chart (Fig. 4.7). The most important parameter in studying localized corrosion is the depth of the deepest pit. In regards to the nature of pitting (which is a random process), sometimes the deepest pit does not truly show the effect of localized corrosion in an alloy. The ASTM G46 ("Standard Practice for Examination and Evaluation of Pitting Corrosion") recommends the use of a pitting chart to record the average pit depth[5]. However, in this study, the average depth of the five deepest pits was used to generate the data presented here. The average pit depth, the deepest pit depth, and the average depth of the five deepest pits for the austenitic and duplex stainless steels are shown in Tables 4.5 and 4.6. It was observed that the edges of the austenitic 304L, 316L and 904L were more susceptible to localized corrosion. There are two reasons for this susceptibility. Firstly, there are residual stresses on the edges after cutting and machining of the specimens. These stress residuals caused stress corrosion cracking on the edges, even though this type of attack was not expected in these experiments. Secondly, the surface conditions on the edges were not the same as on the metal surfaces. Therefore, the pits on these areas were not considered in analyzing the data.

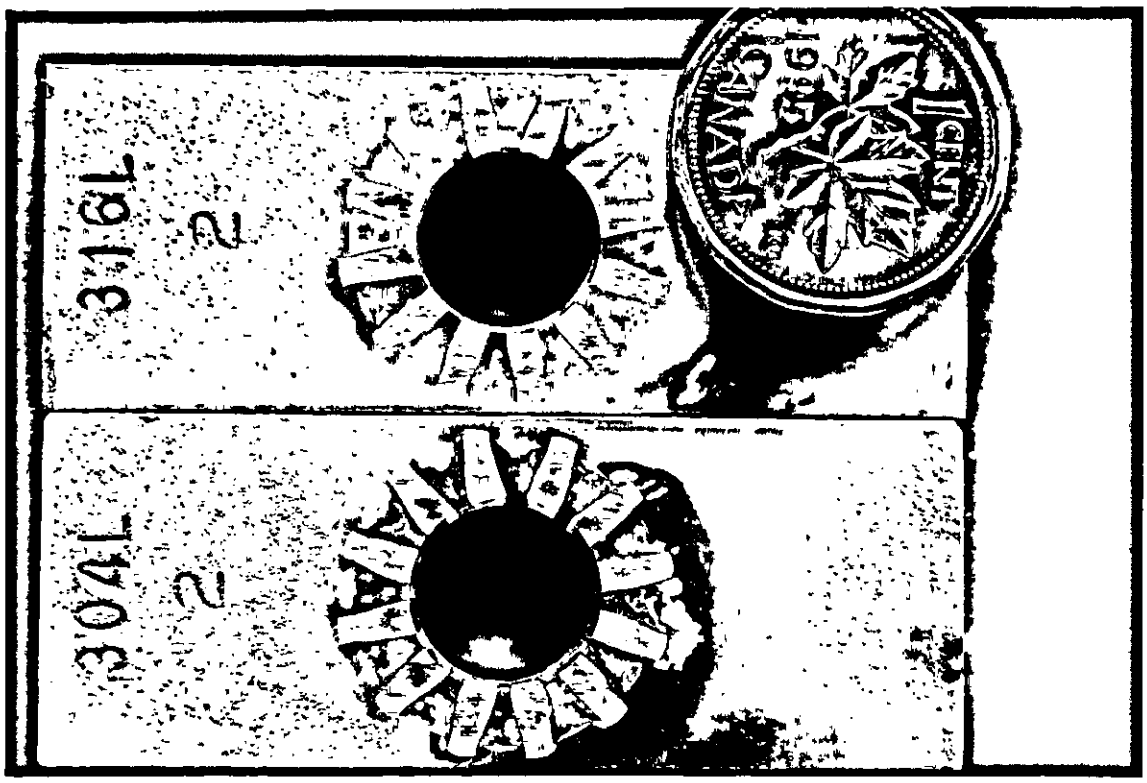

Fig. 4.5 General features of austenitic 304L and 316L after an exposure test

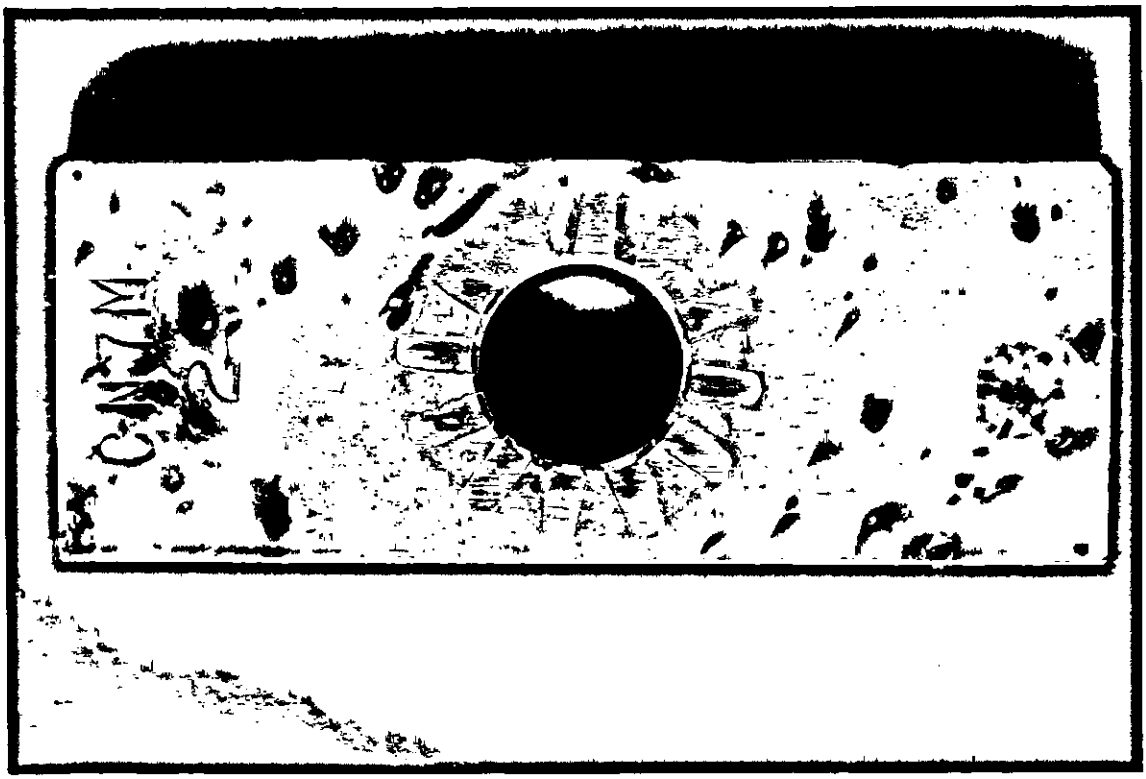

Fig. 4.6 General feature of cast corrosion-resistant CN7M after an exposure test

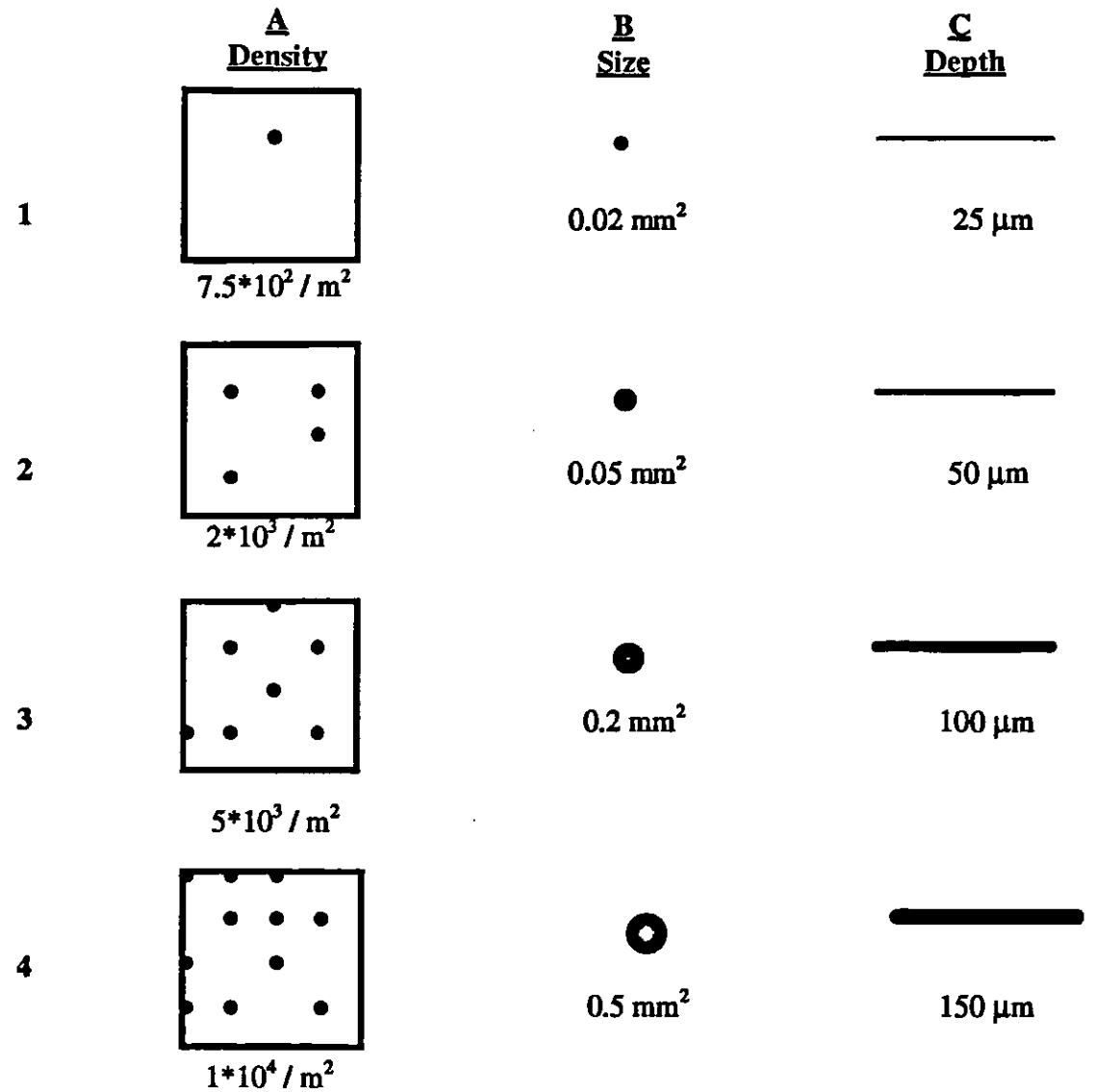

Alloy	% Cr	% Mo	% N	LCRI*	30 days**			60 days**		
304L	18.23	0.24	0.086	20.4	-3	+2	-4	+3	-3	+4
316L	16.33	2.12	0.03	23.8	-3	-2	+3	-3	-3	-4
CN7M	20.23	2.16	0	27.4	+3	+2	-4	-4	+2	+4
CD4MCu	25.52	1.87	0	31.7	+3	2	-3	+4	+2	+3
2205	22.33	2.77	0.177	34.3	+2	+1	2	-3	1	+2
904L	19.9	4.3	0.064	35.1	+1	1	+2	+1	-1	+1
2507	24.87	3.81	0.263	41.6	2	-2	-1	-2	-2	-2
254SMO	20	6.1	0.2	43.3	2	+2	-3	2	-3	+3

* Based on the average of the 5 biggest & deepest pits. The numbers in columns in each of three for 30 and 60 days show, density, size and depth, respectively

♦ The plus and minus sign represent greater and smaller values, respectively

Localized Corrosion Resistance Index = %Cr + 3.3* %Mo + 16* %N

Fig 4.7 Pitting chart for the exposure tests in the potash brine at 90° C

Both 2205 and 2507 duplex stainless steels showed better resistance than what was expected (based on their alloying elements). The deepest pit and the average of the five deepest pits for these two duplex alloys were shallower than the rest of the alloys in this study. Despite the optimum combination of alloying elements, the presence of few deep pits on austenitic alloys 904L and 254SMO lowered their performance rating.

Table 4.5 Pit depth data after exposure tests in Cory potash brine at 90°C for 30 days*

Alloys	The average pit depth (microns)	The average of 5 deepest pits (microns)	The deepest pit (microns)
304L	25	141	220
316L	28	114	145
CN7M	29	148	285
CD4MCu	21	76	102
2205	12	49	60
904L	12	71	215
2507	9	23	60
254SMO	14	86	205

* Data in microns

Table 4.6 Pit depth data after exposure tests in Cory potash brine at 90°C for 60 days*

Alloys	The average pit depth (micron)	The average of 5 deepest pits (micron)	The deepest pit (micron)
304L	61	154	200
316L	39	143	270
CN7M	47	216	240
CD4MCu	28	122	300
2205	24	52	83
904L	19	83	93
2507	13	42	113
254SMO	17	103	250

* Data in microns

4.3 Metallography

The alloys were examined after exposure test as described in the Chapter Three. Some of the photomicrographs of the exposed samples and the results of the SEM study are shown in Fig. 4.8 to 4.13.

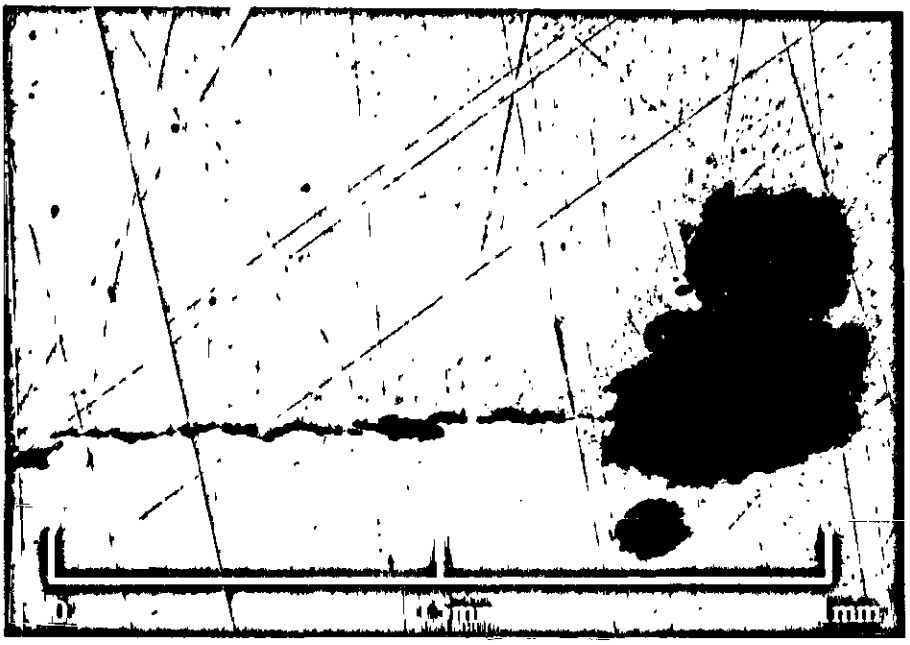

Fig. 4.8 Edges of 304L (60 days), ×100

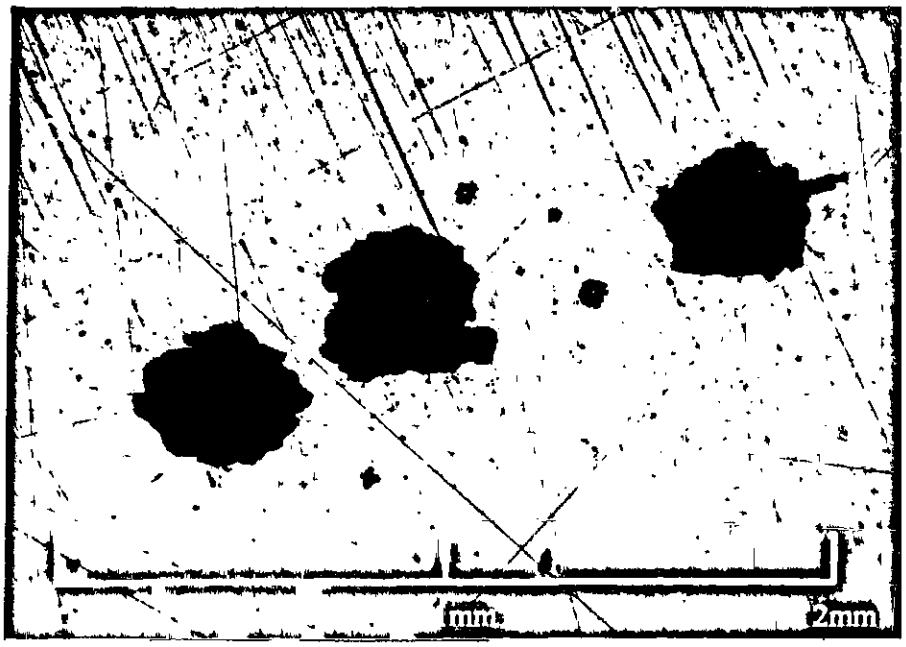

Fig. 4.9 Edges of 304L (60 days), ×50

Fig. 4.10 Edges of 316L (60 days), ×50

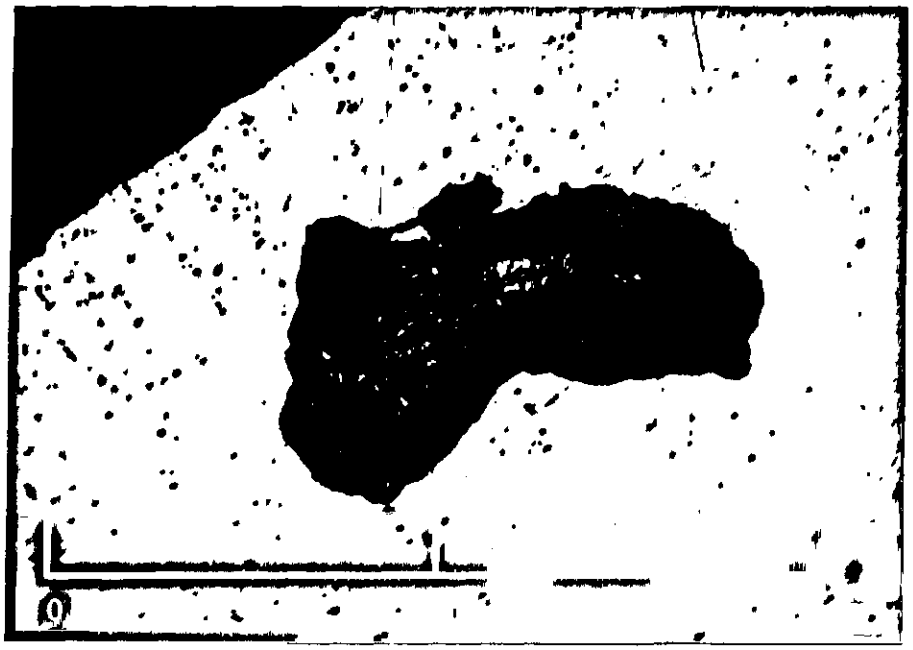

Fig. 4.11 Surface of 254SMO (60 days), ×50

Fig. 4.12 Microstructure of CN7M, austenite (light areas), ferrite (dark areas), ×100

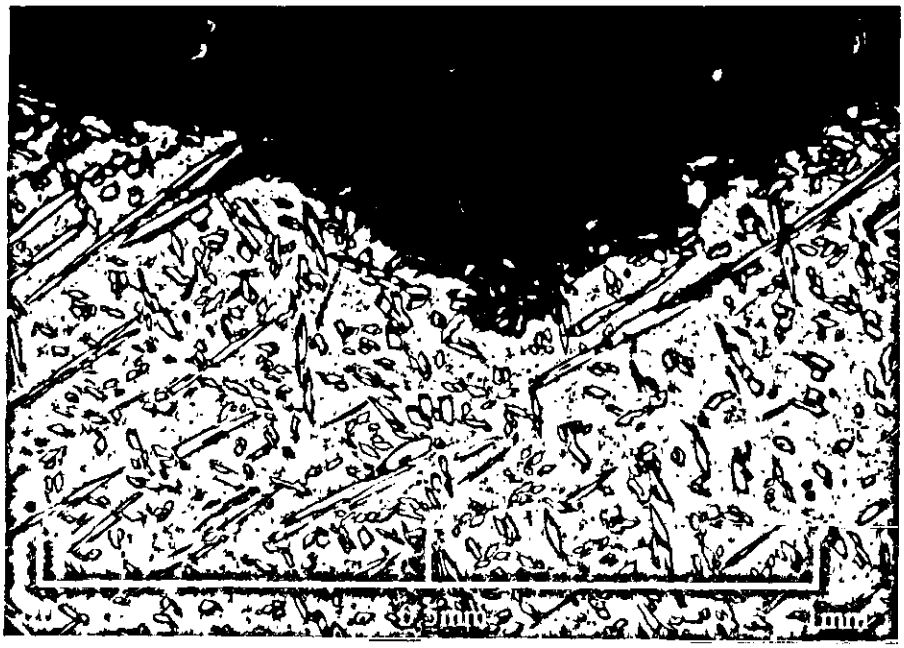

Fig. 4.13 Microstructure of CD4MCu, austenite (light areas), ferrite (dark areas), ×100

5. Discussion

5.1. Electrochemical Polarization

Electrochemical polarization is a valuable method for evaluating the corrosion behavior of alloys. It is fast and reliable for a wide range of alloys. However, there are a few parameters which affect such experiments and create uncertainties in analyzing the results.

In electrochemical polarization, crevice formation is undesirable. However, it inevitably occurs at the Teflon washer located at the working electrode mount (Fig. 3.5). Increasing the torque on the nut may reduce the crevice size; unfortunately a higher torque also assists in the initiation of crevice corrosion by limiting the oxygen diffusion into the crevice. The higher torque also slows down the propagation rate and decreases the hysterisis loop. Most researchers confirm that the crevice potential is lower than the pitting potential[7,12,64]. Therefore, as it is impossible to completely eliminate crevice formation in the presence of compression washers, it is very difficult to find out whether the breakdown potential is due to crevice formation or pitting corrosion. Visual inspection of the specimens after the tests showed different types of attack. For example, cast corrosion-resistant CN7M and Hastelloy C-276 were less corroded at their interface with the washer, while these areas were more corroded for 304L, 316L and 2304.

The other factor which affects the competition between pitting and crevice corrosion is the torque which is inserted on the nut. Although the higher torque moves the breakdown potential to the more active potentials, it slows the propagation of the attacked areas. The pits initiate at higher potentials and repassivate at the lower potentials than the crevices. Thus, the final curve is an altered curve with a lower breakdown potential (which indicates crevice corrosion) and lower the repassivation potential (which indicates pit repassivation as in Fig. 5.1). This may be the main reason for the alteration of the anodic polarization curve, which affects the reproducibility of the tests.

Despite disagreement on the effect of the surface condition on the pitting potential, most studies show the presence of higher concentrations of chromium in passive films on smoother surfaces[16,46,65]. One suggestion is that mechanical polishing covers grain boundaries and inclusions on the metal surface[65]. If we accept this theory, it would be expected that a higher degree of mechanical polishing would have the same effect on the initiation of pitting and crevice corrosion. Most of the previous works confirm the positive effects of finer mechanical polishing on both pitting and crevice corrosion[16,46].

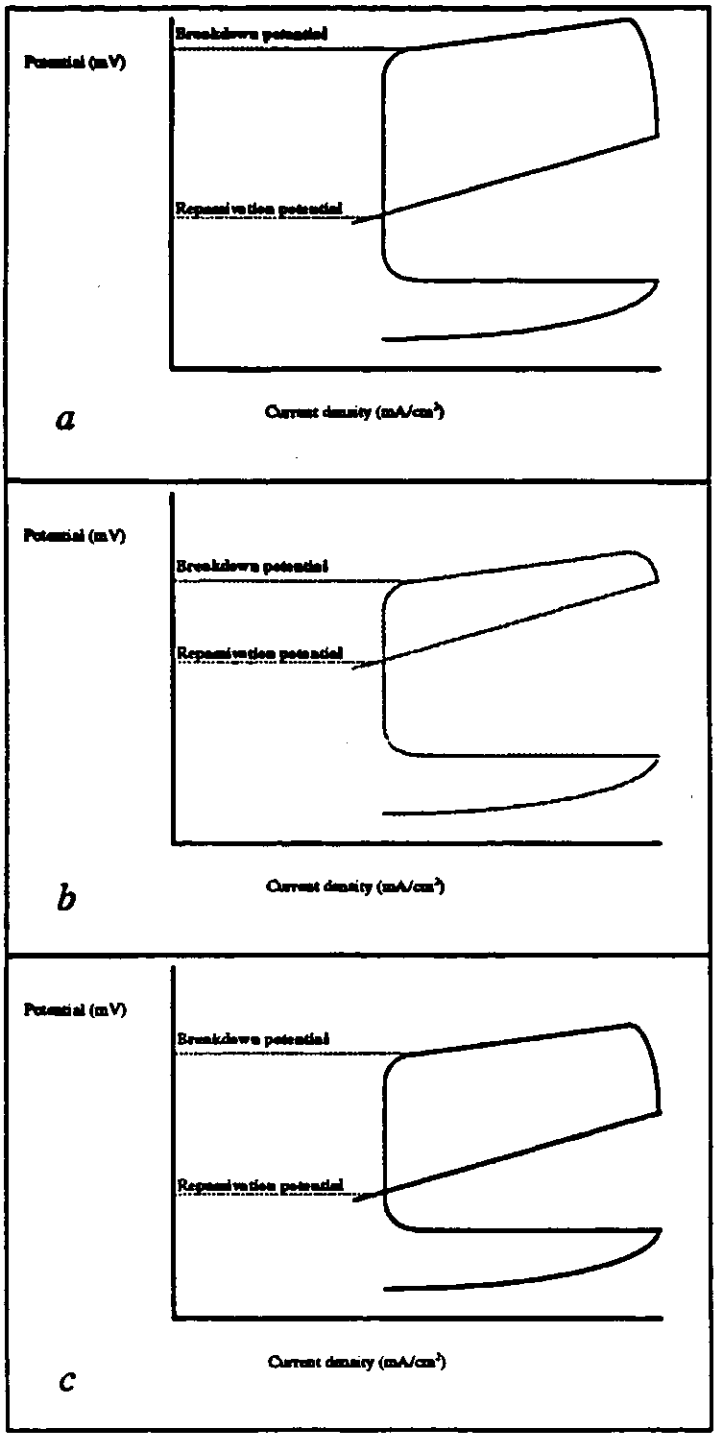

Fig. 5.1 Effect of crevice formation on cyclic polarization curves
(a) the curve for pitting corrosion
(b) the curve for crevice corrosion
(c) the curve for localized corrosion while a crevice has been formed

The effect of chemical treatment was examined by passivating the 904L austenitic in 10% HNO_3 for 20 minutes. Fig. 5.2 shows the electrochemical polarization behavior of 904L with and without chemical treatment. The chemical treatment improved the metal resistance with increasing breakdown potential and decreasing passive current density. Chemical treatment is especially effective in removing the manganese sulfide which segregates on the grain boundary, making this area prone to the initiation of localized corrosion[16,46].

The scanning rate has identical effects on pitting and crevice corrosion. As the scanning rate increases, the breakdown potential shifts into the lower potentials and the hysterisis loop becomes much smaller[65]. The electrochemical polarization of 904L in aerated 0.3N potassium chloride solution confirmed the above statement (Fig. 5.3). The experiment also showed lower passive current density at higher scanning rates. In Chapter Two, it was mentioned that increasing the metal potential increases the passive film thickness until the electrical field across it has the same gradient before changing the potential. However, the passive film can be destroyed because of high electrical fields at high potentials. At higher scanning rates, the passive film cannot grow quickly enough, causing the breakdown of the passive film at lower potentials.

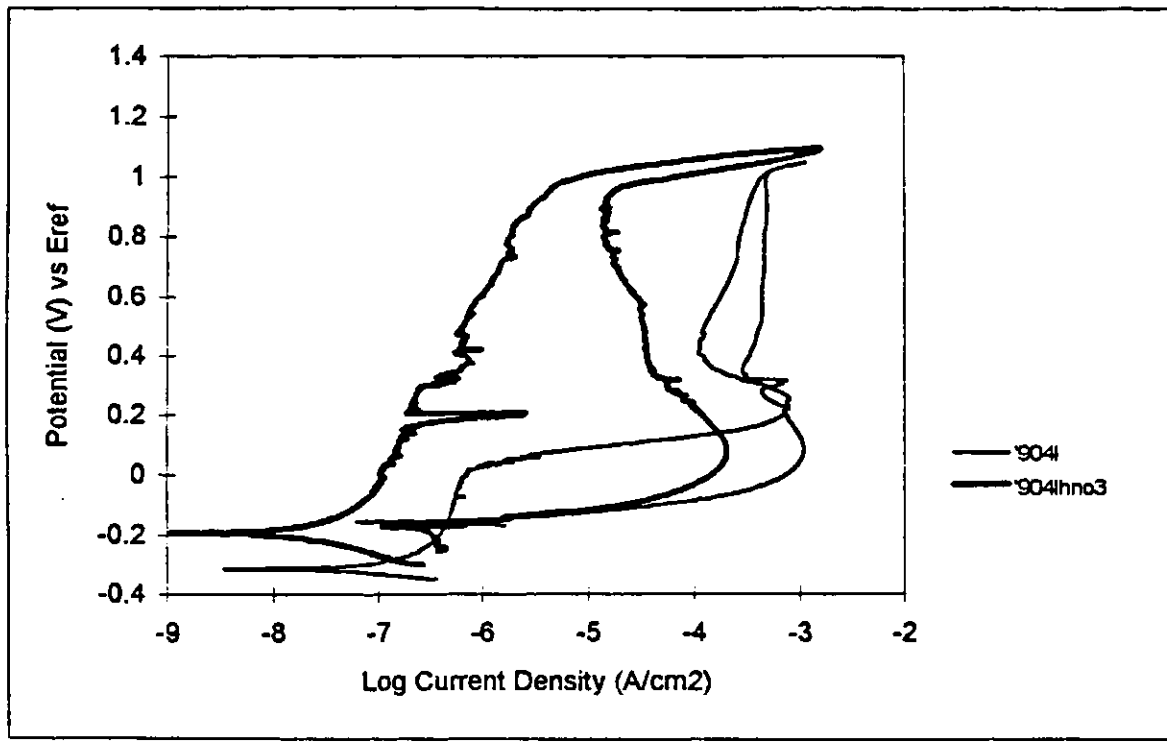

Fig. 5.2 Effect of chemical treatment on electrochemical polarization of 904L without chemical treatment and after 20 minutes immersion in 10% nitric acid

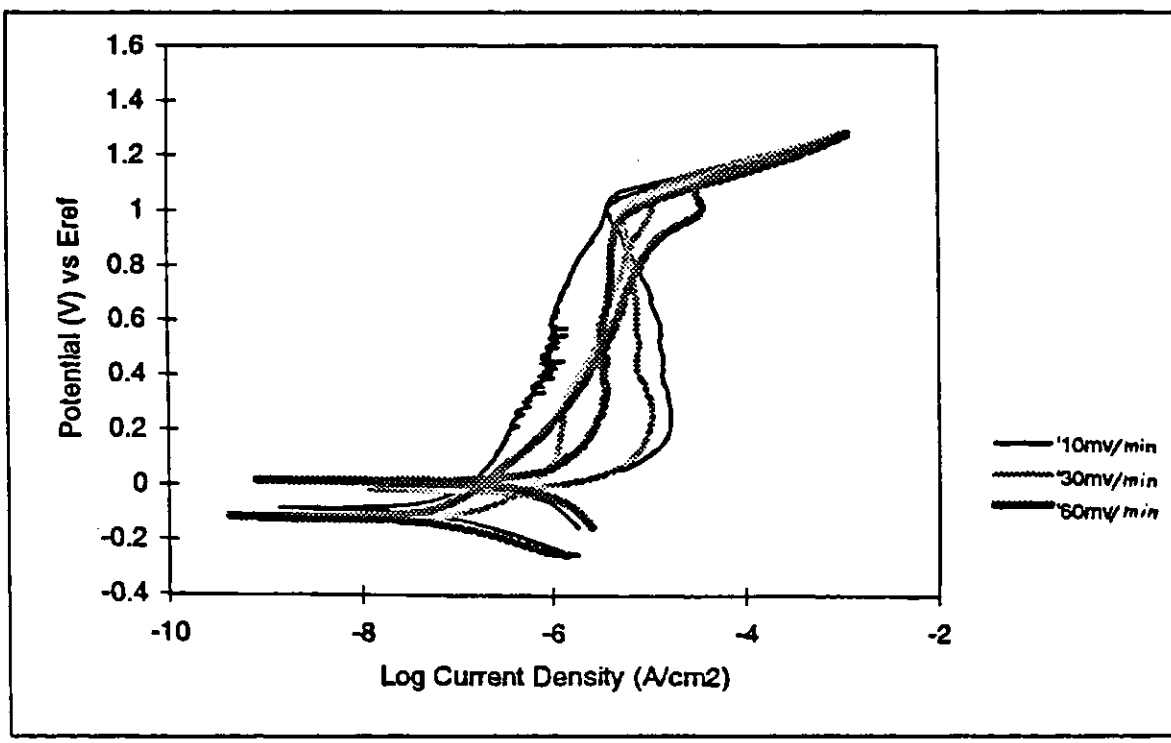

Fig.5.3 Effect of the scanning rate on electrochemical polarization curves

The rotating cylinder is a good apparatus for studying the effect of velocity on corrosion. However, further investigation is required in order to develop its application in corrosion science. In developing an equation for relating the rotation speed to pipe velocity, it was assumed that the corrosion mechanism is controlled only by mass transfer. However, other parameters such as resistance of oxide layer may affect the corrosion mechanism as well. As well, the rotating cylinder cannot be used for two phase flow. In these circumstances it is not surprising that the results from service failure do not correlate with the laboratory tests[7].

5.1.1. Cyclic Polarization

The breakdown and repassivation potentials of the alloys at 22°C and 90°C are shown in Fig. 5.4 and 5.5. The alloys are ranked based on their LCRIs (see Fig. 5.10 for LCRIs values). The 2205 and 2507 duplex stainless steels are very sensitive to high temperatures. This may be the result of two phase interference. 254SMO showed better resistance than any other stainless steel alloy at 90°C. 904L is not very sensitive to temperature and can be used for making equipment which will be utilized in a wide range of operating temperatures. 304L, 316L and CN7M have the same characteristics but with lower resistance which makes them unreliable in high chloride solutions. Cast corrosion resistance CD4MCu has the same repassivation potentials at 22°C and 90°C, but the breakdown potential drops sharply at 90°C. The high breakdown potential for CD4MCu can be related to 25.52 % Cr in its composition. 2304 duplex with 22-23% Cr has almost the same resistance as 316L with 16.3% Cr. This is due to the presence of 2.18% molybdenum in 316L. The better performance of 904L over 304L is due to the

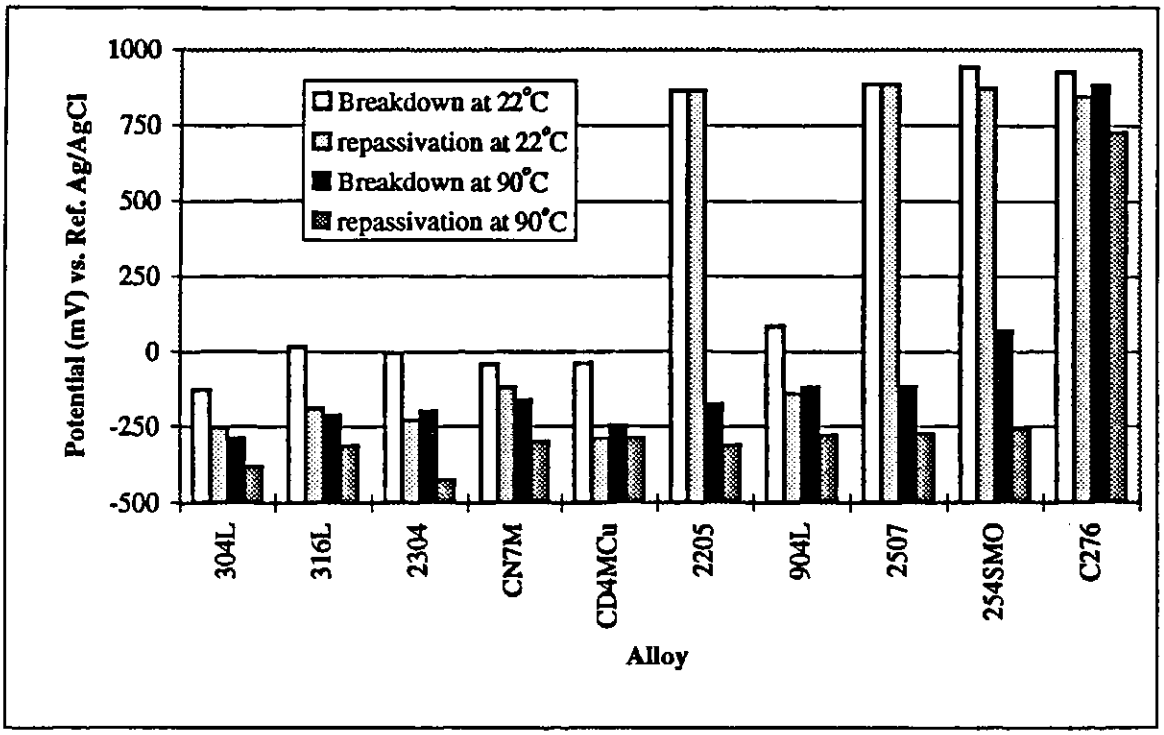

Fig. 5.4 Breakdown & repassivation potentials at stagnant conditions

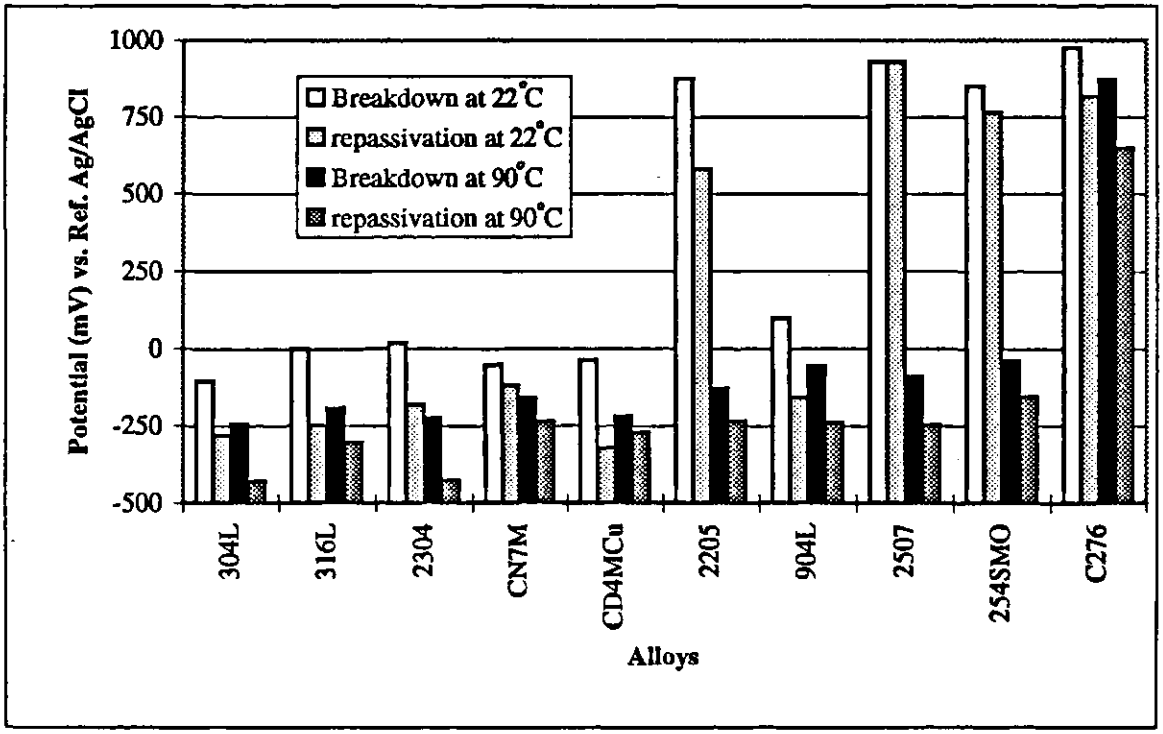

Fig. 5.5 Breakdown & repassivation potentials in flowing conditions

presence of 4.32% molybdenum. The same conclusion can be made by comparing 2304 and 2205 with 0.1-0.64% and 3% molybdenum, respectively. High molybdenum and nitrogen content in 254SMO than in 904L makes the former alloy a more reliable alloy in the high chloride content solutions.

In Chapter Two, it was mentioned that the passivity of an alloy depends mostly on the presence of chromium. Molybdenum slows down the propagation rate of localized corrosion by blocking the active site under the passive film. Analyzing the results of the electrochemical polarization tests shows that high molybdenum content alloys have higher repassivation potential and therefore lower propagation rates during localized corrosion. The comparison between the repassivation potential for 2304 and 316L at 90°C confirms the above statement (Fig. 5.7), while the breakdown potential for these alloys are almost the same (Fig. 5.4 and 5.5).

The effect of flow rate on breakdown potential at 22°C and 90°C are shown in Fig. 5.8 and 5.9. The breakdown potentials in stagnant and flowing conditions are very close to one another, therefore it can be concluded that flow rate does not have a significant effect on the breakdown potential. This agrees with a previous work by Postlethwaite *et al*[52]. The effect of flow rate on the repassivation potential is shown in Fig. 5.6 and 5.7. There is no significant change in the repassivation potential in these two conditions, but as mentioned before, the flowing condition can slow down the propagation rate, especially in shallow pits by sweeping away the high concentration of

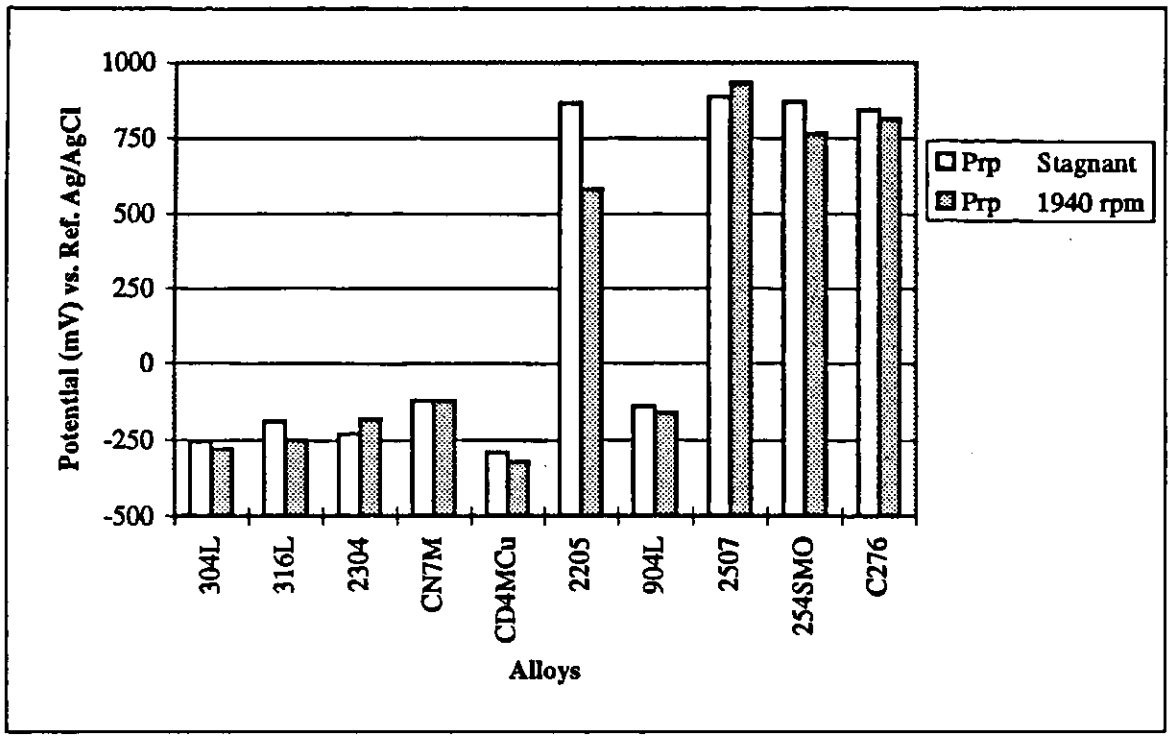

Fig. 5.6 Repassivation potentials at stagnant and flowing conditions at 22°C

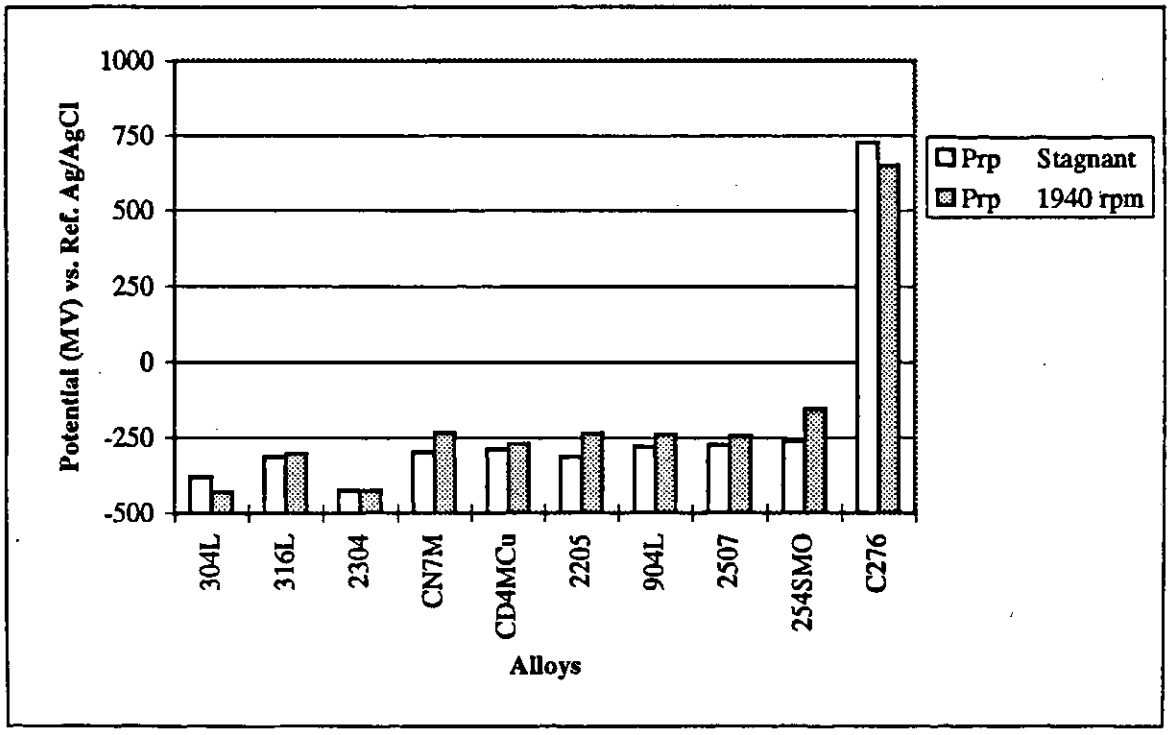

Fig. 5.7 Repassivation potentials at stagnant and flowing conditions at 90°C

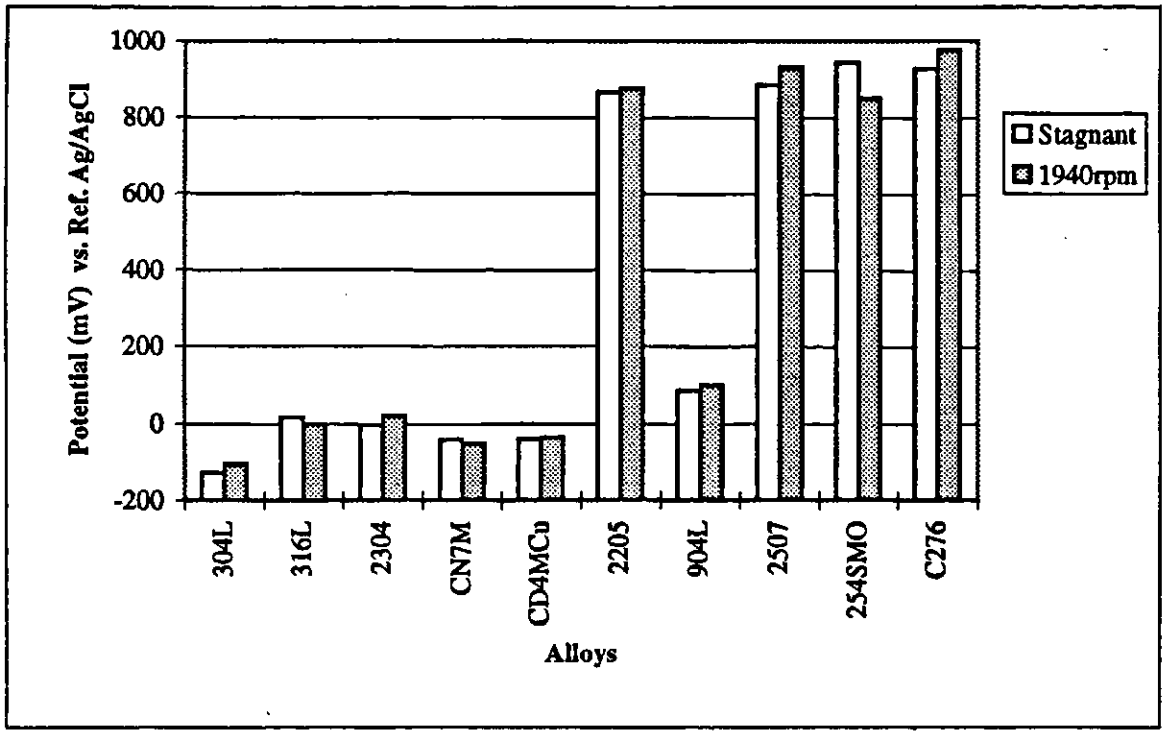

Fig. 5.8 Breakdown potentials at stagnant and flowing conditions at 22°C

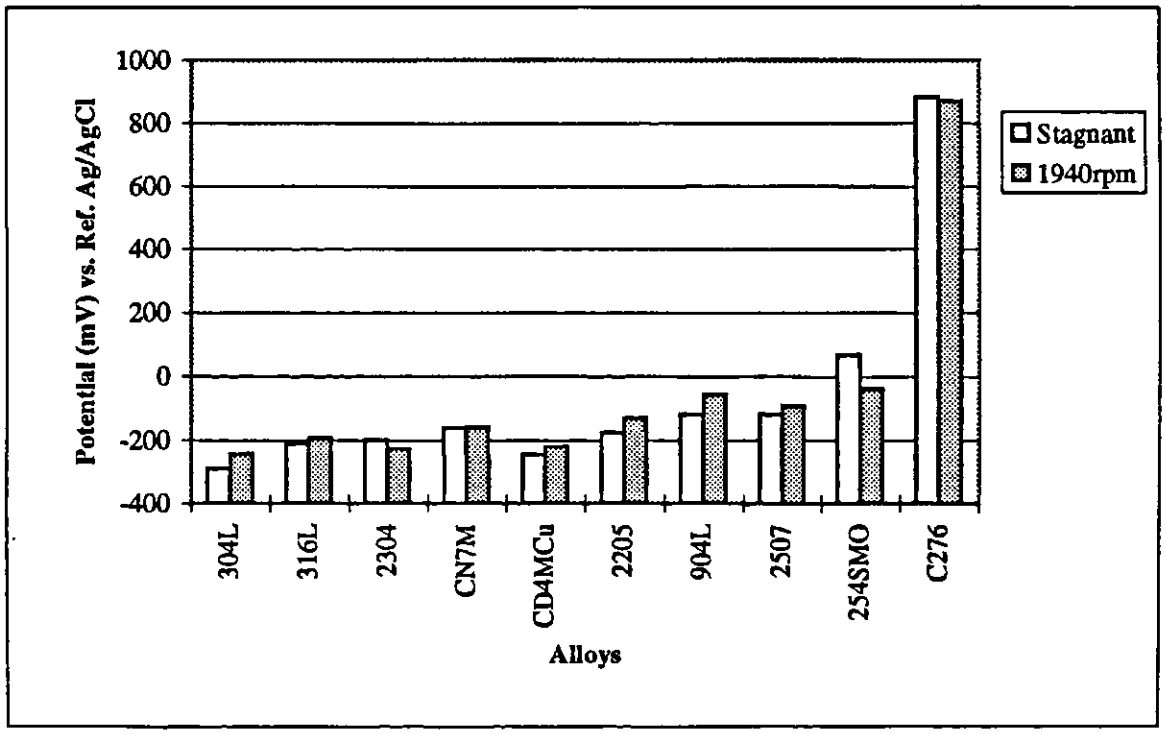

Fig. 5.9 Breakdown potentials at stagnant and flowing conditions at 90°C

hydrogen ions inside the pits[52]. On the other hand, the repassivation potential depends on the pit depth and its value is higher for shallow pits[66]. The repassivation potentials under flowing conditions is higher than under stagnant conditions at 90°C, but at 20°C the repassivation potential is higher in stagnant conditions. Considering the fact that pits are deeper at higher temperatures, the opposite results would have been expected. This observation can be explained by the different transport properties (e.g. viscosity and diffusion coefficient) at different temperatures and higher solubility of the corrosion products at higher temperatures. The corrosion products can plug the pit entrance at lower temperatures.

The passive current density for alloys at different conditions are shown in Fig. 5.10. The passive current density increases for all alloys at higher temperatures, but the passive current density for alloys with a LCRI higher than 33 are less sensitive to the temperature and the flow rate. The passive current density of CD4MCu is higher than other alloys. The non-homogenous casting structure of CD4MCu may be the main reason for its low passive current density.

Electrochemical polarization of Hastelloy C-276 is shown in Fig. 5.11. After passivation of the alloy at a potential of about -235 mV, it stays in the passive state until a potential of about 25 mV where the first transpassive state occurs. The current density in this state increases sharply with increasing the potential for a while until it reaches a more noble potential where the rate of current density change slows down. At the higher potentials the second transpassive zone appears in the potential which is about 875 mV.

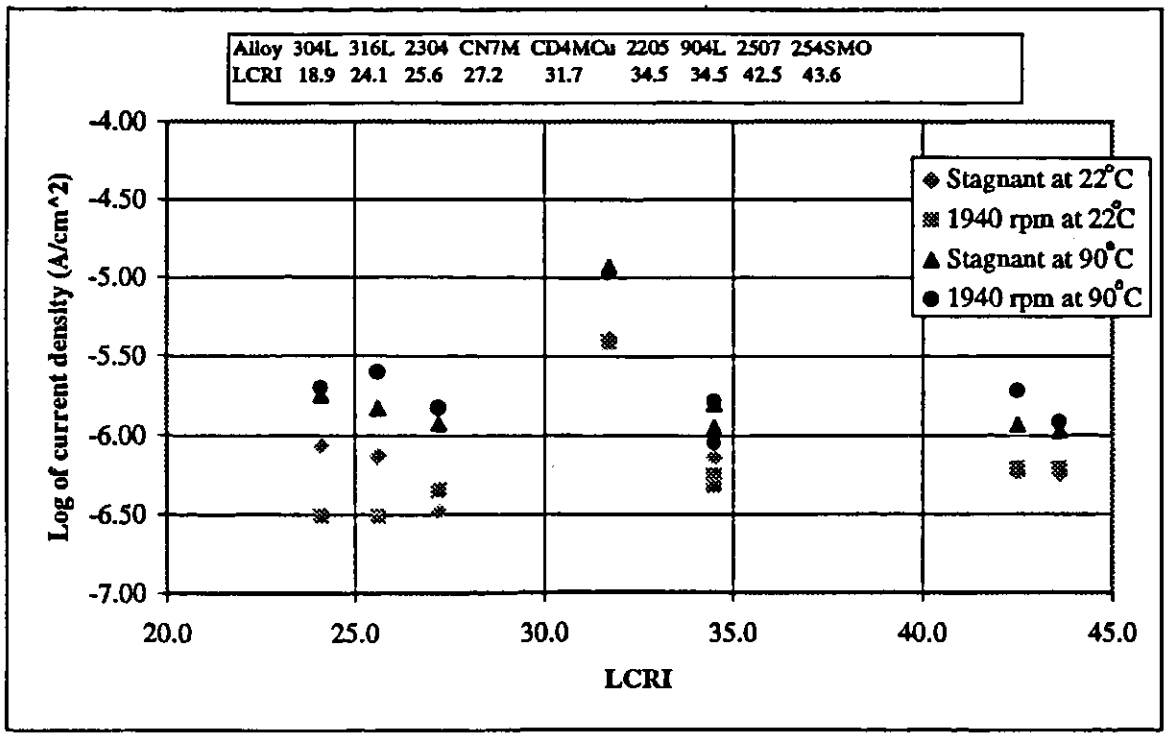

Fig. 5.10 Log of passive current density vs. LCRI

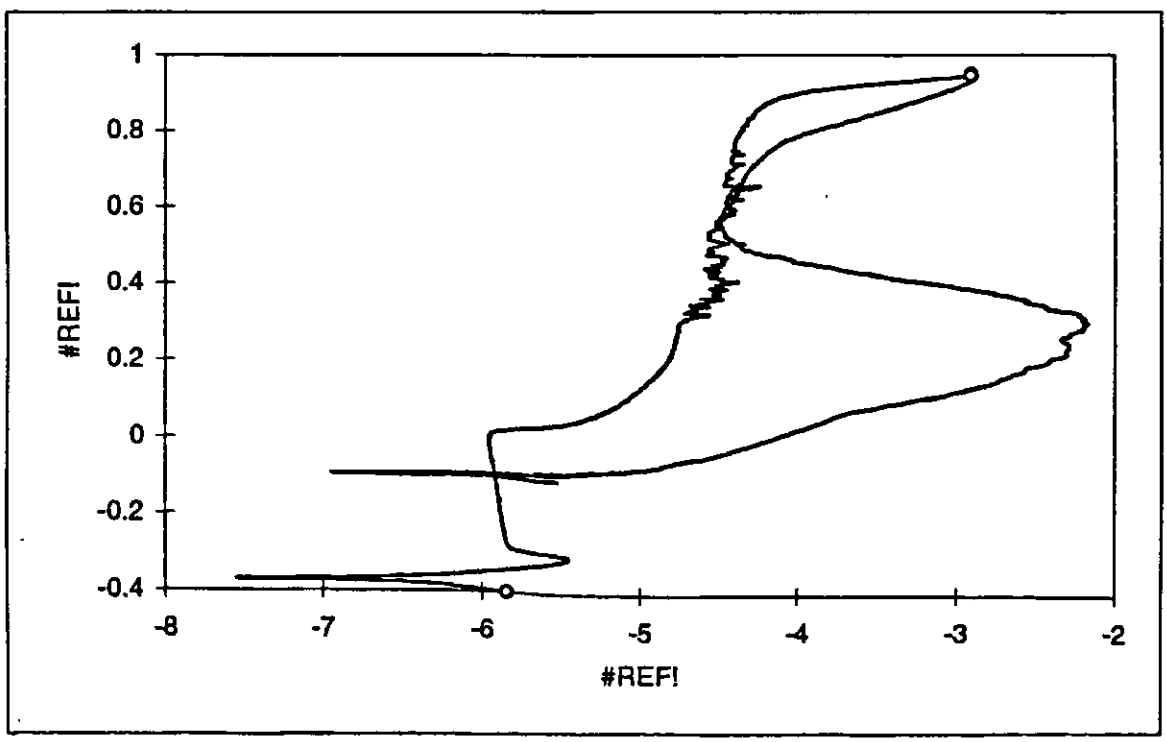

Fig. 5.11 Electrochemical polarization of Hastelloy C-276 at 90°C

It has been reported that the presence of different transpassive zones is related to the dissolution of alloying elements in the Hastelloy C-276[63]. Therefore, the dissolution process in Hastelloy C-276 in the order of passive-transpassive potentials should be iron, nickel, molybdenum, and chromium in the chloride solutions[67]. The higher resistance of Hastelloy C-276 in the chloride solutions is related to dissolution of molybdenum which produces molybdate (MoO_4^{2-}). Molybdate acts as an inhibitor in localized corrosion of stainless steels[63]. Hence, the oxidation reaction of chromium was considered as the breakdown potential for Hastelloy C-276. The absence of this phenomenon in the anodic polarization of Hastelloy C-276 at 22°C confirms the inhibiting effect of molybdate by omitting the first transpassive zone. A similar behavior is also observed in anodic polarization of 904L at 22°C (Appendix C). Therefore, the above theory may be extended for nickel alloys and high nickel austenitic stainless steels.

The presence of two transpassive zones in anodic polarization of CD4MCu may be related to the dissolution of ferrite and austenite phases at different potentials (Fig. 5.12). The microstructure of the exposed alloy is shown in Fig. 5.13. The austenitic pools (light phase) spread around the ferrite matrix (dark phase). It was reported that at lower Corrosion Indices [CI = %Cr + 3.3 (%Mo)], the austenitic stainless steels have higher pitting potentials[39]. Therefore, it can be concluded that the first transpassive zone in the anodic polarization of CD4MCu is related to the oxidation of ferrite and the second transpassive zone to the oxidation of the austenite phase. Fig. 5.13 confirms that the more susceptible phase in the exposure test of CD4MCu is the ferrite phase (see also Fig. 4.12). A similar behavior at lower intensity was observed for duplex stainless steel 2304 (Fig. 5.14). The absence of two transpassive zones in 2205 and 2507 is due to the

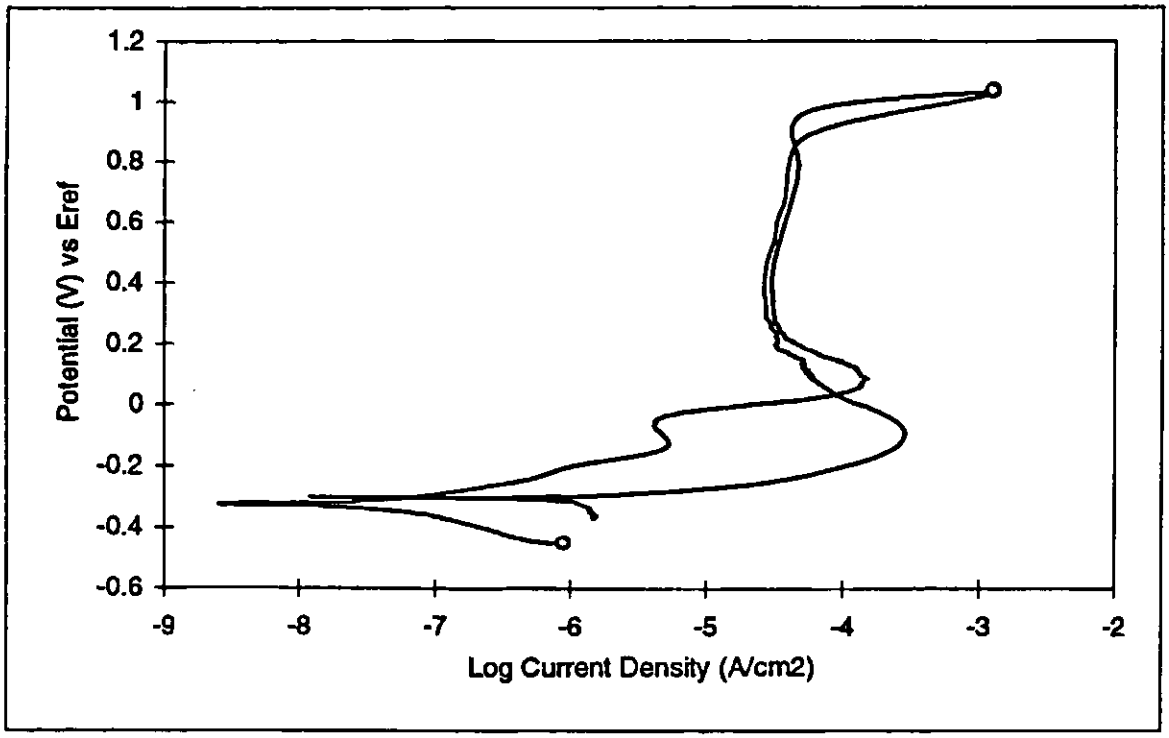

Fig. 5.12 Electrochemical polarization of CD4MCu at 22°C

Fig. 5.13 Microstucture of CD4MCu, x400, austenite (light phase) and ferrite (dark phase)

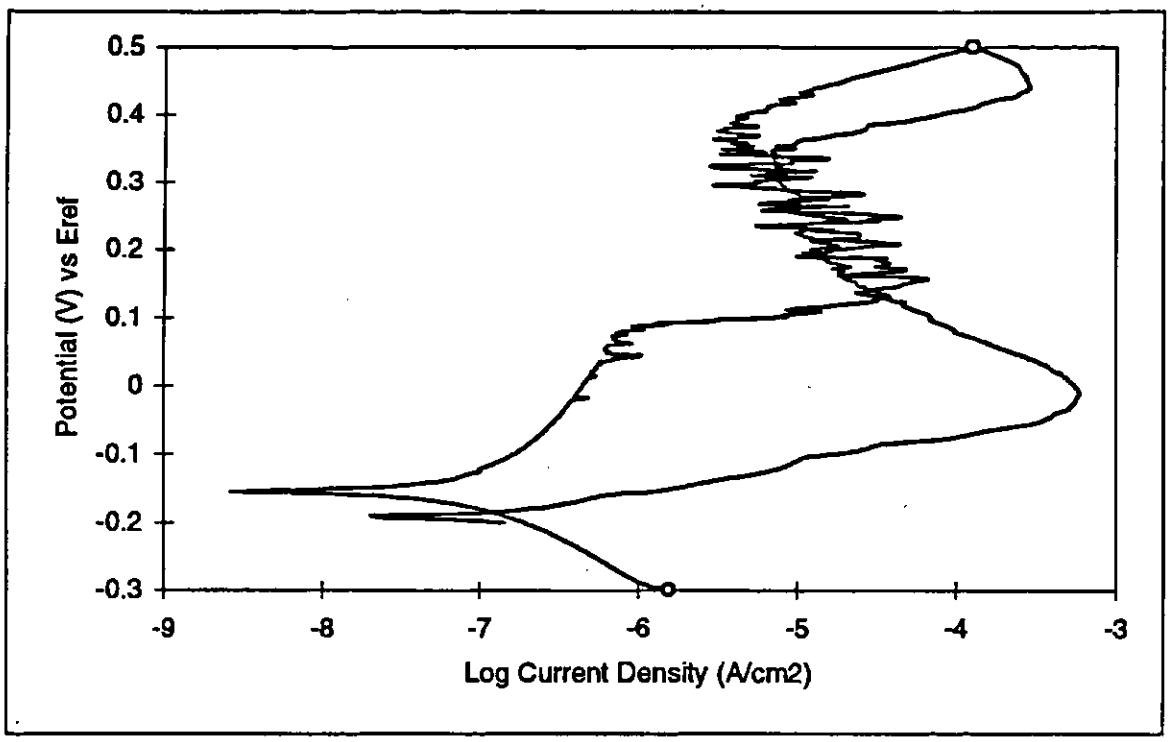

Fig. 5.14 Electrochemical polarization of 2304 at 22°C, aerated

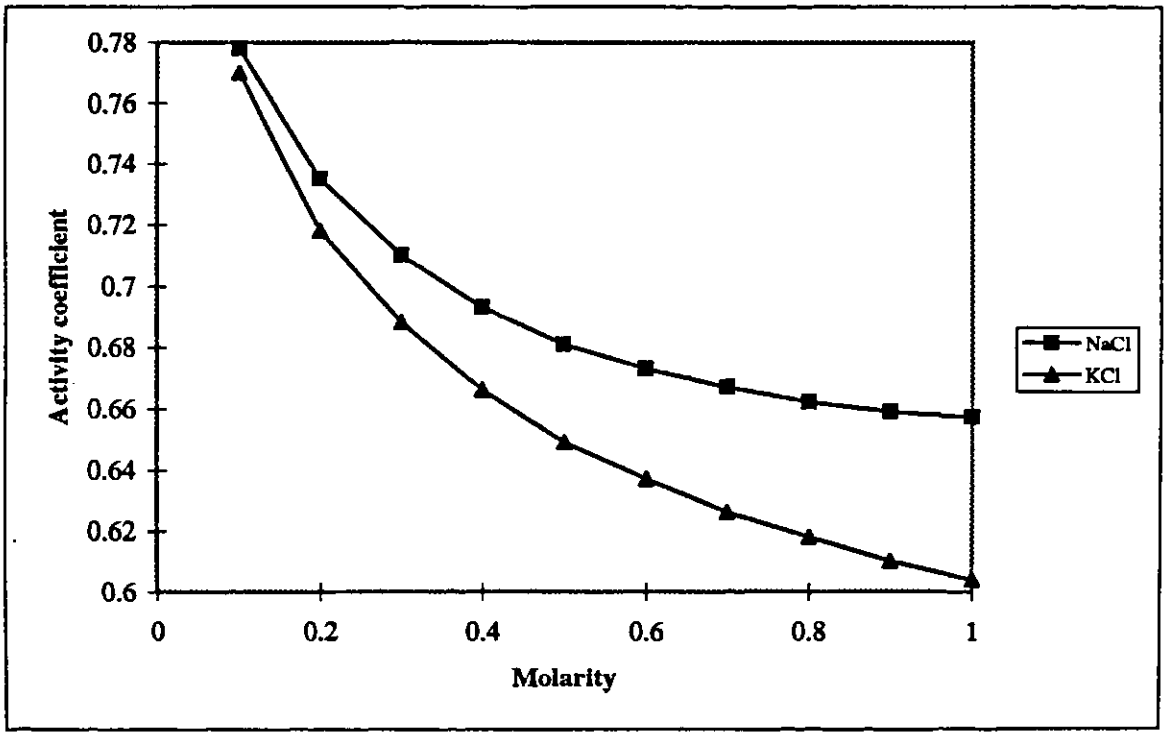

Fig. 5.15 Activity coefficient of alkaline chlorides vs. molarity of the solution

relatively homogenous microstructure of these alloys and the higher chromium and molybdenum concentration of the ferrite phase.

Fig. 5.15 compares the activity of sodium chloride and potassium chloride[31]. The anodic polarization of 304L and 316L austenitic stainless steels in 0.3N sodium chloride and potassium chloride solutions show that in spite of the higher activity of sodium chloride, potassium chloride is more corrosive in aerated solutions (Fig. 5.16.*a* and 5.17.*a*). The more corrosive nature of the potassium chloride solution relates to its higher conductivity in aqueous solutions (Fig. 2.8). The breakdown potential for alloys in the aerated KCl solution is lower than that for alloys in the NaCl solution. The identical anodic polarization behavior of the alloys in the deaerated solutions is unclear (Fig. 5.16.*b* and 5.17.*b*).

The increased pH value in the bulk chloride solution during localized corrosion can be explained by the cathodic reaction (Fig. 4.3 and 4.4). In aerated chloride solutions, the oxygen reduction in the areas around the pits or crevices increases the pH value; while in deaerated solutions the hydrogen evolution reaction reduces the hydrogen ions concentration and increases the pH value in the bulk solution.

The breakdown potentials of the tested alloys are compared with their LCRI in Fig. 5.18 and 5.19. The LCRI can be used for predicting the resistance of alloys at 90°C, but at 22°C LCRI is not a reliable index for ranking alloys, mostly because of the outstanding resistance of duplex 2205 and 2507 and austenitic 254SMO at 22°C.

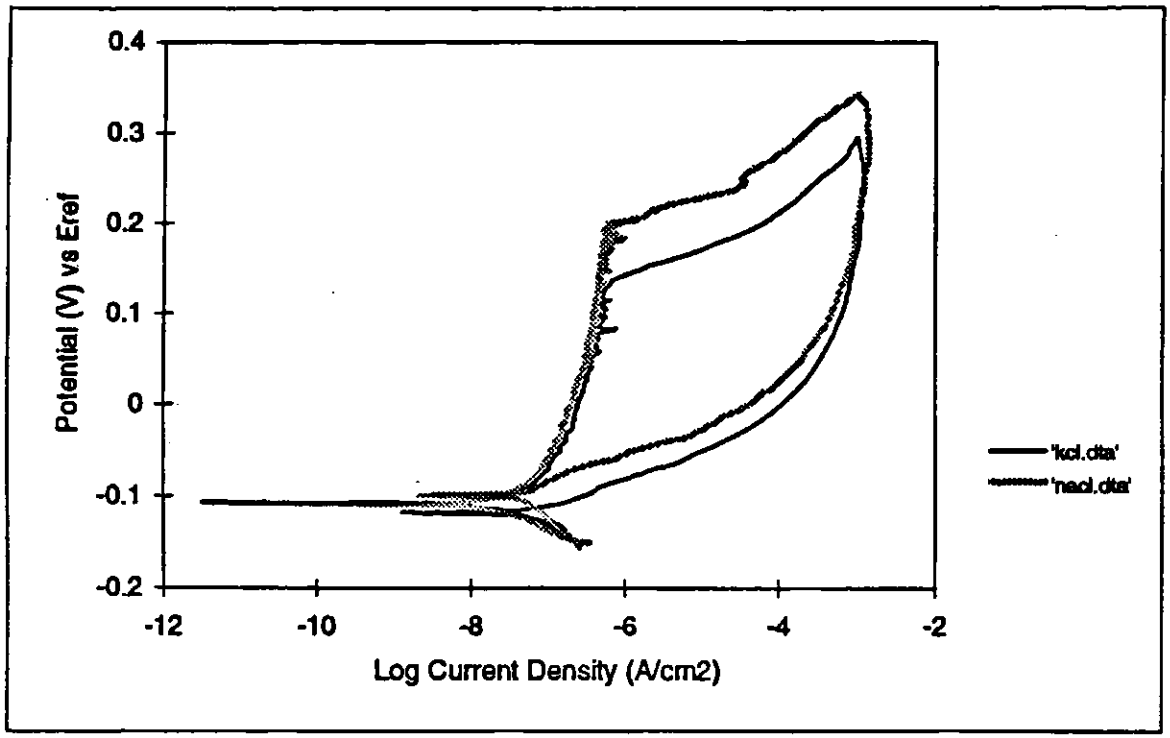

Fig. 5.16.*a* Electrochemical polarization of304L in 0.3N alkaline chlorides, aerated

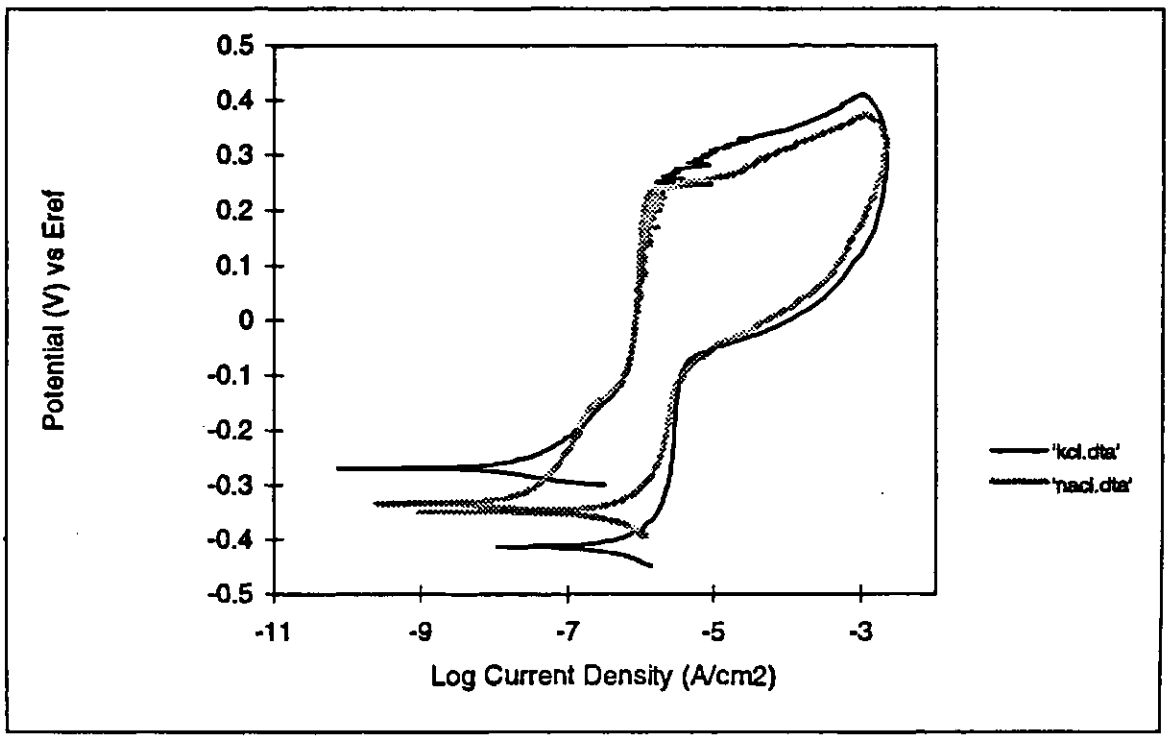

Fig. 5.16.*b* Electrochemical polarization of 304L in 0.3N alkaline chlorides, deaerated

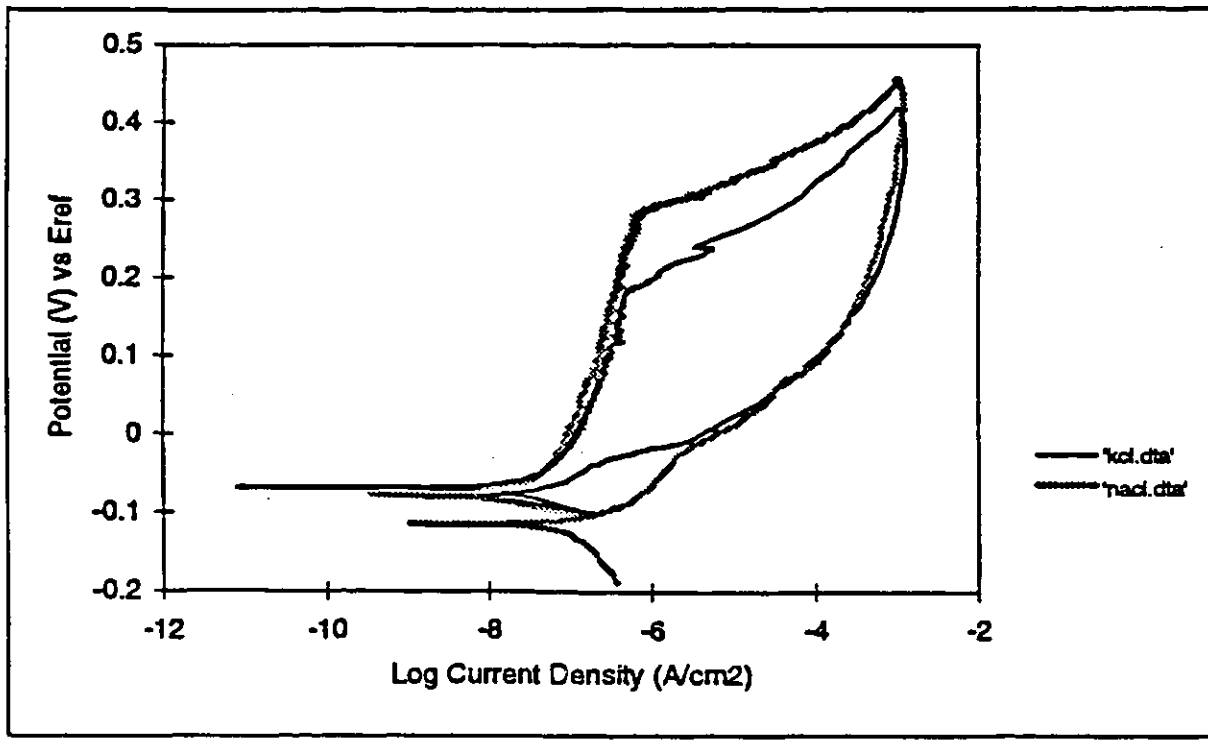

Fig. 5.17.*a* Electrochemical polarization of 316L in 0.3N alkaline chlorides, aerated

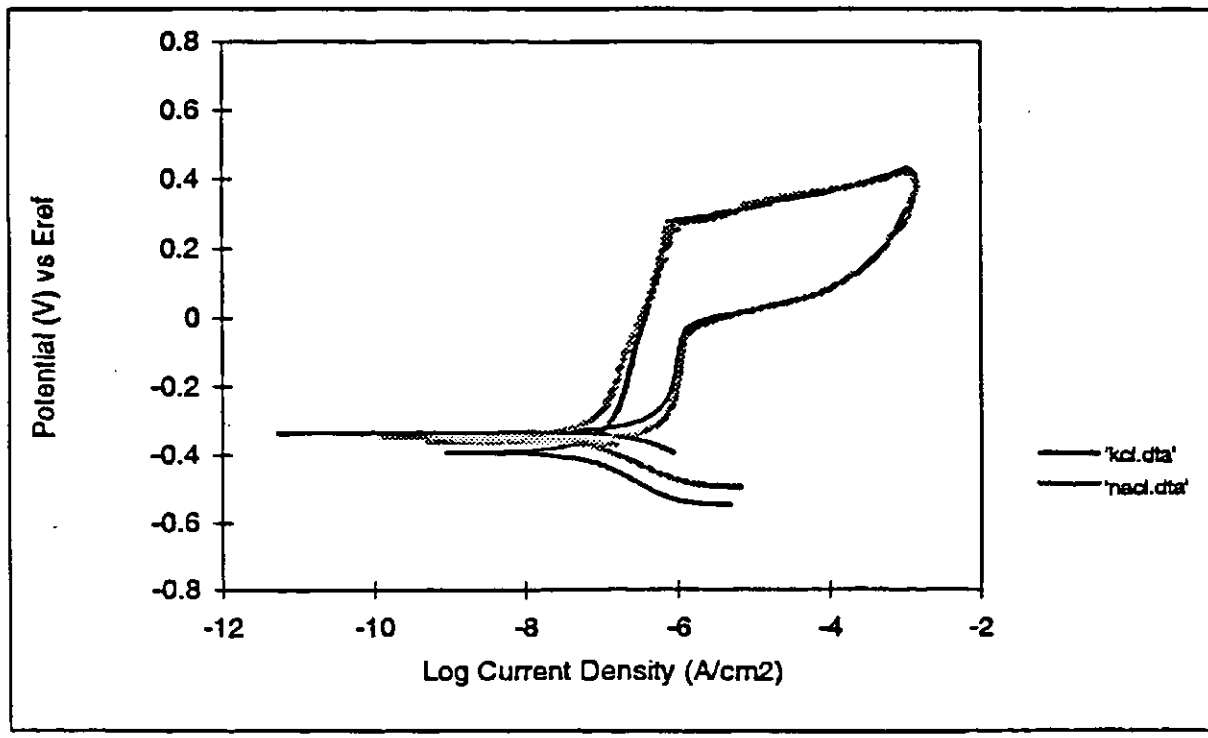

Fig. 5.17.*b* Electrochemical polarization of 316L in 0.3N alkaline chlorides, deaerated

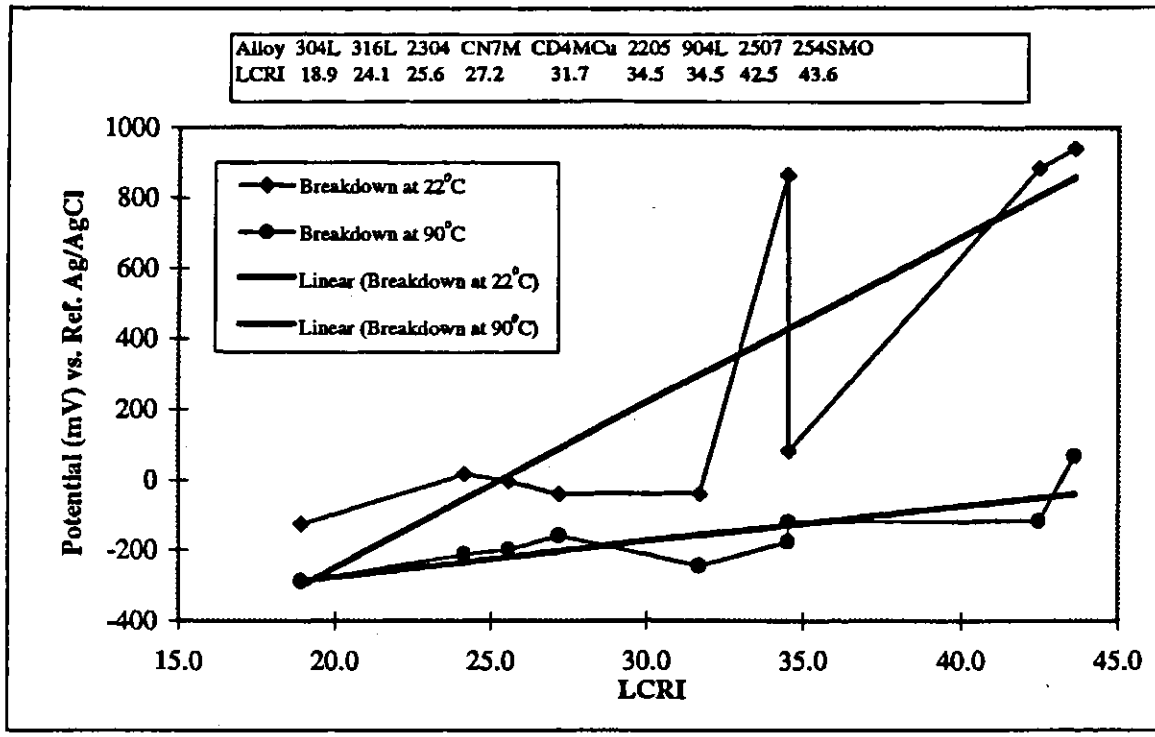

Fig. 5.18 Breakdown potential vs. LCRI under stagnant conditions

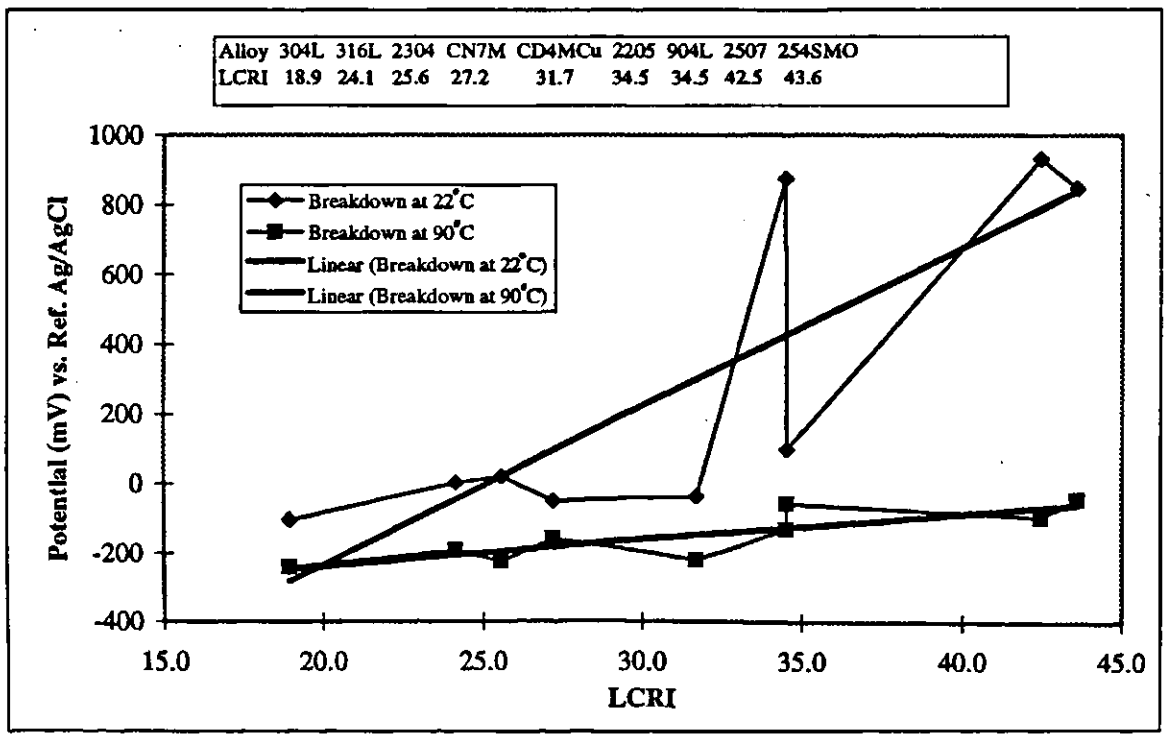

Fig. 5.19 Breakdown potential vs. LCRI under flowing conditions

5.2. Exposure tests

Localized attack is a random process and any defect on the surface of the alloy can produce a pit. The resistance of an alloy to localized corrosion depends on its resistance to initiation and propagation of the attack. Therefore, the number of pits indicates the resistance of alloys to the initiation of pits, while the depth of pits indicates their resistance to the propagation of attack. The results of exposure tests are shown in Fig. 5.20 and 5.21. In localized corrosion, the metal failure is caused by the deepest pit. To determine the general resistance of the metal, the average pit depth is used. However, in this study, in order to account for the random nature of the pitting process, the average depth of the five deepest pits was used in order to analyze the exposure test results.

The samples were immersed vertically in the solution so that their surfaces on both sides were exposed to the environment. However, it should be noted that the upper and lower edges had different locations in the solution. In exposure tests, the specimen edges are extremely prone to corrosion. Pitting was more severe at the edges for austenitic stainless steel 304L, than for 316L and 904L, respectively. The pits on the edges appeared mostly on the upper surface, probably because of the gravity direction in the pitting process and the accumulation of acidic solution at the end of the pits on the upper edge. The presence of pits on the edges protected the area around the pits so that no pits were formed on the metal surface. Thus, it is difficult to determine whether the

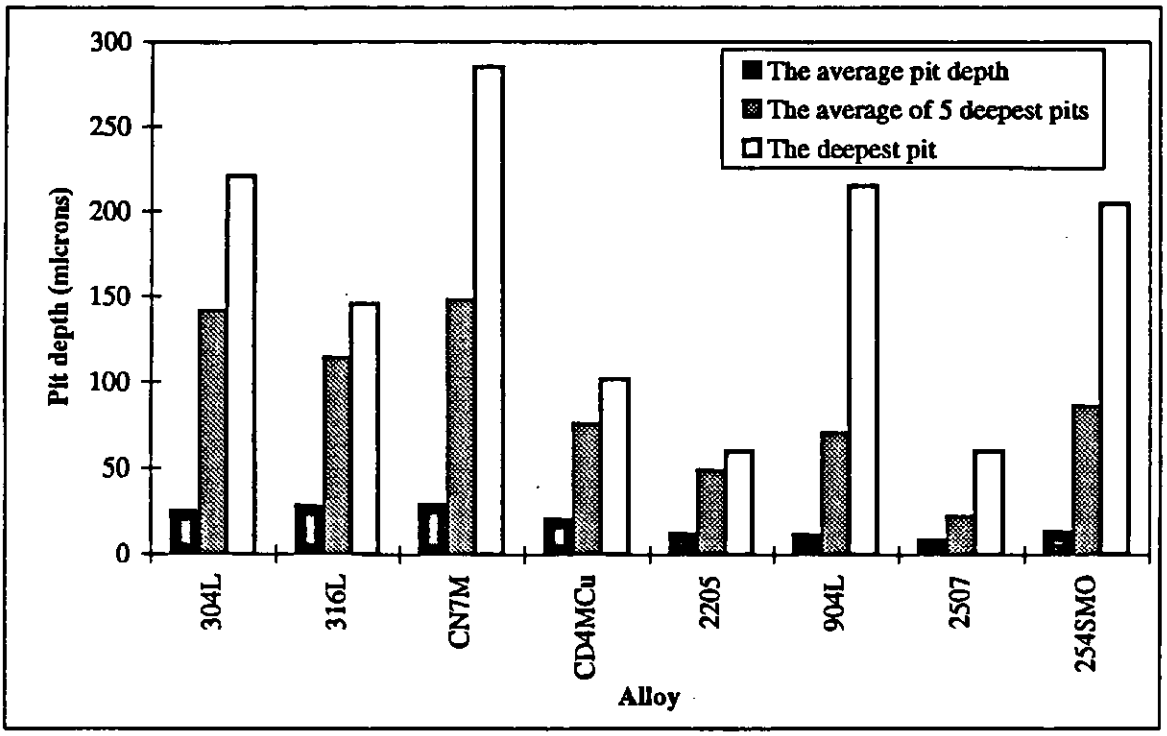

Fig. 5.20 Exposure test results in potash brine after 30 days, 90 C

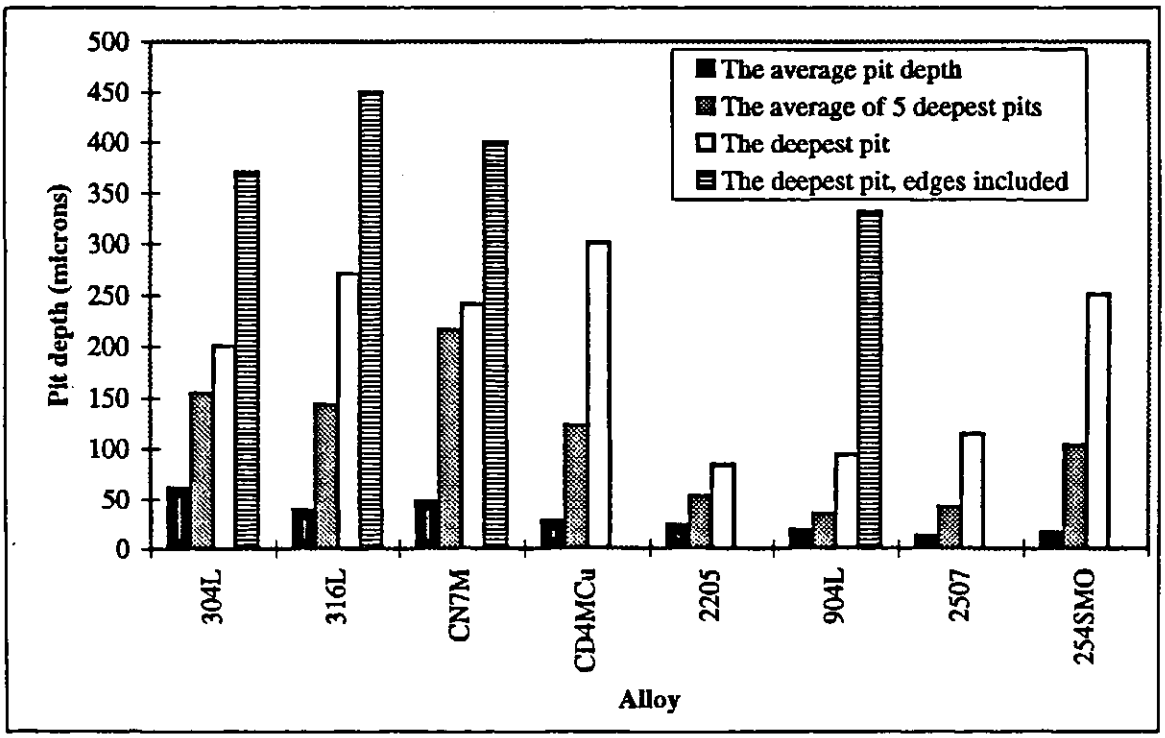

Fig. 5.21 Exposure test results in potash brine after 60 days, 90 C

pits on the edges protected the rest of the sample or the surface itself had enough resistance in the solution. As mentioned in Chapter 4, the other parameters which are involved in edge pitting are the stress residuals on the edges resulting from machining and the coarser surface conditions on the edges which make both these areas more susceptible to localized attack. Extension of the attack at the end of a pit (located on the edge of 316L) is shown in Fig. 5.22. Such a crack is the result of stress corrosion cracking in chloride solutions. Stress corrosion cracking was observed in austenitic 304L and 316L on these areas. When the crack is very deep, it is not possible to relate it to the stress residual during the specimen cutting. Therefore, the stress may also be produced during the process of metal production. In spite of the pit formation on the edges, stress corrosion cracking was not observed in austenitic 904L. It can be related to 24% nickel in austenitic 904L which increases the resistance of the alloy to stress corrosion cracking. Fig. 5.20 and 5.21 show that the deepest pits on 304L, 316L, and 904L are present at the edges. The pits at the edges were not considered in the data analysis, but as mentioned before, the interference of the anodic dissolution of alloys at the edges with cathodic protection of the areas adjacent to the edges is not clear.

Fig. 5.22 Stress corrosion cracking of 316L, ×100

The average of the five deepest pits for the tested alloys show a better resistance for duplex stainless steels than other alloys. High austenitic stainless steel 904L and 254SMO also had a good resistance in the solution. The presence of few wide and deep pits around the crevice area signifies that 254SMO has a lower resistance than 904L, but visual inspection of 254SMO after the tests showed less accumulation of corrosion products on the surface of 254SMO than the other alloys. The pit distribution histograms show the details of pit depth distribution of the alloys (Appendix D).

Cast corrosion-resistant CD4MCu showed better performance than CN7M. The presence of nitrogen in CD4MCu could reinforce the molybdenum effect and increase its resistance in service conditions.

Duplex stainless steel, with its ideal structure, contains equal austenitic and ferritic phases and it is free of intermetallic and nonmetallic compounds[68]. Fig. 5.23

shows the microstructure of 2507. The alloying elements are distributed in ferrite and austenite phases with different ratios; therefore, when studying the corrosion resistance of duplex stainless steels the composition of each phase should be individually considered rather than the overall ratio of the alloying elements. Table 5.1 shows the chemical composition of each phase and the relative LCRI for 2205 and 2507[27]. There is no agreement on the more susceptible phase to localized corrosion in duplex stainless steels. Ujiro *et al* used [%Cr + 3 (%Mo)] as a corrosion index and compared the austenitic and ferritic stainless steels with identical indices. It was mentioned that in the region where the corrosion index exceeds 32, ferritic stainless steels show superior pitting and higher resistance to crevice corrosion resistance compared to austenitic stainless steels. It was also believed that chromium and molybdenum are more effective in ferritic structure than austenitic. Another work refers to preferential attack in the austenitic phase[39].

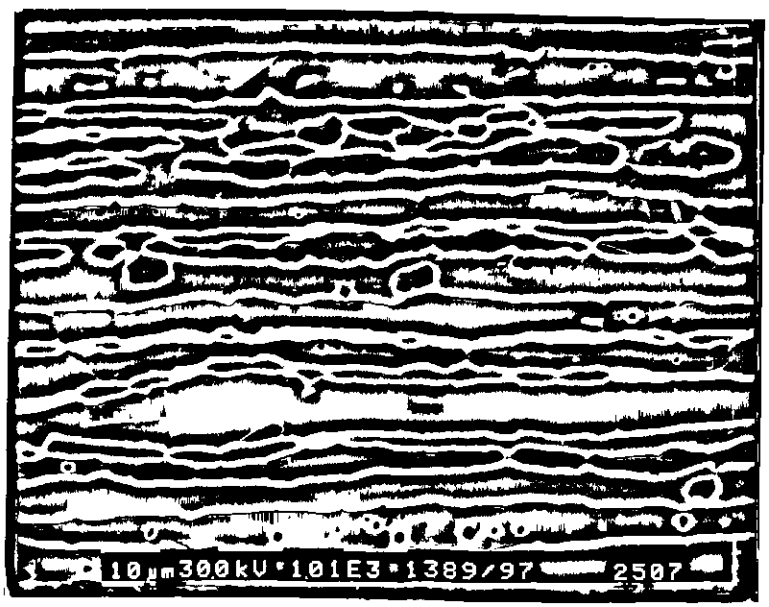

Fig. 5.23 Microstructure of annealed duplex stainless steel 2507

Table 5.1 Chemical composition of each phase in duplex stainless steels[27]

Alloy	Phase	%Cr	%Ni	%Mo	%N	LCRI
2507	Ferrite	26.5	5.8	4.5	0.06	42.5
2507	Austenite	23.5	8.2	3.5	0.48	42.5
2205	Ferrite	24.3	4.1	3.8	0.05	37.6
2205	Austenite	20.2	7.1	2.2	0.24	30.6

All previous works confirm the initiation of localized attack on the phase boundary and propagation of pits in austenitic phase. These investigations were done in Hank's solution, but with different kinds of alloys (wrought and cast)[69,70]. Troman *et al* confirm the initiation of pits at the boundaries. It was shown that in 1M NaCl solution the austenite phase is more susceptible in cast duplex stainless steels, whereas ferrite is more susceptible in wrought stainless steels[71]. Among the disputes about the preferential phase in the localized corrosion of duplex stainless steels, Troman's idea seems more rational. He believes that the behavior of phases in duplex stainless steels differ from single phase because of the presence of phase interfacial boundaries and solute partitioning effects like MnS inclusion and nonmetallic precipitation. The susceptibility of ferrite/austenite interference may be related to phase transformation and segregation effects, resulting in depleted chromium and molybdenum in this interface[71]. The microstructure of austenitic alloys shows precipitation of carbide at grain boundaries. This precipitation consists of Cr_xC_y and Mo_xC_y. In both cases, the depleted area around the carbides are prone to localized corrosion. Due to higher energy of the grain boundaries than the grain itself, attack usually initiates at the depleted areas on the grain boundaries[71].

Sharp reductions in breakdown and repassivation potentials of 2205 and 2507 in electrochemical polarization (Fig. 5.4 & 5.5) may be related to the more susceptible interfacial defects and the greater segregation of chromium and molybdenum in this area at higher temperatures. The SEM examination of 2507 duplex stainless after the exposure test confirmed the initiation of pits in the boundary of phases and their propagation in the ferrite phase as illustrated in Fig. 5.24. The higher resistance of the austenitic phase, in spite of higher chromium and molybdenum content in the ferrite phase relates to the higher solubility of nitrogen in austenite than in ferrite[72]. Consistent with the above statement, it was shown that pitting occurs preferentially in the ferrite phase of high nitrogen content duplex stainless steels and in the austenite phase of low nitrogen duplex stainless steels[71].

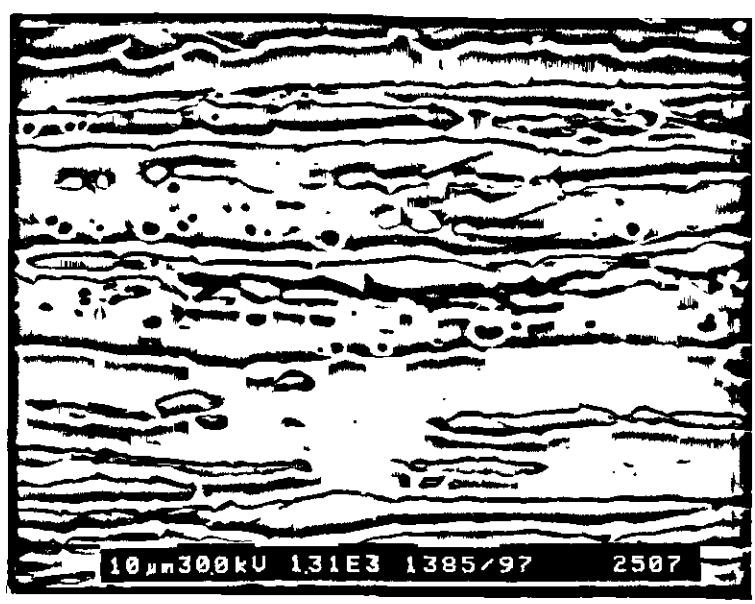

Fig. 5.24 Preferential attack of ferrite phase in localized corrosion of 2507, austenite (light areas), ferrite (dark areas)

The production of a passive film on stainless steel surfaces is due to the presence of chromium, even though chromium, nickel oxide, and iron oxide and hydroxide are present in the passive film[10]. Molybdenum and nitrogen reinforce the metal base. It has been reported that the molybdenum content inside pits is greater than in the metal matrix[35]. Also, the nitrogen content of the oxide film sub-layer increases several times more than its amount in the metal matrix. In the presence of molybdenum, nitrogen produces an ammonium ion which increases the pH in the absence of a passive film and decreases the severity of localized corrosion[35,36].

Statistical evaluation of pitting corrosion of stainless steels has not been studied as much as the other subjects. The statistical study of a specimen after exposure testing can give some information about the distribution of pits (Appendix D), but it is not possible to make a conclusion with respect to long term service conditions. Among the several statistical studies on pitting corrosion, those by Aziz[73] and Crews[74] are more valuable. These studies were focused mainly on the deepest pit and estimating the life time of a pipe in a corrosive media. Unfortunately in the present study it was not possible to perform such a test due to the lack of time.

The general feature of pits on the surface of CN7M is shown in Fig. 5.25 to 5.27. The square small pits are spread around the main pit. The microscopic feature of one of these pits shows its regular geometry. Such a regular shape was observed by the "Edge Pit Technique". An edge pit is the shaped solution cavity produced by the prolonged action of a natural or artificial etchant[75]. Regarding the fact that no etchant was used in producing the square pits on the CN7M, the presence of these pits may be due to the

high corrosion potential of the alloy. The regular shape of the square pits (Fig. 5.26) is related to the intersection of the cleavage planes and an edge dislocation in the alloy matrix. The high energy level of the area around the edge dislocation is the main reason for the formation of pits in this area.

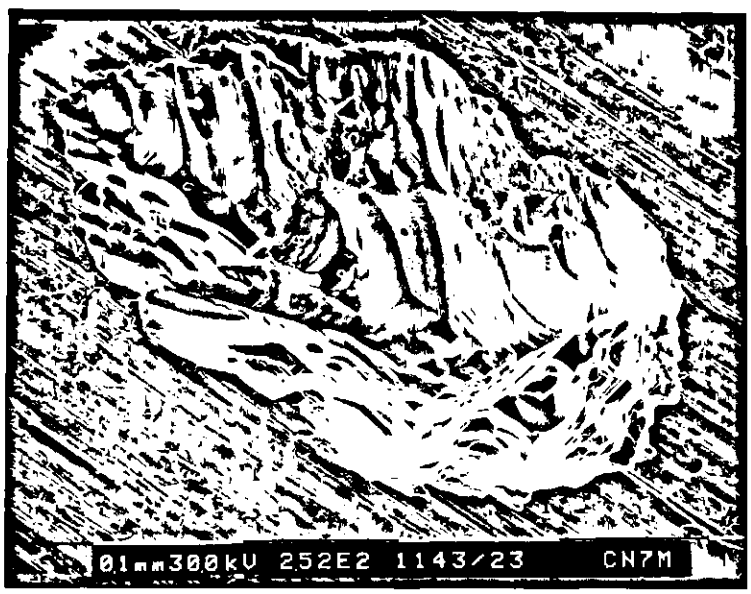

Fig. 5.25 Scanning electron micrograph of CN7M after the exposure test for 60 days

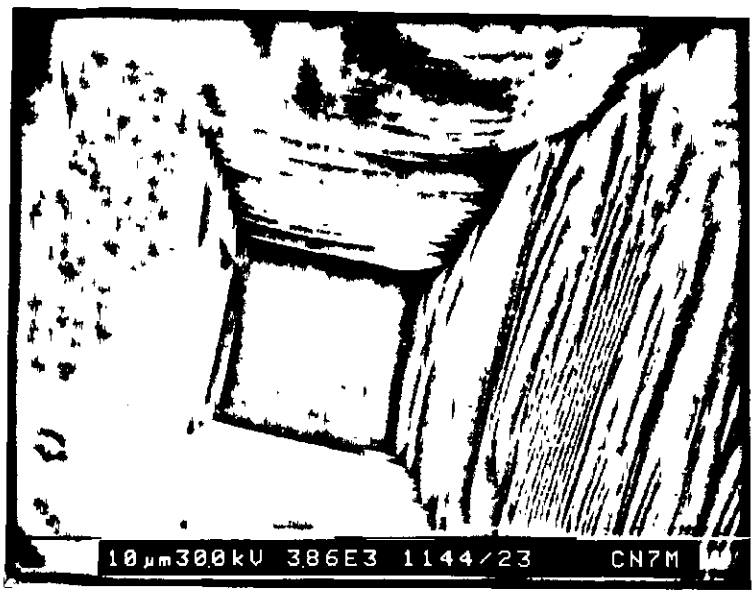

Fig. 5.26 Scanning electron micrograph of a square pit on CN7M

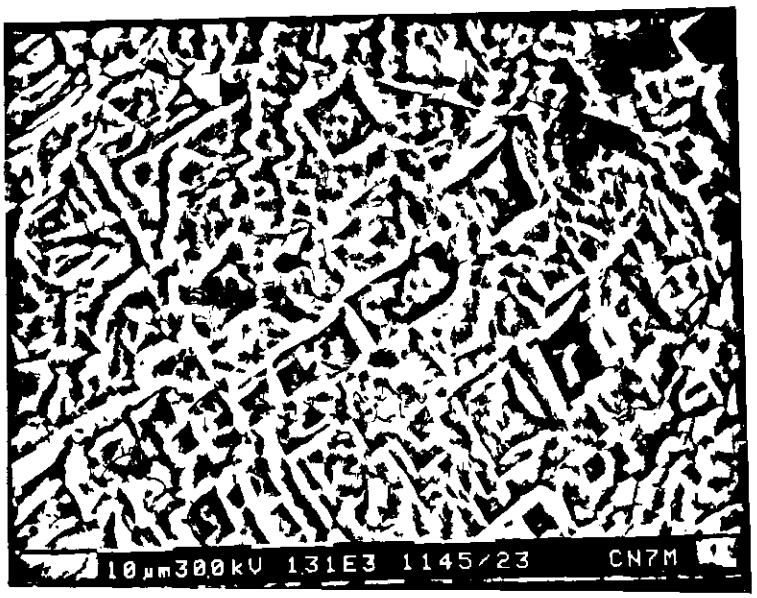

Fig. 5.27 Scanning electron micrograph of initiated square pits on CN7M

The results of the exposure tests are compared to those of electrochemical polarization (Fig 5.28 and 5.29) for austenitic and duplex stainless steels. It was expected that the breakdown potentials increase by increasing LCRI. It was also expected that the pit size would decrease by increasing LCRI. The average pit depth of alloys shows a smooth decrease with increasing LCRI. The higher average pit depth of 316L compared to 304L is due to overlooking the pits on the edges in data analysis. The 2507 duplex steel showed better resistance than the 254SMO austenitic steel in exposure tests. The average depth of the five deepest pits for the 2205 and 2507 duplex shows the better resistance of duplex than the austenitic stainless steels with almost the same LCRI. The sample holder in exposure tests was made of Hastelloy C-276 and no pits were observed on it.

The morphology of pits depends on the metallurgy of the alloy and the chemistry of the environment. Pits may be shallow, elliptical, undercut, or subsurface. Typical pit morphologies are sketched in Fig. 5.30. The pit profiles for some of the alloys are compared with the typical morphologies in Fig. 5.31 to 5.36.

Economics is one of the most important factors in material selection. The purchase cost for some of the tested alloys is listed in Table 5.2. Here it should be mentioned that the fabrication costs for various alloys are close to each other and are independent of the purchase cost.

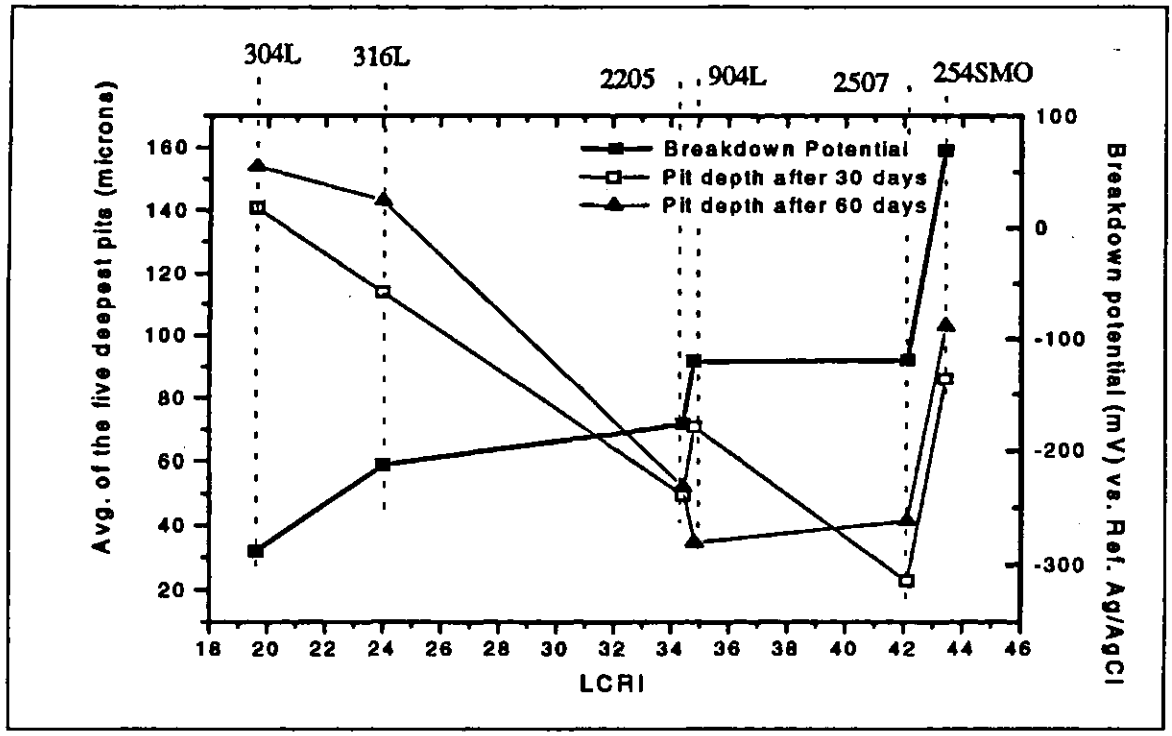

Fig. 5.28 Breakdown potentials and the average depth of five deepest pits vs. LCRIs

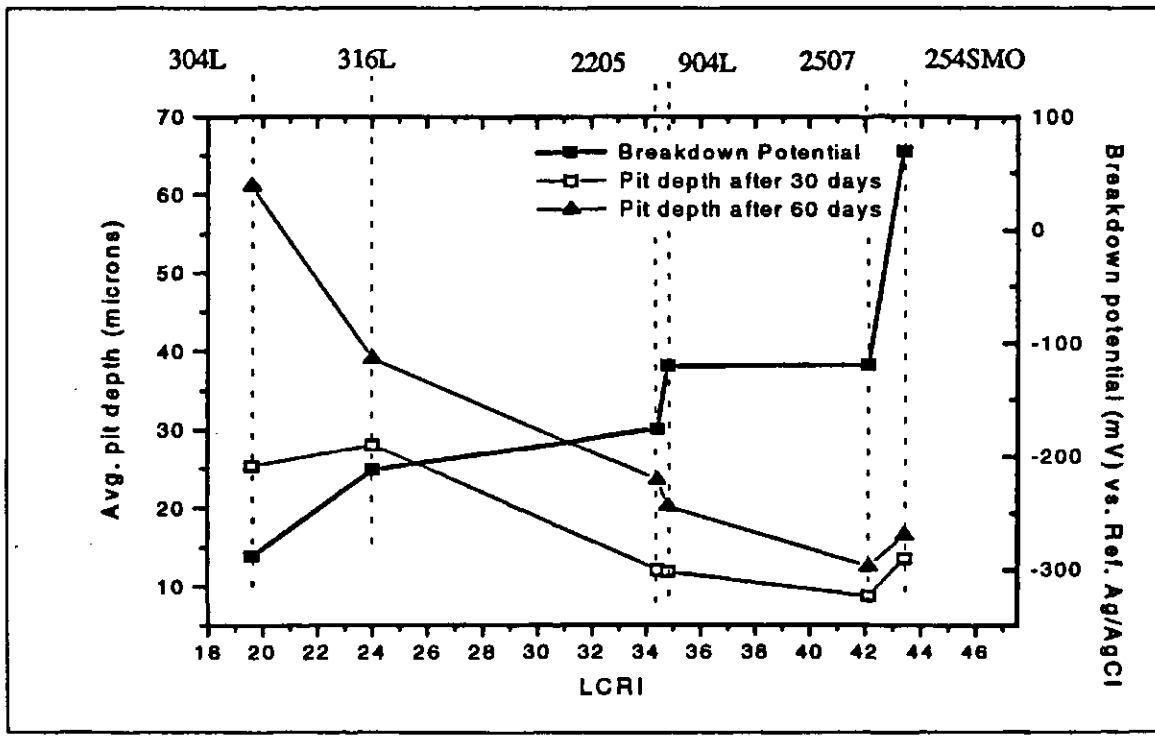

Fig. 5.29 Breakdown potentials and average depth of the pits vs. LCRIs

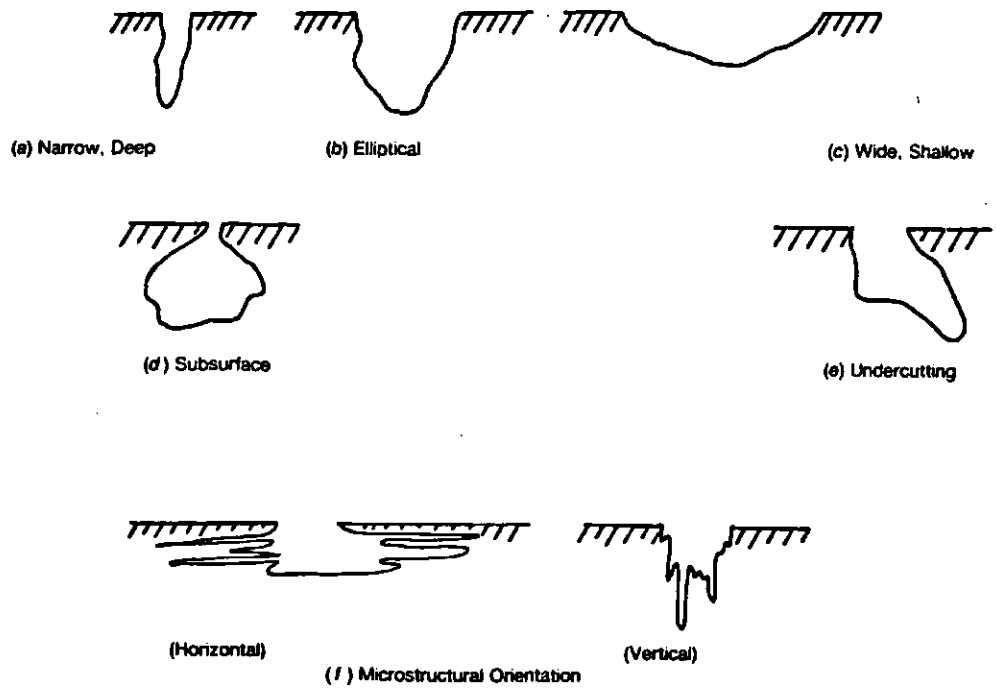

Fig. 5.30 Variation in the cross-sectional shape of pits[5]

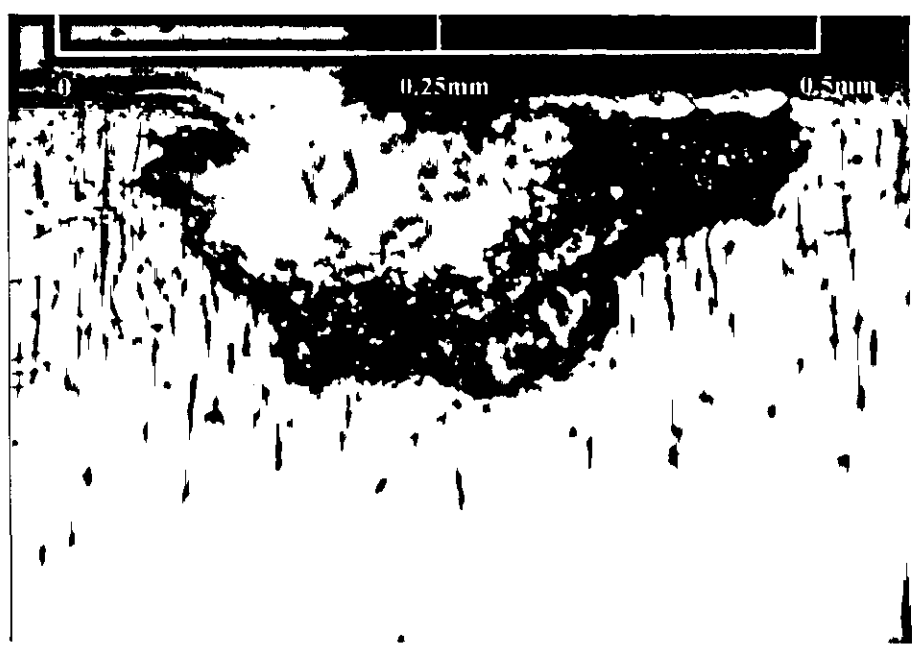

Fig. 5.31 Cross-section of 304L, ×200 (Elliptical)

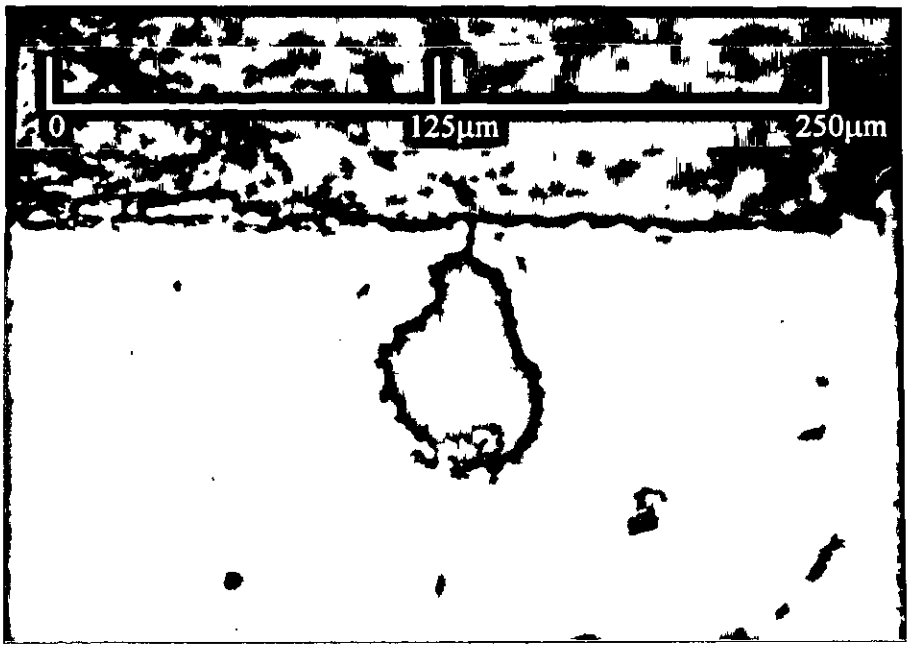

Fig. 5.32 Cross-section of CN7M, ×400 (Subsurface)

Fig. 5.33 Cross-section of 316L, ×200 (Undercutting)

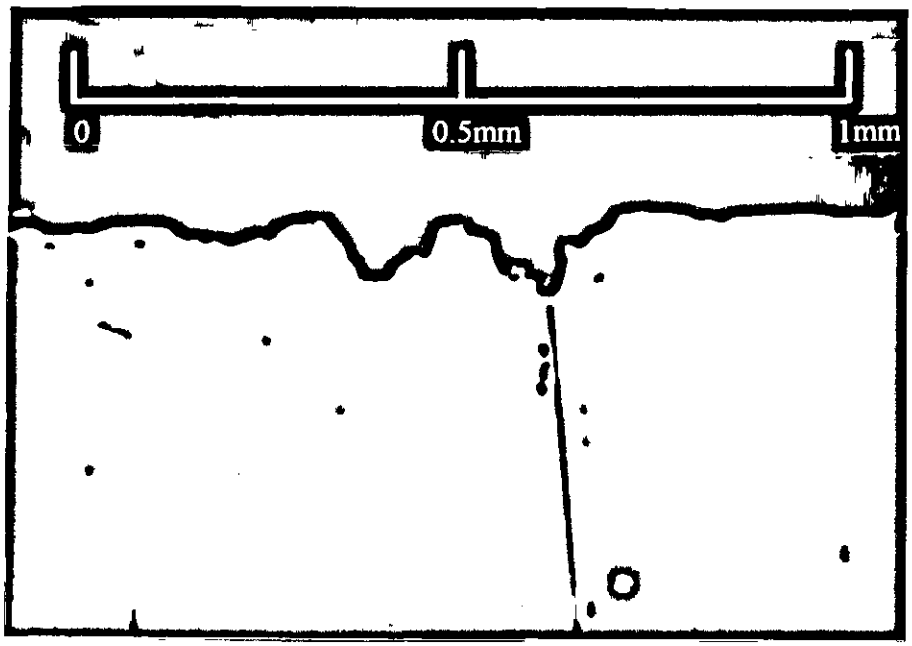

Fig. 5.34 Cross-section of 2205, ×100 (Elliptical)

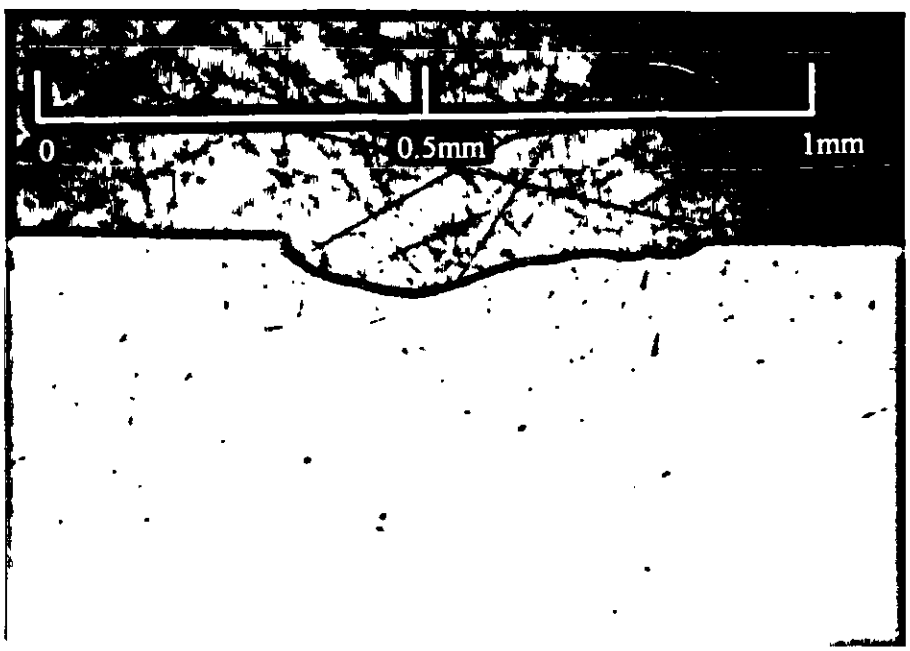

Fig. 5.35 Cross-section of 254SMO, ×100 (Wide, Shallow)

Fig. 5.36 Cross-section of 904L, ×50 (microstructural orientation, vertical)

Table 5.2 Price list for some commercial stainless steel pipes, Sch 40, seamless*

Alloy	304L	316L	904L	2304	2205	2507
Price, $/ft	60.67	68.54	175.44	95.35	110.40	125.32

* Courtesy Edmonton Tube Sales Ltd., November 1995

6. Conclusions

1. Hastelloy C-276 showed an outstanding resistance to localized corrosion in high temperatures and high chloride concentrations. The rest of the alloys show lower resistance depending on the temperature and chloride concentration.

2. Duplex stainless steels which were used in this study had better resistance than the austenitic alloys with the same LCRI in exposure tests; while the electrochemical polarization showed almost identical resistance of austenitic and duplex stainless steels.

3. The effect of alloying elements (chromium, molybdenum and nitrogen) on localized corrosion of stainless steels confirmed the previous studies of other researchers in this regard. However, only the alloys in the same group (i.e. austenitic, duplex) and with identical manufacturing process (i.e. wrought, cast) should be compared to each other based on their alloying elements.

4. LCRI and similar formulas can predict the resistance of alloys in the same group (e.g. austenitic, duplex) to the initiation of localized corrosion specially at high temperatures. However, the exposure test results proved that LCRI is not suitable for predicting the propagation rate of the pits in localized corrosion.

5. Localized attack in high nitrogen content duplex stainless steels initiates on the austenite/ferrite interface, but the attack preferentially propagates in the ferrite phase. The higher resistance of the austenite phase compared to the ferrite phase can be related to the higher solubility of nitrogen in the former.

6. The edges of austenitic stainless steels (304L, 316L and 904L) are very prone to localized corrosion. Stress corrosion cracking can intensify the corrosion attack in these areas in austenitic 304L and 316L. Rough surface conditions are the main cause of initiation of localized corrosion on the edges followed by stress corrosion cracking due to the residual stresses in these areas. Care should be taken during equipment fabrication in this regard.

7. The resistance of cast corrosion-resistant stainless steels is greatly affected by their microstructures. The ferrite phase is more susceptible to localized attack than the austenite phase.

8. Flow rate does not have any significant effect on the breakdown potential of the stainless steels, but it slows down the propagation of the pits by sweeping away the high chloride and acidic solutions around the pits confirming previous studies.

9. 2507, 254SMO, 904L and 2205 are respectively recommended for use in high temperature potash brine. However, the optimum mechanical properties and economical aspects should be considered before material selection.

10. Despite the higher activity of sodium chloride than potassium chloride, the corrosivity of potassium chloride is higher than sodium chloride in aerated solutions. The higher conductivity of potassium chloride is the main reason for this phenomenon. Alloys in deaerated solutions of sodium chloride and potassium chloride have identical anodic behavior with respect to the breakdown and repassivation potentials.

7. Recommendations

1. The presence of solid crystals in potash brines produces a harsh environment for both localized corrosion and erosion-corrosion of stainless steels. Study of erosion-corrosion of stainless steels in potash brines is necessary for material selection.

2. The newly developed electrochemical polarization cell can prevent crevice formation during the test, and give more accurate data for pitting potentials. Hence, its use is recommended[76].

3. The selected alloys in this study were all highly resistant in chloride solutions. Therefore, long term exposure tests (e.g. two years, five years) is recommended to evaluate their resistance in actual industrial conditions.

4. Electrochemical polarization tests should be performed in actual flowing conditions. This gives more accurate results than when performing the test with the rotating cylinder electrode.

5. Monitoring the current density during the exposure test can show the metal state (active, passive) and the characteristic of the passive film in a corrosive environment.

6. The study of existing coating technologies (metallic, non-metallic, plastic, rubber, ceramic and enamel) would open a new avenue in minimizing corrosion problems in potash and other chemical processes.

7. Further study of the resistance of duplex stainless steels to different types of corrosion is recommended since this type of stainless steels has relatively better mechanical properties than austenitic stainless steel and is significantly cheaper.

8. References

1 "Kalium: the Solution", Kalium Canada, Ltd., Regina, Canada

2 Potash and Potash Fertilizers, Report No.14, Stanford Research Institute Stanford (1966)

3 Shreves, R.N., Chemical Process Industries, McGraw Hill, New York, (1977)

4 Noyes, R., "Potash and Potassium Fertilizers", Chemical Process Monograph No.15, Noyes Development Corporation, New Jersy (1966)

5 Annual Book of ASTM Standards , Section 3: Metals Tests Methods and Analytical Procedures,Vol.03.02 "Wear and Erosion; Metal Corrosion", (1992)

6 Szklarska-Simialowska, Z, Pitting Corrosion of Metals, NACE, Houston (1986)

7 Shreir, L.L, R.A. Jarman and G.T. Burstein, Corrosion, Butterworth Heinemann, London (1994)

8 Uhlig, H.H., Corrosion and Corrosion Control, John Wiley & Sons, New York (1971)

9 Burstein, G.T. and P.I. Marshall, Corr. Sci. 24, p.449 (1984)

10 Borex, B. and I. Olefjord, "Preferential Dissolution of Iron During Polarization of Stainless Steels in Acids", Proc. Stainless Steels '84, p.134, GÖteborg, Sweden, Sept. 3-4 1984, The Institute of Metals, London (1985)

11 Fontana, M.G. and N.D. Green, Corrosion Engineering, McGraw Hill, New York (1978)

12 Baboian, R, Corrosion Tests and Standards, NACE, Houston (1995)

13 Bockris, J.O and Shahed U.M. Khan, Surface Electrochemistry, Plenum Press, New York and London (1933)

14 Okamoto, G., Corr. Sci.13, p.471 (1973)

15 Pistorius,P.C. and G.T. Burstein, Corr. Sci. 33, p.1885 (1992)

16 Sedriks, A.J., Corrosion of Stainless Steels, The Electrochemical Society, John Wiley & Sons, New York (1979)

17 Sedriks, A.J., "Metallurgical Aspects of Passivation of Stainless Steels", Proc. Stainless Steels '84, p.125, Göteborg, Sweden, Sept. 3-4 1984, The Institute of Metals, London (1985)

18 Issacs, H.S., Corr. Sci. 29. p.313 (1989)

19 Pourbaix,M., Lectures on Electrochemical Corrosion, Plenum Press, New York-London (1973)

20 Suzuki, T., M. Yamake and Y. Kitamura, Corr. 29, p.18 (1973)

21 Evitts, R. and J. Postlethwaite, Unpublished paper, Univ. of Saskatchewan, Saskatoon, Canada

22 F.B. Pickering, "Physical Metallurgical Development of Stainless Steels", Proc. Stainless Steels '84, p.2, Göteborg, Sweden, Sept. 3-4 1984, The Institute of Metals, London (1985)

23 Lula, R.A., Stainless Steel, ASM, Metals Park, Ohio (1989)

24 Stainless Steel from Avesta Sheffield, Steel Grade, Avesta Sheffield, Information, 9485

25 Van Vlack, L.H., A Textbook of Material Technology, Addition Wesley, Reading, Massachusetts (1973)

26 Perry, R.H., and D. Green, Perry's Chemical Engineers' Handbook, McGraw Hill, New York (1984)

27 Bernhardsson S., "The Corrosion Resistance of Duplex Stainless Steels", Proc. Duplex Stainless Steels '91, p.185, Bourgogne, France, Oct. 28-30 1991

28 Fruytier, D.J.A., "Industrial Experience with duplex Stainless Steel Related to Their Specific Properties", Proc. Duplex Stainless Steels '91, p.497, Bourgogne, France, Oct. 28-30 1991

29 Stainless Steels, American Society of Metals, Materials Park, Ohio (1994)

30 Smith, W.F , Structure & Properties of Engineering Alloys, McGraw Hill, New York (1981)

31 Handbook of Chemistry and Physics, CRC, 76 th Edition, New York (1995/1996)

32 Blackmore, C.E., M.Sc. thesis, Univ. of Saskatchewan, Saskatchewan, Canada (1996)

33 Nadezhdin,A. and D.A. Wensley, "Composition Factors Affecting Resistance of Ni-Cr-Mo-N Alloys to Crevice Corrosion", Material Performance **31** p.57 (1992)

34 Halada, G.P., D.Kim and C.R.Clayton, "Influence of Nitrogen on Electrochemical Passivation of High-Nickel Stainless Steels and Thin Molybdenum-Nickel Films", Corr. 52 p.36 (1996)

35 Moria M. and M.B. Ives, " Surface Segregation of Molybdenum during Pitting Corrosion of a Nickel-Molybdenum Alloy", Corr. 40 p.105 (1984)

36 Kearns, J.R. and H.E. Deverell, " The Use of Nitrogen to Improve the Corrosion Resistance of Fe-Cr-Ni-Mo Alloys for the Chemical Process Industries", Material Performance 26 p.18 (1987)

37 Alfonsson, E. and R. Qvarfort, "Investigation of the Applicability of Some PRE Expressions for Austenitic Stainless Steels", Material Science Forum: Electrochemical Methods in Corrosion Research, Trans Tech Publications, Aedermannsdorf, Switzerland (1992)

38 Muto, I., E. Sato and S. Ito, "Pitting Corrosion Behavior of Stainless Steel in a Marine Environment and Its Estimation Method", Corr. Eng. 42 p.887 (1993)

39 Ujiro, T, K. Yoshioka and R.W. Staehie, "Differences in Corrosion Behavior of Ferritic and Austenitic Stainless Steels", Corr. 50 p.953 (1994)

40 Mat. Tech. Inst. of the Chem. Proc. Ind., Inc MTI manual No.3, Corrosion Test Methods

41 Suutala, N. and M. Kurkela, Proc. Stainless Steels '84, p.240, Göteborg, Sweden, Sept. 3-4 1984, The Institute of Metals, London (1985)

42 Truman, J.E., Proc. Stainless Steels '87, p.111, Brighton, UK, Oct. 26-28 1987

43 Kitada, T., Y. Kobayashi, M. Tsuji, T. Taira, K. Ume and M. Ito, Nippon Kokan Technical Report: Overseaes No.51 p.37 (1987)

44 Ericsson, R., L. Schon and B. Wallen, Proc. of the 8th Scand. Corr. Cong., p.312, Helsinky, Finland (1978)

45 Ogushi, T., "Decline in the Corrosion Resistance of Stainless Steels due to Mechanical Polishing", Corr. Eng. 44 p.321 (1995)

46 Coates, G.R., "Effect of Some Surface Treatments on Corrosion of Stainless Steel", Material Performance. 29 p.61 (1990)

47 Degerbeck, J., Proc. of the 6th Scand. Corr. Cong., Paper No.36, Gothenborg, Sweden (1991)

48 Hultquiat G. and C. Leygraf, Corr. 36 p-126 (1980)

49 Morris, P.E., "Use of Rapid Scan Potentiodynamic Technique to Evaluate Pitting and Crevice Corrosion Resistance of Fe-Cr-Ni Alloys", Galvanic and Pitting Corrosion ASTM-STP 576, ASTM, Philadelphia (1976)

50 Szklarska-Smialowska, S. "The Pitting of Fe-Cr-Ni Alloys", Localized Corrosion, p.312, Int. Corr. Conf., Williamsburg, Virginia, USA, 6-10 Dec. 1971, NACE, Houston (1971)

51 Ives, M.B and M. Zamin, Discussion on "The pitting of Iron-Chromium-Nickel Alloys", Localized Corrosion, p.337, Int. Corr. Conf., Williamsburg, Virginia, USA, 6-10 Dec. 1971, NACE, Houston (1971)

52 Postlethwaite, J., B. Huber and D. Makepeace " Hydrodynamics Effect During Electrochemical and Exposure Pitting Tests with Passive Films", Corr. **42** p.646 (1986)

53 Postlethwaite, J., R.A. Brierly, M.J. Walmsley and S.C Goh, "Pitting at Elevated Temperatures", Localized corrosion, NACE, Houston (1974)

54 Beck, T.R., and S.G. Chan, Corr. **37** p.665 (1981)

55 Silverman, D.C., " Rotating Cylinder Electrode- an Approach for Predicting Velocity Sensitive Corrosion", Corrosion 90, paper 13, Las Vegas, USA ,April 3-27 1990

56 Holser, R.A., G. Prentice, R.B. Pond Jr and R. Guanti, " Use of Rotating Cylinder Electrodes to Simulating Turbulent Flow Conditions in Corrosion Systems", Corr. **52** p.764 (1990)

57 Liu, G., D.A. Tree, and M.S. High, " Relation Between Rotating Disk Corrosion Measurements and Corrosion in Pipe Flow" , Corr. **50** p.584 (1994)

58 Coates, G.E., "Materials for Dealing with Corrosion and Wear Problems in the Potash Industry", Proc. Can. Reg. West Conf. 1995, p.399, NACE, Regina, Saskatchewan, Canada, Feb. 19-22 1995

59 Hirsch, C. and S. Rohani, Unpublished paper, Univ. of Saskatchewan, Saskatoon, Canada

60 Streicher, M.A., " Analysis of Crevice Corrosion Data from Two Sea Water Exposure Test on Stainless Alloys", Corr. **39** p.37 (1983)

61 Metallography Principles and Procedures, Leco® Corporation

62 Postlethwaite, J., " Electrochemical Tests for Pitting and Crevice Corrosion Susceptibility", Can. Metallurgical Quar. **22** p.133 (1983)

63 Cavanaugh, M.A., J.A. Kargol, J. Nickerson, and N.F. Fiore, " The Anodic Dissolution of a Ni Base Superalloy" Corr. **39** p.144 (1983)

64 Johnson, M.J., "Relative Critical Potentials for Pitting Corrosion of Some Stainless Steels", Localized Corrosion-Cause of Metal Failure, STP516, ASTM, (1971)

65 Bond, A.P., "Pitting Corrosion-a Review of Recent Advances in Testing Methods and Interpretation", Localized Corrosion-Cause of Metal Failure, STP516, ASTM, (1971)

66 Newman, R.C. and E.M. Franz, "Growth and Repassivation of Single Pits in Stainless Steel", Corr. **40** p.325 (1984)

67 Pourbaix, M., "Atlas of Electrochemical Equilibria in Aqueous Solutions", Pergamon Press, Brussels (1966)

68 Davison, R.M. and J.D. Redmond, "A Guide to Using Duplex Stainless Steels", Materials & Design **12** p.187 (1991)

69 Sivakumar, M., U. Kamaci Mudali, and S. Rajeswari, " Compatibility of Ferritic and Duplex Stainless Steels as Implant Materials" J. of Material Sci. **28** p.6081 (1993)

70 Ping Cheng, T., W. Ta Tsai, and J. Tung Lee, " Electrochemical and Corrosion Behavior of Duplex Stainless Steels in Hank's Solution", J. of Material Sci. 25 p.936 (1990)

71 Sriram, R and D. Tromans, "Pitting Corrosion of Duplex Stainless Steels", Corr. 45 p.804 (1989)

72 Alfonsson, E. and R. Qvarfort, "Duplex Stainless Steels of Yesterday and of Today-a Pitting Corrosion Investigation", Proc. Duplex Stainless Steels '91, p.839, Bourgogne, France, Oct. 28-30 1991

73 Aziz, P.M., "Application of the Statistical Theory of Extreme Values to the Analysis of Maximum Pit Depth Data for Aluminum", Corr. 12 p.495t (1956)

74 Crews, D.L., "Interpretation of Pitting Corrosion Data From Statistical Prediction Interval Calculations", Galvanic and Pitting Corrosion ASTM-STP 576, ASTM , Philadelphia (1976)

75 Ives, M.B., "Etch Pitting-Theory and Observation", Localized Corrosion, p.78, Int. Corr. Conf., Williamsburg, Virginia, USA, 6-10 Dec. 1971, NACE, Houston (1971)

76 Vafort, R and E. Alfonsson, Proc. of the 11th Scand. Corr. Cong., Paper No.F.79, (1991)

Appendix A

The chemical composition of the samples along with their mechanical properties and manufacturers are shown in "Material Test Report" sheets. The Samples used for electrochemical polarization and exposure tests are marked by * and ♦, respectively.

Metal Samples

P.O. BOX 8 • 152 METAL SAMPLES RD.
MUNFORD, AL 36268
(205) 358-4202 • FAX (205) 358-4515

MATERIAL TEST REPORT

DATE: 02/27/96

CUSTOMER: UNIVERSITY OF SASKATCHEWAN

CUST. ORDER: L216513

M.S. ORDER: 961044

DEAR CUSTOMER:
WE CERTIFY THAT THIS MATERIAL TEST REPORT IS CORRECT TO THE BEST OF OUR KNOWLEDGE AND THAT THE MATERIAL SUPPLIED MEETS THE REQUIRED SPECIFICATIONS.
THANK YOU.

Larry Brandes
QUALITY CONTROL DEPARTMENT

CHEMICAL PROPERTIES

	ALLOY	LOT	AL	C	CR	CU	FE	MN	MO	NI	P	S	SI	TI	OTHERS
*	SAF2507	L118		0.019	24.800	0.130		0.800	3.900	6.800	0.020	0.001	0.330		N-0.300;CO-0.170
*	316L	J965		0.027	16.30	0.17		1.85	2.18	10.27	0.034	0.016	0.50		N-0.04
*	304L	K194		0.030	18.13			1.03		8.79	0.026	0.025	0.59		N-0.0500
♦	2507	J787		0.016	24.87	0.065		0.42	3.81	6.93	0.017	0.001	0.27		N-0.263

PHYSICAL PROPERTIES

ALLOY	LOT	TENSILE - KSI	YIELD - KSI	ELONG - %	R/A - %	HARDNESS	COND.	UNS.	MILL
SAF2507	L118	130.644	95.073	29	72	104		S32507	AVESTA SHEFFIELD
316L	J965	110	76	32	69	HB 215	SOL AN	S31603	GRAND FOUNDRY LTD.
304L	K194	86.0	31.0	57	75	HB 161		S30403	KRUPP STAHL AG
2507	J787	864	595					S32507	SANDVIC

Metal Samples

P.O. BOX 8 • 152 METAL SAMPLES RD
MUNFORD, AL 36268
(205) 358-4202 • FAX (205) 358-4515

MATERIAL TEST REPORT

DATE: 02/02/95

CUSTOMER: UNIVERSITY OF SASKATCHEWAN

CUST. ORDER: K200099

M.S. ORDER: 950503

DEAR CUSTOMER:
WE CERTIFY THAT THIS MATERIAL TEST REPORT IS CORRECT TO THE BEST OF OUR KNOWLEDGE AND THAT THE MATERIAL SUPPLIED MEETS THE REQUIRED SPECIFICATIONS.
THANK YOU.

QUALITY CONTROL DEPARTMENT

CHEMICAL PROPERTIES

HEAT#	LOT	A	C	CR	CU	FE	MN	MO	NI	P	S	SI	TI	OTHERS
* V2304	J496		0.030 MAX	22.0/23	0.10/0.		2.0 MAX	0.10/0.	4.0/5.0	0.035 MAX	0.010 MAX	0.7 MA X		N-0.08/0.15
SLM	D447		0.020	16.52	0.27	BAL	1.77	2.08	10.15	0.030	0.015	0.56		CO-0.12; N-0.119

PHYSICAL PROPERTIES

HEAT#	LOT	TENS. KSI	YIELD KSI	ELONG. %	R/A %	HARDNESS	COND.	UNS	MILL
V2304	J496	99.5	68.5	62	67	Rb/DH/19	ANN	S32304	AVESTA
								R31652	JESSOP

METAL SAMPLES CO.

P.O. BOX 8
RT 1 BOX 152
MUNFORD, AL 36268
(205) 358-4202
FAX (205) 358-4515

MATERIAL TEST REPORT

DATE: 06/14/94

CUSTOMER: UNIVERSITY OF SASKATCHEWAN

CUST. ORDER: K189600

M.S. ORDER: 94-451

DEAR CUSTOMER:
WE CERTIFY THAT THIS MATERIAL TEST REPORT IS CORRECT TO THE BEST OF OUR KNOWLEDGE AND THAT THE MATERIAL SUPPLIED MEETS THE REQUIRED SPECIFICATIONS.
THANK YOU.

QUALITY CONTROL DEPARTMENT

CHEMICAL PROPERTIES

ALLOY	HEAT	AL	C	CR	CU	FE	MN	MO	NI	P	S	SI	TI	OTHERS
17-4PH	D737		0.034	15.51	3.860	BAL	0.45	0.130	4.28	0.020	0.023	0.340		N2-0.016; CB+TA-0.28; T
														B<0.01
17-4PH	D706		.05	15.38	3.20	BAL	.43	.43	4.31	.027	.012	.60		CB-.32; TA-.01
304L	G424		0.02	18.18	0.30	BAL	1.83	0.29	9.74	0.023	0.026	0.30	<0.01	CB-<0.01; CO-0.09; N-0.
														062; TA-<0.01; V-0.08
304L	D768		0.012	18.22	0.250	BAL	1.54	0.240	8.77	0.029	0.022	0.560	<0.01	N2-0.063; CO-0.12; CB-<
														0.01; TA-<0.01
446	C007		0.11	24.35		BAL	0.51			0.024	0.006	0.53		N-0.17
446	0963		0.092	25.97		BAL	1.29			0.017	0.027	0.66		N2-0.18
904L	F752		0.018	20.90	1.50	BAL	1.67	4.44	24.45	0.025	0.009	0.49		N-.035; CO-.17
904L	B390		0.016	20.21	1.36	BAL	1.67	4.32	24.64	0.024	0.003	0.15		
* 2205	F754		.016	21.97	.15	BAL	1.49	3.09	5.85	.024	.001	.59		CO-.06; N-.16

PHYSICAL PROPERTIES

ALLOY	HEAT	TENSILE - KSI	YIELD - KSI	ELONG - %	R/A - %	HARDNESS	COND.	UNS	MILL
17-4PH	D737					BHN 341	ANN	S17400	ALTECH
17-4PH	D706					RC 35		S17400	FAY
304L	G424	100.5	72	39 (2")	70	BHN 217	SOLANN	S30403	AL TECH
304L	D768	92.0	60.0	51	68	BHN 179	ANN	S30403	ALTECH
446	C007	88.95	75.18	24.5	59.3	RB 91		S44600	CROCTUBE
446	0963	78.0	54.9	32.1	64.2	RB 80	ATRDAN	S44600	ROLLED ALLOYS
904L	F752	83.2	37.4	53.7	65.8	BHN 143		N08904	JESSOP
904L	B390							N08904	THYSSEN
2205	F754	109.8	71.2	41.8	71.0	BHN 217		S31803	JESSOP STEEL

METAL SAMPLES CO.

P.O. BOX 8
RT 1 BOX 152
MUNFORD, AL 36268
(205) 358-4202
FAX (205) 358-4515

MATERIAL TEST REPORT

DATE: 06/14/94

CUSTOMER: UNIVERSITY OF SASKATCHEWAN

CUST. ORDER: K169880

M.S. ORDER: 94 [illegible]

DEAR CUSTOMER:
WE CERTIFY THAT THIS MATERIAL TEST REPORT IS CORRECT TO THE BEST OF OUR KNOWLEDGE AND THAT THE MATERIAL SUPPLIED MEETS THE REQUIRED SPECIFICATIONS.
THANK YOU.

QUALITY CONTROL DEPARTMENT

CHEMICAL PROPERTIES

ALLOY	HEAT	AL	C	CR	CU	FE	MN	MO	NI	P	S	SI	TI	OTHERS
430	G017	0.014	0.046	16.28	0.12	BAL	0.41	0.02	0.14	0.023	0.005	0.42		V-0.05; SN-0.02; CO-0. 3; CB-0.01; N-0.037
430	D723	<0.005	0.036	16.60	0.10	BAL	0.50	0.040	0.31	0.028	0.013	0.53		
304LN	D450		0.021	19.80	0.18	BAL	1.80	0.40	8.80	0.034	0.008	0.45		CO-0.12; N-0.124
CN7M	G520		0.056	20.02	3.32	43.591	1.10	2.18	28.79	0.026	0.007	0.91		
316L	H844		0.013	16.12	0.32		1.60	2.01	10.05	0.033	0.025	0.32		CO-.16; N-.05
316L	B778		0.020	17.47	0.360	BAL	1.61	2.390	11.70	0.023	0.025	0.590		CO-0.11; N2-0.085
A53GRB	B620		0.17			BAL	0.65			0.019	0.007	0.02		
347	0986		0.063	17.19	0.18	BAL	1.49	0.[illegible]9	9.30	0.022	0.004	0.51		CO-0.03; TA-0.006; C+T 0.80
347	H276		0.052	17.14	0.25	BAL	1.78	0.23	9.96	0.021	0.002	0.47		CB+TA-.80

PHYSICAL PROPERTIES

ALLOY	HEAT	TENSILE - KSI	YIELD - KSI	ELONG - %	R/A - %	HARDNESS	COND.	UNS	MILL
430	G017	85.7	75.5	18.0	73.0	BHN 160		S43000	LTV STEEL
430	D723						ANN	S43000	ALTECH
304LN	D450	86.5	41.4	60.0	71.0	BHN 174	ANN	S30453	JESSOP
CN7M	G520							J95150	TEXAS STAINLESS
316L	H844	99.7	81.9	35 (2")	65.4	RB 95		S31603	INDUSTRIAL ALLOYS
316L	B778	95.0	73.0	42.0	73.0	BHN 197	ANN	S31603	ALTECH
A53GRB	B620	70.1	46.9	42.0				K03005	LABARGE
347	0986	106.0	79.0	43.0	70.0	BHN 235		S34700	ALTECH
347	H276	104.8	79.7	42 (2")	68.6	BHN 240		S34700	SOUTHERN TOOL STEEL

METAL SAMPLES CO.

P.O. BOX 8
RT 1 BOX 152
MUNFORD, AL 36268
(205) 358-4202
FAX (205) 358-4515

MATERIAL TEST REPORT

DATE: 06/14/94

CUSTOMER: UNIVERSITY OF SASKATCHEWAN

CUST. ORDER: KIH9XM

M.S. ORDER: 94054

DEAR CUSTOMER:
WE CERTIFY THAT THIS MATERIAL TEST REPORT IS CORRECT TO THE BEST OF OUR KNOWLEDGE AND THAT THE MATERIAL SUPPLIED MEETS THE REQUIRED SPECIFICATIONS.
THANK YOU.

QUALITY CONTROL DEPARTMENT BF

CHEMICAL PROPERTIES

	ALLOY	HEAT	AL	C	CR	CU	FE	MN	MO	NI	P	S	SI	TI	OTHERS
*	2205	G614		0.016	22.20		BAL	1.52	3.00	5.60	0.025	0.002	0.34		N-0.15
	C276	J196		0.003	15.47		5.70	0.48	15.10	BAL	<0.005	0.002	0.03		CO-1.32;V-.15;W-3.31
*	C276	D968		<0.00	15.48		5.88	0.46	15.60	BAL	0.008	0.002	0.04		CO-0.43; V-0.12; W-3.91

PHYSICAL PROPERTIES

ALLOY	HEAT	TENSILE - KSI	YIELD - KSI	ELONG - %	R/A - %	HARDNESS	COND.	UNS	MILL
2205	G614	111.8 KSI	71.7 KSI	44.1 (2")	83.1	RB 98	SOL AN	S31803	AVESTA
C276	J196	111.0	46.0	67.0	ASTM B574		ANLD	N10276	HAYNES INT'L
C276	D968	109.0	59.0	69.0				N10276	CABOT

Metal Samples

P.O. BOX 8 • 152 METAL SAMPLES RD.
MUNFORD, AL 36268
(205) 358-4202 • FAX (205) 358-4515

MATERIAL TEST REPORT

DATE:

CUSTOMER:

CUST. ORDER:

M.S. ORDER:

DEAR CUSTOMER:
WE CERTIFY THAT THIS MATERIAL TEST REPORT IS CORRECT TO THE BEST OF OUR KNOWLEDGE AND THAT THE MATERIAL SUPPLIED MEETS THE REQUIRED SPECIFICATIONS.
THANK YOU.

QUALITY CONTROL DEPARTMENT DC

CHEMICAL PROPERTIES

ALLOY	LOT	AL	C	CR	CU	FE	MN	MO	NI	P	S	SI	TI	OTHERS
*						BAL.								
* CD4MCU	J315		0.022	25.52	2.89	52.96	0.78	1.87	5.04	0.039	0.019	0.86		

PHYSICAL PROPERTIES

ALLOY	LOT	TENSILE - KSI	YIELD - KSI	ELONG - %	R/A - %	HARDNESS	COND.	UNS	MILL
CD4MCU	J315	103.766	73.65	60.6			ANNLD	J93370	TEXAS STAINLESS

Metal Samples

P.O. BOX 8 • 152 METAL SAMPLES RD.
MUNFORD, AL 36268
(205) 358-4202 • FAX (205) 358-4515

MATERIAL TEST REPORT

DATE: 04/10/95

CUSTOMER: UNIVERSITY OF SASKATCHEWAN

CUST. ORDER: K202990

M.S. ORDER: 951879

DEAR CUSTOMER:
WE CERTIFY THAT THIS MATERIAL TEST REPORT IS CORRECT TO THE BEST OF OUR KNOWLEDGE AND THAT THE MATERIAL SUPPLIED MEETS THE REQUIRED SPECIFICATIONS.
THANK YOU.

QUALITY CONTROL DEPARTMENT

CHEMICAL PROPERTIES

ALLOY	LOT	AL	C	CR	CU	FE	MN	MO	NI	P	S	SI	TI	OTHERS
254SMO	K731													
904L	K660		0.014	19.900	1.490		1.510	4.300	24.200	0.019	0.0001	0.420		CO-0.360; N-0.064
304L	E673		0.026	18.23	0.25	BAL	1.79	0.24	8.83	0.030	0.018	0.61		CO-0.10; N-0.086
316L	J974		0.02	16.33	0.23		1.84	2.12	10.17	0.028	0.0003	0.52		N-0.03
2205	D316		0.02	22.33		BAL	1.83	2.77	5.82	0.023	0.003	0.33		N2-.117
CD4MCU	J315		0.022	25.52	2.89	62.96	0.78	1.87	5.04	0.039	0.019	0.86		
CN7M	A081		0.01	20.23	3.16	BAL	0.46	2.16	28.86	0.009	0.007	0.39	28.86	
C276	K198		0.002	15.41		5.29	0.47	15.52	BAL.	<0.005	0.002	<0.02		CO-0.39; V-0.15; W-3.65

PHYSICAL PROPERTIES

ALLOY	LOT	TENSILE - KSI	YIELD - KSI	ELONG - %	R/A - %	HARDNESS	COND	UNS	MILL
254SMO	K731							S31254	AVESTA SHEFFIELD
904L	K660	91.0	43.0	50.0		BB 82		N08904	AVESTA
304L	E673	85.8	46.9	54		Rb 82		S30403	J&L SPECIALTY
316L	J974	88.500	44.000	56		80.HRB	ANLD.	S31603	ALLEGHENY LUDLUM
2205	D316	112.0	85.0	40				S31803	CREUSOT LOIRE
CD4MCU	J315	103.766	73.65	60.6			ANNLD	J93370	TEXAS STAINLESS
CN7M	A081	68.95	28.20	55.0	62.0			N08020	CSCO
C276	K198	102.000	60.000	62.0		1RB 90	ANLD	N10276	HAYNES INT.

Appendix B

The general technical information of the electrochemical corrosion measurement system (Gamry CMS 100) and the rotating electrode are shown in this appendix.

CMS100

Electrochemical Corrosion Measurement System

The CMS100 Corrosion Measurement System uses proven electrochemical techniques to investigate corrosion problems. You can extract both mechanistic information and predicted corrosion rates from electrochemical corrosion experiments. Best of all, the experiments run in hours, not weeks or months. The CMS100 is especially useful when you need to evaluate many samples in a limited time.

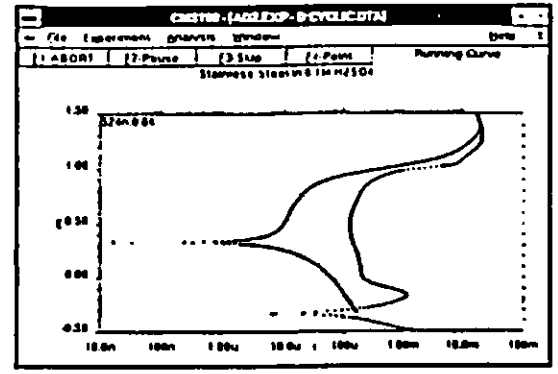

The CMS100 offers an unprecedented combination of flexibility, power and ease of use. Using the Microsoft Windows® environment, you can run standard experiments at the click of a button. But when a standard technique isn't enough, you can modify the technique or create a new one using our powerful Explain™ script language. Data is automatically transferred into Microsoft Excel® for analysis and presentation via user accessible routines. From there, you can export results to your favorite database.

The heart of the CMS100 is a state-of-the-art potentiostat/galvanostat contained inside your AT compatible computer. This instrument offers research grade features such as multiple autoranged current scales, current interrupt iR compensation, 16 bit D/A and A/D conversion, automatic calibration, and extensive filtering and stability compensation. A single laboratory computer can drive up to 4 potentiostats performing 4 different experiments, dramatically raising sample throughput without the cost of additior computers.

Gamry Instruments offers the CMS100 in cost-effective desktop and portable systems. The CMS100 provides the high performanc and flexibility that you need to perform electrochemical corrosion measurements today and in the future.

And finally, when simple modifications won't suffice, our staff can create custom applications to fit your specific needs.

CMS100

Electrochemical Corrosion Measurement System

Features

- Electronics on two plug-in cards for ISA bus, 286/386/486 computers -- no bulky external potentiostat
- Cards powered from computer power supply eliminating extra cables and clutter
- Up to 4 potentiostats in one computer share a single operator interface
- 8 decade, autoranging current measurement
- Potentiostat electrically isolated from computer for use with autoclaves or mechanical stress apparatus
- Current interrupt iR compensation for work in resistive media
- Auxiliary I/O -- 2 analog inputs, 1 analog output, 4 digital inputs, 4 digital outputs
- Easy to use graphical user interface based on Microsoft Windows
- Standard corrosion experiments preprogrammed for routine use
- User modifiable scripts serve as the basis for new experiments
- Autoranging real time graphical display for experiment monitoring
- Data presentation and calculations in customizable Microsoft Excel
- Presentation quality graphical output on most common output devices
- Numerical treatment includes Tafel fits, polarization resistance and integration

AFMSRX
Rotator

Highlights

- High performance system: rapid acceleration
- Speed may be modulated from an external source (square wave, sine wave, etc)
- Bi-polar power supply improves dynamic performance
- Chemical resistant base
- Use with Disk or Ring-Disk type electrodes
- Silver carbon contact brushes
- Voltage output proportional to rotational speed
- Speed range to 10,000 RPM
- Ideal for use in hydrodynamically modulated systems
- Low Cost, High Quality

Description

Pine Instrument Company's AFMSRX Rotator is a solid state controlled servo-system designed to operate in an application which requires the electrode speed to be modulated by a sine, square or other type waveform. The outstanding acceleration characteristics of the system allow electrode speed to follow the input signal with little error. This feature is particularly desirable for use in hydrodynamically modulated applications.

The outstanding dynamic performance of the AFMSR Rotator System is due to the use of a high speed, low inertia, permanent magnet DC motor and a high voltage, bi-polar power supply. The positive power supply voltage is approximately twice the motor's rating. A dual protection scheme is employed to protect the motor from both demagnetization and overheating: an instantaneous electronic current limit set at 10 amps, and a thermal type circuit breaker.

The rotational speed of the electrode may be precisely controlled by a four digit pushbutton pot on the front panel, or by application of an externally generated voltage applied to a jack on the front panel. The rotational speed is adjustable to within 1% of the digital pot setting from 50 to 10,000 RPM. A voltage signal which is proportional to the electrode speed is available at the output jack, also located on the front panel.

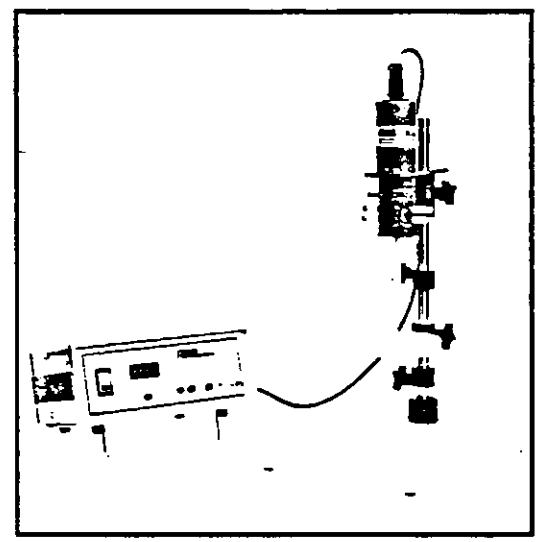

AFMSRX shown with optional electrode

The body of the rotator may be easily raised or lowered; a cell shelf is provided whose height is easily adjusted. These features facilitate introduction and removal of the cell. The base is made of a chemically resistant material.

The AFMSRX has been designed to accommodate both Disk and Ring-Disk type electrodes. Electrical connections are made to the electrode by silver carbon brushes — two each for the disk and ring — to provide consistent, reliable contact.

Pine Instrument Company manufactures a wide range of electrode types and produces many custom units to the customer's specifications. Consult the factory for details.

Specifications:

Power:	115 VAC or 230 VAC, 50/60 HZ factory connected
Weight:	Electronic Control Unit (ECU) 11.5 lbs. Body — Base Assembly 23 lbs.
Operation Temperature:	10°C to 40°C
Dimensions:	ECU — 11⅜" W x 10⅛" D x 5¾" H; Base — 11" x 15" x ¾"
Motor:	1/50 HP permanent magnet DC
Motor Power Supply:	+45 VDC, -20 VDC
Speed Control:	Closed loop servo-system; temperature compensated tach generator is mounted on the motor shaft and provides rotational speed information
Speed Range:	50 to 10,000 RPM
Accuracy:	Better than 1% of digital pot setting
Controls:	Lighted On-Off switch Digital pot to set speed: four digits
Front Panel Connections:	Input jack for controlling speed via external source. Output jack gives a voltage proportional to the rotational speed: 1 V/1000 RPM ±1%. Common jack is DC common, isolated from the case. Ground terminal is connected to the case and the ground lead of the power cord.
Max Slew Rate of Motor:	Approximately 300,000 RPM/sec (no load)
Bandwidth:	@1000 RPM peak to peak modulation, 2000 RPM base speed: >50 HZ.—1db.
Motor Protection:	1.5 amp thermal type circuit breaker

Hardware Supplied

1 Electronic Control Unit
1 Body - Base Assembly (includes motor-tach)

Documentation Supplied

Instruction Manual
Inspection Sheet

Warranty

The AFMSRX manufactured by Pine Instrument Company is warranted to be free from defects in material and workmanship for a 6 month period from date of shipment to original purchaser and used under normal conditions. The obligation under this warranty being limited to replacing or repairing any part or parts which shall upon examination disclose to Pine Instrument's satisfaction to have been defective and shall have been returned freight prepaid and clear of encumbrances to Pine Instrument Company in Grove City, Pa. within the warranty period. This warranty being expressly in lieu of all other warranties, expressed or implied and all other obligations or liabilities. All specifications are subject to change without notice.

Pine Instrument Company
101 Industrial Drive
Grove City, PA 16127 U.S.A.
(412) 458-6391

3/88 Printed in USA

Appendix C

The polarization curves of the tested alloys are shown in this section.

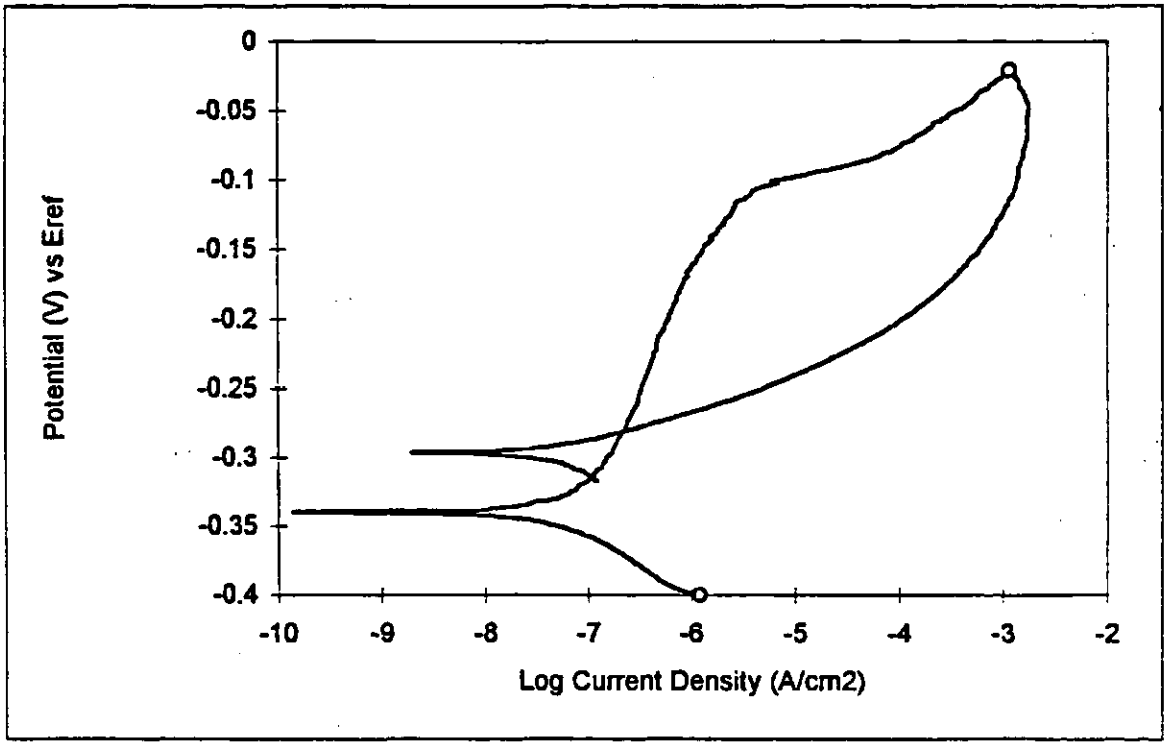

Fig. C.1 304L at 22°C, deaerated (1940 rpm)

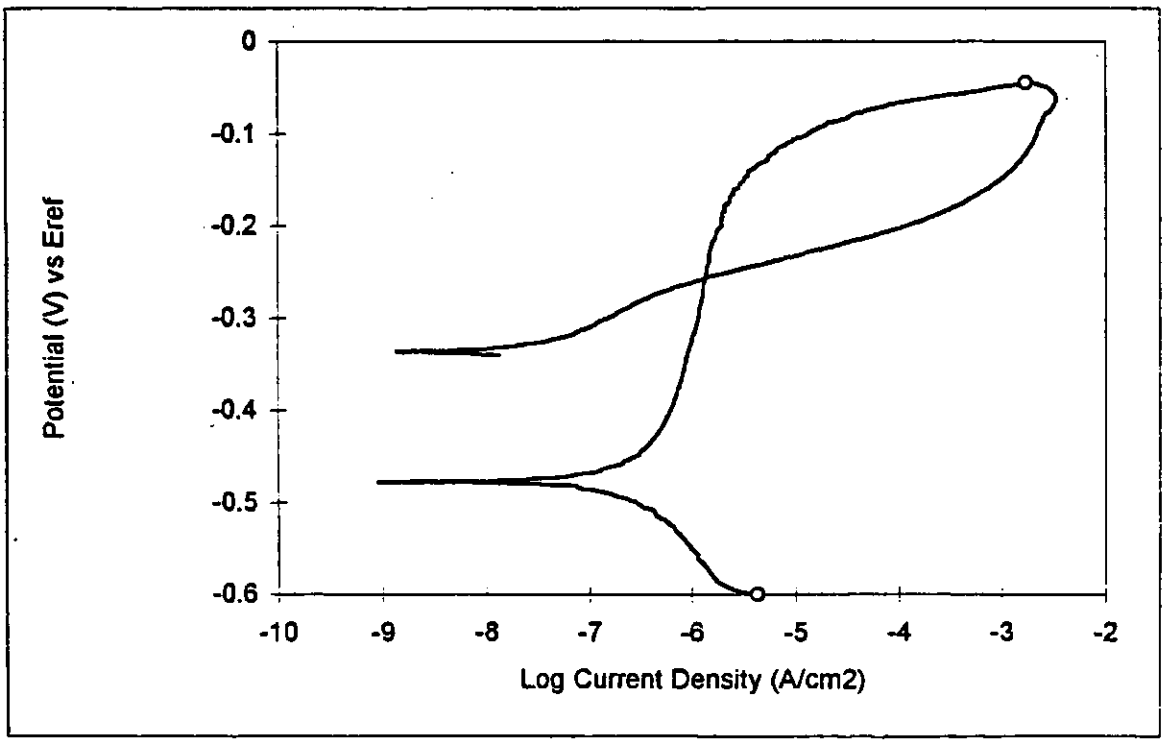

Fig. C.2 304L at 22°C, deaerated (Stagnant)

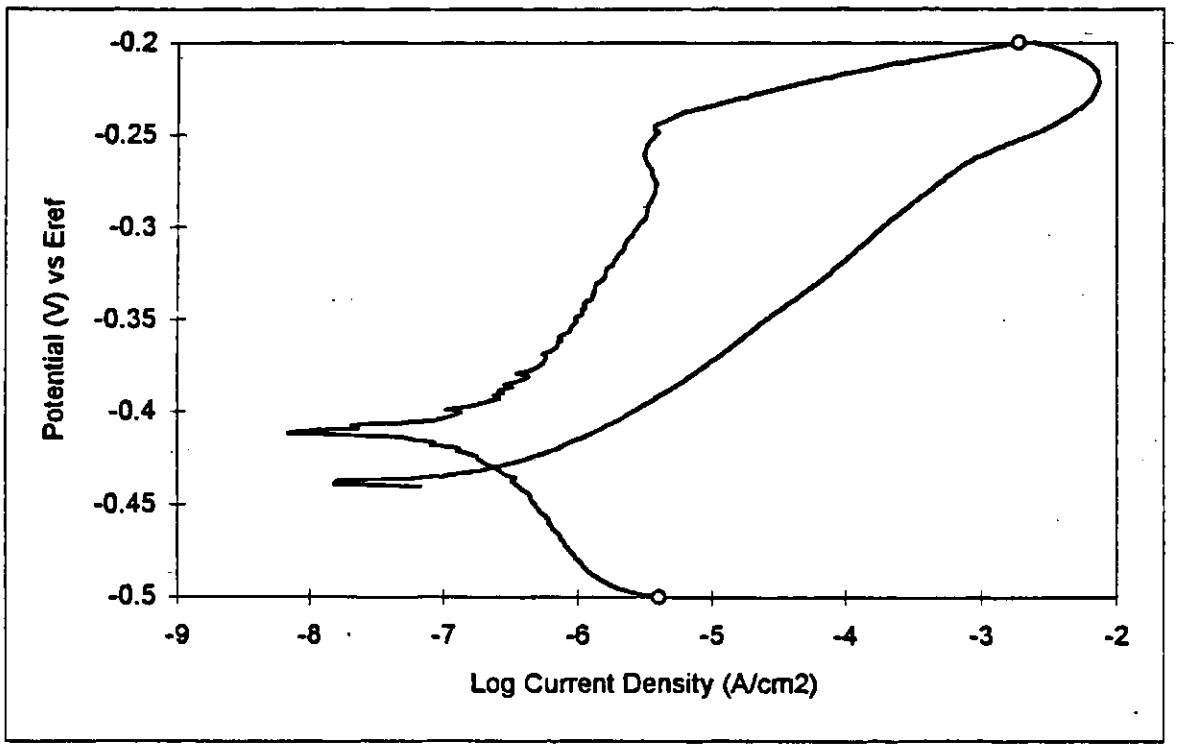

Fig. C.3 304L at 90°C, deaerated (1940 rpm)

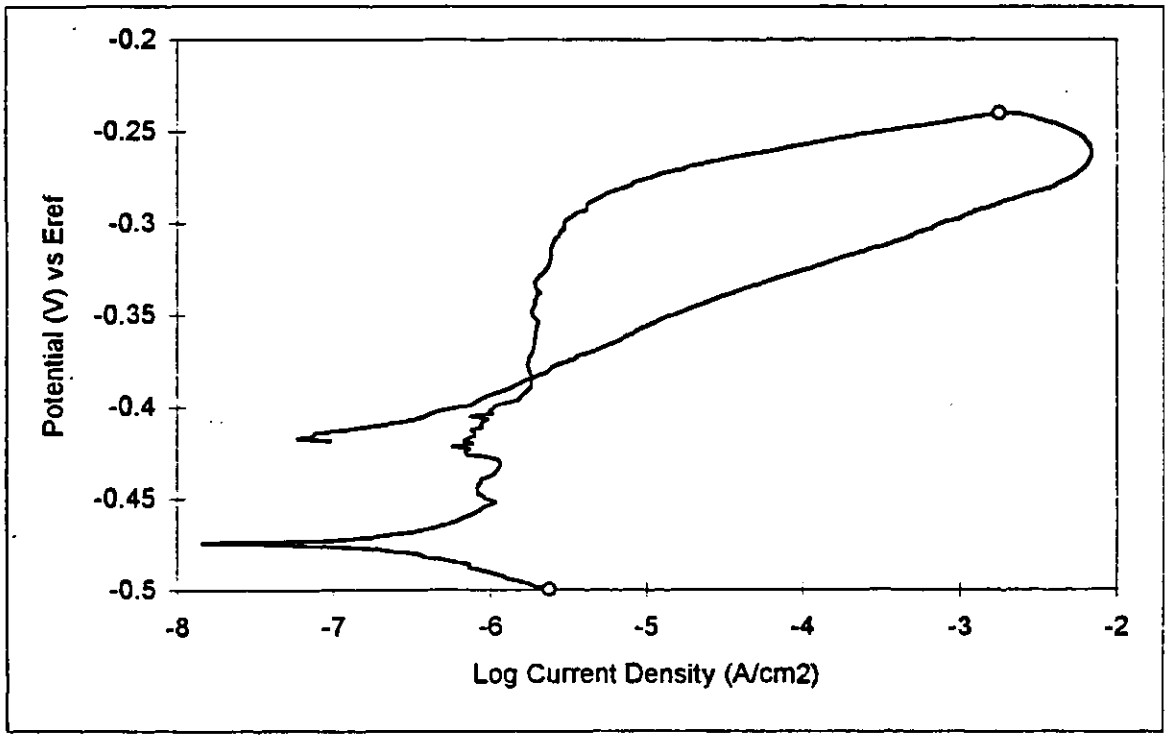

Fig. C.4 304L at 90°C, deaerated (Stagnant)

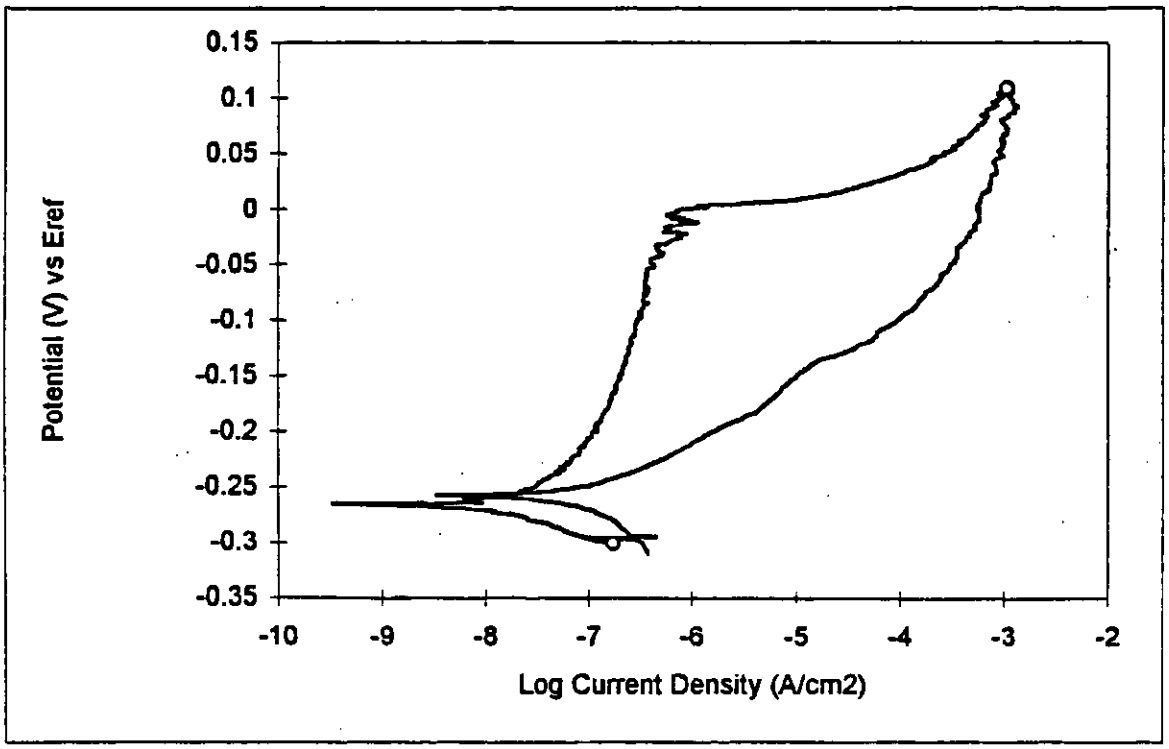

Fig. C.5 316L at 22°C, deaerated (1940 rpm)

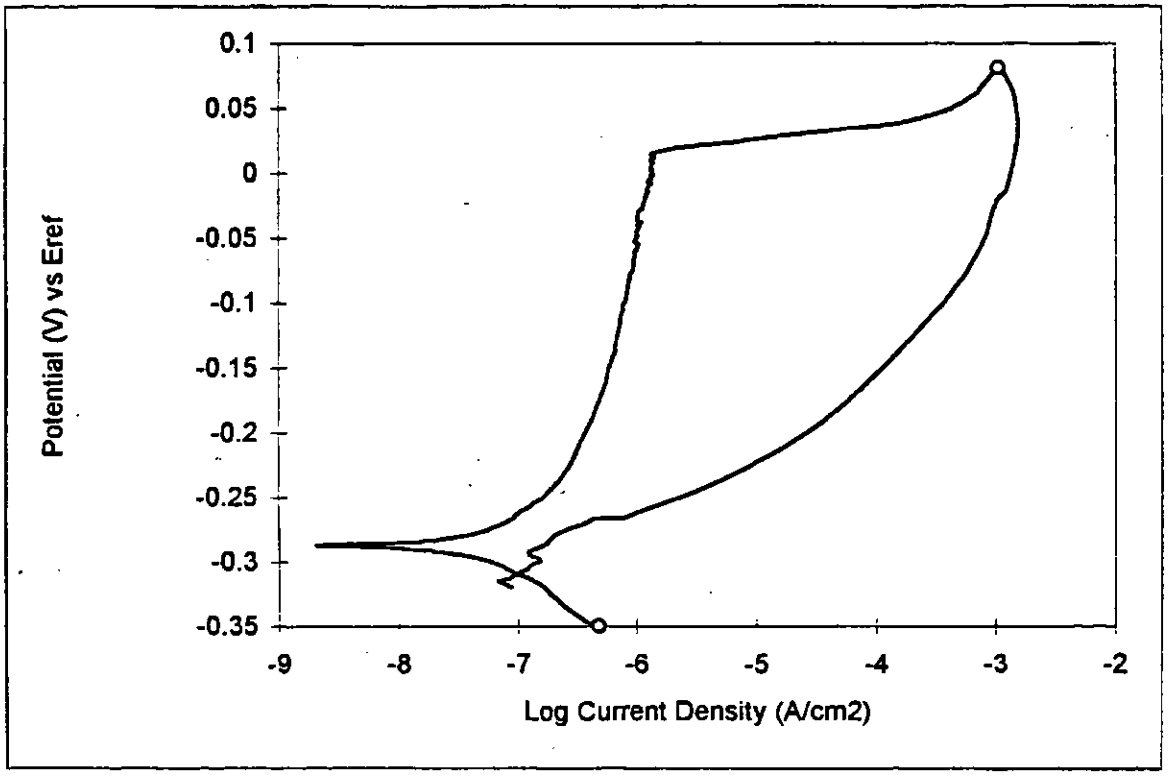

Fig. C.6 316L at 22°C, deaerated (Stagnant)

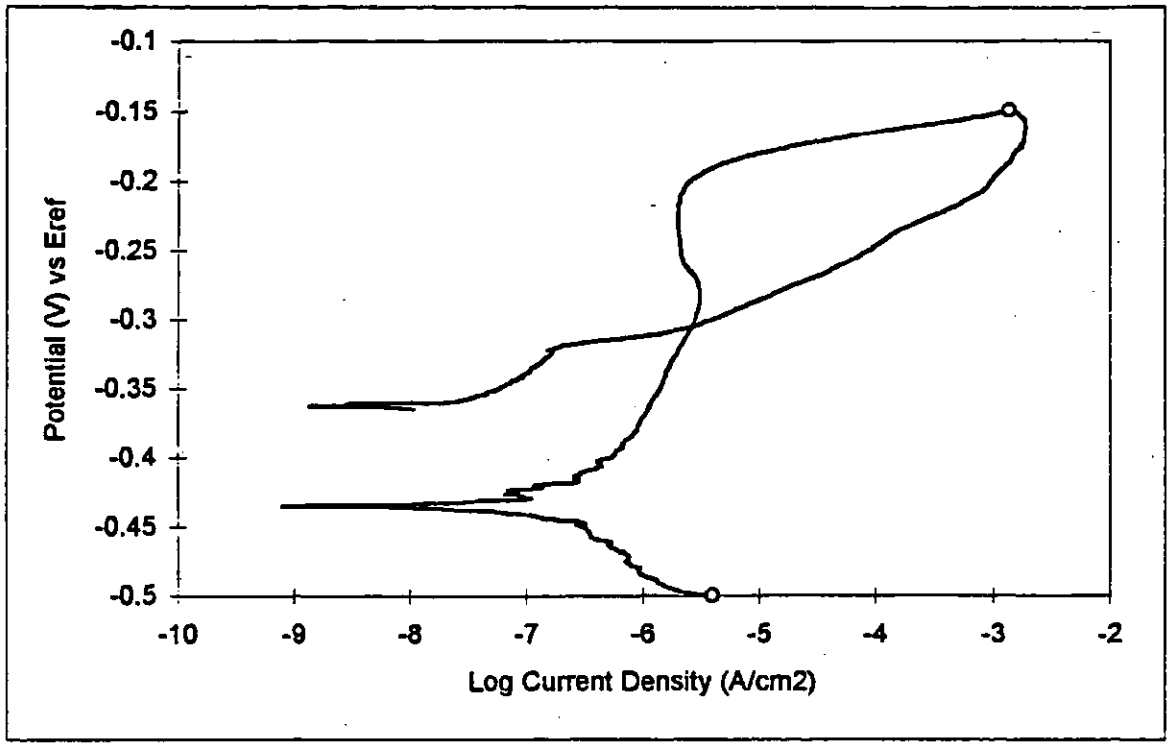

Fig. C.7 316L at 90°C, deaerated (1940 rpm)

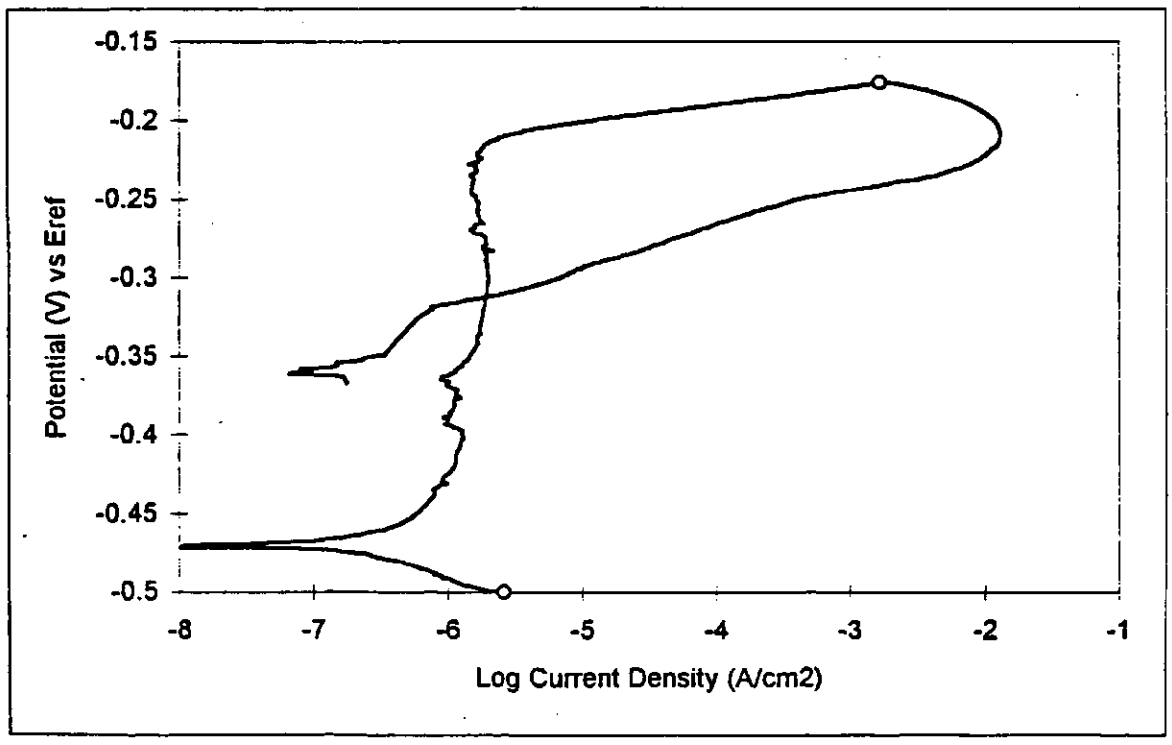

Fig. C.8 316L at 90°C, deaerated (Stagnant)

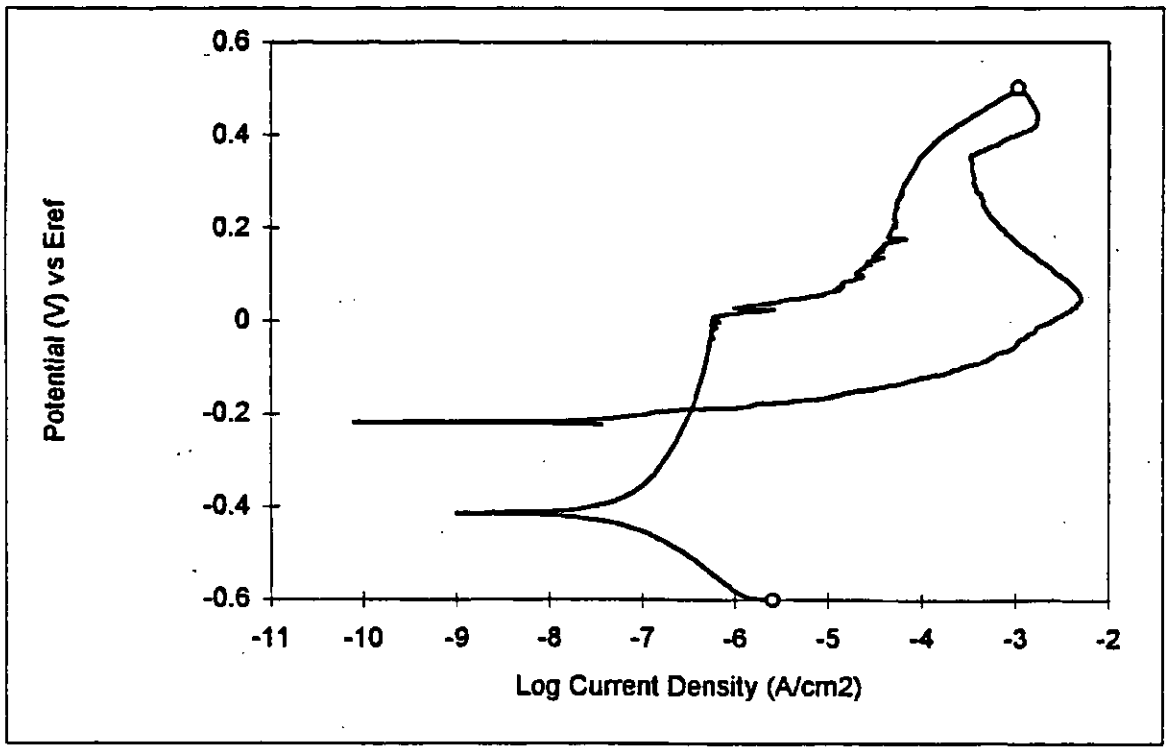

Fig. C.9 2304 at 22°C, deaerated (1940 rpm)

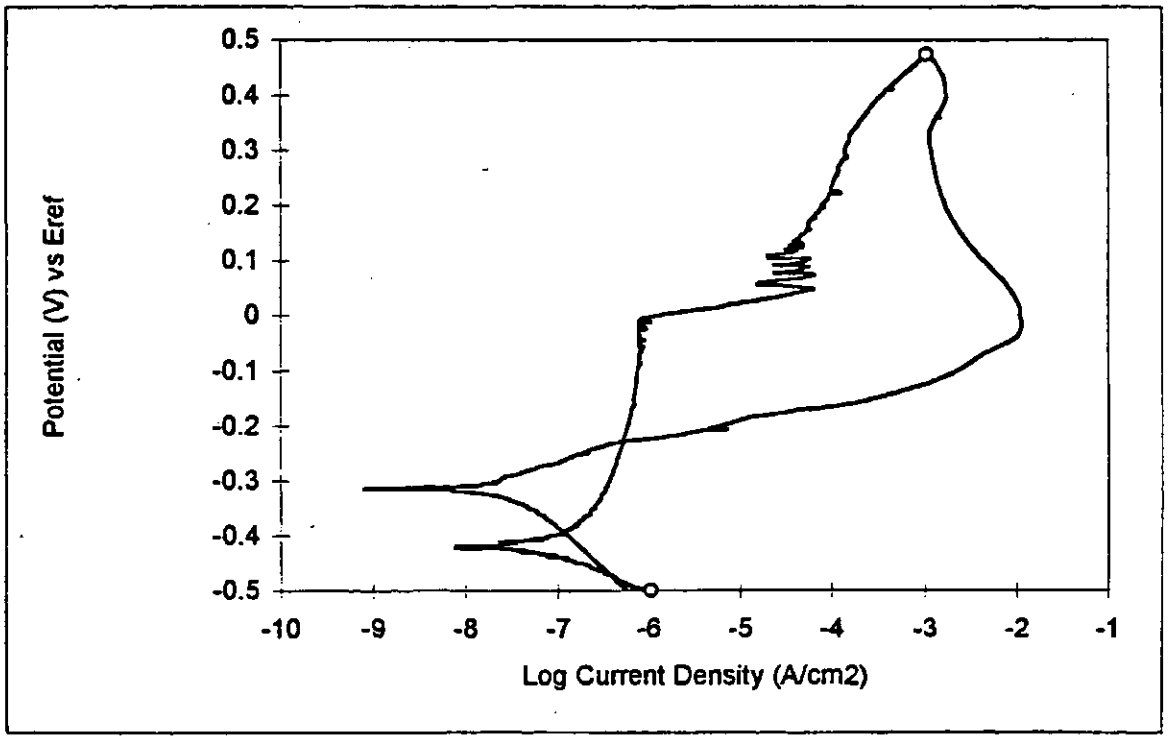

Fig. C.10 2304 at 22°C, deaerated (Stagnant)

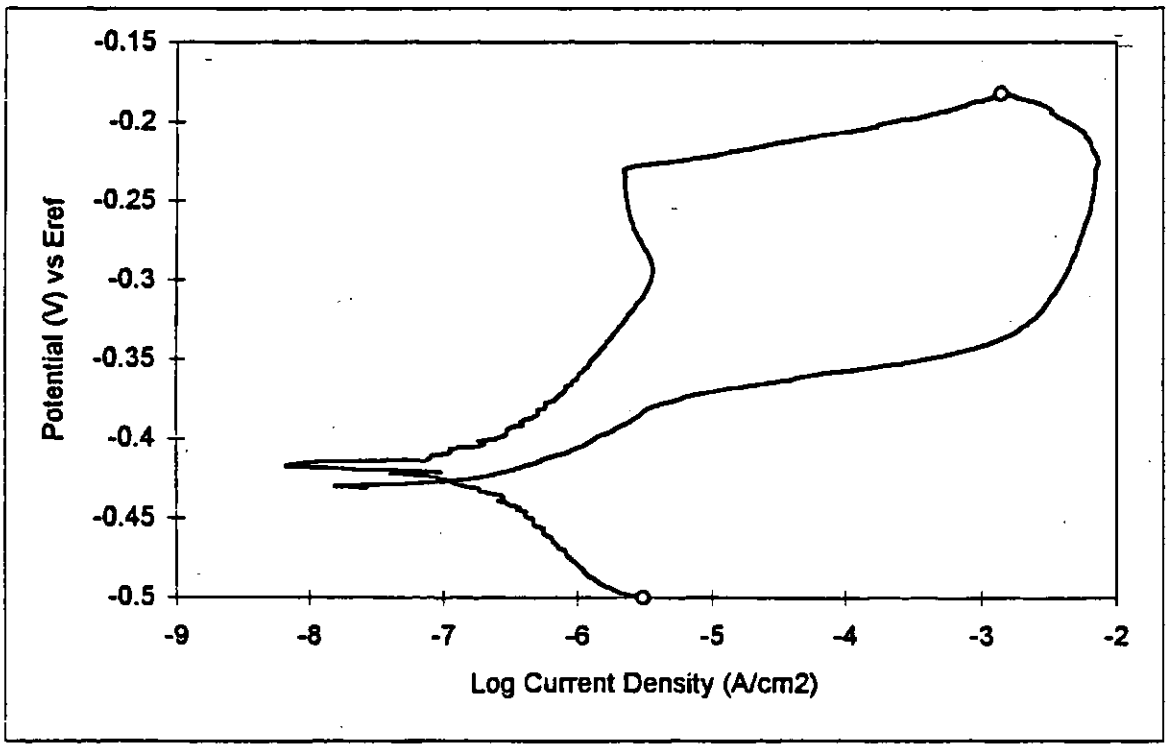

Fig. C.11 2304 at 90°C, deaerated (1940 rpm)

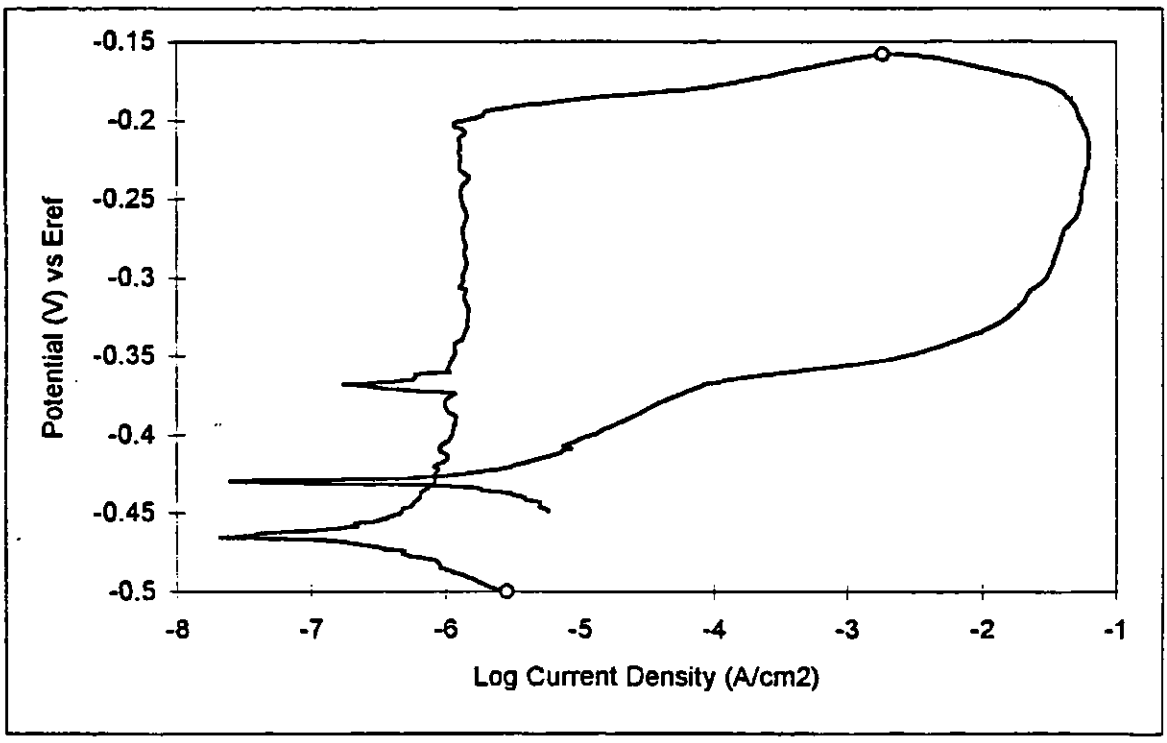

Fig. C.12 2304 at 90°C, deaerated (Stagnant)

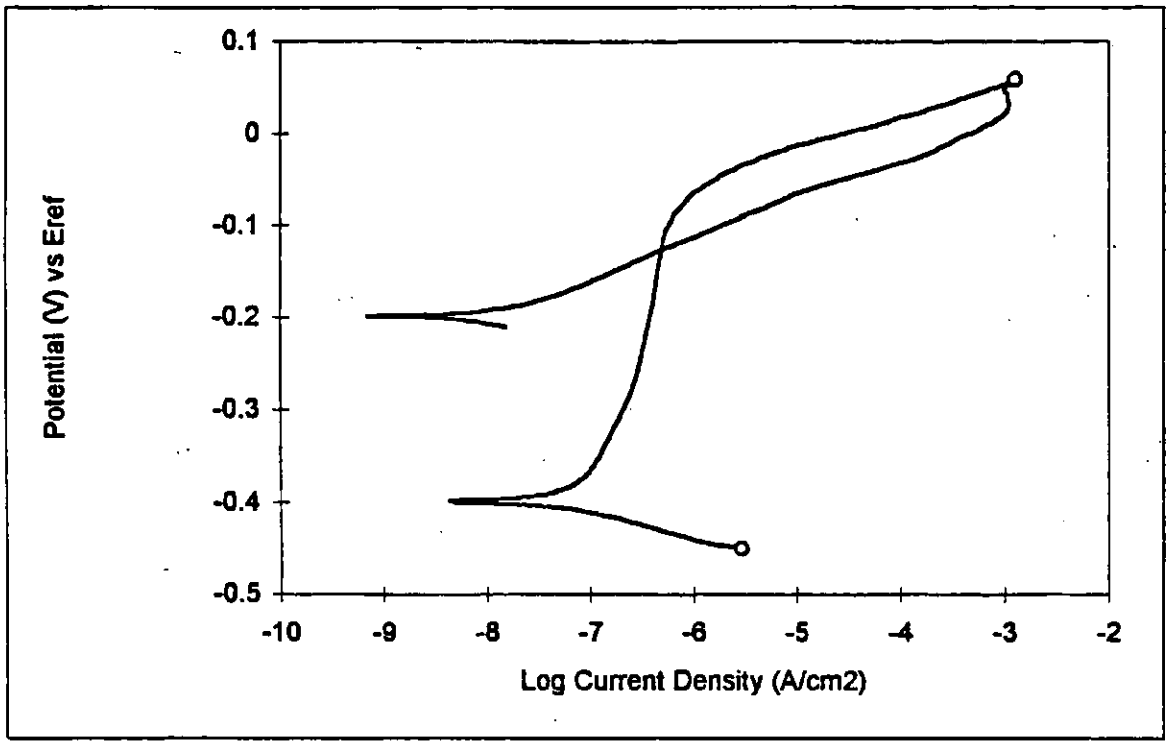

Fig. C.13 CN7M at 22°C, deaerated (1940 rpm)

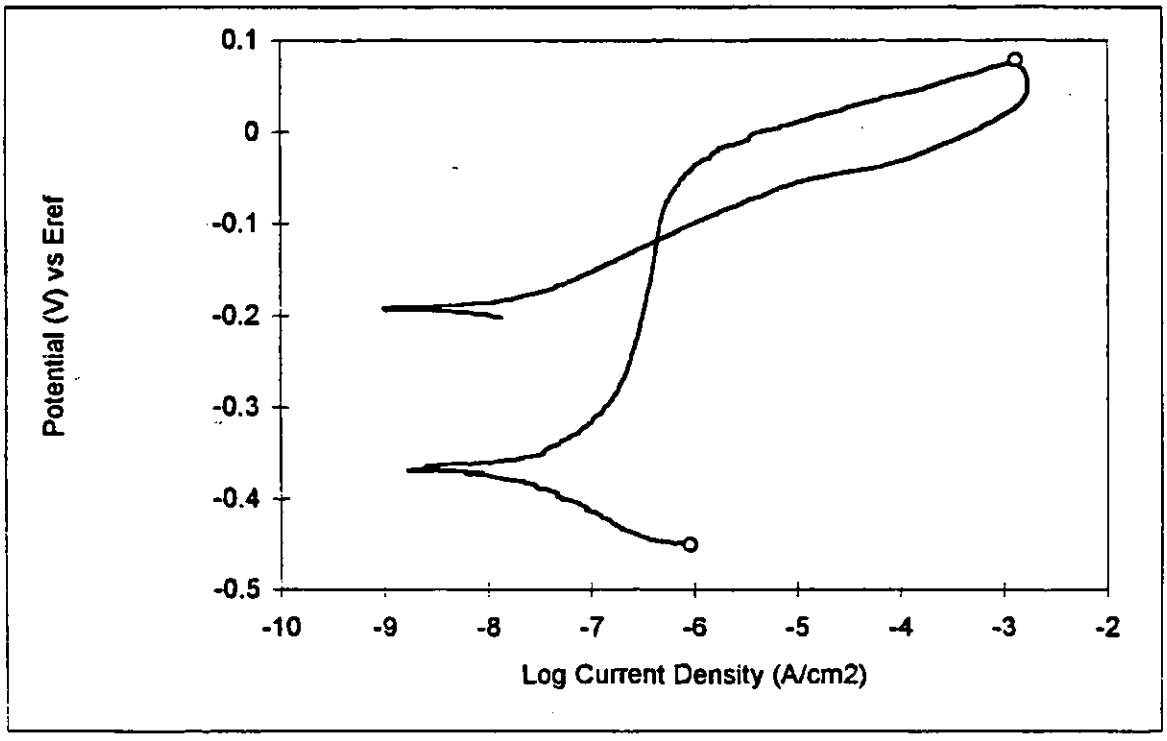

Fig. C.14 CN7M at 22°C, deaerated (Stagnant)

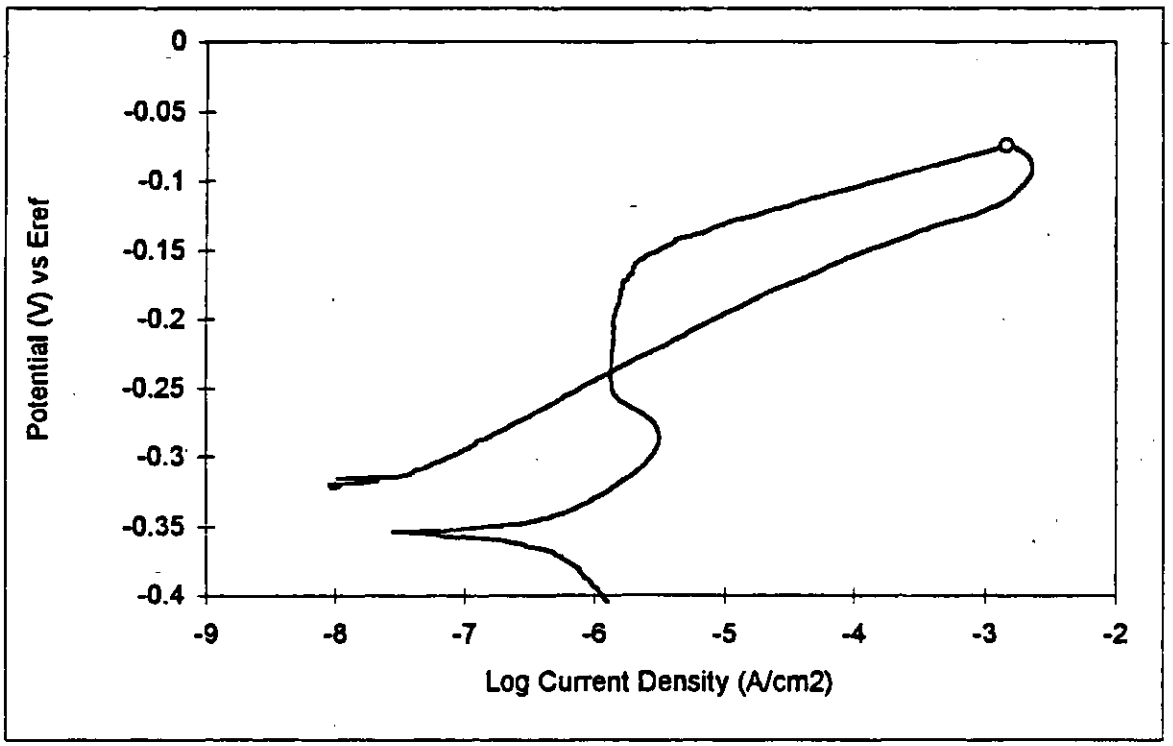

Fig. C.15 CN7M at 90°C, deaerated (1940 rpm)

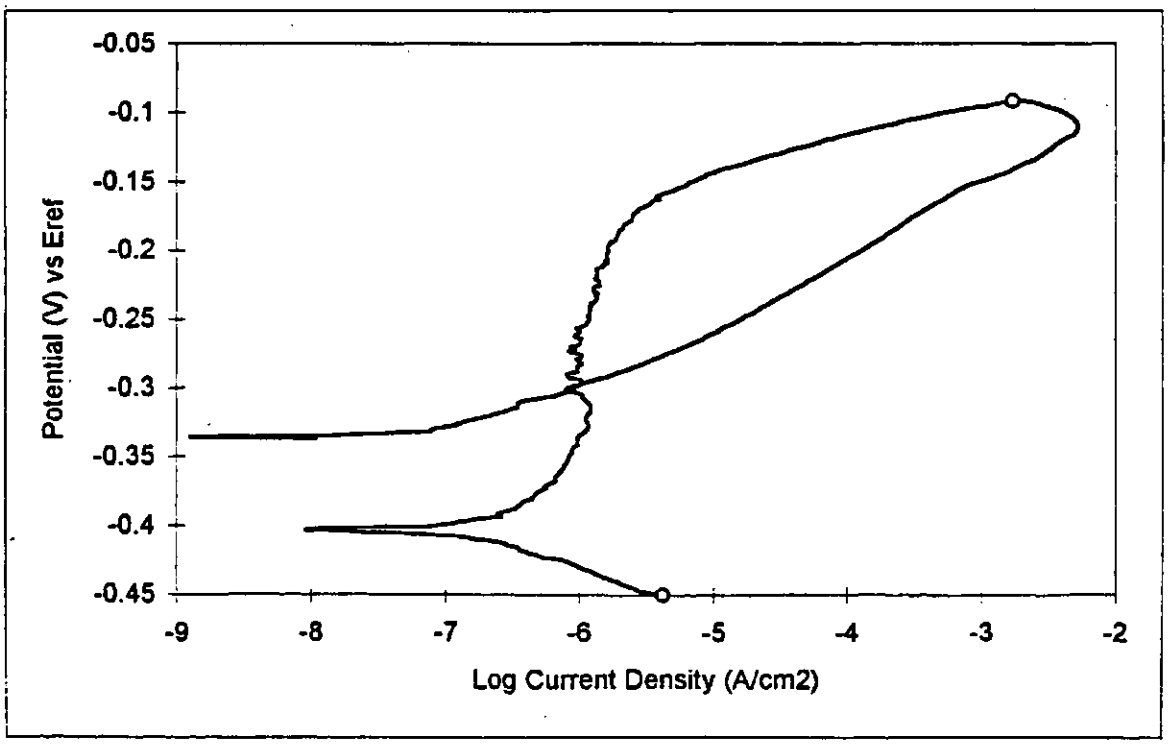

Fig. C.16 CN7M at 90°C, deaerated (Stagnant)

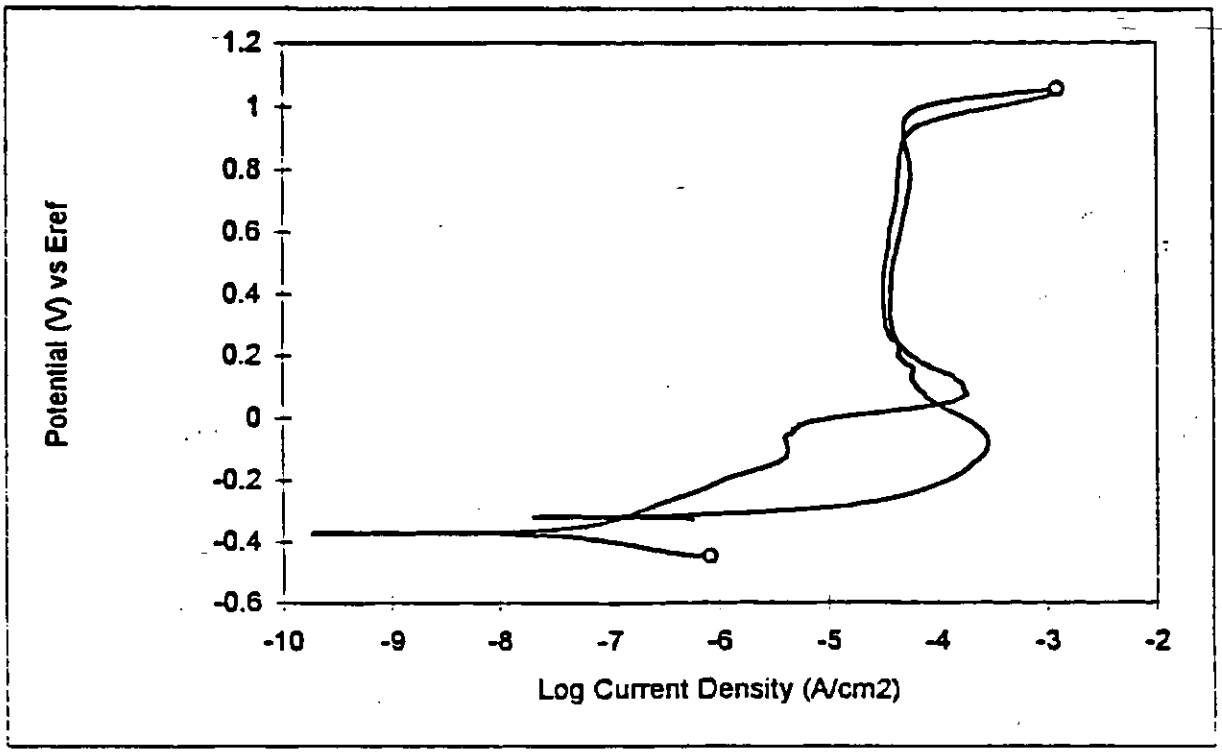

Fig. C.17 CD4MCu at 22°C, deaerated (1940 rpm)

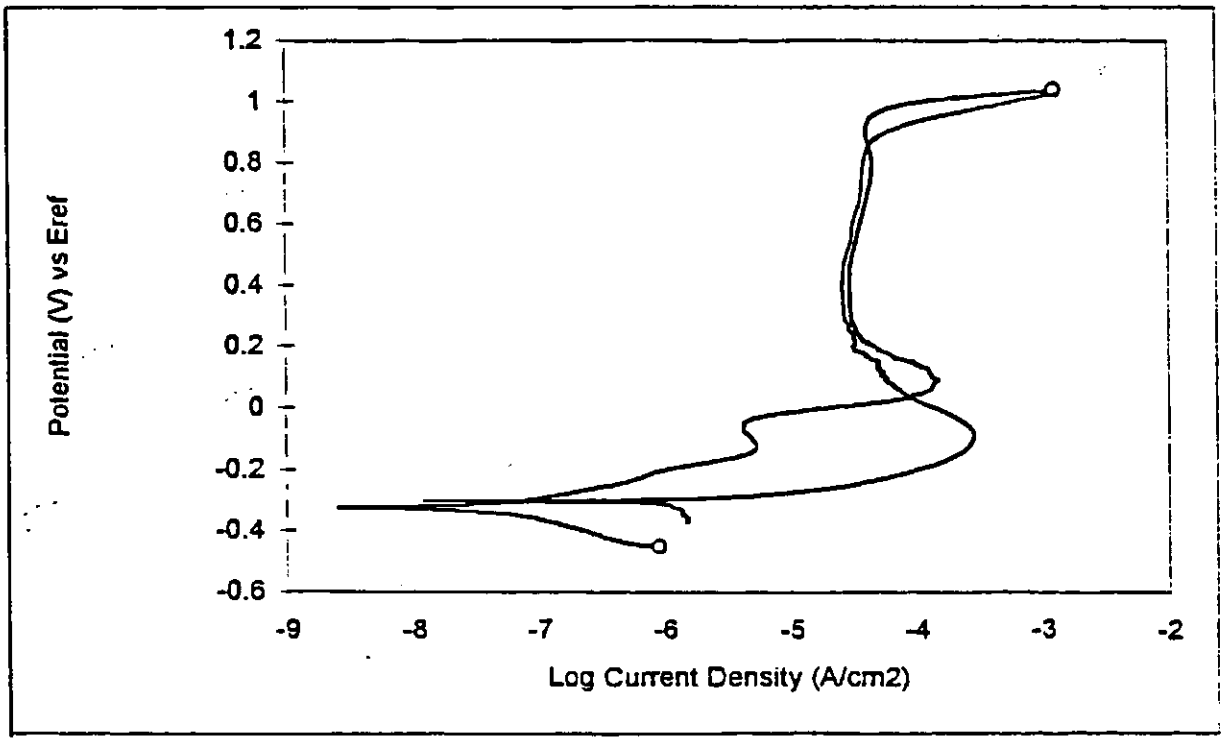

Fig. C.18 CD4MCu at 22°C, deaerated (Stagnant)

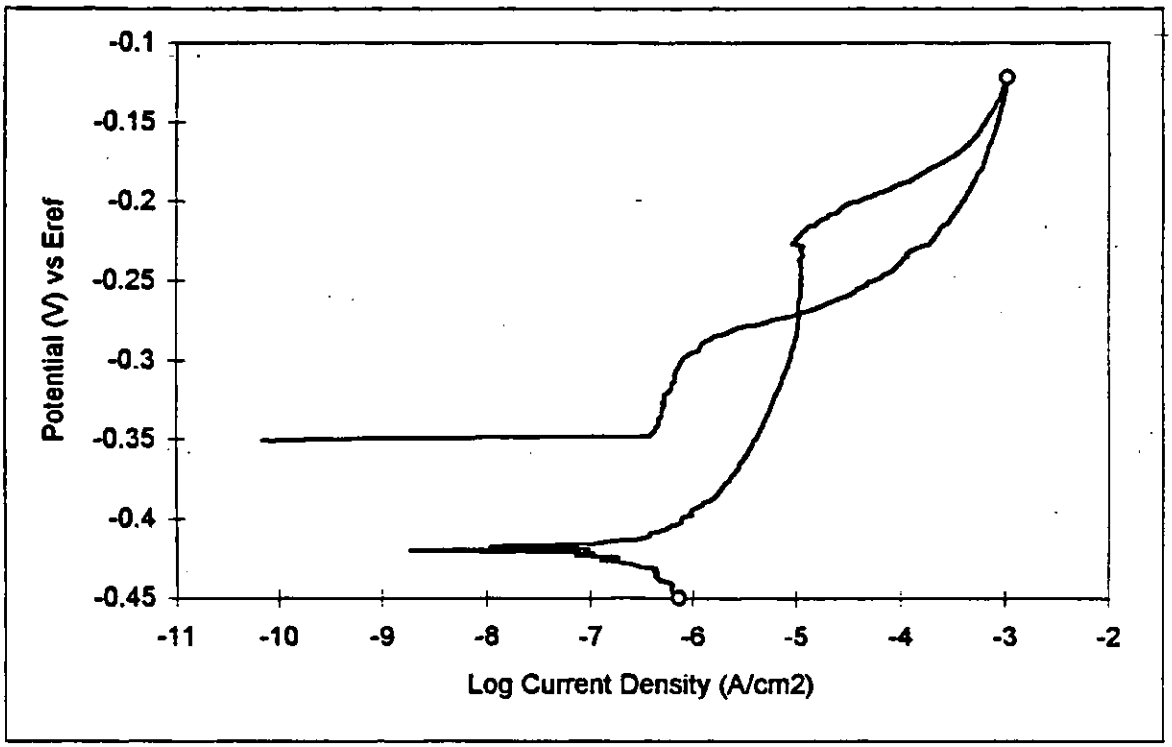

Fig. C.19 CD4MCu at 90°C, deaerated (1940 rpm)

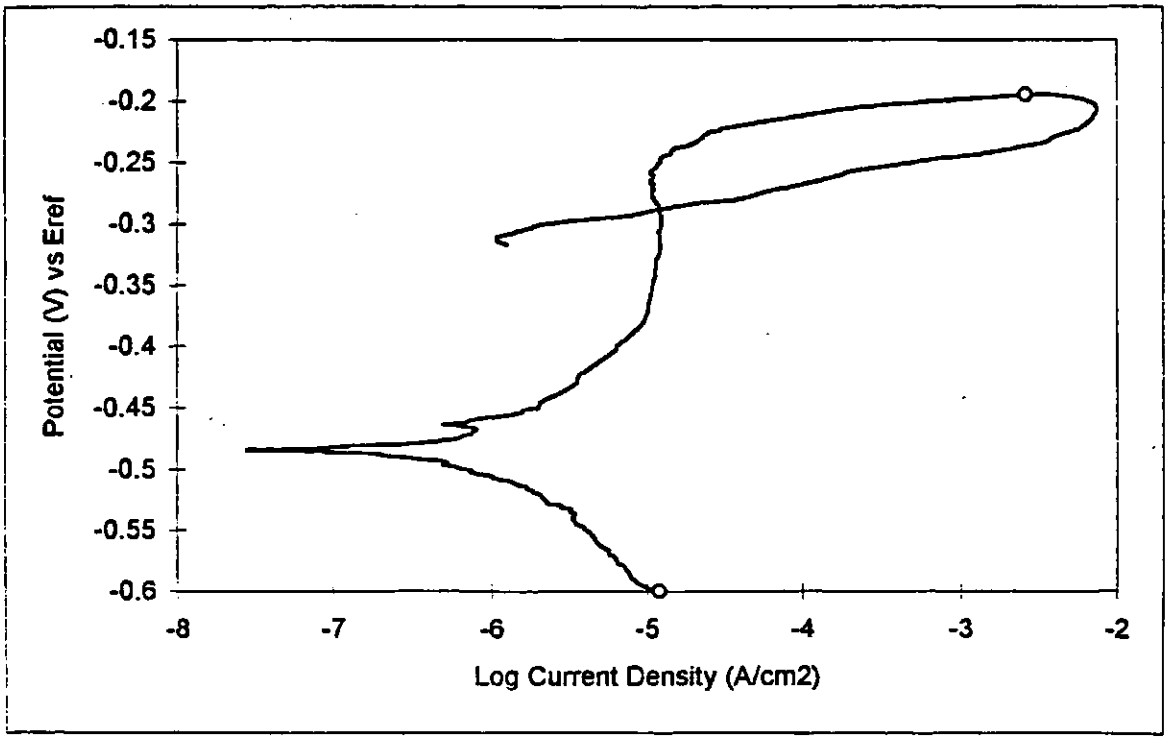

Fig. C.20 CD4MCu at 90°C, deaerated (Stagnant)

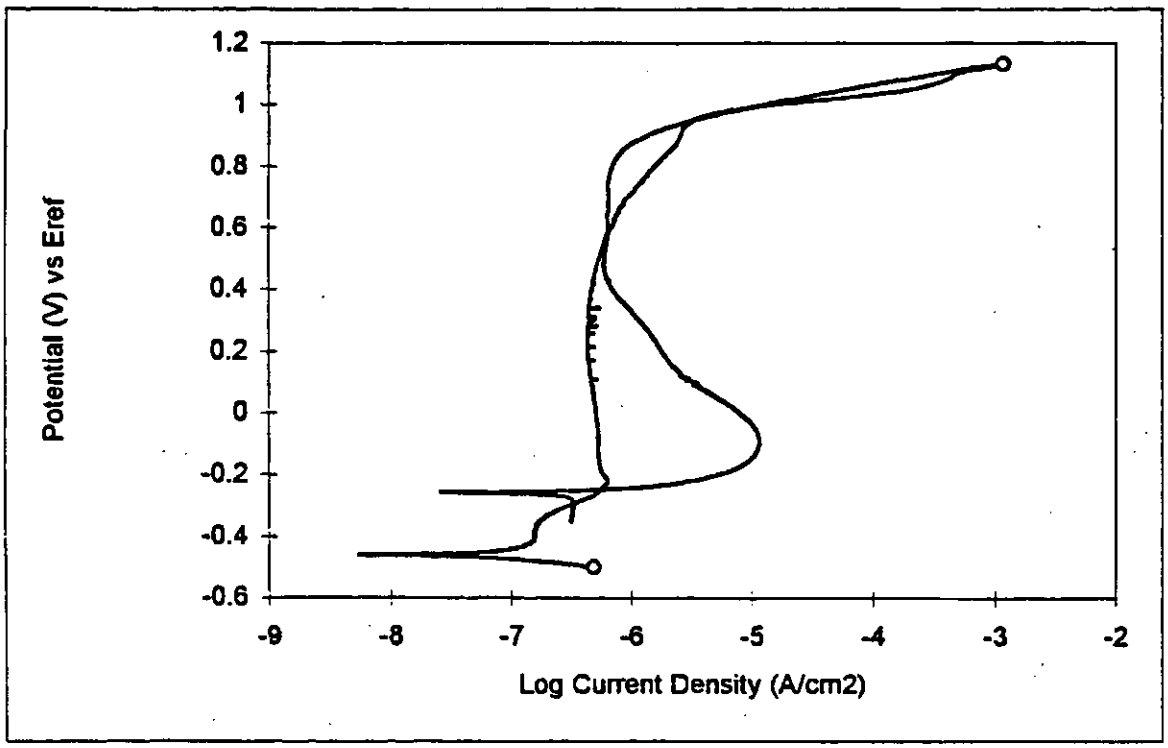

Fig. C.21 2205 at 22°C, deaerated (1940 rpm)

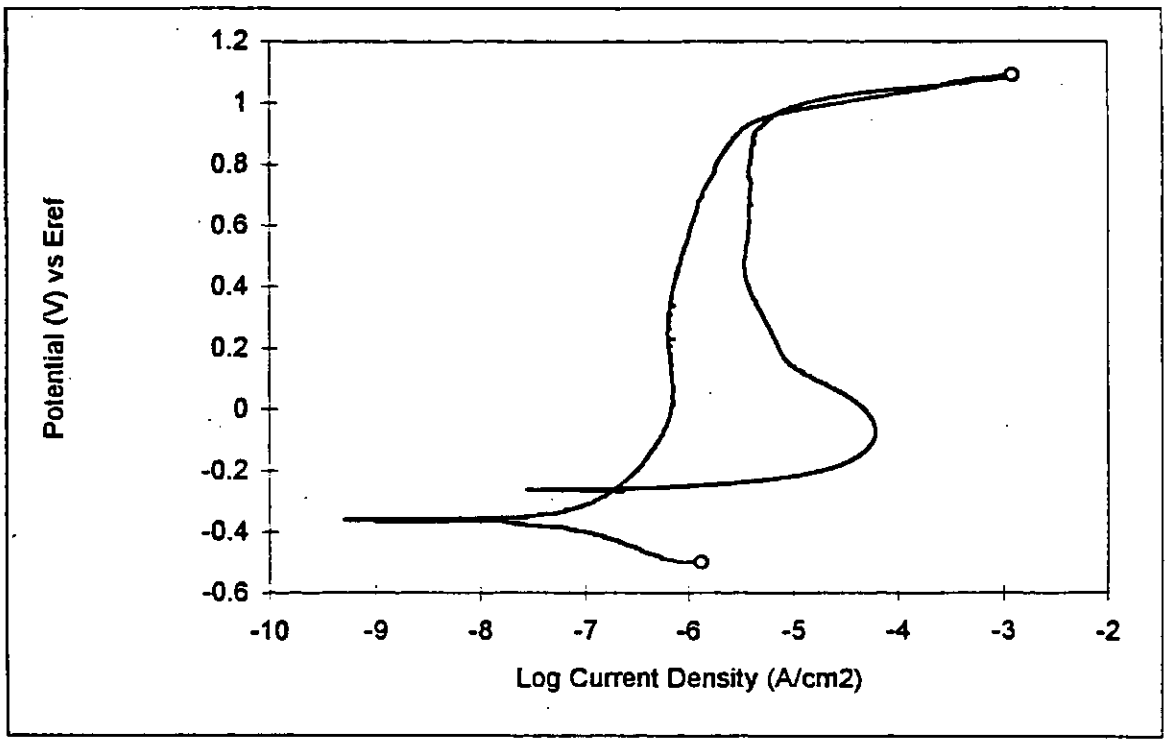

Fig. C.22 2205 at 22°C, deaerated (Stagnant)

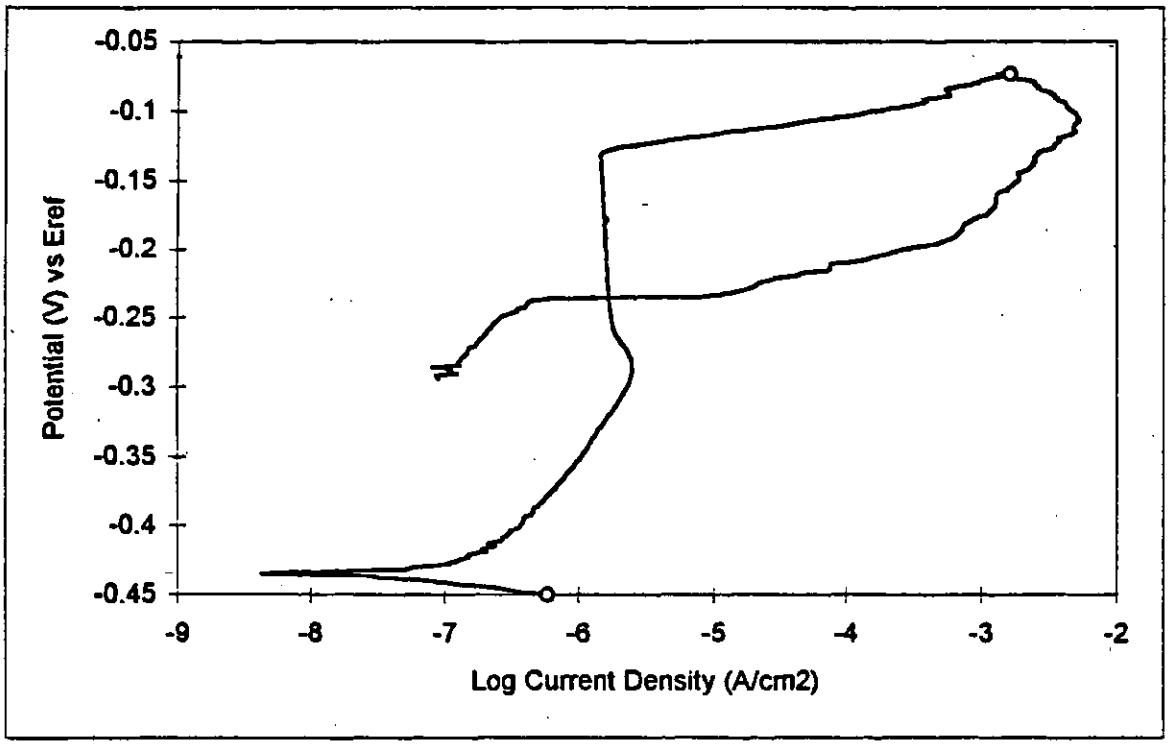

Fig. C.23 2205 at 90°C, deaerated (1940 rpm)

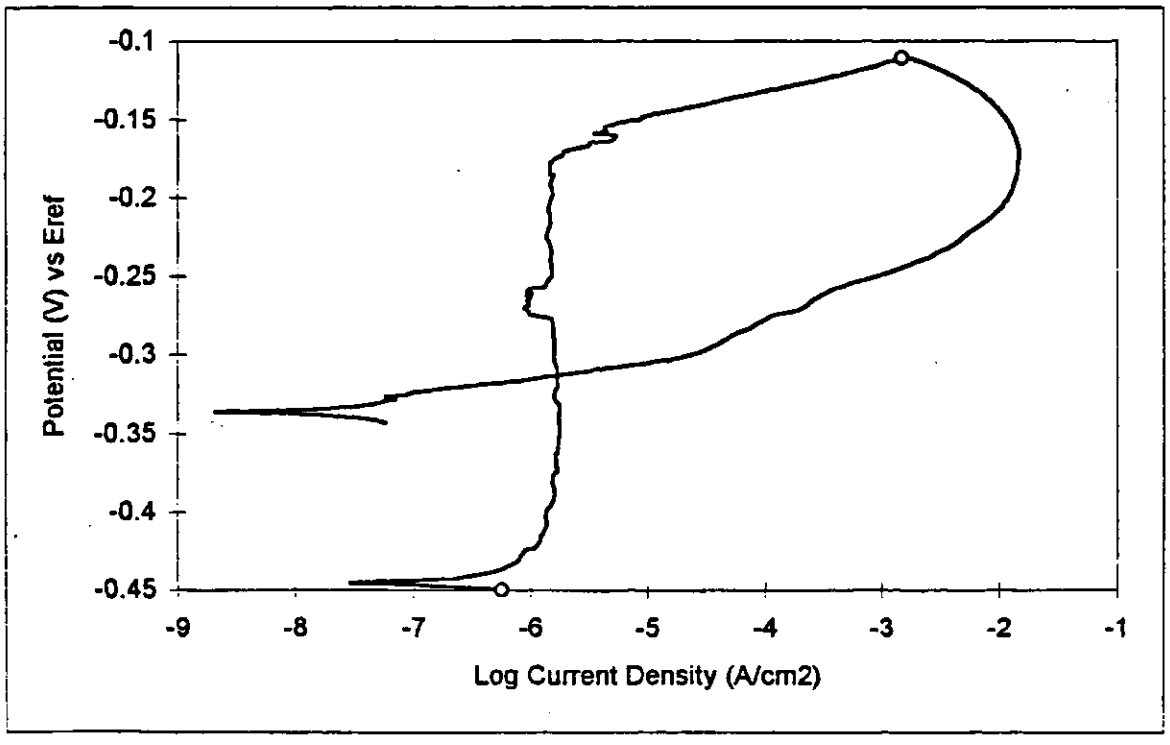

Fig. C.24 2205 at 90°C, deaerated (Stagnant)

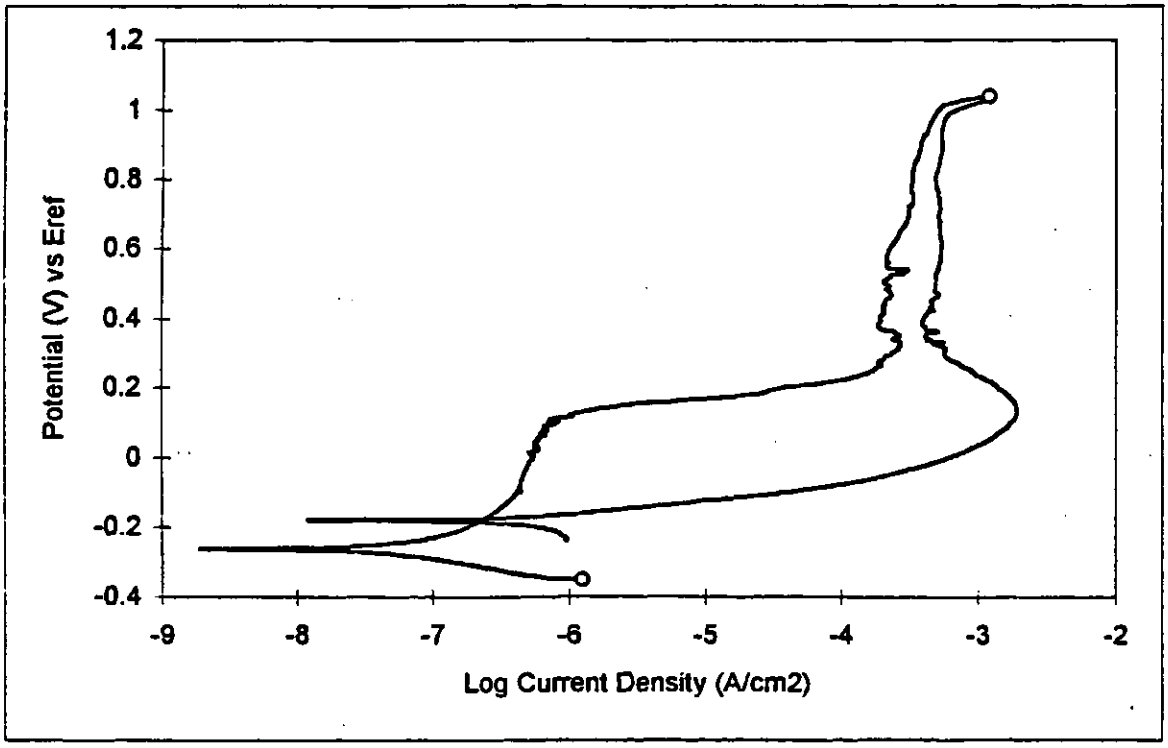

Fig. C.25 904L at 22°C, deaerated (1940 rpm)

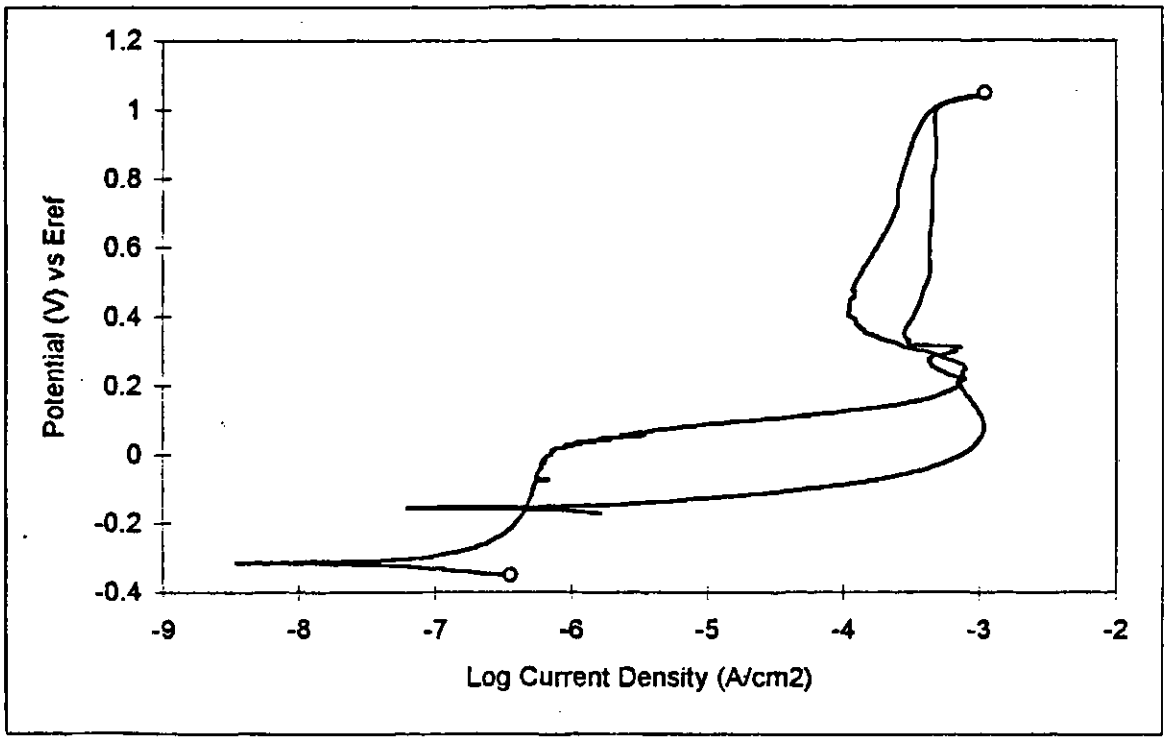

Fig. C.26 904L at 22°C, deaerated (Stagnant)

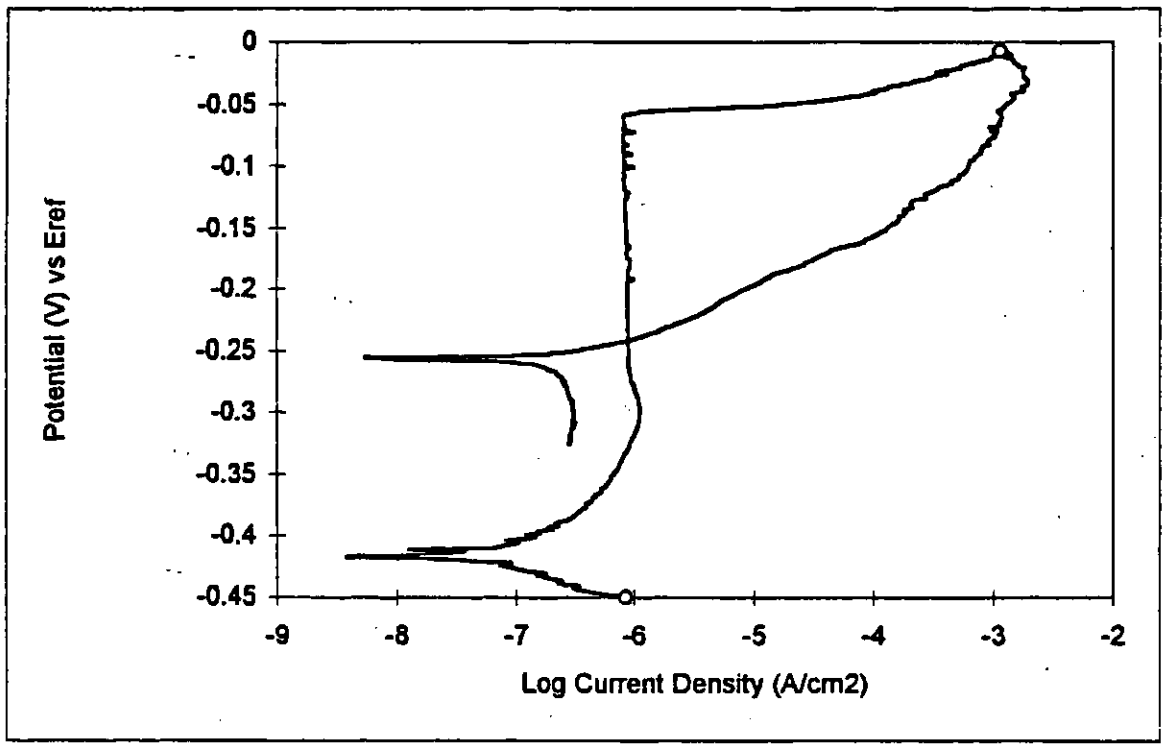

Fig. C.27 904L at 90°C, deaerated (1940 rpm)

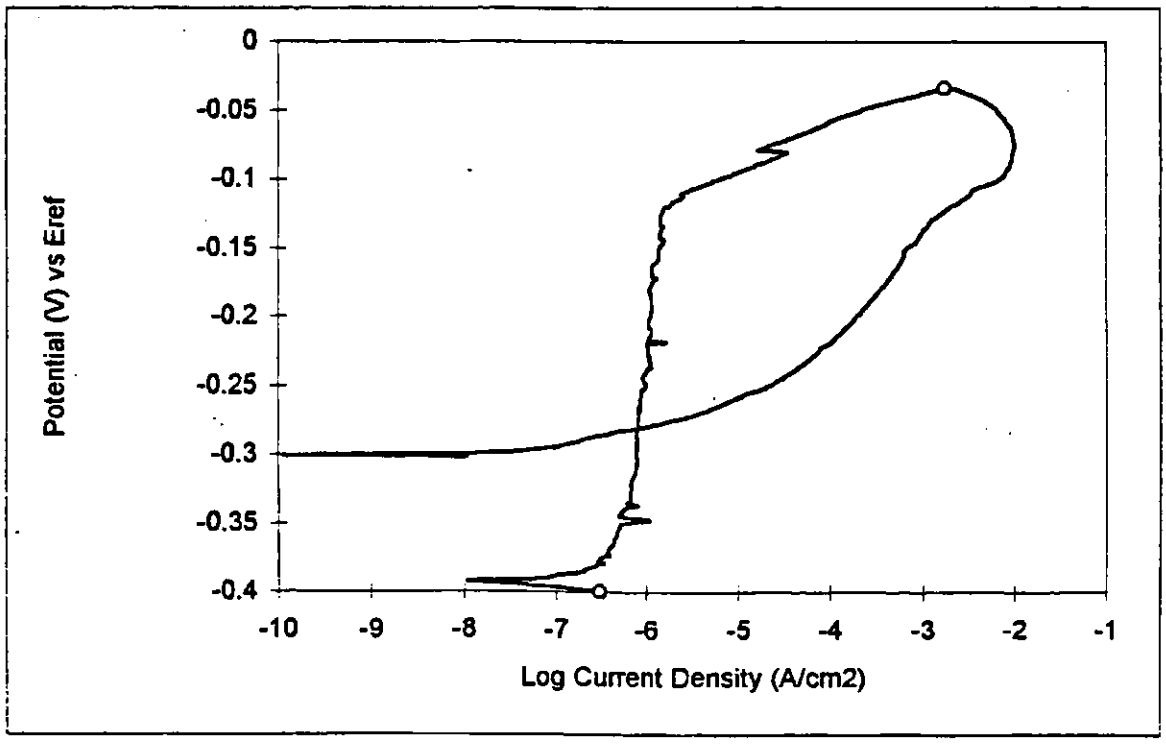

Fig. C.28 904L at 90°C, deaerated (Stagnant)

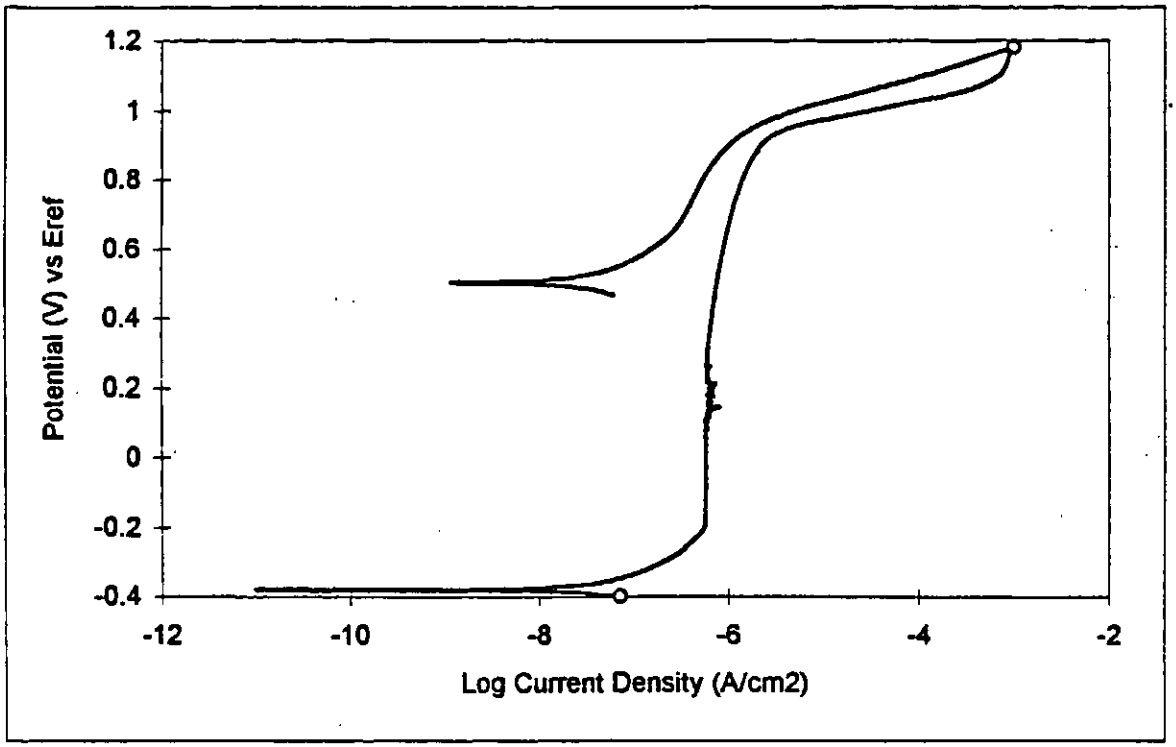

Fig. C.29 2507 at 22°C, deaerated (1940 rpm)

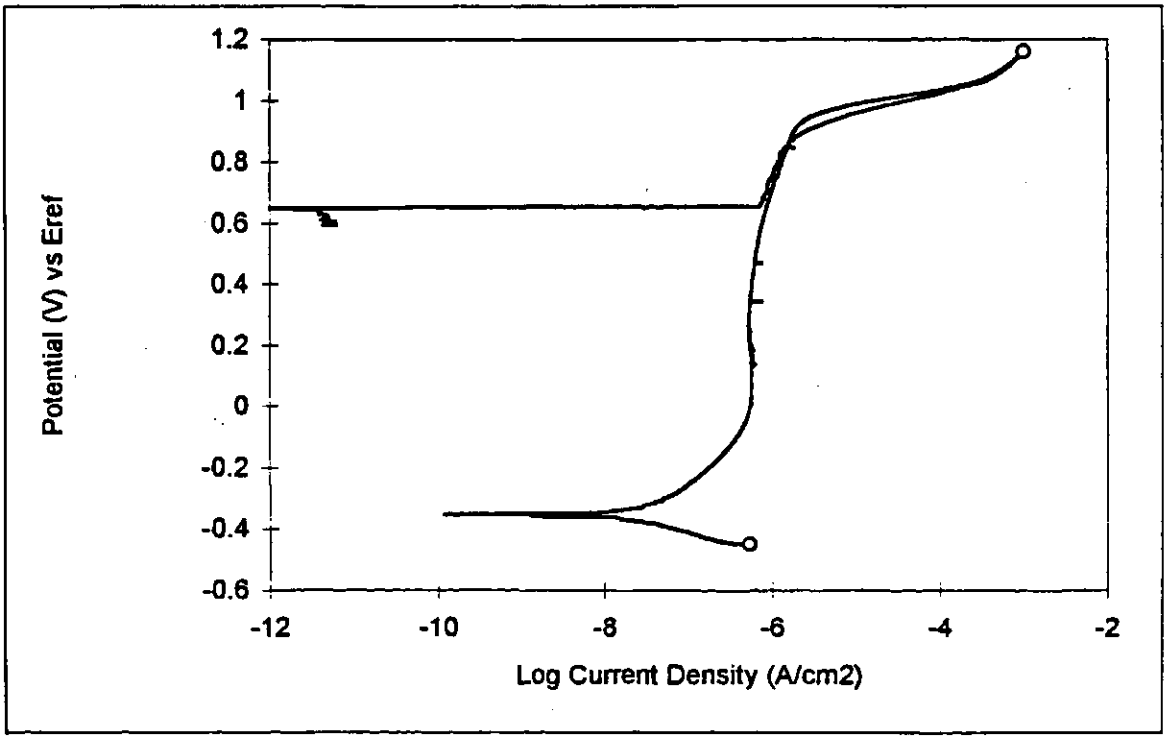

Fig. C.30 2507 at 22°C, deaerated (Stagnant)

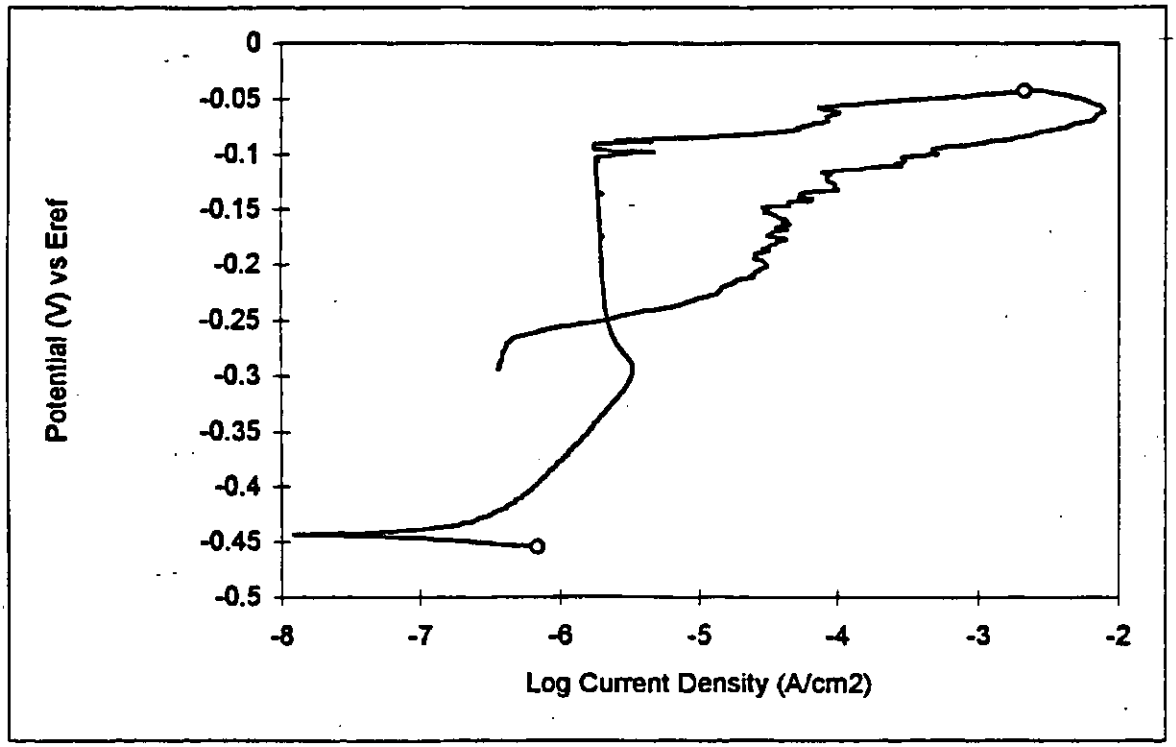

Fig. C.31 2507 at 90°C, deaerated (1940 rpm)

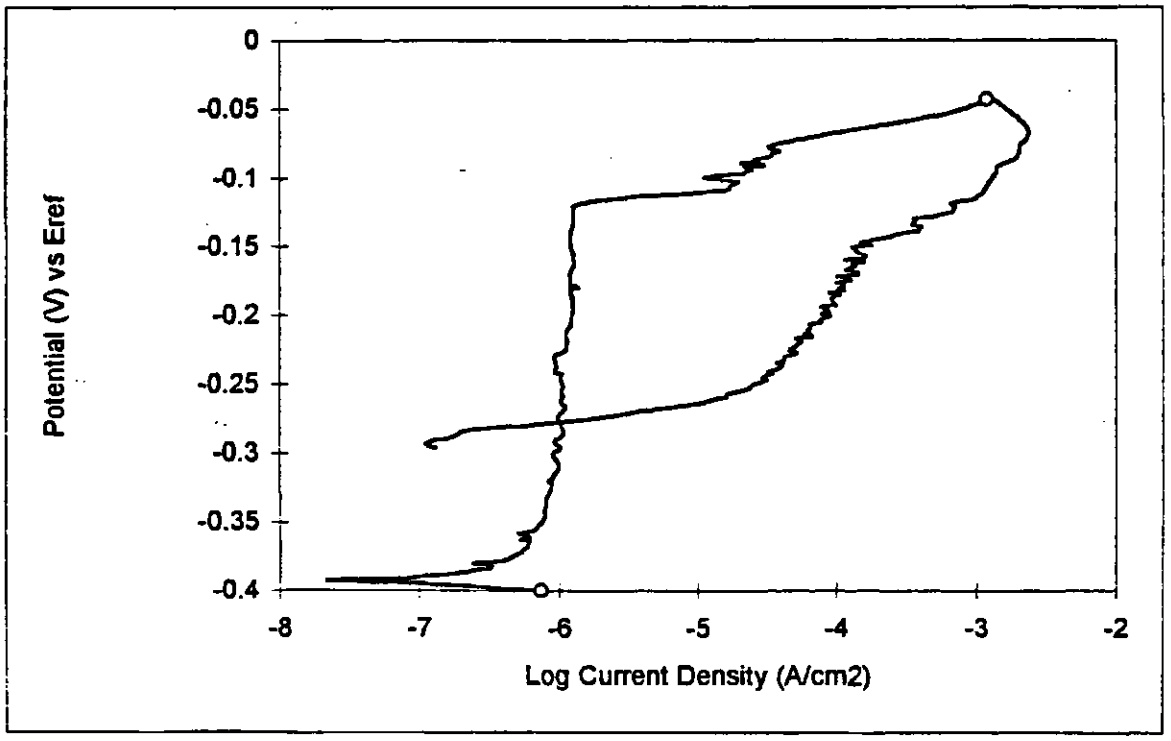

Fig. C.32 2507 at 90°C, deaerated (Stagnant)

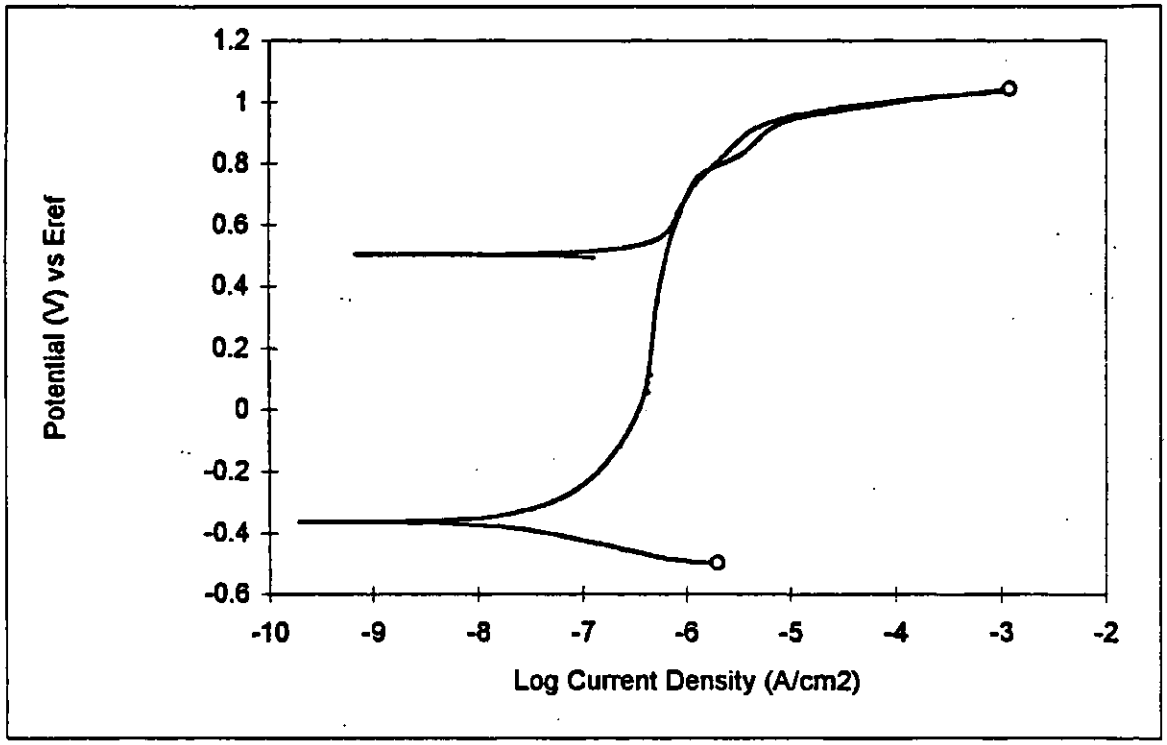

Fig. C.33 254SMO at 22°C, deaerated (1940 rpm)

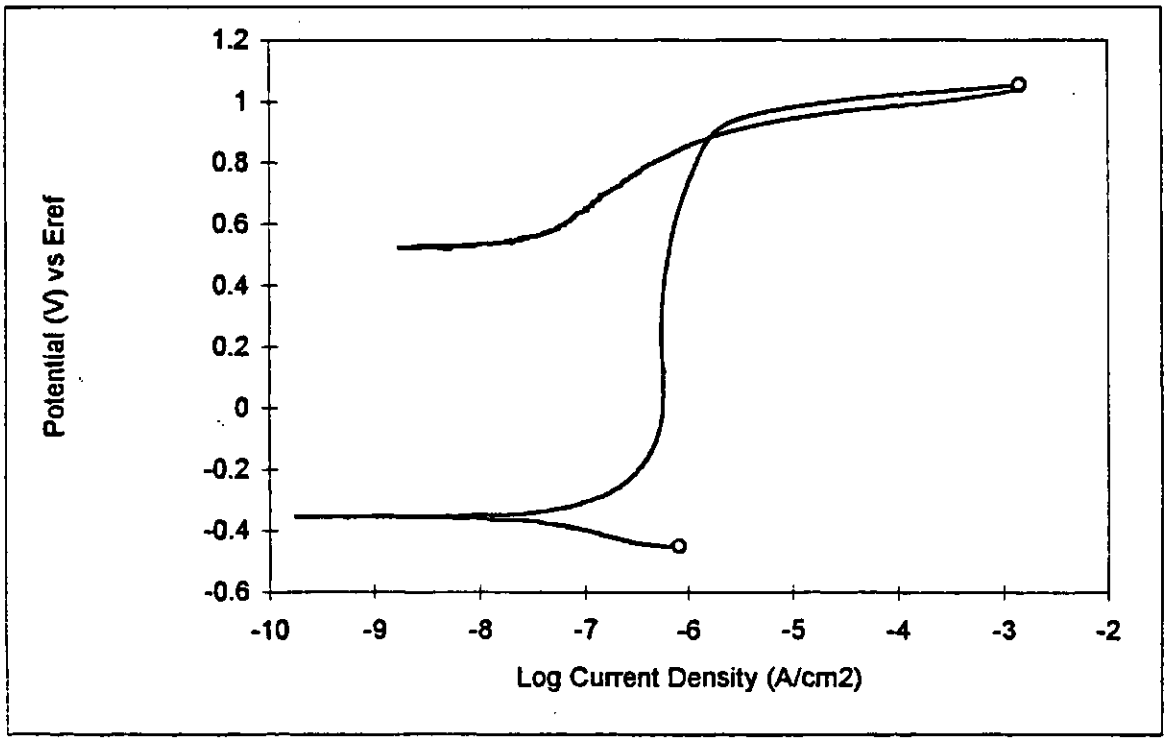

Fig. C.34 254SMO at 22°C, deaerated (Stagnant)

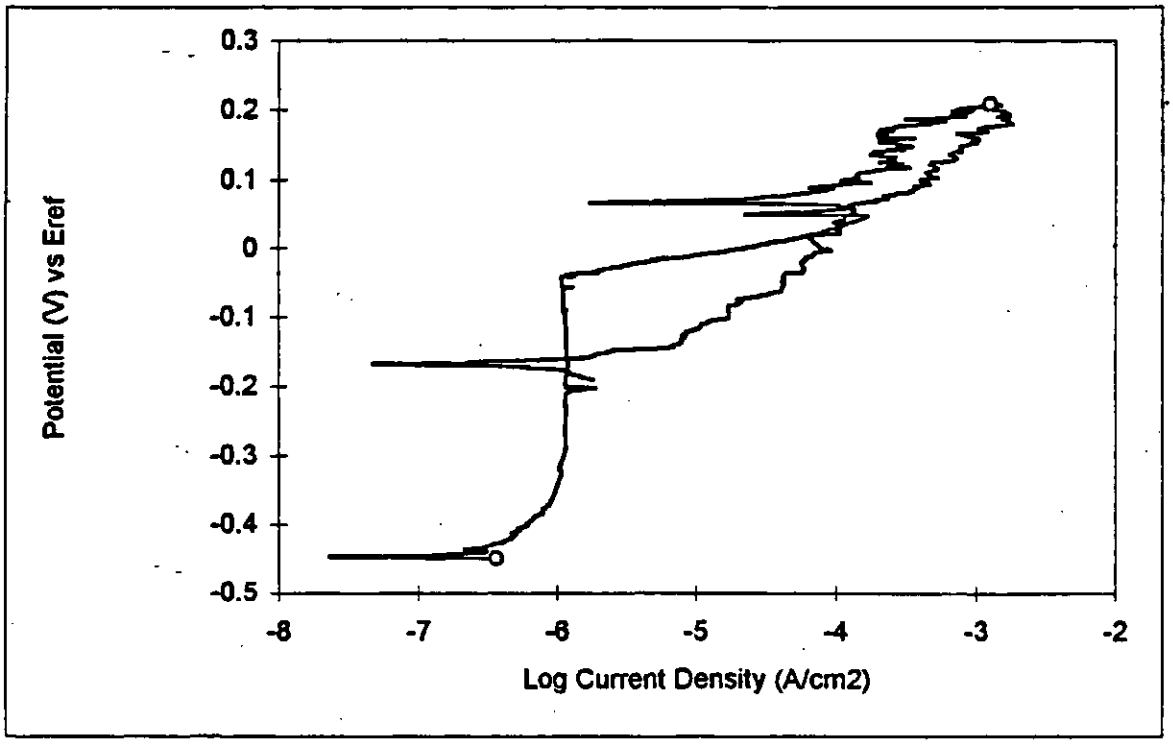

Fig. C.31 254SMO at 90°C, deaerated (1940 rpm)

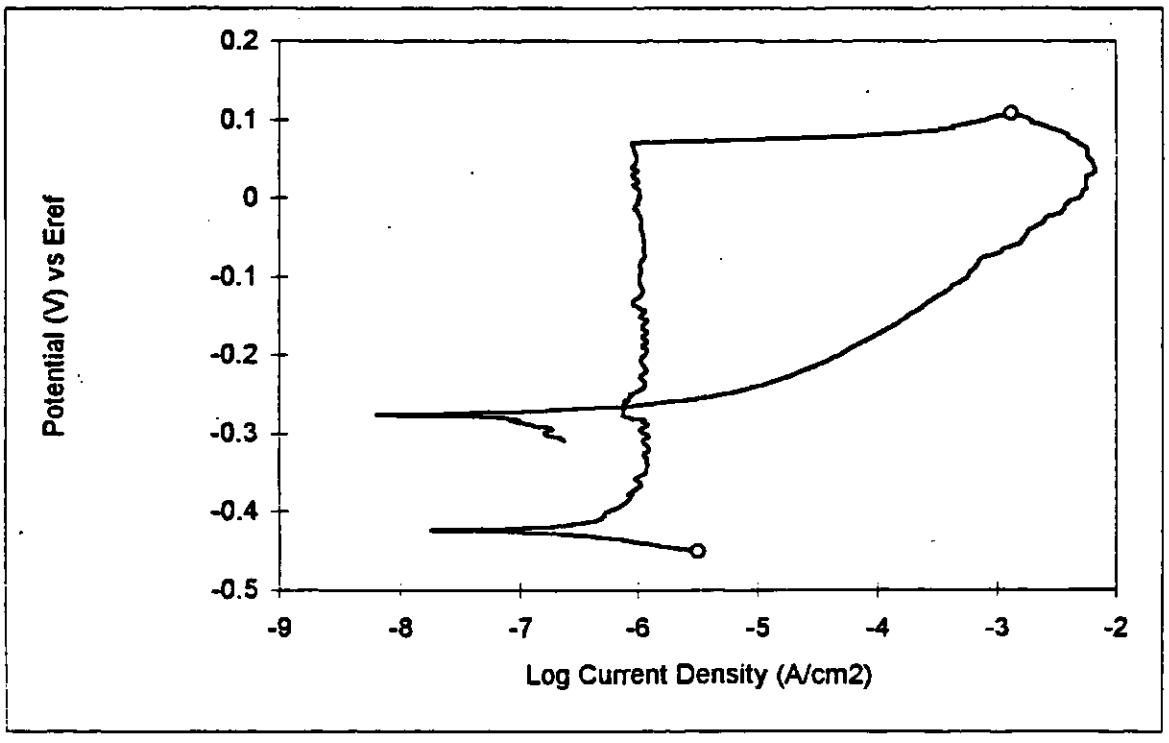

Fig. C.32 254SMO at 90°C, deaerated (Stagnant)

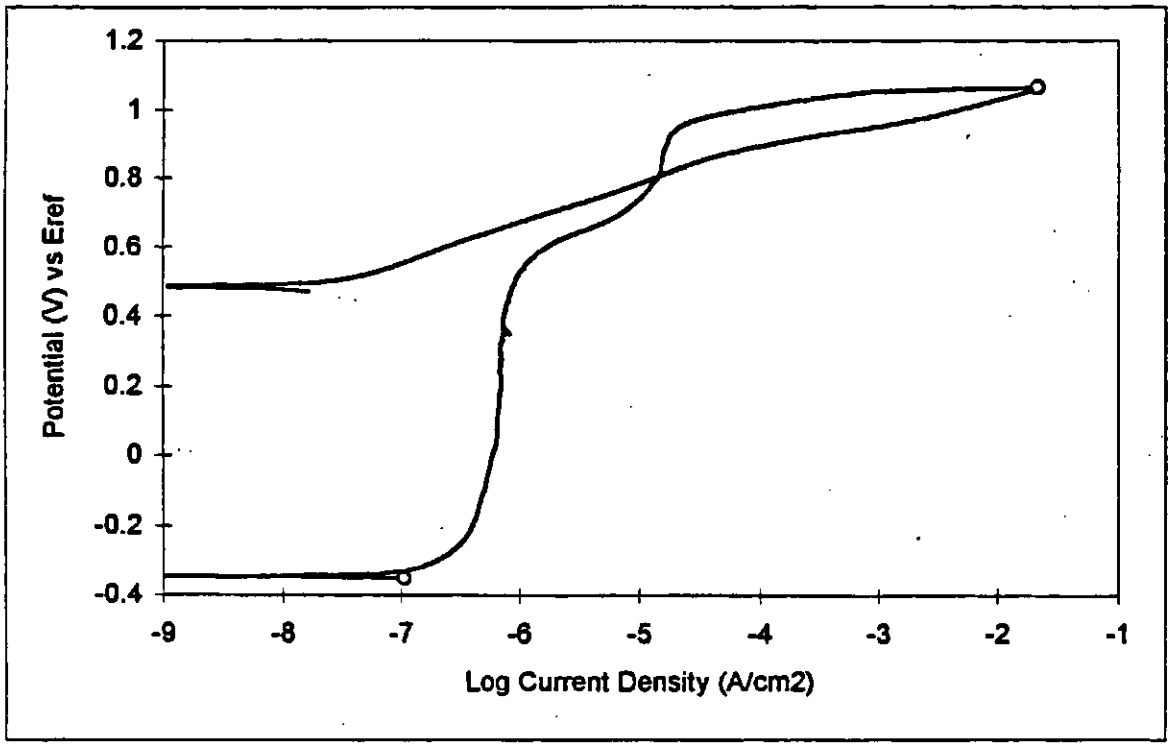

Fig. C.37 C276 at 22°C, deaerated (1940 rpm)

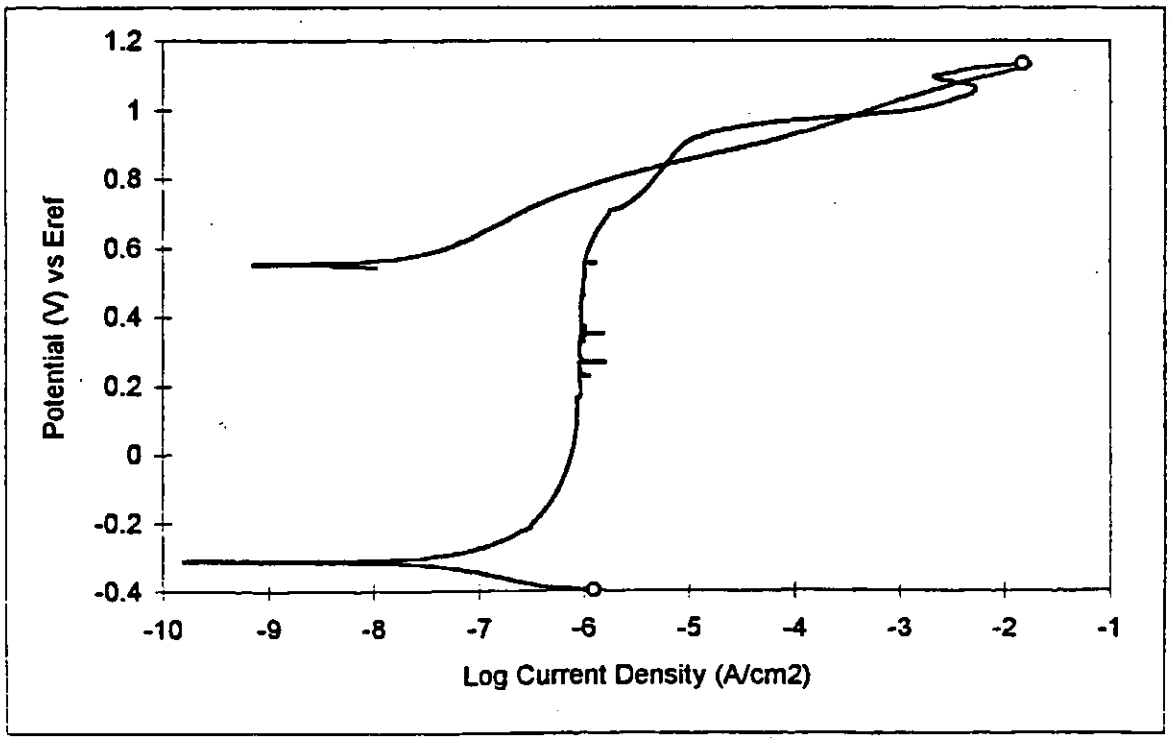

Fig. C.38 C276 at 22°C, deaerated (Stagnant)

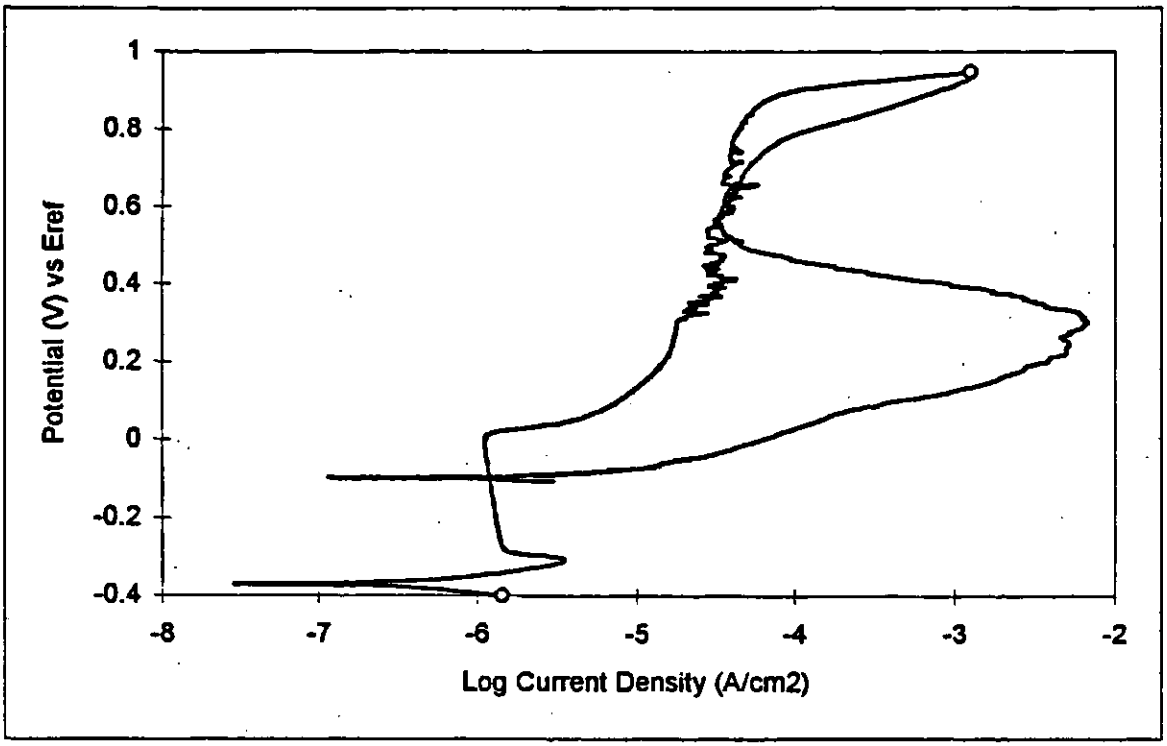

Fig. C.39 C276 at 90°C, deaerated (1940 rpm)

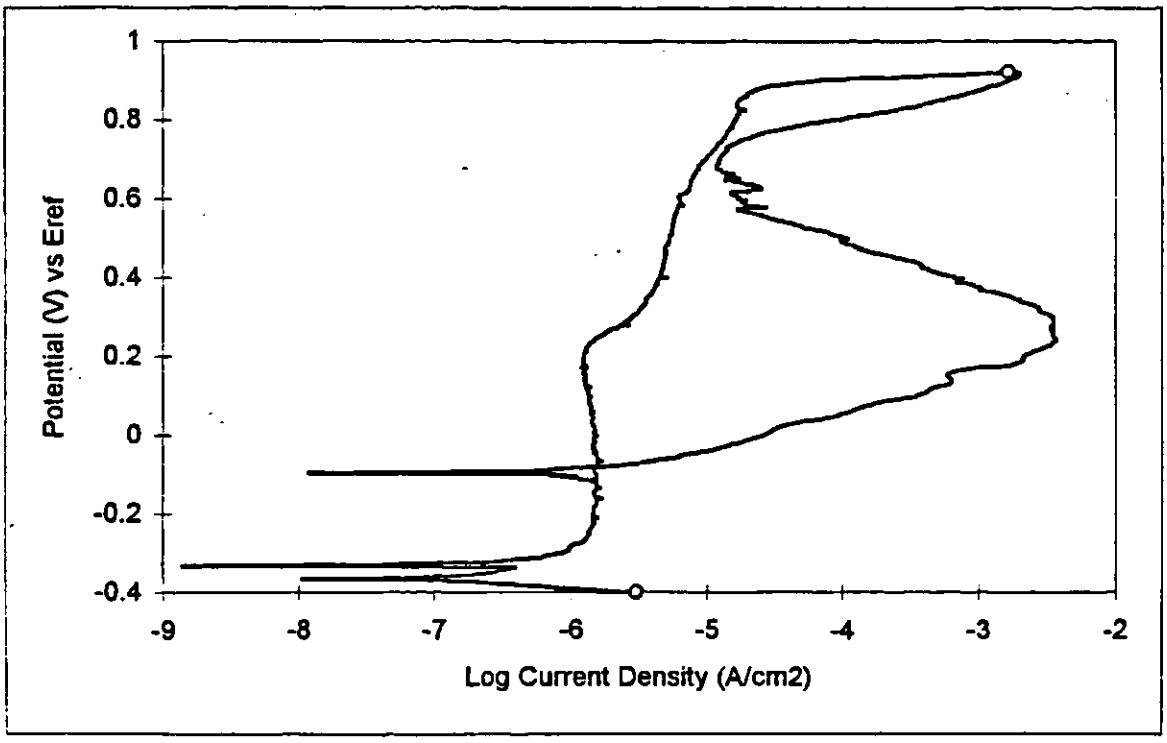

Fig. C.40 C276 at 90°C, deaerated (Stagnant)

Appendix D

The pit depth distribution of samples after the exposure test are shown in this appendix.

Bin	*Frequency*	*Cumulative %*
10	30	29.41%
20	41	69.61%
50	21	90.20%
100	5	95.10%
200	5	100.00%
300	0	100.00%
More	0	100.00%
	102	

Bin: pit depth in microns

Frequency: number of pits

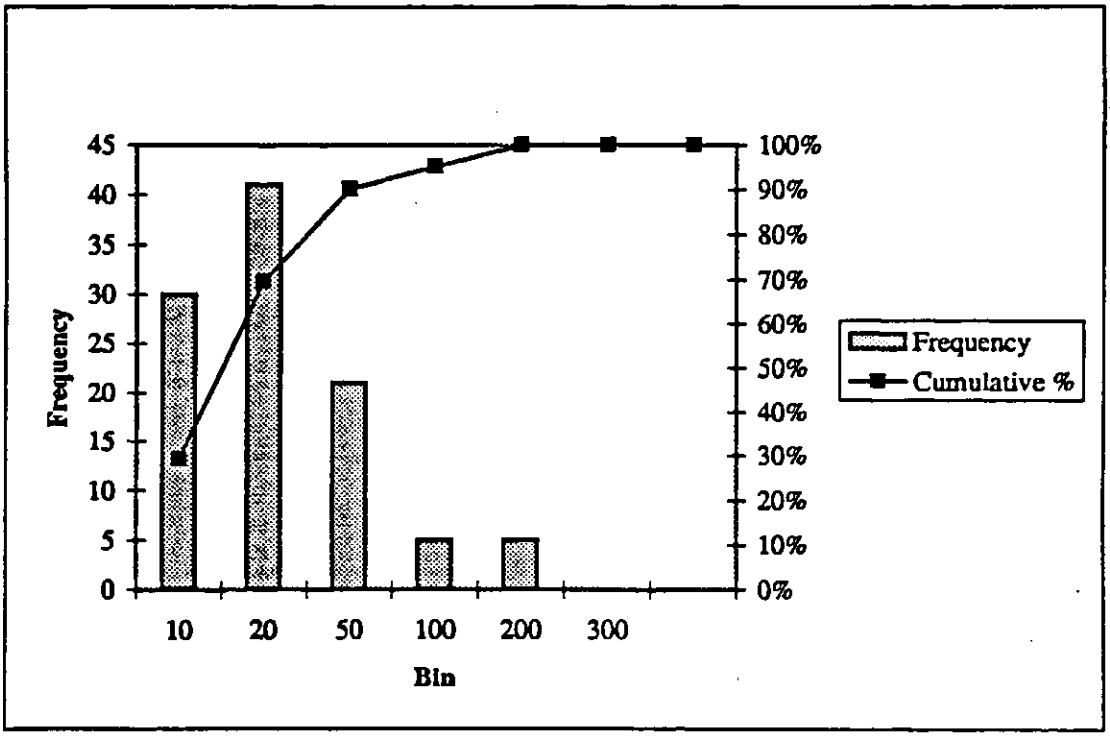

Fig. D1 Pit distribution for 304L after 30 days at 90°C

Bin	*Frequency*	*Cumulative %*
10	0	.00%
20	6	5.08%
50	64	59.32%
100	39	92.37%
200	9	100.00%
300	0	100.00%
400	0	100.00%
More	0	100.00%
	118	

Bin: **pit depth in microns**

Frequency: **number of pits**

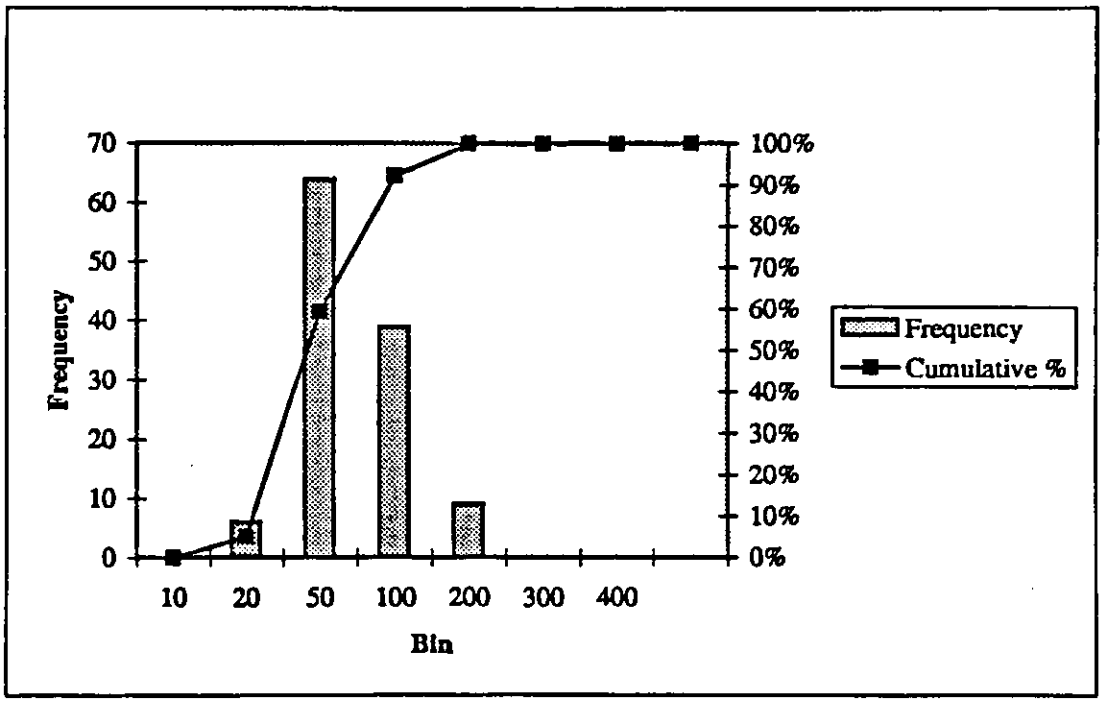

Fig. D2 The pit distribution for 304L after 60 days at 90°C

Bin	*Frequency*	*Cumulative %*
10	34	36.96%
20	19	57.61%
50	21	80.43%
100	16	97.83%
200	2	100.00%
300	0	100.00%
More	0	100.00%
	92	

Bin: pit depth in microns

Frequency: number of pits

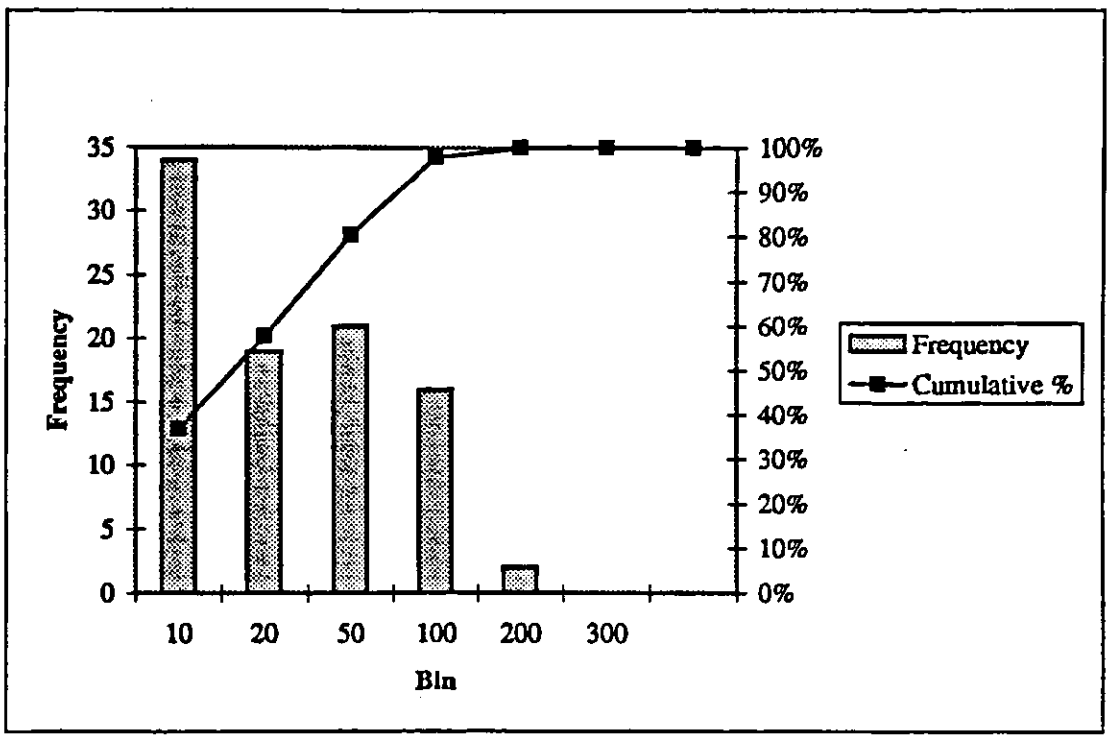

Fig. D3 Pit distribution for 316L after 30 days at 90°C

Bin	*Frequency*	*Cumulative %*
10	12	12.77%
20	27	41.49%
50	24	67.02%
100	28	96.81%
200	2	98.94%
300	1	100.00%
400	0	100.00%
More	0	100.00%
	94	

Bin: pit depth in microns

Frequency: number of pits

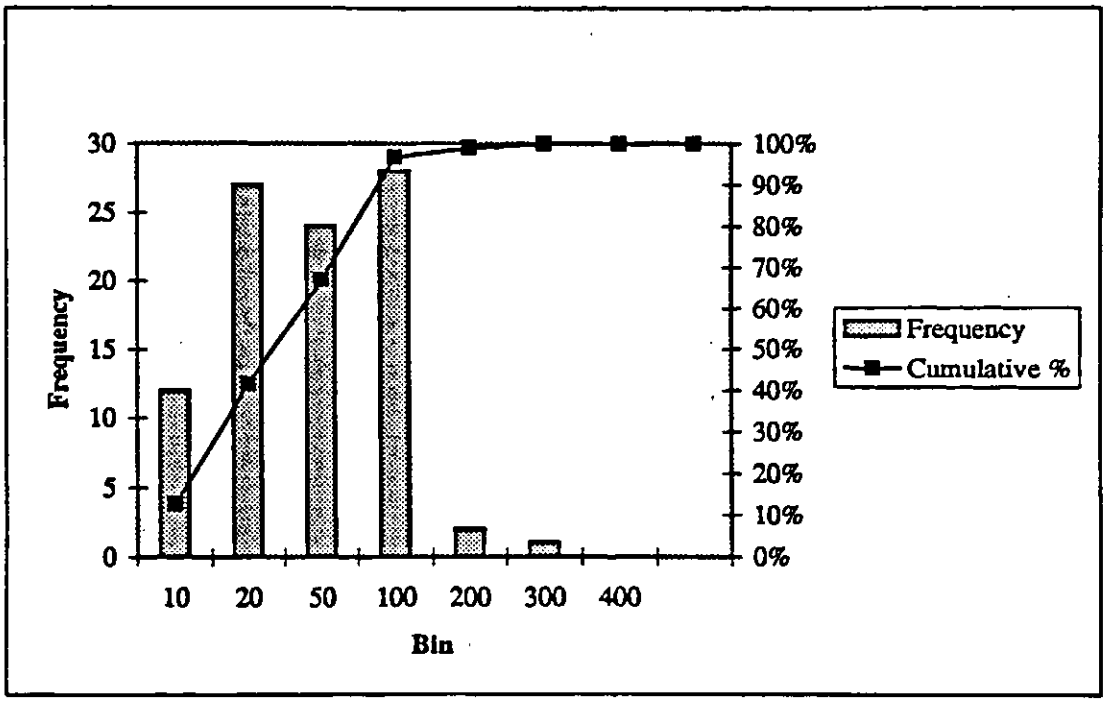

Fig. D4 The pit distribution for 316L after 60 days at 90°C

Bin	*Frequency*	*Cumulative %*
10	46	65.71%
20	3	70.00%
50	6	78.57%
100	12	95.71%
200	2	98.57%
300	1	100.00%
More	0	100.00%
	70	

Bin: pit depth in microns

Frequency: number of pits

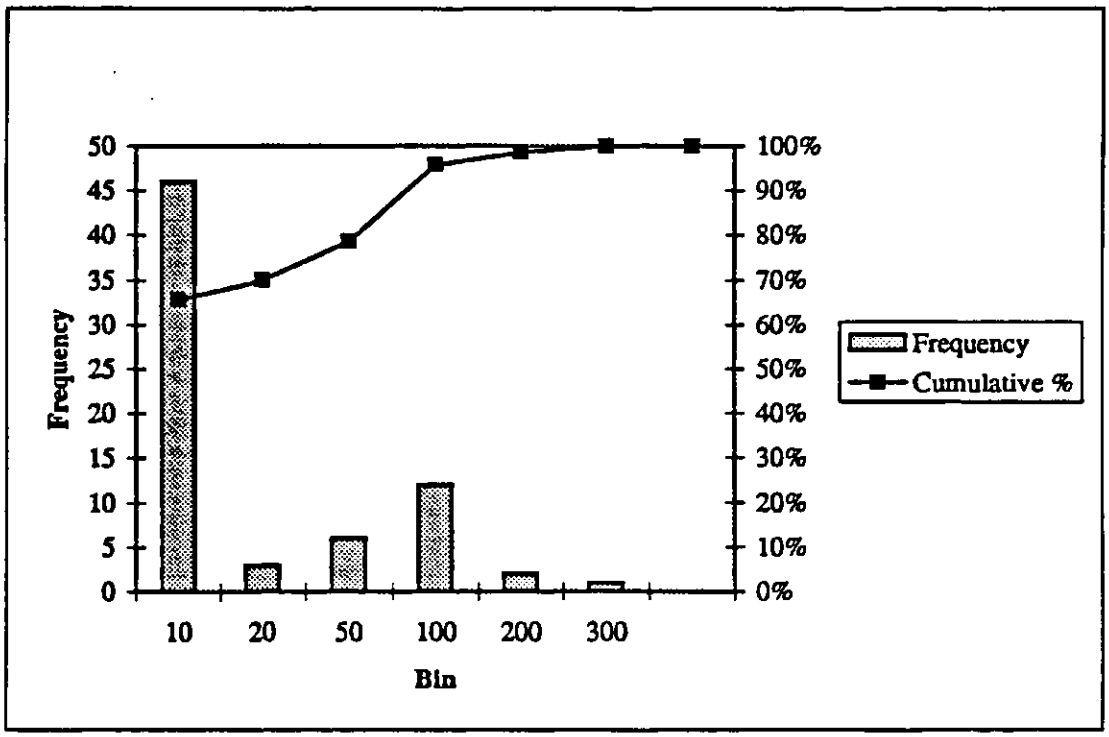

Fig. D5 Pit distribution for CN7M after 30 days at 90°C

Bin	*Frequency*	*Cumulative %*
10	49	70.00%
20	0	70.00%
50	2	72.86%
100	0	72.86%
200	16	95.71%
300	3	100.00%
400	0	100.00%
More	0	100.00%
	70	

Bin: **pit depth in microns**

Frequency: **number of pits**

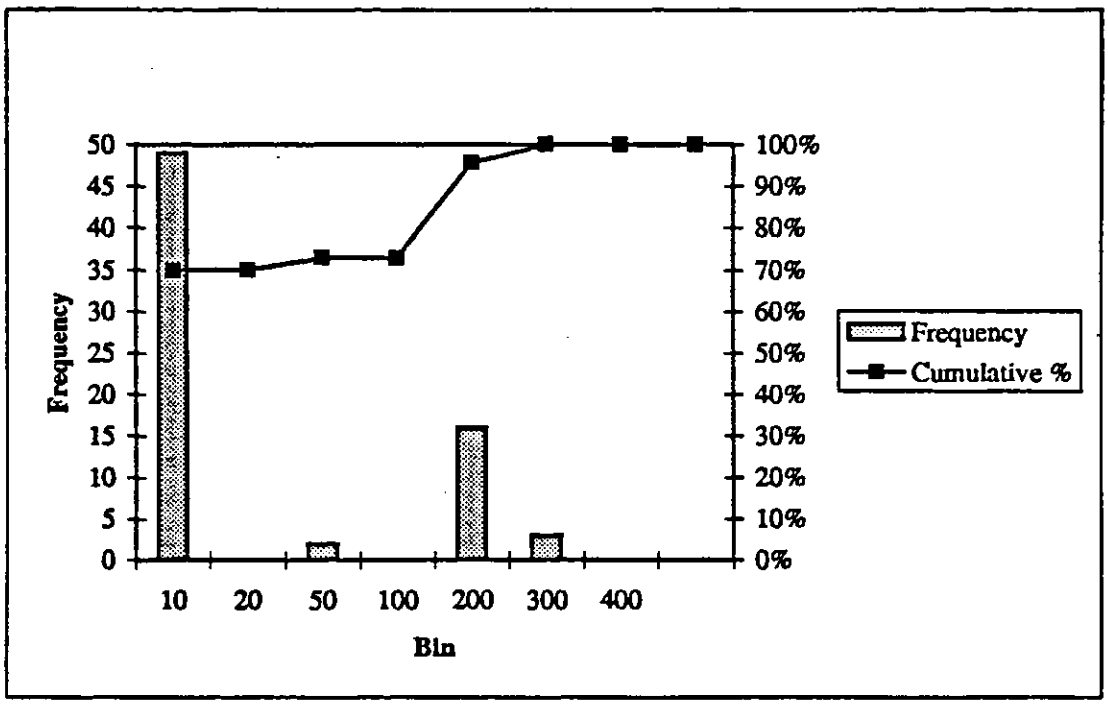

Fig. D6 The pit distribution for CN7M after 60 days at 90°C

Bin	*Frequency*	*Cumulative %*
10	21	52.50%
20	7	70.00%
50	8	90.00%
100	3	97.50%
200	1	100.00%
300	0	100.00%
More	0	100.00%
	40	

Bin: pit depth in microns

Frequency: number of pits

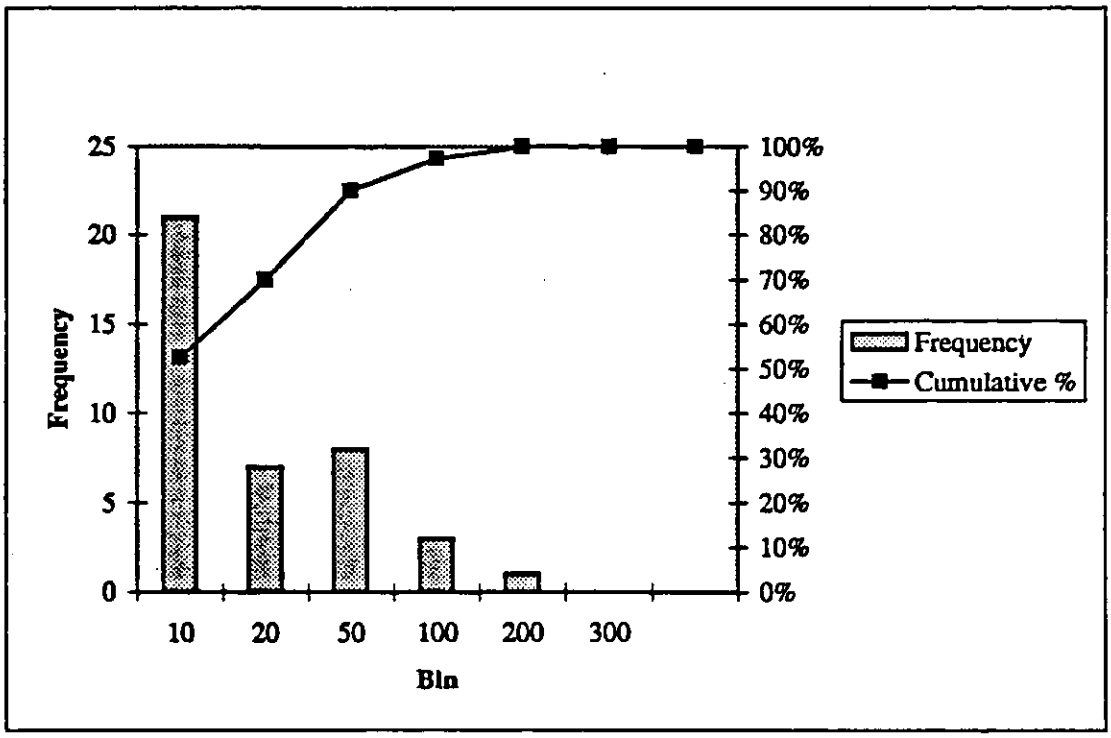

Fig. D7 Pit distribution for CD4MCu after 30 days at 90°C

Bin	*Frequency*	*Cumulative %*
10	0	.00%
20	122	80.26%
50	15	90.13%
100	13	98.68%
200	1	99.34%
300	1	100.00%
400	0	100.00%
More	0	100.00%
	152	

Bin: pit depth in microns

Frequency: number of pits

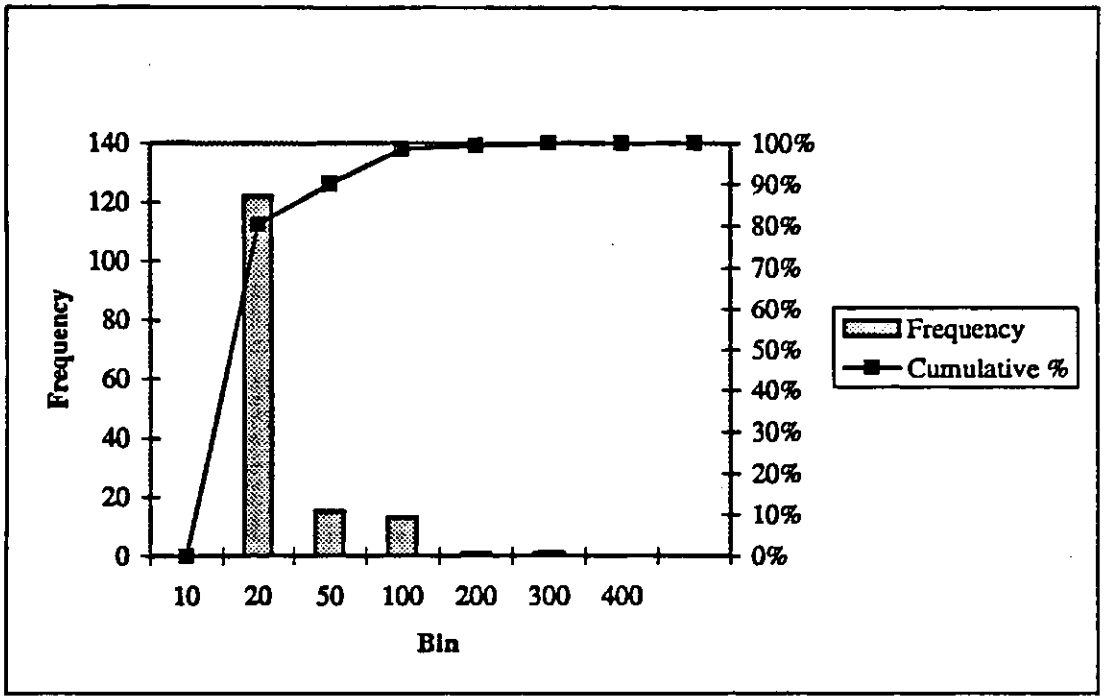

Fig. D8 The pit distribution for CD4MCu after 60 days at 90°C

Bin	*Frequency*	*Cumulative %*
10	20	71.43%
20	3	82.14%
50	3	92.86%
100	2	100.00%
200	0	100.00%
300	0	100.00%
More	0	100.00%
	28	

Bin: pit depth in microns

Frequency: number of pits

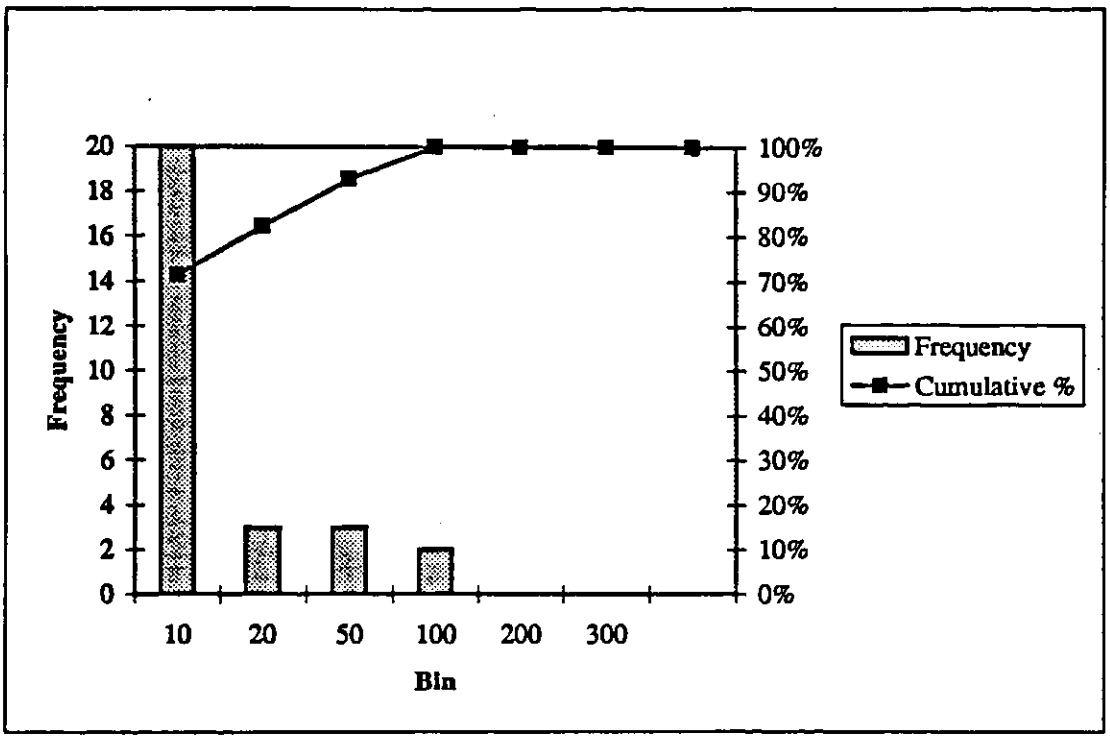

Fig. D9 Pit distribution for 2205 after 30 days at 90°C

Bin	*Frequency*	*Cumulative %*
10	10	25.64%
20	8	46.15%
50	20	97.44%
100	1	100.00%
200	0	100.00%
300	0	100.00%
400	0	100.00%
More	0	100.00%
	39	

Bin: **pit depth in microns**

Frequency: **number of pits**

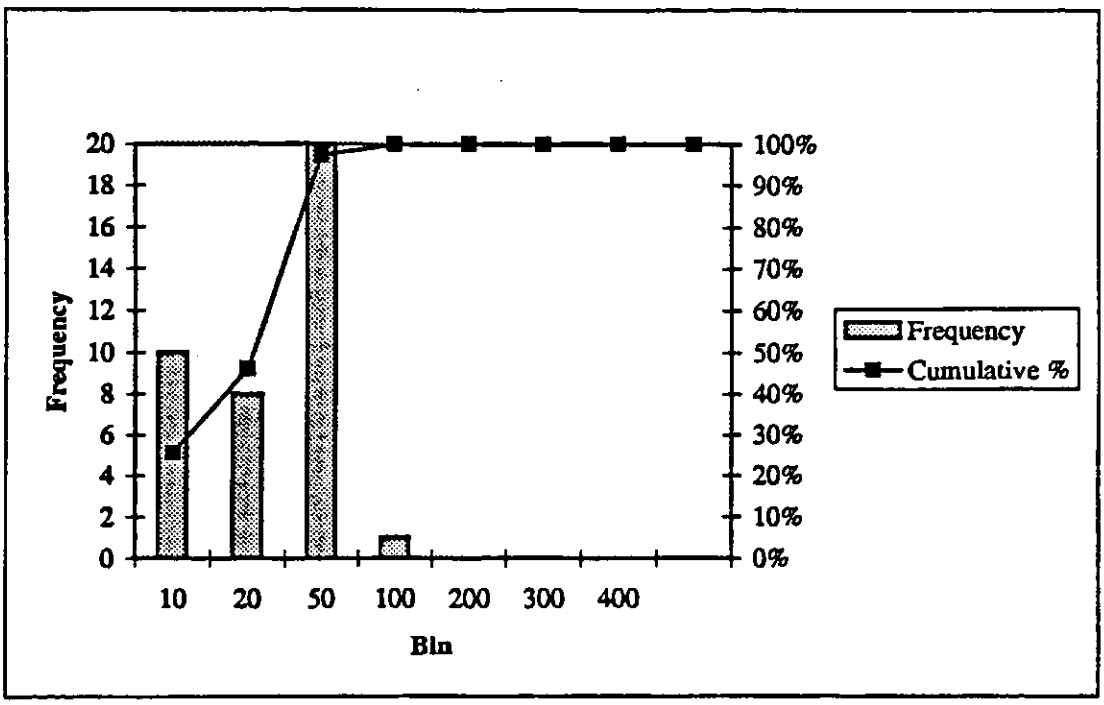

Fig. D10 The pit distribution for 2205 after 60 days at 90°C

Bin	*Frequency*	*Cumulative %*
10	50	80.65%
20	8	93.55%
50	3	98.39%
100	0	98.39%
200	0	98.39%
300	1	100.00%
More	0	100.00%
	62	

Bin: pit depth in microns

Frequency: number of pits

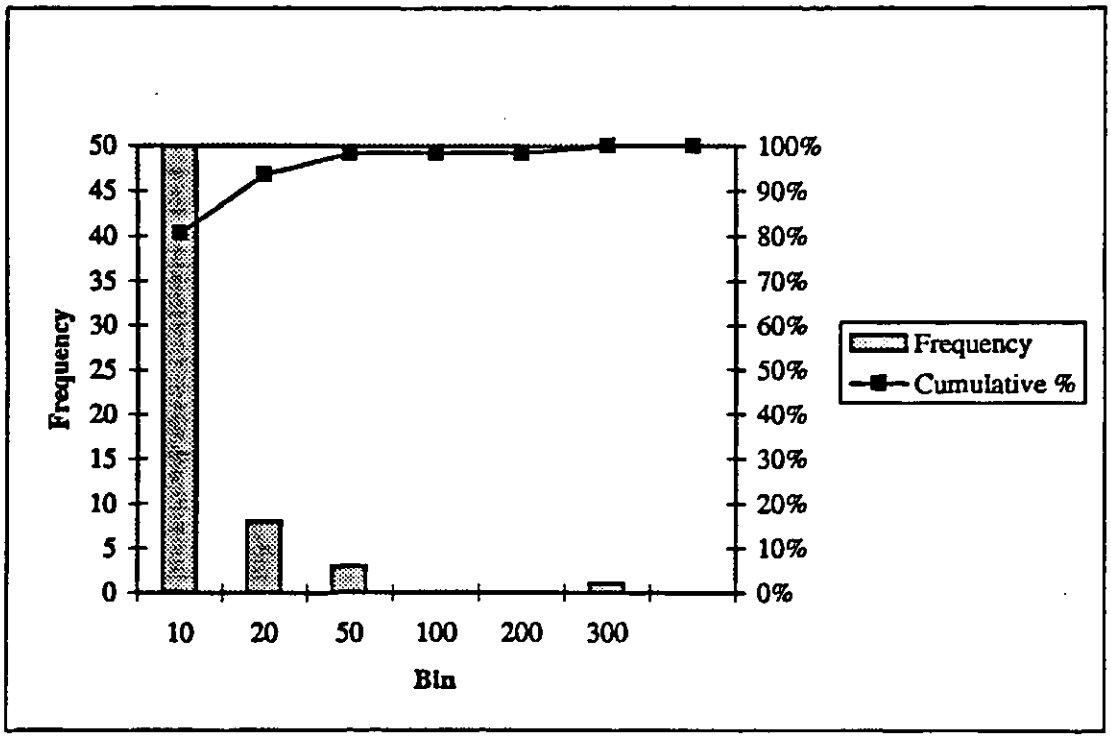

Fig. D11 Pit distribution for 904L after 30 days at 90°C

Bin	*Frequency*	*Cumulative %*
10	0	.00%
20	84	97.67%
50	1	98.84%
100	1	100.00%
200	0	100.00%
300	0	100.00%
400	0	100.00%
More	0	100.00%
	86	

Bin: **pit depth in microns**

Frequency: **number of pits**

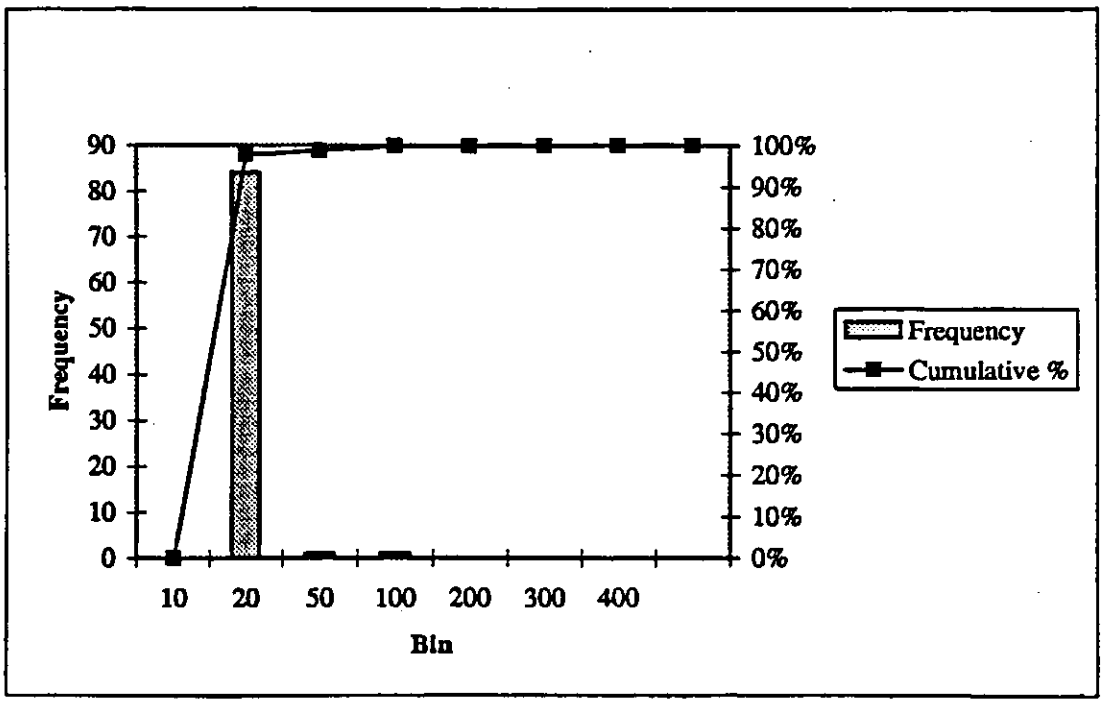

Fig. D12 The pit distribution for 904L after 60 days at 90°C

Bin	*Frequency*	*Cumulative %*
10	14	77.78%
20	3	94.44%
50	0	94.44%
100	1	100.00%
200	0	100.00%
300	0	100.00%
More	0	100.00%
	18	

Bin: pit depth in microns

Frequency: number of pits

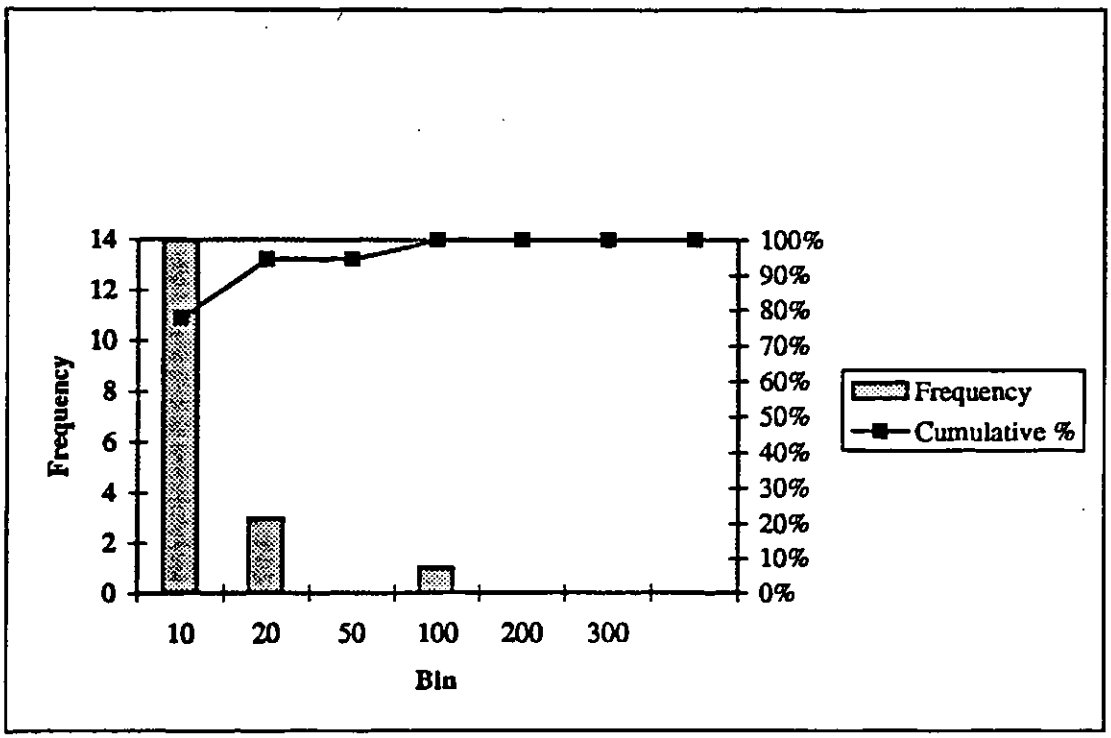

Fig. D13 Pit distribution for 2507 after 30 days at 90°C

Bin	*Frequency*	*Cumulative %*
10	20	80.00%
20	2	88.00%
50	2	96.00%
100	0	96.00%
200	1	100.00%
300	0	100.00%
400	0	100.00%
More	0	100.00%
	25	

Bin: pit depth in microns

Frequency: number of pits

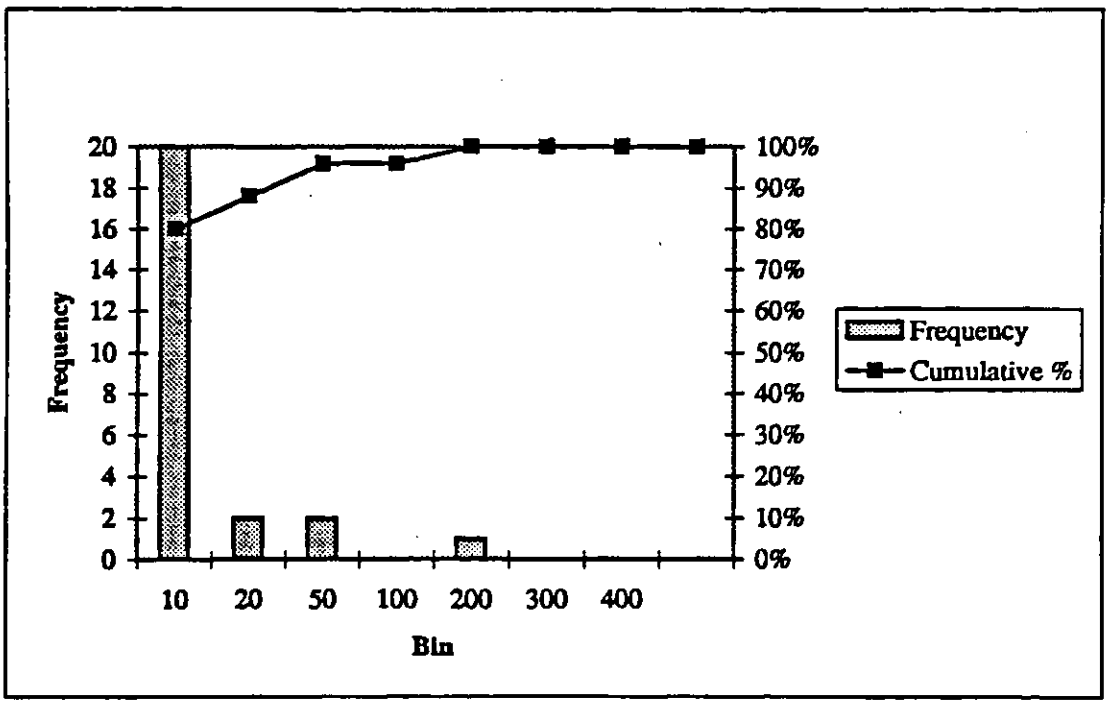

Fig. D14 Pit distribution for 2507 after 60 days at 90°C

Bin	*Frequency*	*Cumulative %*
10	42	75.00%
20	5	83.93%
50	6	94.64%
100	2	98.21%
200	0	98.21%
300	1	100.00%
More	0	100.00%
	56	

Bin: **pit depth in microns**

Frequency: **number of pits**

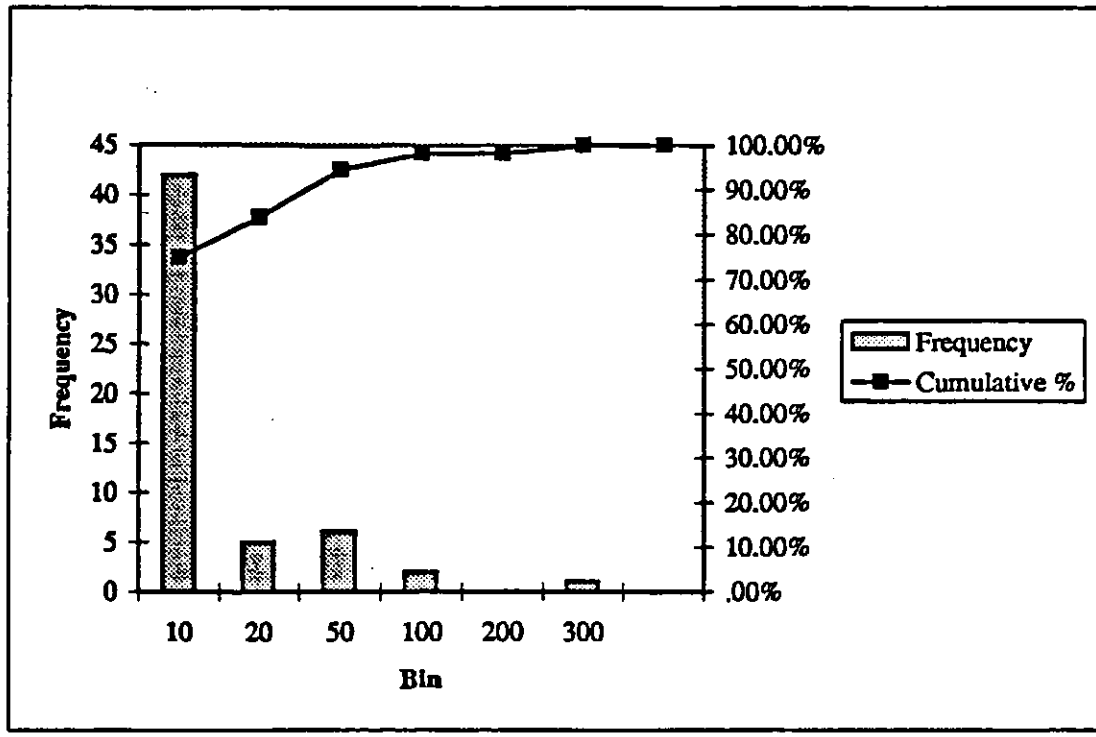

Fig. D15 Pit distribution for 254SMO after 30 days at 90°C

Bin	*Frequency*	*Cumulative %*
10	46	71.88%
20	0	71.88%
50	15	95.31%
100	1	96.88%
200	1	98.44%
300	1	100.00%
400	0	100.00%
More	0	100.00%
	64	

Bin: pit depth in microns

Frequency: number of pits

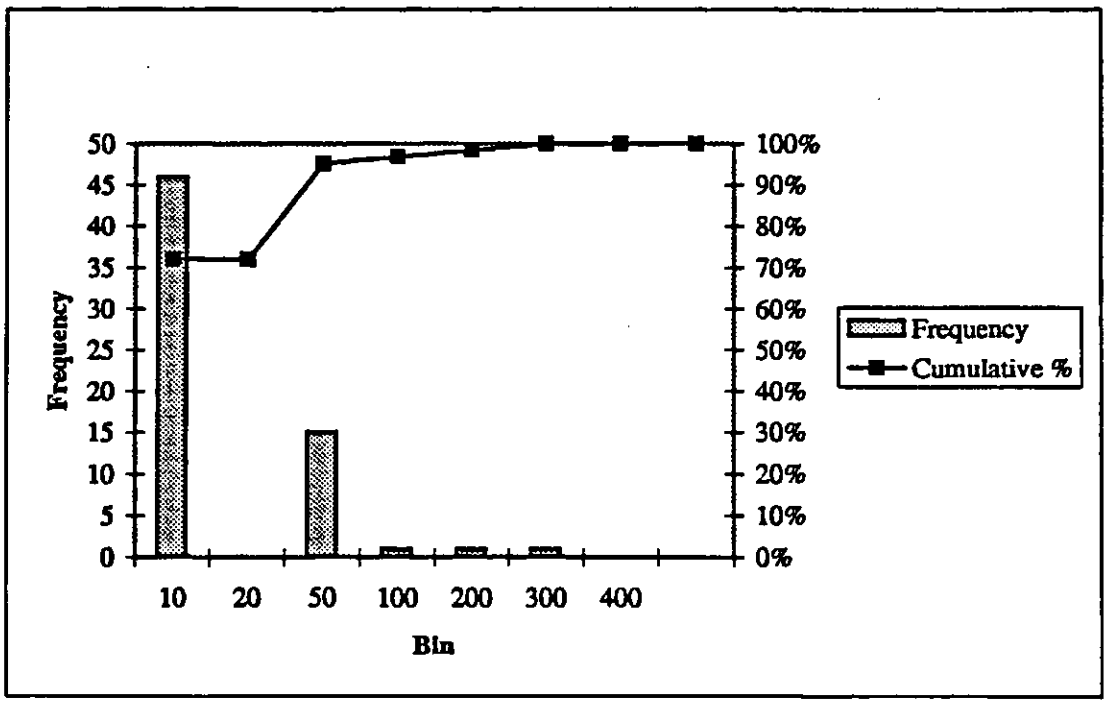

Fig. D16 The pit distribution for 254SMO after 60 days at 90°C